The P Cluster of the *Azotobacter vinelandii* Nitrogenase Complex: Effects of Substitution at the Cluster-bridging Residue, α-Cys88

by

John S. Cantwell

Dissertation submitted to the faculty of the
Virginia Polytechnic Institute and State University
in partial fulfillment of the requirements for the degree of

DOCTOR OF PHILOSOPHY

in

Biochemistry

APPROVED:

_____
W.E. Newton, Chairman

_____ _____
J.S Chen D.R. Dean

_____ _____
E.M. Gregory P.J. Kennelly

January, 1998

Blacksburg, VA

The P Cluster of the *Azotobacter vinelandii* Nitrogenase Complex:
Effects of Substitution at the Cluster-bridging Residue, α-Cys88

by

John S. Cantwell

Committee Chairman: William E. Newton
Department of Biochemistry

(ABSTRACT)

The major focus of the research in our laboratory is the investigation of the role of the nitrogenase component, the MoFe protein, in the catalytic mechanism of biological nitrogen fixation. This dissertation research centers on the role(s) of the P cluster, one of the two unique FeS clusters of the MoFe protein, in the electron transfer mechanism of nitrogenase.

Prior to the solution of the x-ray crystal structure of the *Azotobacter vinelandii* MoFe protein, it was had been determined which of the highly conserved cysteinyl residues of this protein were likely P cluster ligands. After elucidation of the crystal structure, it became evident that cysteine-88 of the α-subunit (α-Cys88) and cysteine-95 of the β-subunit (β-Cys95) could play important roles in maintaining and/or perturbing the conformation of the double-cubane structure by virtue of their bridging positions. It was found that three out of ten bacterial strains with substitutions at the α-Cys88 ligand retained significant catalytic activity. We investigated the effects of these substitutions on the overall structural, kinetic and spectroscopic parameters. The results of prior studies suggested a role for the P clusters in accepting, storing, and then delivering the electrons received from the Fe protein. Therefore, we asked whether α-Cys88 substitution resulted in perturbed functioning of the overall catalytic mechanism and more importantly what these differences reveal about the normal mechanism of nitrogenase.

Alterations in the bridging cysteine α-88 affected the rate of substrate reduction which can be explained in part by production of cluster-less MoFe protein. Electron flux,

NaCl concentration, and reductant concentration titration assays revealed a significant uncoupling of the ATP hydrolysis rate from the substrate reduction rate in the α-88Cys-to-Gly MoFe protein. Rapid kinetic analysis revealed decreased electron tranfer rates in all three of the α-Cys88 altered MoFe proteins when compared to the wild-type MoFe protein. The intermolecular electron transfer rate was lowered in the α-88Cys-to-Asp MoFe protein, while the intramolecular electron transfer rate was limiting in the α-88Cys-to-Gly and α-88Cys-to-Thr MoFe proteins. These results indicated a role for the α-88 position in controlling electron flow through the P cluster.

Another significant finding centers on the spectroscopic signals derived from one of these α-88Cys substituted MoFe proteins. The α-88Cys-to-Gly MoFe protein possesses a unique S=1/2 EPR signal in the native, dithionite-reduced state that was shown to be due to a one-electron-oxidized P cluster. This new paramagnetic center was evidence for the dramatic perturbation of the electromagnetic properties of the P cluster by the α-88Cys-to-Gly substitution. Additionally, both Mössbauer and magnetic circular dichroism spectroscopies have also demonstrated significant changes in the electromagnetic environments of the P clusters of these α-88Cys altered MoFe proteins and that each substitution affected the P cluster differently. The novel EPR signal was exploited in order to follow the sequence of electron transfer events in the nitrogenase reaction.

Finally, altered nitrogenase component proteins were combined and analyzed in an attempt to distinguish which particular step(s) are perturbed in the overall enzymatic reaction.

ACKNOWLEDGMENTS

I would like to express my sincere gratitude to the following individuals who have all contributed to my graduate education in one way or another. First and foremost I'd like to thank my major advisor, mentor, and good friend Dr. William E. Newton for his patience, guidance, trust, and good humor over the entire 12 years that I have had the pleasure to work for him. The confidence that Bill instilled in me was critical to my decision to continue my education at Virginia Tech. Equally important has been my association with Dr. Karl Fisher over the last four years. I have no doubt that this research project would not have progressed as far as it did without Karl's expert advice, criticism, support and friendship. I will truly miss our many thought-provoking discussions on nitrogenase, science, and life in general over many a mug-full of Mill Mt. coffee. Many thanks are owed to Dr. Dennis Dean and the past and present members of his laboratory, particularly Dr. John Peters and Valerie Cash. Their assistance and facilities were critical to the molecular biological phase of my research. They always made me feel welcome and for that I am indebted to them. I would like to thank the other members of my committee, Drs. Chen, Gregory and Kennelly, for their advice, attention, and extreme patience during my six year tenure as a PhD. candidate. My coworkers and fellow graduate students, both past and present, deserve my appreciation for the camaraderie and laughs provided by all. My gratitude also goes out to our understaffed and overworked support staff, particularly Ross Willis who was always willing and able to assist on various equipment and technical problems that arose periodically. Finally, I'd like to thank my fiancee, Charlene Tanaka, for her support, patience, laughter and love during our record-breaking long distance relationship over the past seven years.

TABLE OF CONTENTS

LIST OF FIGURES

Figure **Page**

LIST OF TABLES

Table **Page**

ABBREVIATIONS

ADP	Adenosine 5’ diphosphate
ATP	Adenosine 5’ triphosphate
Av	*Azotobacter vinelandii*
Av1	Component 1 of *Azotobacter vinelandii* nitrogenase; MoFe protein
Av2	Component 2 of *Azotobacter vinelandii* nitrogenase; Fe protein
$Av2_{ox}$	Oxidized Fe protein from *Azotobacter vinelandii*
CD	Circular Dichroism
Cp	*Clostridium pasteurianum*
Cp2	Component 2 of *Clostridium pasteurianum* nitrogenase; Fe protein
DEAE	Diethylaminoethyl cellulose
ΔA	Absorbance change
$\Delta\varepsilon$	Molar absorptivity change
EDTA	Ethylene diamine tetraacetic acid
EPR	Electron paramagnetic resonance spectroscopy
FeMoco	Iron molybdenum cofactor
GHz	Gigahertz
^{1}H NMR	Proton nuclear magnetic resonance spectroscopy
HEPES	N-[2-Hydroxylethyl]piperazine-N’-[2-ethanesulfonic acid]
k	Rate constant
kD	Kilodalton(s)
kHz	kilohertz
K_m	Michaelis Menten constant
k_{obs}	Observed rate constant
Kp	*Klebsiella pneumoniae*
Kp1	Component 1 of *Klebsiella pneumoniae* nitrogenase; MoFe protein
Kp2	Component 2 of *Klebsiella pneumoniae* nitrogenase; Fe protein
$Kp2_{ox}$	Oxidized Fe protein from *Klebsiella pneumoniae*

MCD	Magnetic circular dichroism
MgADP	Magnesium adenosine 5’ diphosphate
MgATP	Magnesium adenosine 5’ triphosphate
M^N	Reduced FeMoco
M^{OX}	Oxidized FeMoco
M_r	Molecular mass
mV	Millivolt(s)
mW	Milliwatt(s)
$Na_2S_2O_4$	Sodium dithionite
nif	nitrogen fixation gene
Nif-	Inability to grow on N_2
Nif+	Ability to grow on N_2; diazotrophy
Nif^{slow}	Slow growth on N_2
NMF	N-methylformamide
PAGE	Polyacrylamide gel electrophoresis
Pi	Inorganic phosphate
P^N	Reduced P cluster
P^{OX}	Oxidized P cluster
S	Electron paramagnetic spin state
SDS	Sodium dodecyl sulfate
$SO_2^{\cdot -}$	Thionite radical
$S_2O_4^{2-}$	Dithionite ion
T	Tesla
$t_{1/2}$	Doubling time or half-life
Tris	Tris (hydroxymethyl) aminomethane
UV	Ultraviolet

CHAPTER I.
LITERATURE SURVEY

A. Introduction

Nitrogen is an essential component for two of the major building blocks of all life forms on this planet, namely nucleic and amino acids. Although nearly 80% of the earth's atmosphere is composed of nitrogen in the form of dinitrogen (N_2) gas, this is metabolically unavailable to higher plants and animals. Nitrogen typically enters the food chain in the form of ammonia (NH_3) or nitrate (NO_3^-). In fact, the conversion of dinitrogen to ammonia (i.e. nitrogen fixation), both biologically and synthetically, represents the rate-limiting step in the global nitrogen cycle. With this fact in mind, it is no wonder that "fixed" nitrogen is very often the limiting soil nutrient in U.S. and world agriculture. Although there are several methods of forming fixed nitrogen from dinitrogen, the biological process, performed exclusively by prokaryotes, is still responsible for the major portion (estimated at 100-175 million metric tons annually; Burns & Hardy, 1975). Lightning strikes may produce 10 million metric tons while industrial fixation by the Haber-Bosch process yielded around 80 million metric tons in 1989 (Hardy, 1993). Clearly biological nitrogen fixation research can impact life on this planet in several ways.

1. The Impact of Nitrogen Fixation

a. Environmental - In developed nations, the problem of limiting soil nitrogen is solved by the application of fertilizers, either man-made or organic forms like manure. However, the efficiency of plant utilization of fertilizer nitrogen is usually 50% or less. Some unassimilated fertilizer can be converted by microbial action to nitrate, which leaches into groundwater tables, thus becoming a source of water pollution and a human health hazard. In addition, denitrifying bacteria can convert nitrate to dinitrogen (N_2) and nitrous oxide (N_2O) which is a greenhouse gas capable of contributing to global warming. As the world population continues to increase, it is likely that these imprudent agricultural practices will necessarily increase to meet the demands for higher crop yield.

Biological nitrogen fixation, whether performed by symbiotic or free-living bacterial species, is essentially pollution-free because ammonia production is tightly controlled at the genetic and biochemical levels. There is no wasted excess of fixed nitrogen in the biological system.

An often overlooked environmental impact of industrially produced ammonia is the danger of transporting anhydrous ammonia from the commercial plants to the distribution centers in large tankers. The potential of an ammonia spill, although slight, is a serious risk because this chemical is highly toxic. The dangers to livestock and humans has been demonstrated in the media frequently. The issue of transportation of anhydrous ammonia also contributes to air pollution by fossil fuel emissions.

b. Economic - The Haber-Bosch method of nitrogen fixation is the major industrial process for nitrogen fertilizer production. In 1995, ammonia was sixth on the list of manufactured chemicals in the U.S. based on production volume, and first when measured by a per mole basis (Kirschner, 1996). The synthetic reaction is an energy-intensive one requiring high pressures of 300 atms. and elevated temperatures of 500°C. Large quantities of fossil fuels are required to attain the necessary catalytic conditions. Obviously, as these non-renewable energy sources become more and more scarce, the cost of synthetically-produced ammonia will rise. Alternatively, biological nitrogen fixation has minimal energy costs aside from the ATP requirement because it occurs at an atmospheric pressure of 1 atm. and a temperature of 20°C. Evolution has performed the ultimate cost-benefit analysis in creating the nitrogenase complex.

c. Basic Biochemistry - Biochemical research into the workings of nitrogen fixation are generally centered on the enzyme complex nitrogenase. Aside from all of the agronomic reasons for studying this enzyme, there are a multitude of more basic biochemical issues involved. Some of the more prominent areas of interest include: 1. Electron transfer reactions and pathways in proteins, both inter- and intramolecular; 2. Protein-protein association and dissociation mechanisms; 3. Nucleotide binding and hydrolysis as a signal transducing system and conformational control method; 4. Complex

metal cluster involvement in enzymatic catalysis; and 5. Prosthetic group assembly and insertion into polypeptides. These topics represent an abbreviated list of the diverse areas of biochemical research that are overlapping aspects of nitrogenase investigations. Nitrogenase research also demonstrates the utility of various spectroscopic techniques as probes into enzymatic mechanism and chemistry.

2. The Overall Reaction

Biological nitrogen fixation is the catalytic process performed by the nitrogenase complex, a two-component metalloenzyme system consisting of the Fe and MoFe proteins (see Figure 1). The overall reaction requires a source of electrons, protons and a minimum of two MgATP molecules hydrolyzed per electron transferred. A minimal chemical equation can be written as follows:

$$\mathbf{N_2 + 8e^- + 8H^+ + 16MgATP \rightarrow 2NH_3 + H_2 + 16MgADP + 16\ Pi}$$

There are a few important details concerning the nitrogenase reaction that are apparent from the overall reaction: 1. For every molecule of dinitrogen reduced, there is an obligate evolution of one molecule of H_2. 2. For every electron transferred by the enzyme complex, a minimum of two molecules of MgATP are hydrolyzed. 3. As the enzyme complex turns over, MgADP will begin to build up unless reconverted to MgATP. This last detail has important consequences because it is known that MgADP is an inhibitor of nitrogenase action (Bulen *et al.*, 1965). 4. The standard free energy change, $\Delta G°$, for the biological process using ferredoxin as reductant is -15 kcal/mol (Alberty, 1994), i.e. favoring ammonia synthesis. Therefore, even though MgATP is required, it does not serve an energy coupling role.

3. The Nitrogenase Complex and it's Nomenclature

Nitrogenase is composed of two metalloproteins that have various names based on common observations of each. The first and larger component is the MoFe protein, whereas the second smaller component is the Fe protein (see Figure 1). In each case the protein derives its name from the metal centers therein. The MoFe protein contains two

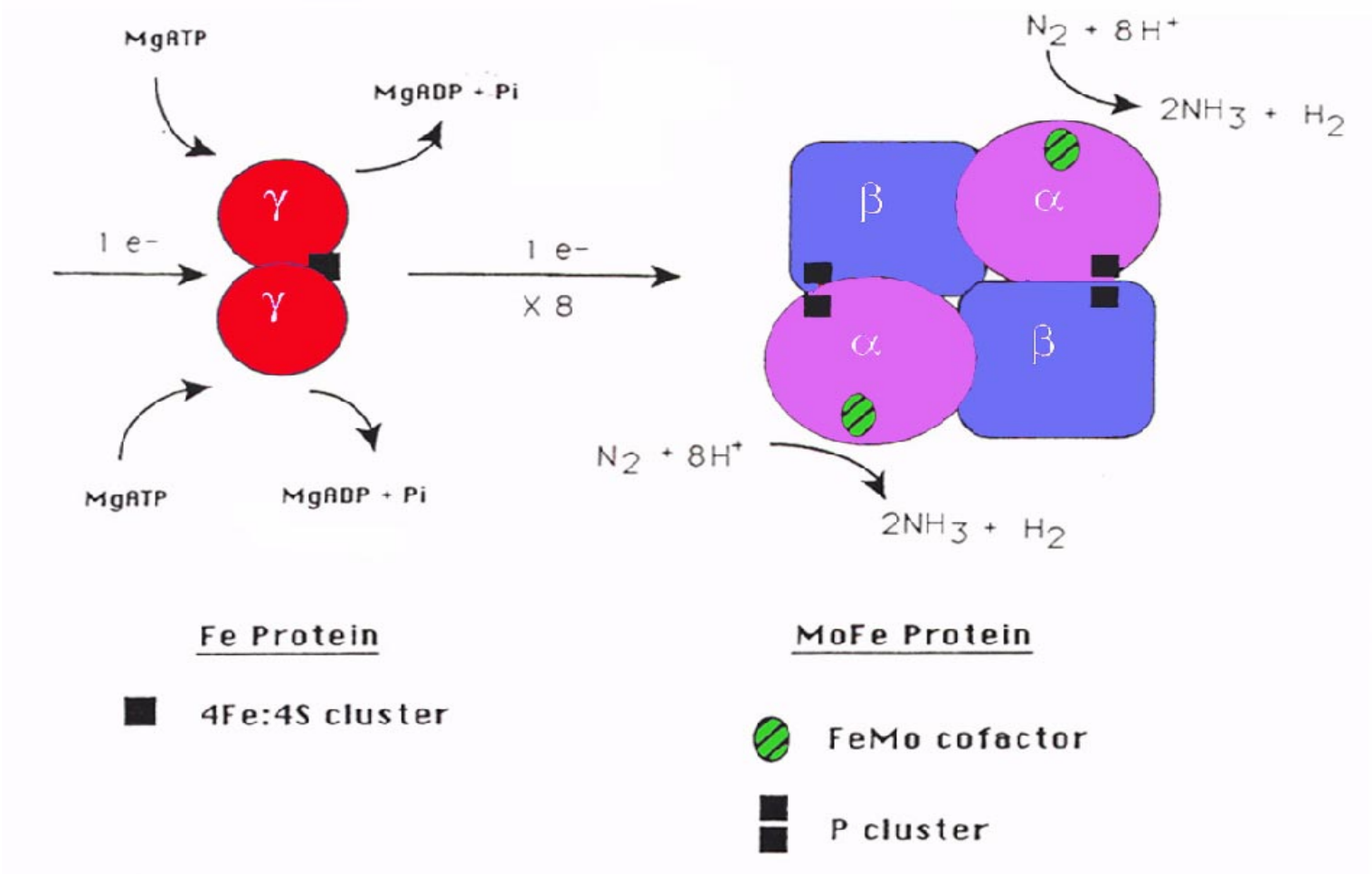

Figure 1: Schematic Diagram of the Nitrogenase Complex and the Generalized Nitrogen Fixation Reaction

types of unique metalloclusters, the iron-molybdenum cofactor (FeMoco), and the Fe-S cluster known as the P cluster; the Fe protein contains one Fe_4S_4 cluster, thus the origins of the respective protein nomenclatures. The MoFe protein is also referred to as component 1 and the Fe protein is called component 2 based on their respective elution positions from a DEAE-cellulose anion exchange column during purification. A two letter genus (upper-case) species (lower-case) designation followed by the numbers 1 or 2 therefore indicates the MoFe or Fe protein from that species, e.g. Av1 denotes the MoFe protein from *Azotobacter vinelandii*, and Kp2 indicates the Fe protein from *Klebsiella pneumoniae*. Less commonly used designations for the nitrogenase components are dinitrogenase for the MoFe protein and dinitrogenase reductase for the Fe protein.

4. The Nitrogen-Fixing Organisms

One of the striking features of nitrogenase is its exclusive location in prokaryotes. To date, the enzyme and, therefore, the ability to fix nitrogen (i.e., diazotrophy) has been found in prokaryotes only. Remarkably, nitrogen-fixing bacteria come in a wide variety of life styles and survival strategies. Examples include: the strict anaerobe, *Clostridium pasteurianum*, the facultative species, *Klebsiella pneumoniae*, the photosynthetic species, *Rhodobacter capsulatus*, the cyanobacteria, *Anabaena*, the legume symbiont, *Rhizobium meliloti*, the archaeal methanogen, *Methanosarcina barkeri 227*, and the strict aerobe utilized in our studies, *Azotobacter vinelandii*. The genes for the structural subunits of nitrogenase have been sequenced from many of these bacterial species and a high degree of homology exists among all of the deduced amino-acid sequences. This fact stands as a testament to the convergence in design that is necessary to catalyze the reduction of N_2 to NH_3.

Although the nitrogenases from various nitrogen-fixing bacteria are similar, the methods of protecting this highly oxygen (O_2) labile metalloenzyme from inactivation are quite diverse. Strategies range from the obvious, such as existing in O_2-limited or anaerobic environments, like *K. pneumoniae* and *C. pasteurianum*, to the more complex, such as the production of oxygen-excluding compartments in *Anabaena* or *R. meliloti*.

Although the problem of oxygen inactivation has multiple solutions, there appears to be only one effective solution to diazotrophy.

5. The Multiple Substrates of Nitrogenase

In addition to the biologically relevant reduction of dinitrogen by nitrogenase, the enzyme can also reduce several other small molecules (see Table 1). Most notable is the reduction of acetylene (C_2H_2) to ethylene (C_2H_4; Dilworth, 1967). This reaction is often used as an indicator of nitrogenase activity in cell lysates and purified preparations. Acetylene is a competitive inhibitor of dinitrogen reduction but dinitrogen is a non-competitive inhibitor of acetylene reduction. This trend in inhibition patterns may result from binding of substrates to different oxidation states of the MoFe protein rather than to different sites on the enzyme. An abbreviated list of alternative substrates of nitrogenase includes nitrous oxide (N_2O; Hoch *et al*., 1960; Jensen & Burris, 1986), cyanide (HCN; Hardy & Knight, 1967; Li *et al*., 1982), azide (N_3^-; Schöllhorn & Burris, 1967), nitrite (NO_2^-; Vaughn & Burgess, 1989), and cyanamide ($NCNH_2$; Miller & Eady, 1988a).

Another significant reaction catalyzed by nitrogenase is hydrogen (H_2) production (Burns & Bulen, 1965; Bulen & LeComte, 1966). In the absence of all other substrates, the nitrogenase complex will reduce protons to molecular hydrogen. This reaction is testament to the reductive capabilities of the enzyme; even under an inert atmosphere such as argon or helium, nitrogenase will form product. H_2 is also a competitive inhibitor of N_2 reduction (Hwang et al., 1973). The extent of inhibition is known to be controlled by the level of electron flux through the nitrogenase system as well as the partial pressure of H_2 (Hageman & Burris, 1980; Wherland *et al*., 1981; Guth & Burris, 1983, see Section I.F.2.a). Hydrogen production is also a useful kinetic tool for analyzing nitrogenase function because carbon monoxide (CO) normally inhibits the reduction of all substrates except proton reduction (Hardy *et al*., 1965).

Table 1: Multiple Substrates of Nitrogenase

	Reactants		**Products**
1.	$N_2 + 6H^+ + 6e^-$	$\rightarrow$	$2NH_3$
2.	$N_2H_4 + 2H^+ + 2e^-$	$\rightarrow$	$2NH_3$
3.	$2H^+ + 2e^-$	$\rightarrow$	H_2
4.	$C_2H_2 + 2H^+ + 2e^-$	$\rightarrow$	C_2H_4
5.	$C_2H_4 + 2H^+ + 2e^-$	$\rightarrow$	C_2H_6
6.	$HCN + 6H^+ + 6e^-$	$\rightarrow$	$CH_4 + NH_3$
7.	$HCN + 4H^+ + 4e^-$	$\rightarrow$	CH_3NH_2
8.	$CH_3NC + 6H^+ + 6e^-$	$\rightarrow$	$CH_4 + CH_3NH_2$
9.	$CH_3NC + 4H^+ + 4e^-$	$\rightarrow$	CH_3NHCH_3
10.	$HN_3 + 6H^+ + 6e^-$	$\rightarrow$	$N_2H_4 + NH_3$
11.	$N_3^- + 3H^+ + 2e^-$	$\rightarrow$	$N_2 + NH_3$
12.	$N_2O + 2H^+ + 2e^-$	$\rightarrow$	$N_2 + H_2O$
13.	$NO_2^- + 7H^+ + 6e^-$	$\rightarrow$	$NH_3 + 2H_2O$
14.	$NCNH_2 + 6H^+ + 6e^-$	$\rightarrow$	$CH_3NH_2 + NH_3$
15.	$NCNH_2 + 8H^+ + 8e^-$	$\rightarrow$	$CH_4 + 2NH_3$
16.	$CH_2\text{-}N{=}N + 6H^+ + 6e^-$	$\rightarrow$	$CH_3NH_2 + NH_3$
17.	$CH_2\text{-}N{=}N + 8H^+ + 8e^-$	$\rightarrow$	$CH_4 + 2NH_3$
18.	$3CH{=}CHCH_2 + 6H^+ + 2e^-$	$\rightarrow$	$CH_2CH_2CH_2 + 2CH_3CH{=}CH_2$
19.	$CO_2 + 2H^+ + 2e^-$	$\rightarrow$	$CO + H_2O$
20.	$COS + 2H^+ + 2e^-$	$\rightarrow$	$CO + H_2S$

Adapted from Yates, 1992.

B. Genetic Organization of the *nif* Regulon

The organization and regulation of the genes required for competent nitrogenase was revealed in the early 1980's at the Unit of Nitrogen Fixation at the University of Sussex, U.K., and the Department of Bacteriology and Center for Studies of Nitrogen Fixation at the University of Wisconsin, U.S.A. The researchers utilized the facultative species *Klebsiella pneumoniae* because of its similarities to *Eschericia coli,* which had proven to be a valuable tool for various molecular biological manipulations. Because *K. pneumoniae* was the first organism to have its nitrogen fixation gene cluster cloned and sequenced, it is the paradigm for all sequence homology comparisons among nitrogen-fixing bacteria. The individual genes of the nitrogen fixation gene cluster are designated by the three-letter acronym, *nif*, followed by a single capital letter. Correspondingly, the gene product is designated by the acronym Nif followed by the same single capital letter. Up to 20 *nif* genes have been described from the 24 kilobase *nif* cluster from *K. pneumoniae*. These genes are organized into eight contiguous transcriptional units (See Figure 2).

1. Nitrogenase and Electron Transporter Structural Genes

The *nif* genes encoding the polypeptides of nitrogenase include *nifH* which codes for the Fe protein, *nifD* which codes for the α-subunit, and *nifK* which codes for the β-subunit of the MoFe protein respectively. The *nifJ* and *nifF* genes encode the electron transport proteins, pyruvate:flavodoxin oxidoreductase and a flavodoxin, respectively.

2. FeMoco Biosynthesis Genes

A majority of the genes in the *nif* cluster appear to function in metal cluster biosynthesis, insertion, or maturation. The *nifB* and *nifQ* genes are proposed to be involved in early steps of iron-molybdenum cofactor (FeMoco; see section I.D.2.c) synthesis; the *nifQ* gene product appears responsible for molybdenum assimilation into FeMoco (Imperial *et al*., 1984). The *nifE* and *nifN* gene products probably express a macromolecular scaffold necessary for FeMoco biosynthesis (Paustian *et al*., 1989; Roll

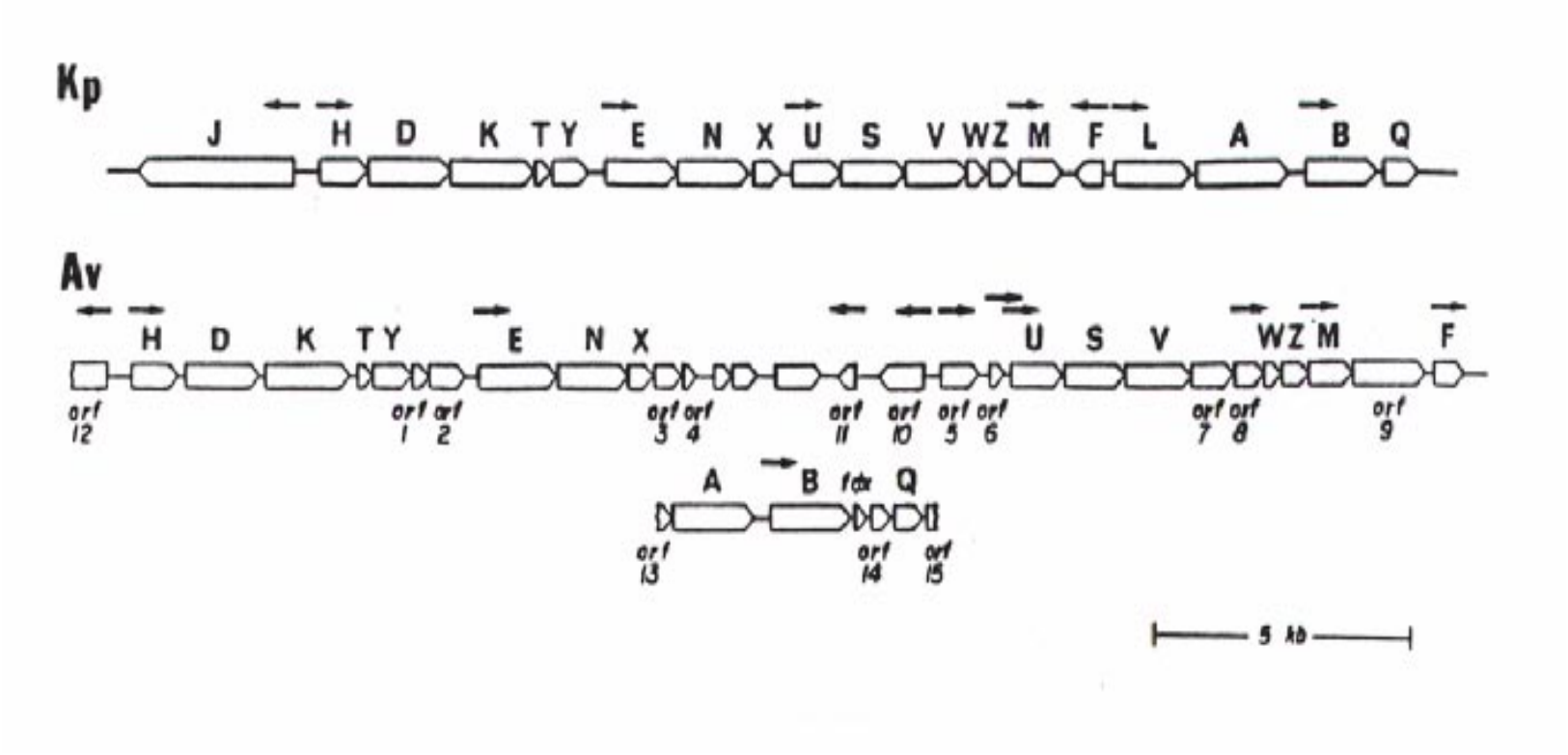

Figure 2: Genetic Organization of the *nif* gene clusters from *K. pneumoniae* and *A. vinelandii*

Arrows indicate the position and direction for known or proposed transcription initiation sites. Adapted from Dean & Jacobson, 1992.

et al., 1995). This supposition is based in part on high sequence homology between *nifEN* and *nifDK* deduced amino acid primary structure (Brigle *et al*., 1987b). The *nifV* gene product is agreed to be homocitrate synthase, whose product, homocitrate, is key component of the FeMo cofactor (Hoover *et al*., 1987). Recently, using an *in vitro* FeMoco synthesis assay it has been shown that the *nifX* gene product is also necessary FeMoco biosynthesis (Shah *et al*., 1997).

3. Fe-S Cluster Biosynthesis Genes

The gene products of *nifS* and *nifU* are possibly involved in iron-sulfur (FeS) cluster synthesis. It is now known that *nifS* codes for a pyridoxal phosphate-containing cysteine desulfurase (Zheng *et al*., 1993; Zheng & Dean, 1994), and thus is potentially responsible for providing sulfur for cluster synthesis. The function of *nifU* is less clear, but it may play a similar role in providing Fe (Fu *et al*., 1994). It is interesting to note that deletion of either *nifS* or *nifU* from *A. vinelandii* results in a 10-fold reduction in Fe protein activity and a 3-fold reduction in MoFe protein activity, while a *nifUS* double deletion results in almost complete elimination of Fe protein activity and more than a 10-fold reduction in MoFe protein activity (Jacobson *et al*., 1989b). These results support the contention that NifU and NifS affect both Fe and MoFe protein activity, but the gene products are unlikely to be involved in the same physiologic function. Also, because the individual *nifU* or *nifS* genes can be deleted without complete loss of component protein activity, there may exist counterparts of these *nif* genes outside of the *nif* regulon that perform similar functions but are not tied specifically to nitrogen fixation.

4. Genes of Unknown Function

Fe protein activity is affected by one other gene, namely *nifM*. It was originally proposed that NifM was required for insertion of the FeS center into apo-Fe protein (Howard *et al*., 1986). Based on sequence comparisons it has been shown that NifM is highly homologous to a family of peptidyl prolyl isomerases (Rudd *et al*., 1995). These enzymes are responsible for the *cis*-to-*trans* conversion of proline residues in polypeptides.

nif genes whose functions remain unknown include *nifT*, *nifW*, and *nifZ*. The *nifT* gene encodes the smallest peptide of the *nif* cluster, 72 amino acids, and its deletion does not affect nitrogen-fixation capability. Both the *nifW* and *nifZ* gene appear to affect MoFe protein activity but are not required for diazotrophic growth. The analysis of a deletion mutant suggests that *nifZ* has a role in FeMoco formation or insertion (Jacobson *et al*., 1989b). Recent work a *nifW* deletion strain from *A. vinelandii* (Kim *et al*., 1994) and *R. capsulatus* (Masepohl et al., 1993) demonstrates that this gene may affect the homocitrate moiety of the FeMoco of the MoFe protein.

5. Regulatory Genes

The *nifA* and *nifL* genes are involved in regulation of expression of the other *nif* operons by transcriptional control. NifA is a *nif*-specific transcriptional activator protein (Dixon *et al*., 1980; Buchanan-Wollaston *et al*., 1981) that interacts with the RNA polymerase σ-factor, σ^{54} (the product of *rpoN*), to initiate transcription at *nif* promoters (Morett & Buck, 1989). The *nifL* product is a negative control element that operates by inactivating NifA, and responds to O_2, NH_4^+, and the levels of certain amino acid (Merrick *et al*., 1982). The *nifLA* operon is in turn controlled by the *ntr* (*nit*rogen *r*egulation) system. The *nifLA* promoter is also σ^{54}-dependent and requires the activator NtrC (Minchin *et al*., 1989). It is the NtrC protein that indirectly responds to the nitrogen status of the cell and thereby regulates the need for nitrogenase (Reitzer *et al*., 1989).

6. Differences in the *nif* Regulons of *K. pneumoniae* and *A. vinelandii*

Although the previous discussion on the *nif* genes is based on *K. pneumoniae*, the genetic organization is nearly identical in *A. vinelandii* with just a few exceptions (Jacobson *et al*., 1989a). There is no *nifJ* gene in *A. vinelandii*, and this fact may relate to the differences between strict aerobic and microaerobic metabolisms. The organization of the *A. vinelandii nif* gene cluster is non-contiguous; there are several open reading frames (orfs) interspersed between the *nif* operons, and the *nifLA* and *nifBQ* transcriptional units are together on a cluster separate from the rest of the *nif* gene cluster. The protein encoded by the *nifY* gene seems to have a defined function in *K. pneumoniae*

but no function has yet to be found for the same gene product in *A. vinelandii*. The current data support the contention that NifY in *K. pneumoniae* acts as a chaperone protein during the process of FeMoco insertion into apo-MoFe protein (Homer *et al*., 1993).

7. Alternative Nitrogenases

Two molybdenum-independent nitrogenases have been discovered: one containing vanadium (V), and another containing only iron (Fe). The expression of either of these alternative nitrogenases is repressed by the presence of molybdate in the growth media. The vanadium-iron protein (VFe protein) has thus far been found in several organisms including *A. vinelandii* (Bishop *et al*., 1986), *Azotobacter chroococcum* (Robson *et al*., 1986) and *Anabaena variabilis* (Kentemich *et al*., 1988) and the structural genes have been cloned and sequenced. The VFe protein has subunits which are highly homologous in amino-acid sequence to the Mo-dependent version including the residues that ligate the metalloclusters. The VFe protein, however, also possesses a small (~15 kD), extra δ-subunit that is essential for activity. Thus, the overall subunit structure is an $\alpha_2\beta_2\delta_2$ hexamer, and is encoded by the *vnf*DGK genes (Robson *et al*., 1989).

There are distinct catalytic differences between the VFe and MoFe proteins. The VFe protein is capable of reducing C_2H_2 to C_2H_6 in addition to C_2H_4 (Dilworth *et al*., 1987), whereas the MoFe protein can reduce C_2H_2 to C_2H_4 efficiently, and C_2H_4 to C_2H_6 inefficiently, but cannot reduce C_2H_2 to C_2H_6. One consequence of the nitrogenase catalytic mechanism is that for some substrates there is more than one reduction product and the allocation of electrons to a particular product is dictated by various factors including electron flux. Electron flux is the rate of transfer of electrons through the enzymatic system. For nitrogenase, flux can be controlled by a number of factors including, reductant and ATP concentrations, and the molar ratio of Fe and MoFe proteins. Under a N_2 atmosphere and high electron flux, the VFe protein allocates a much larger percentage of its electrons to H_2 formation than does the MoFe protein (65% vs. 30%), i.e. in the VFe protein, N_2 does not compete with protons effectively for electrons

compared to the Mo-nitrogenase. The VFe protein, however, is more efficient at reducing N_2 at low temperatures (30°C - 5°C) than the MoFe version (Miller & Eady, 1988b).

The third nitrogenase system, also known as Fe-nitrogenase or nitrogenase-3, has been cloned and sequenced from *A. vinelandii* (Pau *et al*., 1989), *R. capsulatus* (Schneider *et al*., 1991), and *Rhodospirillum rubrum* (Ludden *et al*. , 1993). Like the VFe protein, FeFe protein consists of three subunits encoded by the *anf*DGK operon. Purification of this protein from *A. vinelandii* has yielded products with varying subunit composition, and much lower specific activities for NH_3 and C_2H_4 formation than the Mo- and V-nitrogenases (Chisnell *et al*., 1988). The third system is the least well-studied, but present research has revealed it to be similar to the V-nitrogenase system in that it preferentially allocates electrons to H^+ under a 100% N_2 or 10% C_2H_2 atmosphere.

C. The Fe Protein

1. Structural Features

The Fe protein component of the nitrogenase complex is a γ_2 homodimer with an M_r of 64 kilodaltons (kD) encoded by the *nifH* gene. It contains one Fe_4S_4 cluster that bridges a cleft between the two identical subunits. Each subunit possesses both a Walker A-type (GX_4GKS/T; Walker *et al*., 1982; Robson, 1984) and Walker B-type (DXXGD; Walker *et al*., 1982;) nucleotide-binding motif that together form the MgATP-binding site. Thus, there are two Mg-ATP binding sites per dimer. Cysteinyl residues 97 and 132 are the ligands to the Fe_4S_4 cluster, i.e. two cysteines per subunit and therefore four cysteine ligands, one per Fe atom, for the entire dimeric protein. (Hausinger & Howard, 1983; Howard *et al*., 1989; Georgiadis *et al*., 1992). (Note: *A. vinelandii* primary sequence numbering will be used unless otherwise noted.)

The crystal structure of the Fe protein has been determined to a resolution of 2.9-❹ (Georgiadis *et al*., 1992). Each subunit has a α/β type domain fold consisting of an eight-stranded β sheet core, with seven of the eight strands in parallel orientation, surrounded by nine α helices (see Figure 3). Each subunit is approximately 40-❹ in

length along the two-fold axis of symmetry, and approximately 35-❹ by 45-❹ in girth. The quaternary structure of the dimer has been described as an iron butterfly or iron lungs with the metal center occupying the head or heart position and the molecular 2-fold rotation axis passing through this cluster. The dimer has an overall length of 40-❹ and a cross section of 45-❹ by 75-❹ perpendicular to the symmetry axis.

The Fe_4S_4 cluster appears to be highly solvent exposed with both Fe-ligating cysteines 97 and 132, occupying positions at the amino-terminal end of α helices, each of which follow a β strand-loop structure. NH-S hydrogen bonds, between amide nitrogens from α helix residues and the cluster sulfides and cysteine sulfhydryls, provide stabilizing electrostatic associations with the cluster. In addition to the bridging metallocluster, there are several Van der Waals and polar interactions that contribute to dimerization to the extent that these may be principal subunit stabilizers in the absence of the Fe_4S_4 cluster.

The nucleotide-binding region was identified in the crystal structure as residues Gly-9 through Ser-16 and again this assignment agreed with the previous discovery of a Walker A-type motif (β strand-loop-α helix) based upon sequence homologies. Molybdate ions from the crystallization solution were fortuitously bound to the residues of the loop region between Gly-9 and Lys-15, perhaps mimicking the γ-phosphate group of MgATP. Due to the prominent electron densities of the molybdate and Fe_4S_4 cluster, a distance of ~20-❹ was clearly measured between the two entities. Therefore, the two sites are unlikely to come into intimate contact with one another at any point during catalysis. Both regions, however, are located at the subunit interface and this fact may impact the mechanism for coupling electron transfer with

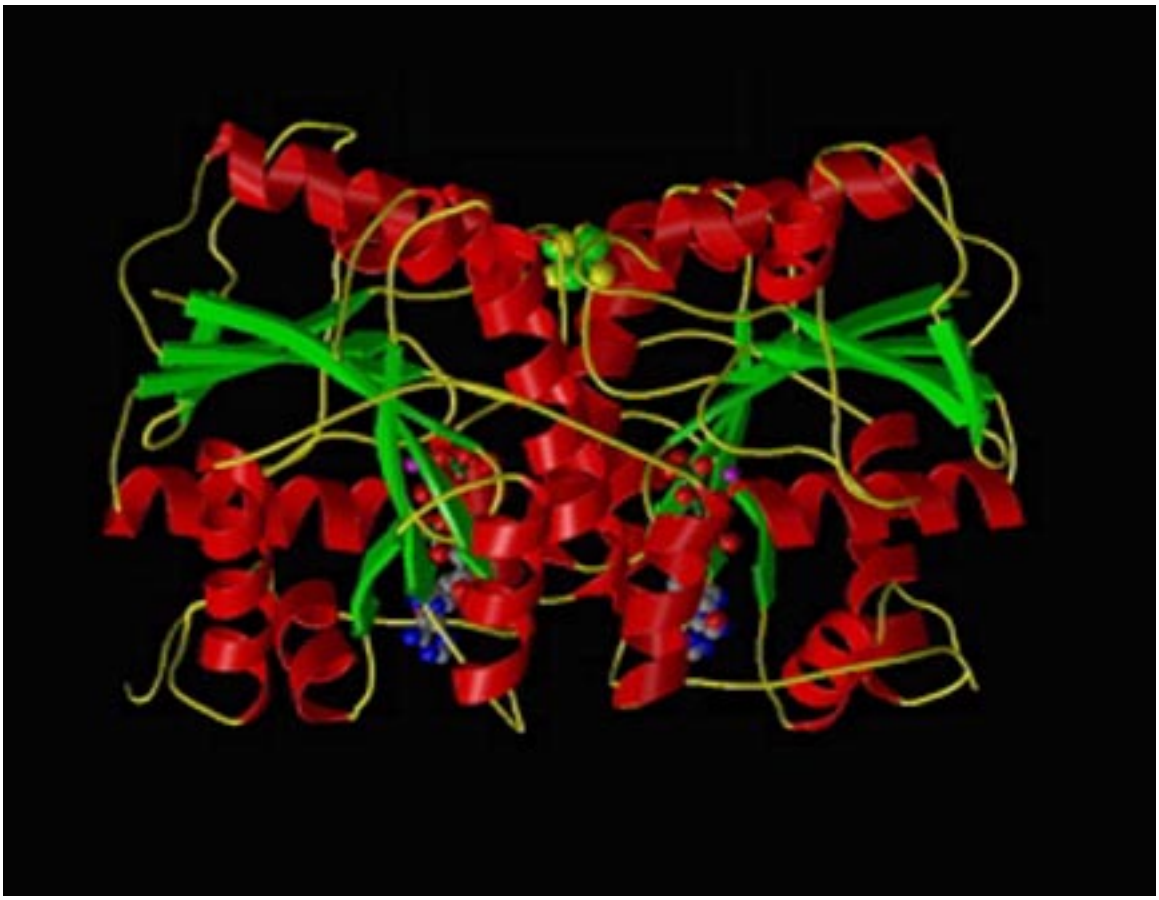

Figure 3: Ribbons Diagram of the Fe Protein

α-helices are shown in red, β-strands in green, random coils in yellow. The Fe_4S_4 cluster is represented as space-filling, green and yellow spheres at the bottom of the homodimer cleft.

ATP hydrolysis. The Walker B-type motif was also identified by the crystal structure as residues Asp-125 through Asp-129 and, in the absence of MgATP, the Asp-125 residue was hypothesized to form an inter-subunit salt bridge to the Lys-15 of the Walker A-type motif.

There are basically three major contributions of Fe protein to the overall mechanism of nitrogen fixation: 1. it is the signal transducing mechanism whereby ATP hydrolysis is coupled to efficient unidirectional transfer of electrons; 2. it is the obligate donor of electrons to MoFe protein; and 3. it is required for both the biosynthesis and insertion of the FeMo cofactor of the MoFe protein. There are several lines of evidence to support each of these deduced functions of the Fe protein component of the nitrogenase complex.

2. Electron Donation to the MoFe Protein

Spectroscopy has been instrumental in determining the pathway by which electrons flow from Fe protein to MoFe protein to substrate. Electron paramagnetic resonance (EPR) spectroscopy is able to detect single unpaired electrons and the influence of the immediate electronic environment on these paramagnetic systems. Early investigations by EPR spectroscopy demonstrated that, as the Fe protein from *C. pasteurianum* and *A. vinelandii* goes from an oxidized to a reduced form, the EPR signal goes from an EPR "silent", diamagnetic state to an S=1/2 state with a broadened "rhombic" signal in the g=2 region of the spectrum (Orme-Johnson *et al*., 1972). Addition of MgATP to the reduced Fe protein sharpens this signal into an "axial" spectrum. The MoFe protein in the presence of the chemical reductant, dithionite ($Na_2S_2O_4$), was found to have a distinct EPR signal with g-values at 4.3, 3.7, and 2.0 and the shape of this signal was unaffected by addition of MgATP or reduced Fe protein alone. When the Fe and MoFe proteins were combined with MgATP (in a regenerating system), and excess dithionite, the MoFe signal intensity declined by >90% as the MoFe protein assumes a more reduced state, while the Fe protein signal appears as a mixture of the reduced, MgATP-bound and free states. A similar experiment was performed, but with limiting dithionite and the inclusion of methylviologen in order to monitor dithionite

exhaustion. It was found that, as the reductant was exhausted over a 15 min. period through turnover of the enzymatic system, the intensity of the MoFe protein signal returned to it's original intensity while the Fe protein EPR signal disappeared completely. The conclusion of these experiments was that the Fe protein donates electrons to the MoFe protein and consequently loses its EPR signal as it is oxidized, and the MoFe protein initially loses it's EPR signal as it is reduced (excess dithionite condition), but then regains this signal as it donates those electrons to substrate (limiting dithionite condition). Similar experiments with the *K. pneumoniae* nitrogenase (Smith *et al*., 1972; 1973) resulted in the same conclusion, i.e., that reducing equivalents pass from dithionite to Kp2, and then in a MgATP-dependent reaction to Kp1 where electrons are finally passed on to substrate.

Although it is generally accepted that the Fe protein is a one-electron donor to the MoFe protein there have been alternative hypotheses for the mode of action of the Fe protein in the nitrogenase reaction. Most of the earlier controversies surrounded the unusual EPR signal of Fe protein. The S=1/2 spin EPR spectra integrated to much less than one electron per mole of protein. When the EPR spectra of reduced MgATP-bound and nucleotide-free forms of Kp2 were interpreted by computer simulations they indicated the presence of two interacting paramagnetic centers which could be close enough together to quench additional EPR signals (Lowe, 1978). This conclusion was supported by integrations on the EPR spectra of Av2 in the presence of 50% ethylene glycol and MgADP that yielded values of more than one electron per mole of protein (Braaksma *et al*., 1982). Much of the controversy of the EPR integrations was resolved by the simultaneous discovery of an S=3/2 spin species in the dithionite-reduced state of Fe protein (Lindahl et al., 1985; Watt & McDonald, 1985). The additional signal together with the S=1/2 signal integrated to approximately one spin per mole of Fe protein. Thus, there no longer remains much support for a second paramagnetic center in the Fe protein, however, the debate on the electron-donating capabilities of this redox-active protein continues. Recently, a fully-reduced form of the *A. vinelandii* Fe protein Fe_4S_4 cluster has been reported. Kinetic, microcoulometric, EPR and reactivity measurements of this

Fe protein suggest that an all ferrous $Fe_4S_4^0$ cluster-containing Fe protein can be prepared by chemical reduction with ultra-pure methylviologen and dithionite. In combination with MoFe protein, the $Fe_4S_4^0$ cluster-containing Fe protein was able to produce both H_2 and reduce C_2H_2 to C_2H_4 in nitrogenase turnover assays in the absence of added reductant. This result suggests that, under certain conditions, the Fe protein can act as a two-electron donor to the MoFe protein and this may be the relevant mechanism *in vivo*.

3. Nucleotide Switch Mechanism

The arrangement of the Fe protein's metallocluster and MgATP binding sites in the crystal structure verified the predictions of numerous spectroscopic, electrochemical, chemical, and site-directed mutagenesis experiments. Some of these experimental techniques have been invaluable in comparing and analyzing the effects of nucleotide additions and amino acid substitutions on the structure and function of the Fe protein. From some of the earliest experiments with the purified component proteins of the nitrogenase complex, it became evident that MgATP exerted its effect on the overall reaction in part by binding to the Fe protein (Bui & Mortenson, 1968). Using the electron paramagnetic resonance (EPR) spectroscopic signal of the Fe protein, the effect of nucleotide binding was definitively demonstrated (Zumft *et al*., 1973). The nucleotide-free state of the Fe protein exhibits a "rhombic" signal at the $g = 2$ region of the magnetic field. The spectrum has g-values typical of Fe_4S_4-cluster-containing proteins and arises from the S = 1/2 spin state of the metallocenter in its reduced state (3 Fe^{3+}, 1Fe^{2+} for an overall cluster charge of 1+). This signal becomes more "axial" in shape after binding of MgATP. This signal change was interpreted as deriving from significant alteration of the peptide environment surrounding the Fe_4S_4 cluster (Lowe, 1978).

In a similar way, the circular dichroism (CD) spectra in the visible region (300 nm - 600 nm) furnishes a sensitive method for detecting structural changes in the Fe_4S_4 cluster upon binding of MgATP or MgADP (Stephans *et al*., 1979). In a study using dye-oxidized Kp2 and Av2 researchers found that when both proteins were in the oxidized state the CD spectra of the Fe protein changed dramatically upon addition of MgATP. The CD spectra exhibited virtually identical changes upon MgADP addition. However,

neither of these nucleotides changed the CD spectra of reduced Kp2 or Av2 (Stephans *et al*., 1982). It was speculated that the binding of nucleotides in oxidized Fe proteins promote greater structural changes than those induced in reduced Fe proteins.

The effect of metal chelating agents on the Fe protein provided additional information on cluster conformation (Walker & Mortenson, 1974), and has been used repeatedly to test the effect of various compounds and amino acid substitutions on the Fe protein. The MgATP-bound form of the Fe protein is considerably more susceptible to chelation of its metallocenter by compounds like orthophenanthroline and α,α'-bipyridyl than the nucleotide-free form. This suggests that the Fe_4S_4 cluster is more solvent exposed in the MgATP- and MgADP-bound Fe protein which is in accordance with the previous interpretation of a conformational shift in the cluster peptide environment upon nucleotide binding. In a similar fashion, the addition of nucleotides increased the sensitivity of the Fe protein to O_2. The Fe proteins from all species to date are highly O_2-sensitive with half-lives ($t_{\bigstar}$) for activity of ~45 sec. in air. This increased sensitivity would also agree with the interpretation of increased exposure of the Fe_4S_4 cluster when nucleotides are bound.

Another useful criteria by which to compare and contrast changes or additions to the Fe protein structure is the measurement of the midpoint potential of the Fe_4S_4 cluster. The midpoint potential of the Fe_4S_4 cluster decreases ~120 mV (from -296 mV to -420 mV) upon MgATP or MgADP binding, rendering it a stronger reductant. This finding led to the belief that the sole function of MgATP in nitrogenase is to promote electron transfer from the Fe_4S_4 cluster to the MoFe protein.

a. Substitutions in the Walker A site - Experiments performed on forms of the *A. vinelandii* Fe protein whose Walker A-type site has been altered by site-directed has led researchers to propose roles for both Lys-15 (Seefeldt *et al*., 1992) and Ser-16 (Seefeldt & Mortenson, 1993) within this motif. When Lys-15 was substituted with glutamine, the resultant Fe protein, K15Q, was unable to support diazotrophy, acetylene-reduction, and ATP-hydrolyzing abilities yet retained wild-type metal content and a typical rhombic,

nucleotide-free EPR signal. (Note: substitutions in the Fe protein will be designated by the one-letter-amino-acid code for the wild-type residue, followed by the primary sequence position number, followed by the one-letter-amino-acid code for the substitution.) Addition of MgATP failed to elicit the axial signal nor did it increase the susceptibility of iron from the cluster to chelation by α, α'-bipyridyl. K15Q Fe protein had a 3-fold reduction in its affinity for MgATP relative to the wild-type proteins affinity, but affinity for MgADP was unchanged. Based on these results, it was suggested that Lys-15 interacts with the γ-phosphate by charge interaction, and that this interaction is essential for a conformational change required for nitrogenase activity. The K15Q Fe protein reacted with the cross-linking reagent 1-ethyl-3-(3-dimethylaminopropyl) carbodiimide (EDC) and the β-subunit of the MoFe protein in the same fashion as the wild-type Fe protein, leading the authors to conclude that this interaction between the component proteins of nitrogenase is not the catalytically relevant one, but that the MgATP-bound induced conformation of the Fe protein is necessary for enzymatic competence.

Mutant strains producing Fe proteins with Ser-16 substituted with Ala, Cys, Asp, or Gly, would not grow diazotrophically. However, a serine-to-threonine substitution yielded an Fe protein, S16T, with partial activity and, in direct contrast to the K15Q substituted Fe protein, an 11-fold higher affinity for MgATP (K_m of 20 μM for S16T vs. 220 μM for wild-type). Like the K15Q variant, the K_m of the S16T protein for MgADP was unchanged. The overall effects of the Ser-to-Thr replacement is a 5.3-fold increase in the catalytic efficiency (k_{cat}/K_m) over wild-type Fe protein, and greater nitrogenase activity over wild-type at of low MgATP concentrations. The S16T Fe protein also had drastically reduced activity in the presence of MnATP when compared to wild-type Fe protein. Taken together these data support a role for Ser16 in which its hydroxyl group interacts with the Mg^{2+} of bound MgATP.

b. Substitutions in the Walker B site - A novel model of how nucleotide binding may provide a gating mechanism for electron transfer in nitrogenase was developed from

analysis of the Fe protein of *A. vinelandii* in which aspartyl residue 125 was substituted by glutamate (D125E; Wolle *et al*., 1992). The mutant strain, DJ576, possessing this alteration was incapable of diazotrophic growth, substrate reduction, and ATP hydrolysis. However, the altered Fe protein retained the ability to induce the cluster-exposing conformational switch driven by MgATP binding and, additionally, MgADP, ATP, and ADP also induced this rearrangement. The model suggests that, in wild-type Fe protein, there are two distinct nucleotide-binding modes and each mode has a specific function. Initially, MgATP binds in an orientation parallel to the two-fold symmetry axis, which could sever an inter-subunit salt bridge between Lys-15 and either Asp-125 or Asp-39 or both. In this mode, the nucleotide would induce the amino acids responsible for hydrolysis to transmit the occurrence of a conformational change to the cluster. After hydrolysis and γ-phosphate release, the MgADP would shift into the second binding mode, which is perpendicular to the symmetry axis and has inter-subunit contacts. This second mode would be similar to the position of the MgADP in the 2.9-❹ crystal structure of the Fe protein from *A. vinelandii* (Georgiadis *et al*., 1992). According to the model, this orientation of MgADP prevents electrons from being "back donated" from the MoFe protein to the Fe protein, i.e., guarantees unidirectionality of electron flow.

Based on its position in the x-ray crystal structure and its inclusion in the Walker B-type motif, the aspartic acid at position 129 was targeted for replacement (Lanzilotta *et al*., 1995). One mutant strain produced an altered Fe protein with a glutamate in place of the aspartate (D129E). The D129E Fe protein was found to bind MgATP and MgADP, undergo the nucleotide-induced conformational changes, and dock with the MoFe protein in much the same way as wild-type Fe protein. The D129E version, however, could not hydrolyze MgATP, transfer electrons to the MoFe protein, or reduce substrates. These observations suggested the existence of subtle differences between the D129E and wild-type Fe proteins and a role for the Asp-129 as a base facilitating nucleophilic attack, via a water molecule, on the γ-phosphate of bound MgATP. The slightly higher affinity (1.6-fold) for binding MgATP and the more rapid rate of chelation of Fe^{2+} in the presence of

MgATP for D129E Fe protein demonstrate that the Glu substitution has tighter nucleotide binding and produces the conformational change that influences cluster exposure to the external environment. The EPR and CD spectra suggest that the longer side chain in glutamate relative to aspartate result in slight perturbations of the Fe_4S_4 cluster environment. In fact, the D129E nucleotide-free CD spectrum resembles the wild-type MgADP-bound spectrum. Thus, the D129E Fe protein behaves in nearly identical fashion to the wild-type protein up to the point of the events that occur in conjunction with or as a result of ATP hydrolysis.

Another important site-directed mutant in the Walker B-type motif is the *A. vinelandii* mutant strain which produces an Fe protein with a deletion for leucine at position 127 (L127Δ). This amino acid was targeted for deletion because of its location between the nucleotide-contact residue Asp-125 and the Fe_4S_4 cluster-ligating residue Cys-132. The resultant Fe protein has the unique ability to bind MoFe protein in the absence as well as in the presence of bound nucleotides and can still transfer an electron, albeit at an extremely reduced rate, but will not dissociate from the MoFe protein and, therefore, will not form products (Ryle & Seefeldt, 1996; Lanzilotta *et al*., 1996). In the initial report, the nucleotide-free L127Δ Fe protein was found to have ^{1}H nuclear magnetic resonance (^{1}H NMR), EPR, and CD spectroscopic signals that were very similar to the signals from MgATP-bound wild-type Fe protein (Ryle & Seefeldt, 1996). This altered Fe protein also had similar Fe chelation assay results and a nearly identical redox potential (-410 mV vs. -420 mV) as the MgATP-bound wild-type. In a subsequent publication (Lanzilotta *et al*., 1996), an L127Δ Fe protein-MoFe protein mixture was found to form an extremely tight complex in the absence of MgATP, and this complex revealed a stoichiometry of 1.7 L127Δ Fe protein holoenzyme bound per tetrameric MoFe protein. Stopped-flow spectrophotometry showed that electron transfer occurred between the L127Δ Fe protein and the MoFe protein in the absence of nucleotide at a rate 700-fold lower than between wild-type, MgATP-bound Fe protein and MoFe protein. An important conclusion of these findings is that ATP hydrolysis may not be a necessary

precursor of electron transfer itself, but rather may function in the dissociation of the Fe protein-MoFe protein complex after this event.

Recently there has been recognition of the Fe protein's structural and functional similarities to diverse systems that also utilize nucleotide-dependent switch mechanisms (Howard & Rees, 1994; Thorneley, 1992). Such systems include actomyosin, the GTP-hydrolyzing p21ras, the recA protein, and membrane-bound transporters. It has been suggested that the Fe protein structure is an ancestral form of a nucleotide-binding protein that has been recruited during the evolution of a variety of biological systems that use the energy transduction of ATP hydrolysis to drive different functions (Koonin, 1993).

4. FeMo-cofactor Biosynthesis and Insertion

The Fe protein's importance in the biosynthesis of the FeMo cofactor was demonstrated during complementation assays with specific mutant strains in *A. vinelandii* (Robinson *et al*., 1986). In these experiments a FeMoco- deficient strain UW45 (*nifB*$^-$) was mixed with either a *ΔnifD, ΔnifK, ΔnifDK,* or *ΔnifHDK* deletion strain. In all but the *ΔnifHDK* strain, some reconstitution of FeMoco activity was observed.

There are conflicting results on whether a catalytically active Fe protein is required for biosynthesis or not. Mutant strains from *K. pneumoniae* (Filler *et al*., 1986) and *A. vinelandii* (Robinson *et al*., 1987) with *nifH* deletions had lost catalytic activity, yet retained in vitro FeMoco biosynthetic activity. Similarly *nifM* mutants which produce a catalytically inactive Fe protein, are still able to produce fully active MoFe protein. However, site-directed mutants from *A. vinelandii* with Ser for Cys substitutions at the Fe_4S_4 cluster ligands were unable to support FeMoco biosynthesis (Howard *et al*., 1989). It seems that the Fe protein operates differently in FeMoco biosynthesis than it does in reduction of the MoFe protein.

Subsequent experiments dealing with the Fe protein's function in maturation of competent MoFe protein led to the proposal of a requirement for an Fe-protein-MgATP complex in FeMo-cofactor insertion into apo-MoFe protein (Robinson *et al*., 1989). This study utilized a *nifH* deletion strain, but other research on reconstitution of apo-MoFe

protein from an *A. vinelandii nifB* mutant only required the addition of purified FeMo-cofactor (Paustian *et al*., 1990). These contradictory results are difficult to assess because there may be inequality in the apo-MoFe proteins derived from a *nifH* as opposed to a *nifB* mutant strain.

D. The MoFe Protein

1. The Overall Structure

The x-ray crystal structure of the MoFe protein component of the nitrogenase complex from *A. vinelandii* was initially determined at 2.7-❹ resolution (Kim & Rees, 1992a,b) and then again at 2.2-❹ resolution (Chan *et al*., 1993) and finally at 2.0-❹ resolution (Peters *et al*., 1997). The overall composition is that of an $\alpha_2\beta_2$ heterotetramer with a M_r of ~230 kD (see Figure 4). The α-subunit (~57 kD) is encoded by the *nifD* gene, while the β-subunit (~59 kD) is encoded by the *nifK* gene. The total cluster content consists of 2 Mo (molybdenum), 30 Fe (iron), and 32 S^{2-} (sulfide) atoms per holoenzyme. The metal atoms are organized into two pairs of distinct and unique metal clusters, the FeMo- cofactors and the P clusters (also referred to as the 8Fe clusters). The FeMo-cofactors are located within each of the α-subunits (one cluster per subunit), while the P clusters are situated at the αβ-subunit interface. The overall tertiary structures of the two subunits are very similar. Both consist of three domains of the α-helical/β-sheet motif, and each subunit contains one wide, shallow cleft between the three motifs; in the α-

Figure 4: Ribbons Diagram of an αβ-subunit of the *A. vinelandii* MoFe Protein

The α-subunit is shown in purple and the β-subunit in blue. Both P cluster and FeMo-cofactor are represented as green (Fe), yellow (S), and magenta (Mo) space-filling spheres. The P cluster is seen at the center bottom of the model between the two subunits while the FeMo-cofactor is to the upper left of the P cluster.

subunit, the FeMoco sits at the bottom of this cleft. Tetrameric interactions are predominantly between the helices of the two β-subunits. In addition, ligands from both β-subunits provide a cation binding site, possibly for calcium, that aids in tetrameric stabilization. The tetramer interface is composed of an ~8-❹ diameter open channel ~35-❹ in length, formed by a barrel comprised of six α-helices, that also represents the tetrameric 2-fold axis of symmetry. For practical purposes, it is helpful to think of the MoFe heterotetramer as a dimer of structurally and functionally identical αβ units. Extensive interactions exist between the α and β subunits, and each dimer has a pseudosymmetrical 2-fold axis, separate from the tetrameric axis of symmetry, that passes through the P cluster pair. The P clusters are hemmed by two wide, shallow clefts that may provide the Fe-protein docking site.

2. The FeMo-cofactor

a. Structure - The x-ray diffraction data from the MoFe proteins of *A.vinelandii* (Kim & Rees, 1992a,b), *C. pasteurianum* (Kim *et al*., 1993) and *K. pneumoniae* (Lawson *et al*., 1997), all agree on the composition, structure, and location of the iron-molybdenum cofactor (FeMoco; see Figure 5). The FeMo-cofactor is buried ~10-❹ below the protein surface of the α-subunit. The consensus is that FeMoco is a $Mo_1Fe_7S_9$-homocitrate metallocluster that is essentially composed of two subclusters, $Mo_1Fe_3S_3$ and Fe_4S_3, that are bridged by 3 sulfides (S^{2-}) that link the opposing Fe atoms from each subcluster in a trigonal arrangement. The distance of separation between these bridged, trigonal Fe atoms is significantly longer than the distance between Fe atoms within the same cluster, 3.6-❹ versus 2.7-❹. This extra distance gives rise to a 4.5-❹ cavity in the center of the FeMoco structure. Another unique feature of the FeMo-cofactor is the coordinatively unsaturated, and potentially reactive, trigonal Fe atoms surrounding this cavity. This atomic arrangement is unprecedented in model compounds and has a possible role in substrate binding and activation.

(R)-homocitrate is an integral component of the FeMoco. It is coordinated to the Mo atom by its 2-hydroxyl and 2-carboxyl groups. The crystal structure confirms the

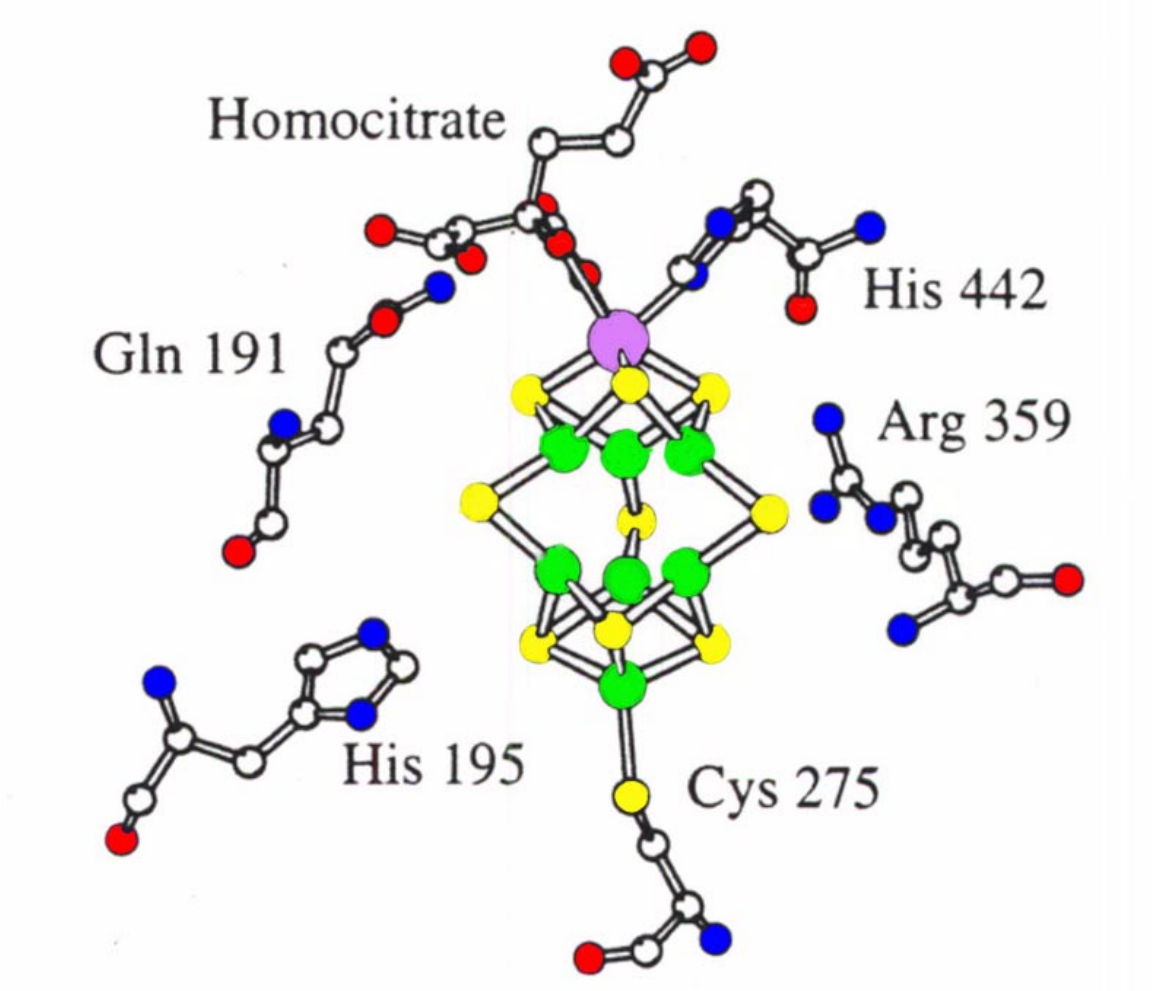

Figure 5: Ball and Stick model of the *A. vinelandii* FeMo-cofactor, homocitrate, ligands, and polypeptide environment

Fe atoms are shown in green, sulfur atoms in yellow, molybdenum atom in purple, nitrogen atoms in blue, and oxygen atoms in red. Adapted from Peters *et al*., 1995a.

predictions of site-directed mutagenesis experiments that the FeMoco is ligated to the α-subunit of the MoFe protein by just two residues, α-Cys275 and α-His442 (Brigle *et al.*, 1987a; Kent *et al*., 1989; Govezensky & Zamir, 1989). α-Cys275 is covalently bound to Fe1 (Kim-Rees model designation) at one end of the cluster, and α-His442 binds the Mo atom at the opposite end of the cluster. The Mo atom is hexacoordinate and therefore exhibits octahedral coordination geometry, which is consistent with earlier EXAFS data (Eidsness *et al*., 1986; Conradson *et al*., 1987).

As early as 1990, x-ray anomalous diffraction crystallography was able to distinguish the approximate distance of separation between the electron-dense metal centers of the MoFe protein from *C. pasteurianum* (Bolin *et al*., 1990). The two FeMocos are ~70-❹ apart from each other, while the center-to-center distance between FeMoco and the P cluster is ~19-❹. The higher resolution structures also agree with these distance approximations. The separation of the FeMo-cofactors precludes any bridged binding of substrates between the pair, while the proximity of the P cluster and FeMoco suggests the potential of interaction between them.

b. Spectroscopy of FeMoco - Fortunately for nitrogen fixation researchers, the iron-molybdenum cofactor possesses a biologically unique EPR signal, which arises from a 3/2 spin state (g=2.0, 3.7, and 4.3). This signal is a useful spectroscopic fingerprint that is detectable in the dithionite-reduced state of whole cells, crude extracts, purified MoFe proteins, and the isolated FeMoco. The S=3/2 signal has been employed in experiments demonstrating the role of FeMoco as the active site of nitrogenase as well as identifying amino acids in the FeMoco proximal environment that are critical for nitrogenase action. The previously mentioned EPR experiments of Orme-Johnson *et al.* in *A. vinelandii* and Smith *et al.* in *K. pneumoniae* (see Section I.C.2) demonstrated the sequence of electron transfer events in nitrogenase. The bleaching of the S=3/2 signal prior to evolution of product suggested that substrate was bound to this EPR-active center.

The EPR signal of the FeMoco has also been effectively exploited in electrochemical titration experiments on the MoFe protein from *A. vinelandii*. The

purpose of these experiments was to quantitate the midpoint potentials of the redox centers of the MoFe protein and to assign the S=3/2 EPR signal to a particular redox center. These redox centers were previously identified by Mössbauer and EPR spectroscopic analyses of thionine-oxidized MoFe protein, and the two metal centers were labeled "M" for the EPR-active FeMoco, and "P cluster" for the metal center which was diamagnetic in the native, reduced state of the MoFe protein (Zimmerman *et al*., 1978). Electrochemical titrations of oxidized MoFe protein established two redox regions, one at -290 mV and one at -480mV (Watt *et al*., 1980). Each redox center required three electrons for complete reaction. Selective reduction of the -290 mV redox region caused the development of the S=3/2 EPR signal of the FeMo-cofactor, while reduction at the -480 mV region produced no visible change in the EPR signal intensity. Subsequent experiments included monitoring of the UV-visible spectrum of the MoFe protein as it underwent step-wise reduction by methyl viologen or oxidation by methylene blue, thionine, or indigosulfonate (Watt *et al*., 1981). The major conclusion of this work was that the P clusters are selectively oxidized first followed by the FeMo-cofactors. Conversely, the sequential reduction of oxidized MoFe protein occurs first at the FeMoco redox center followed by the P cluster. Thus, the sequence of electron transfer within the MoFe protein appears to flow from the more negative redox centers, the -480 mV P clusters, to the more positive redox centers, the -290 mV FeMo-cofactors.

c. FeMoco *in vitro* biosynthesis - The ability to isolate FeMoco has been instrumental in the investigations into the biosynthetic pathway of this complex metallocenter. Evidence for the molecular identity of the nitrogenase active site came with the discovery of a method for extraction and isolation of the iron-molybdenum cofactor from *A. vinelandii* (Shah & Brill, 1977). The procedure consisted of acid-denaturation of purified MoFe protein, base titration to the isoelectric point (pI), and extraction of the exposed FeMoco by N-methylformamide (NMF). It was subsequently discovered that not only could this extracted cofactor impart full activity to certain FeMoco-deficient mutants of *A. vinelandii* and *K. pneumoniae*, but it was also responsible for the trademark EPR signal of the MoFe protein. The purification of

FeMoco led to predictions of its imminent structural elucidation that, due to the organic solvent extractant, were never realized. As previously mentioned (see Section I.B.2), it is now known that at least six *nif* genes are required for FeMoco synthesis, *nifB, E, N, V, Q,* and *H*. *In vitro* addition of isolated FeMoco to mutant strains with deletions for some of these genes (*Δnif B, E, N,* or *H*) resulted in full reconstitution of enzymatic activity (Ugalde *et al*. 1984; Robinson *et al*., 1989). An earlier version of a completely *in vitro* FeMoco synthesis system required a minimum of molybdate, ATP, homocitrate, the Fe protein, and the *nifBEN* gene products (Shah et al., 1986). Further utilization of the *in vitro* FeMoco synthesis system in *A. vinelandii* has found that an additional subunit, γ, is involved in the reconstitution of apo-MoFe protein (FeMoco deficient). Attachment of this subunit to the apo-MoFe protein yields an $\alpha_2\beta_2\gamma_2$-subunit composition, that is proposed to be the FeMoco-activatable form of MoFe protein (Allen *et al*., 1993). The attachment of γ is thought to require both MgATP and Fe protein. The *in vitro* system has recently been employed in characterizing the product of the *nifB* gene (Shah *et al*., 1994). NifB apparently synthesizes a low molecular weight metal cluster referred to as NifB-co, which is possibly an Fe-S cluster precursor of the FeMo-cofactor of mature MoFe protein. Accumulation of data from the *in vitro* synthesis of FeMoco, such as that presented here, will hopefully lead to the complete understanding of the sequence the individual steps involved in the construction of this intricate metallocluster.

d. Substitutions in the FeMoco peptide environment - Another benefit of the FeMoco purification procedure was the implication of an amine-rich environment for the FeMoco in the MoFe protein. It was reasoned that perhaps NMF mimics the peptide surroundings of FeMo-cofactor in the MoFe protein. This hypothesis, in part, led to the selection for mutagenesis of certain amino acid residues with amine containing side groups. An alternative basis for mutagenesis selection utilized the amino acid sequence homology comparisons between the *nifD* gene product and the product of the *nifE* genes, the proposed FeMoco-scaffold protein. This strategy yielded two important *A. vinelandii* mutant strains, DJ178 which produced a MoFe protein with an asparagine substituted for

a histidine at position α-195 (α-195HN), and DJ255 which has a lysine substituted for α-191 glutamine to give an (α-191QK) altered MoFe protein (Scott *et al*., 1990). (Note: From this point forward altered MoFe proteins will be designated by the greek letter defining their location in either the α- or β-subunit, followed by the residue number of the substituted site, followed by the one letter amino acid code for the wild-type residue at this position, and then the one letter amino acid code for the substituting residue.) In dramatic contrast to wild-type *A. vinelandii*, both strains had a Nif $^-$ phenotype (i.e. could not grow diazotrophically), whereas crude extracts of these strains produced EPR spectra altered in lineshape and *g* value, and were able to reduce C_2H_2 to C_2H_6. This last distinction of ethane formation is significant for two reasons. First, it indicated that a single amino acid substitution changed both the EPR spectrum and the substrate-reduction properties, a strong indicator that both the EPR spectrum and substrate-reduction arise from the same entity. Second, C_2H_6 from C_2H_2 is a feature of the vanadium-dependent nitrogenase system and is used a test for the presence of this alternative nitrogen fixing system *in vivo* (Dilworth *et al*., 1987).

The altered MoFe proteins were purified from both of these mutant strains and further characterized. The α-191QK MoFe protein was also distinguished by increased sensitivity to CO inhibition of proton reduction (Scott *et al*., 1992). In wild-type MoFe protein a 10% CO atmosphere will divert all electrons to H_2 evolution under an 100% Argon, 10% C_2H_2/90% Ar, or 100% N_2 atmosphere without any loss of total electron flux. However, the α-191QK MoFe protein exhibited a significant reduction in H_2 evolution under all three atmospheres in the presence of various concentrations of CO and thus a reduction in total electron flux. The CO-sensitive proton reduction pattern is also a trait of the *nifV* $^-$ mutant strain from *K. pneumoniae* (McLean & Dixon, 1981), which was later found to possess a compromised FeMoco (Hawkes *et al*., 1984) that had citrate in place of homocitrate (Liang *et al*., 1990). To rule out this explanation for CO-sensitive proton reduction in the α-191QK MoFe protein, the FeMoco from this protein, as well as the FeMoco from wild-type MoFe protein, were extracted and used in

heterologous reconstitution experiments with either α-191QK or wild-type FeMoco-deficient MoFe proteins. The end result was that regardless of the FeMoco source, both the distinctive EPR spectra and ethane production patterns were determined by the peptide environment of the apo-MoFe proteins and not the source FeMo-cofactors. The similarities between the α-191QK and NifV$^-$ altered forms of the MoFe protein led to the suggestion that α-Gln191 interacted with homocitrate (Scott *et al*., 1992) and was confirmed by the structural model which positions the α-Gln191 residue in a hydrogen-bonding arrangement with a terminal carboxylate of homocitrate.

Ensuing inquiry into the role of the α-195His residue revealed an additional mutant strain, DJ528, from *A. vinelandii* that synthesizes an altered form of the MoFe protein with a glutamine substitution at this position (α-195HQ). This strain is Nif $^-$, yet is capable of near wild-type C_2H_4 and H_2 evolution levels (Kim *et al*. 1995). It was found that N_2 acts as a potent inhibitor of both of these nitrogenase activities, possibly by binding to a common active site. It was found that the inhibition constant (K_i) for CO inhibition of C_2H_2 reduction for α-195HQ MoFe protein was 8-fold more sensitive than wild-type MoFe protein, i.e. CO binds with a much higher affinity to the α-195HQ protein relative to the wild-type protein. It was reasoned that the glutamine substitution might make an Fe atom in the cofactor structure more accessible to attack by CO. The crystal structure is in accordance with the suggestion that the glutamine might be able to simulate the ε-nitrogen of the imidazole ring of α-His195 which is close enough (3.14-❹) to a bridging sulfide to form a NH-S hydrogen bond. N_2 also uncouples MgATP hydrolysis from proton reduction in the α-195HQ MoFe protein without altering the rate of MgATP hydrolysis, which supports the long-held contention that bound substrate acts as an effective electron sink during the nitrogenase catalytic mechanism.

Another interesting amino acid substitution in the FeMoco environment is the histidine exchange for arginine at position α-277 (α-277RH; Shen *et al*., 1997). This residue was targeted for substitution due to its proximity to the FeMoco ligand α-275Cys

and its potential role in the pathway for the entry/exit of substrates/products. This same channel might also serve in FeMoco insertion (Kim & Rees, 1992b). This later proposition was based on the x-ray crystal structure analysis that noted a potential channel in the FeMoco vicinity formed by residues α-Arg277, α-Ser192, and α-Gly356. A prominent feature of the α-277RH MoFe protein is its EPR signal which exhibits two sets of signals; the major pair at *g*=4.25 and 3.63 are close to the wild-type values and account for 80% of the overall intensity, and a minor pair at *g*=4.52 and 3.48 account for the remaining 20% of the signal intensity. The EPR signal perturbation may result either from two different orientations of the FeMoco or perhaps from different turnover intermediate states of the FeMoco. However, none of the catalytic differences in the altered MoFe protein could be assigned to the unique EPR signal. Another noteworthy difference between wild-type and α-277RH MoFe proteins was the substituted protein's inability to bind or reduce N_2, even though this variant MoFe protein reduced protons (H^+) and C_2H_2 at ~50% of the wild-type rate. This observation was interpreted to mean that the α-277RH MoFe protein could not attain the more reduced redox states necessary to bind and reduce N_2. A completely unexpected finding from analysis of the α-277RH MoFe protein involved the pattern of CO inhibition of C_2H_2 reduction. Instead of the typical hyperbolic response of increasing specific activity with increasing concentrations of C_2H_2 in the presence of CO, the altered MoFe protein responded in a sigmoidal pattern which indicates cooperativity. Thus CO induces cooperativity between at least two C_2H_4 evolving sites on the FeMoco of the α-277RH MoFe protein.

All three of the aforementioned amino acids of the FeMoco domain are hydrophilic in nature which may impact substrate/product entry/exit pathways. In addition to these three residues, positively charged amino acids (including α-Arg96 and α-Arg359) are packed around the central bridging region of the FeMoco. This structural feature may be necessary for the electrostatic coordination of the negatively charged FeMoco. Also the net positive charge may stabilize any negatively charged intermediates generated during nitrogenase turnover. Whatever the true purpose of the FeMoco

proximal peptides, site-directed mutagenesis in this region demonstrates the fine tuning of substrate binding, reduction, and inhibition patterns by these important residues. The corresponding perturbation of the electronic and magnetic properties of the FeMoco (alteration of the S=3/2 EPR signal) by replacement of these residues, is further support for the FeMo-cofactor's assignment as the active site of the nitrogenase complex.

3. The P Cluster

Although there is near universal agreement on the structure and function of the FeMo-cofactor, the same cannot be said for the other unique metallocluster of the MoFe protein, the P cluster. The current supposition is that the P clusters are involved in the acceptance and storage of electrons from the Fe protein, and their subsequent delivery to bound substrate at the FeMoco reduction site. Although the evidence to support this hypothesis is circumstantial, recent experiments utilizing spectroscopic and kinetic techniques on both wild-type and site-substituted forms of the MoFe protein have advanced the popularity of this proposal.

a. Structure - The resolution of the x-ray crystal structure of the MoFe proteins of *C. pasteurianum* and *A. vinelandii* in the early 1990's clarified many of the structural questions surrounding the P clusters. Initially, the low resolution 7.0-❹ image of the *C. pasteurianum* MoFe protein identified two P clusters per tetramer with each cluster arising from the pairing of two Fe_4S_4 clusters (Bolin *et al*., 1990). It also approximated the distances between P cluster and FeMoco at ~19-❹ and the separation of the P clusters on each αβ-dimeric half of the holoenzyme at ~70-❹. This view was substantially improved upon with the 2.8-❹ resolution x-ray crystal structure of the MoFe protein and its accompanying metalloclusters from *A. vinelandii* (Kim & Rees, 1992a). Many of the structural predictions based on the site-directed mutagenesis and spectroscopic data were verified by the crystal model. The P cluster was first described as an Fe_8S_8 cluster that is ligated at the αβ subunit interface by six cysteinyl (three from each subunit) and one serinyl residue (see Figure 6). More specifically, the P cluster was modeled at that time

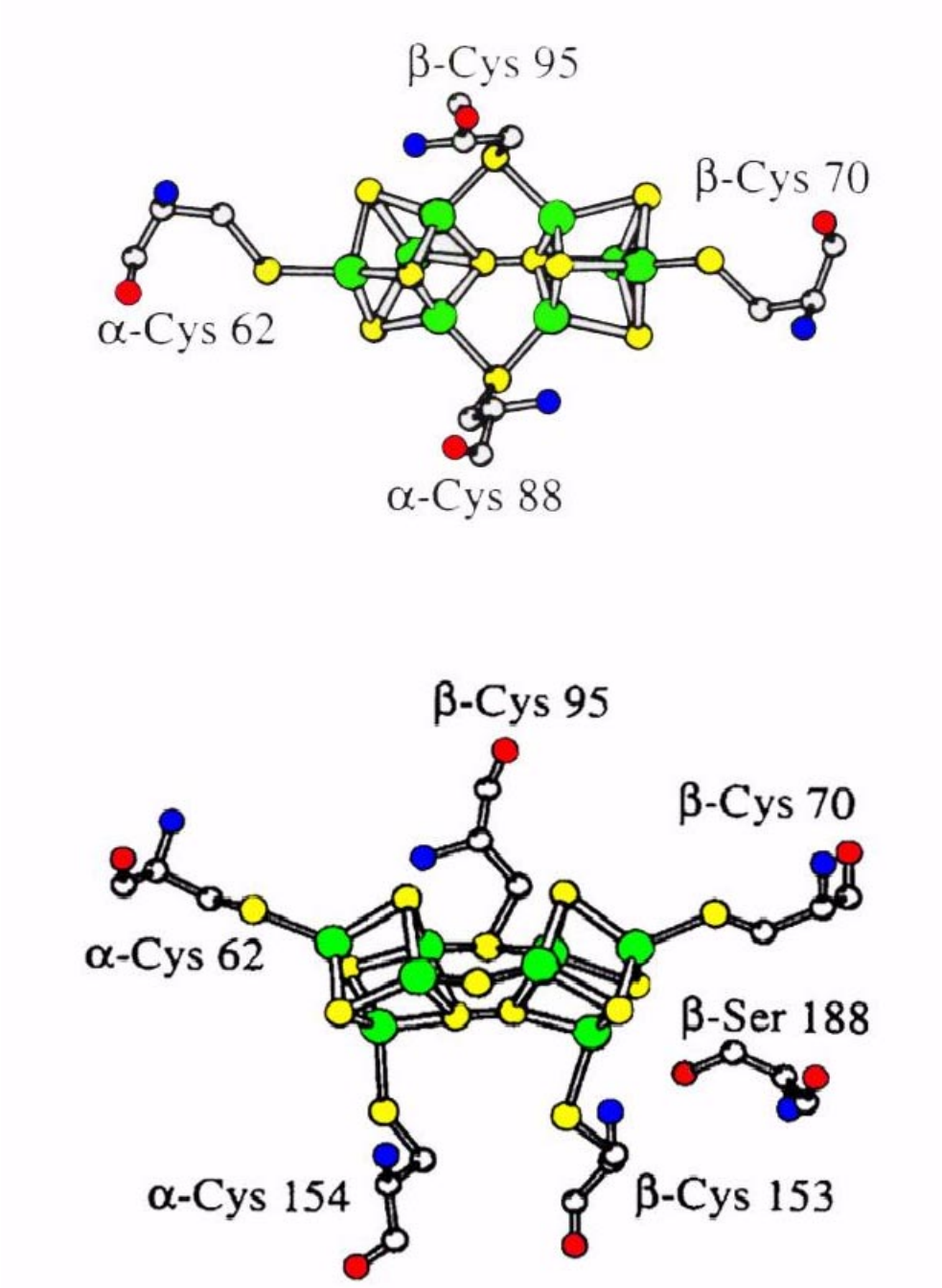

Figure 6: Ball and Stick Model of the *A. vinelandii* P cluster and Surrounding Ligands These two orientations of the P cluster are related by a 90° rotation about the x-axis. Fe atoms are shown in green, sulfur atoms in yellow, nitrogen atoms in blue, and oxygen atoms in red. Adapted from Peters *et al.*, 1995a.

as a pair of Fe_4S_4 cubanes connected together through two bridging cysteinyl ligands, α-Cys88 and β-Cys95, and a disulfide bond (~2.1-❹; Chan *et al.*, 1993) between sulfurs at adjacent corners of the two cubanes. The other ligands include α-Cys62, α-Cys154, β-Cys70, β-Cys153, and β-Ser188. The β-Cys153 and β-Ser188 are both coordinated to the same Fe atom (designated Fe6 in the model), while the three remaining cysteines form covalent bonds with peripheral Fe atoms. The P cluster is about 10-❹ below the protein surface and the pseudosymmetrical 2-fold axis that relates the α and β subunits passes through the cluster. The closest distance between metal sites on the P cluster and FeMoco is ~14-❹ occurring between Fe3 of the P cluster (ligated by α-Cys62) and Fe6 of FeMoco. P clusters on separate αβ subunit pairs are ~67-❹ apart from center to center. In contrast to the hydrophilic environment of the FeMo-cofactor, the P cluster is surrounded by mainly hydrophobic residues and these are conserved in the MoFe protein primary sequence of other nitrogen-fixers.

b. Spectroscopic signals of the P cluster - The appellation of "P cluster" derived from the identification of Fe-S clusters that were distinguishable from the FeMoco during early Mössbauer and EPR investigations on reversibly oxidized MoFe protein from *A. vinelandii* (Zimmerman *et al.*, 1978). Core extrusion of Fe-S centers from the MoFe proteins of *C. pasteurianum* and *A. vinelandii* using o-xylyl-α-α'-dithiol with subsequent ligand exchange with p-CF_3-C_6H_4-SH resulted in the identification of approximately four Fe_4S_4 clusters that accounted for nearly 100% of the non-FeMoco iron (Kurtz *et al.*, 1979). Taken together, these experiments mistakenly identified the P clusters as Fe_4S_4 clusters, and this view remained the case for nearly a decade.

A new concept of P cluster structural stoichiometry resulted from a quantitative EPR analysis of a unique S=7/2 system derived from thionine-oxidized MoFe protein from *A. vinelandii, K. pneumoniae,* and *Azotobacter chroococcum* (Hagen *et al.*, 1987). The new interpretation proposed an 8 Fe atom-containing P cluster with a 1:1 ratio of P cluster to FeMoco in the MoFe protein of nitrogenase. This new view of the P cluster metal content sparked a controversy (McLean *et al.*, 1987, Lindahl *et al.*, 1988) that

continued for nearly five years until the resolution of the crystal structure by x-ray diffraction.

Successive research in the early 1990's also utilized EPR and Mössbauer spectroscopies to characterize distinct oxidation states of the P clusters mainly from the *A. vinelandii* MoFe protein (Surerus *et al*., 1992, Pierik *et al*., 1993; Tittsworth & Hales, 1993). The combined analyses provide a sequence of redox levels of the P cluster with each level correlating to a unique EPR spin state, and in some cases with a midpoint potential value (Pierik *et al*., 1993). The MoFe protein is again considered as two functionally equivalent $\alpha\beta$ subunits each with it's own P cluster. The sequence advances from the fully reduced state, P^N or P state, to the one-electron-oxidized P^+ state, followed by the two-electron-oxidized P^{OX1} or P^{2+} state, and then the three-electron-oxidized P^{OX2} or P^{3+} state (see Table 2). There is also an additional oxidation from P^{OX2} to $P^{SUPEROX}$ that results in irreversible damage to the P cluster. An interesting model of P cluster oxidation assumes that the paramagnetism is not delocalized over the entire 8Fe structure but instead occurs on each Fe_4S_4 half of the double cubane structure. As each half is oxidized a unique spin state is established and if both halves become oxidized spin coupling between them could generate an integer-spin signal. This model of P cluster oxidation might also explain the equal probability of $P \rightarrow P^+$ and $P^+ \rightarrow P^{2+}$ transitions that is found in oxidation of the P clusters using limiting thionine (Tittsworth & Hales, 1993).

c. Substitutions to the P cluster ligands and proximal residues - While the debate raged on, molecular biologists applied their techniques to determining the amino acid positions for protein ligation to the metal centers of the MoFe protein from *A. vinelandii* (Brigle *et al*. 1987) and *K. pneumoniae* (Kent *et al*., 1989, Kent *et al*., 1990). Utilizing both interspecies MoFe protein and α-β subunit sequence homologies, an alignment map of the conserved cysteinyl and histidyl residues was constructed (Dean *et al*., 1990). The conserved cysteines were then grouped into five primary sequence "domains" in the α-subunit (I-V), and three domains in the β-subunit (I-III). The first three domains of the α-

subunit aligned with the three β-subunit domains including a His-Gly-X-X-Gly-Cys in Domain II. It was suggested that the spatial arrangement of the conserved cysteines and histidines met the requirements for the four separate, yet structurally similar domains thought necessary to bind the P clusters (still thought of as four Fe_4S_4 clusters). In the initial set of experiments, the conserved residues of Domains I, II, and III of the MoFe protein α-subunit certain were targeted for site-directed mutagenesis, these included α-Cys62, α-His83, α-Cys88, and α-Cys154. The data included measurements of the diazotrophic growth rates, C_2H_2-reduction rates, and whole-cell S=3/2 EPR spectra of a variety of *A.vinelandii* mutant strains with amino acid replacements in these potential P cluster ligands. The results indicated that α-Cys62 and α-Cys154 were probably essential to MoFe protein activity but that α-His83 and α-Cys88 were not. A subsequent analysis targeted the conserved cysteines in Domains I-III of the MoFe protein β-subunit; β-Cys70, β-Cys95, and β-Cys153 (May *et al*., 1991). Using the same criteria as in the previous experiments, it was concluded that β-Cys70 and β-Cys95 were essential while β-Cys153 was not. Two of the β-Cys153 mutant strains, DJ122 (Cys-to-Ser substitution) and DJ219 (Cys deleted), both retained about 50% of the wild-type diazotrophic growth rates and crude extract C_2H_2-reduction activity, and 100% of the S=3/2 EPR signal intensity. The MoFe protein from DJ122 was purified and further tested for numerous substrate-reduction patterns for comparison to wild-type MoFe protein. This altered protein was indistinguishable from wild-type with the notable exception of response to an electron flux titration. In such an experiment, the availability of electrons is controlled by the molar ratio of the Fe protein to MoFe protein because, as the concentration of reduced Fe protein increases, the MoFe protein specific activity increases to its maximal velocity (V_{max}) for product formation. The β-153CS altered and wild-type MoFe proteins exhibit the same specific activities up to a 1:1 Fe protein to MoFe protein molar ratio but beyond

Table 2: Multiple Redox Levels of the P cluster

Name*	**Alternate Name****	**Redox Potential†**	**Spin State**	**Comments**
P^{N}	P	-307 mV	0	As isolated, dithionite-reduced state
$P^{semi\text{-}ox}$	P^{+}	-307 mV	1/2, 5/2	Transient state in oxidative titrations
P^{Ox1}	P^{2+}	+90 mV	3, 4	Excited state, parallel mode EPR at g=12
P^{Ox2}	P^{3+}	+345 mV	1/2, 7/2	Mixed spin state of unknown origin
$P^{superox}$	-	-	>2	Irreversible damage

* Adapted from Pierik *et al*., 1993

** Adapted from Tittsworth & Hales, 1993

† Midpoint potential for transition to next oxidation level, $P^{n} \rightarrow P^{n+1}$

that the β-153CS altered protein's activity slows dramatically relative to wild-type such that the V_{max} of the altered MoFe protein is half of that of wild-type MoFe protein. The intriguing interpretation of this finding is that the intramolecular delivery of electrons within the MoFe protein of strain DJ122 has been slowed by the β-153CS substitution. Therefore, if this is correct, then β-Cys153 is probably a P cluster ligand and that P clusters function in intramolecular delivery of electrons to the FeMo-cofactor.

The parallel research being performed in *K. pneumoniae* (Kent *et al*. 1990) discovered similar results for the equivalent conserved cysteines in *A. vinelandii* with the exception of a double mutant strain, pHK17, that has an α-89CA/β-94CA substitution in the MoFe protein (*Kp* numbering). Each of the single mutations resulted in strictly Nif- phenotypes, however, when the substitutions are combined in one strain, the product is a nitrogenase with impaired activity. The inference is that the double substitution results in compensating structural rearrangements that allow the MoFe protein some decreased function in substrate reduction. Subsequent purification of the MoFe protein from the pHK17 mutant strain yielded a heterogeneous mixture of MoFe proteins with differing specific activities (Yousafzai *et al*., 1996). The specific activities of the MoFe proteins was found to be directly proportional to the EPR intensity of the S=3/2 signal. This led to the conclusion that the substitutions at the P cluster bridging cysteines leads to potential loss of EPR-active FeMoco, and that the Cys-to-Ala substitution does not affect the rate-limiting step in enzyme turnover.

With the advent of the crystal structure, a new criterion for selection of amino acid residue replacement had been created. Quick advantage was taken of this situation with the site-directed substitution of β-Tyr98 in the MoFe protein from *A. vinelandii* (Peters *et al*., 1995b). This conserved residue is situated in a potential electron transfer pathway between the P cluster and the FeMo-cofactor, thus its substitution might affect intramolecular electron transfer and overall substrate reduction activities. A histidine for tyrosine substitution (β-98YH) yielded an altered MoFe protein that had wild-type MoFe protein metallocluster structure and electronic properties as determined by EPR and

magnetic circular dichroism spectroscopy (MCD). The β-98YH MoFe protein, however, had lowered diazotrophic growth rates and decreased substrate-reduction rates, particularly under a 10% C_2H_2/90% Ar atmosphere, where the total electron flux, as measured by electron pairs diverted to product(s), was ~30% of the wild-type flux. Under a 100% Ar or N_2 atmosphere, the β-98YH MoFe protein has ~50% of the wild-type reduction rates. Addition of 10% CO to the C_2H_2-reduction assays for the β-98YH MoFe protein increases the electron flux from 30% to 54% of the wild-type rates, and ATP hydrolysis is more coupled to substrate reduction in the presence of CO (+CO = 6.5 ATP/$2e^-$ vs. -CO = 11.3 ATP/$2e^-$). The most significant catalytic difference attributable to the histidine substitution is the rate of component protein dissociation as measured by stopped-flow spectrophotometry. Initially the β-98YH MoFe protein displays a wild-type dissociation rate of 6.0 sec^{-1} for the first 300 msec, then the rate drops more than 2-fold to 2.5 sec^{-1}. Based on the reaction conditions and the time necessary for the slowing of dissociation rate, it was calculated that 2.4 electrons had been delivered to the MoFe protein before the turnover rate decreased. The authors interpreted these results to mean that the P clusters normally accumulate two electrons from the Fe protein and then shuttle these on to FeMoco where substrates are reduced. In the β-98YH MoFe protein, the intramolecular electron transfer pathway between P cluster and FeMoco has been disrupted and a lower electron transfer rate is the consequence. After one or two rounds of intermolecular electron transfer the P clusters become saturated and this slows the component protein dissociation rate.

d. Electron donation to the P cluster - As demonstrated in the previous example, stopped-flow spectrophotometry has proven useful in ascertaining P cluster function. Investigators followed the pre-steady-state absorbance changes that occur in the wild-type MoFe protein from *K. pneumoniae* during the first 500 msec of nitrogenase turnover (Lowe *et al.*, 1993). An additional absorbance increase was observed at the 430 nm wavelength typically used in these experiments when nitrogenase was turning over in the presence of 100% Ar or N_2, compared to 100% C_2H_2. Using kinetic simulation

programs, it was determined that the time required for the appearance of this extra absorbance change coincides with that for the attainment of the E_4 redox state of the MoFe protein (see Section I.F.2.b). E_4 is the stage at which the Thorneley-Lowe model predicts that MoFe protein is irreversibly committed to N_2 reduction. Therefore, because this absorbance change is detected only under gas atmospheres where the MoFe protein reaches the E_4 redox state, i.e. Ar and N_2, and cannot be attributed to intermolecular electron transfer, then its must be due to intramolecular electron transfer and the most likely explanation is oxidation of the P cluster as it transfers its electrons to the FeMo-cofactor.

Tandem EPR experiments were also run in which a nitrogenase turnover system was mixed in the presence of either 100% C_2H_2, N_2, CO, or Ar, and frozen in EPR tubes within 5 sec. The resulting spectra revealed a broad feature between *g*=6 and *g*=4 and, in the N_2 and Ar samples, sharp signals at *g*=5.4 and 5.7. These EPR signals are similar to the signals seen in thionine-oxidized MoFe protein that are hypothesized to arise from a S=7/2 spin state of oxidized P clusters.

As further proof of the P clusters role as electron transfer mediators, an artificially oxidized state of the MoFe protein from *A. vinelandii* was used in order to follow the distinct EPR signals of the P clusters in a one-electron turnover experiment (Lanzilotta & Seefeldt, 1996). The MoFe protein was oxidized by 2 equivalents of electrons, using indigo sulfonate (IDS), to the P^{2+} state where the FeMoco and P cluster are both paramagnetic and the reduction of these metal centers can be followed by loss of signal intensity. The FeMoco signal arises from a spin 3/2 system (S=3/2) and, because it is half-integer spin, it could be measured using the typical perpendicular mode EPR, whereas the P^{2+} clusters with S=3 are in an integer spin state and, therefore, their EPR signals can only be measured using parallel mode EPR. As sources of reductants, two forms of the Fe protein were used. The first was wild-type Fe protein, in the presence and absence of MgATP, and the second was an altered form of the Fe protein, L127Δ, that mimics the MgATP-bound conformation in the absence of nucleotide (see Section

I.C.3.b). The MgATP-bound wild-type Fe protein as well as the MgATP-free L127Δ altered Fe protein was able to perform a one-electron transfer to the MoFe protein. Unlike the wild-type Fe protein, the L127Δ altered Fe protein forms an irreversible, tight complex with the MoFe protein, and therefore only a single electron is transferred before cessation of enzymatic activity due to the inability of complex dissociation. Intermolecular electron transfer from the L127Δ Fe protein was confirmed by loss of both the S=1/2 EPR signal of the altered Fe protein upon oxidation and the S=3 EPR signal of the P^{2+} cluster of the acceptor MoFe protein as it is reduced from the P^{2+}-state to the P^{1+}-state with no observable change in the S=3/2 FeMoco EPR signal. Using wild-type Fe protein in the presence of MgATP caused a loss both S=1/2 and S=3 EPR signals, plus a notable decrease in the S=3/2 signal intensity as some of the FeMoco was reduced beyond the dithionite-reduced state. If the same reactants were mixed in the absence of MgATP or in the presence of MgADP, there was no signal intensity loss in any of the three EPR peaks. This result confirmed that the reduction of the P^{2+}-oxidation state of the MoFe protein is dependent on a MgATP-bound conformation of the Fe protein and is not due to nonspecific electron transfer. The two major conclusions from these data are first, that the P cluster is an immediate electron acceptor from the Fe protein and second, that only the MgATP-bound conformation of the Fe protein, and not MgATP hydrolysis, is all that is required for primary electron transfer to the P cluster.

An analogous experiment utilizing an incomplete form of the MoFe protein from *A. vinelandii* also demonstrated electron transfer from the Fe protein to the P cluster (Ma *et al*., 1996). The source material in this experiment was an apo-MoFe protein purified from strain DJ54, that results from a deletion in the *nifH* gene. The apo-MoFe protein is reconstituted with an altered form of the FeMo-cofactor, referred to as the MoFe cluster, which contains the Mo-Fe-S portion of FeMoco but appears to lack the homocitrate moiety (Ma *et al*., 1994). The end product of this reconstitution is a MoFe protein that can induce MgATP hydrolysis in the Fe protein and must, therefore, form a complex with it, but this altered MoFe protein does not reduce substrate. It does, however, accept an

electron from the Fe protein and this leads to the appearance of a sharp EPR signal at g=1.94 which is assigned as arising from the P cluster and integrates to one spin per P cluster. What is not known is whether this state is more oxidized or more reduced than the P^N native state of the P cluster in dithionite-reduced wild-type MoFe protein.

e. Revised structure of the P cluster - Recently, the x-ray crystal structure of the MoFe protein from *A. vinelandii* has been refined to 2.0-❹ resolution in two different oxidation states that were confirmed by EPR spectroscopy (Peters *et al*., 1997). A major difference is observed in these latest structures when compared to earlier versions of the MoFe protein x-ray crystal structure, and that difference is in the P cluster structure and ligation. The P cluster in both oxidation states is comprised of eight Fe and seven S atoms (see Figure 7). In the oxidized state, designated P^{OX}/M^{OX}, the eight Fe atoms are coordinated by the usual six conserved cysteine residues, β-Ser188, and additionally by the backbone amide N of α-Cys88. In the reduced state, designated P^N/M^N, the Oγ of β-Ser188 and backbone amide N of α-Cys88 bonds are no longer coordinated to P cluster Fe atoms. Instead, these cluster ligands are exchanged for coordination to the central S atom of the P cluster, creating a central hexacoordinate sulfur with distorted octahedral geometry. This updated version of the P cluster structure agrees with the earlier *C. pasteurianum* (Bolin *et al*., 1993) and more recent *K. pneumoniae* (Lawson *et al*., 1997) MoFe protein structures. The structural differences result in movement of Fe5 and Fe6 by 1.4-❹ and 0.9-❹, respectively, towards the central S upon reduction. This net movement agrees with previous EXAFS data that indicate a contraction of Fe-Fe distances upon reduction of the P clusters (Christiansen *et al*., 1995). It was proposed that the earlier P cluster structure was actually determined on crystals with both oxidation states and so both structures present. This mixture could then account for the misinterpretation of the early data, which led erroneously to the inclusion of a disulfide bond and a Fe_8S_8 cluster in the original structure.

The recent structural analysis of the P cluster implicates a new function for these metallocenters in the nitrogenase mechanism, the coupling of electron and proton transfer

during substrate reduction. As the P cluster oxidizes from P^N to P^{OX}, there would be an accompanying release of two protons from the β-Ser188 hydroxyl and α-Cys88 amide groups as they deprotonate to form Fe-O and Fe-N bonds, respectively.

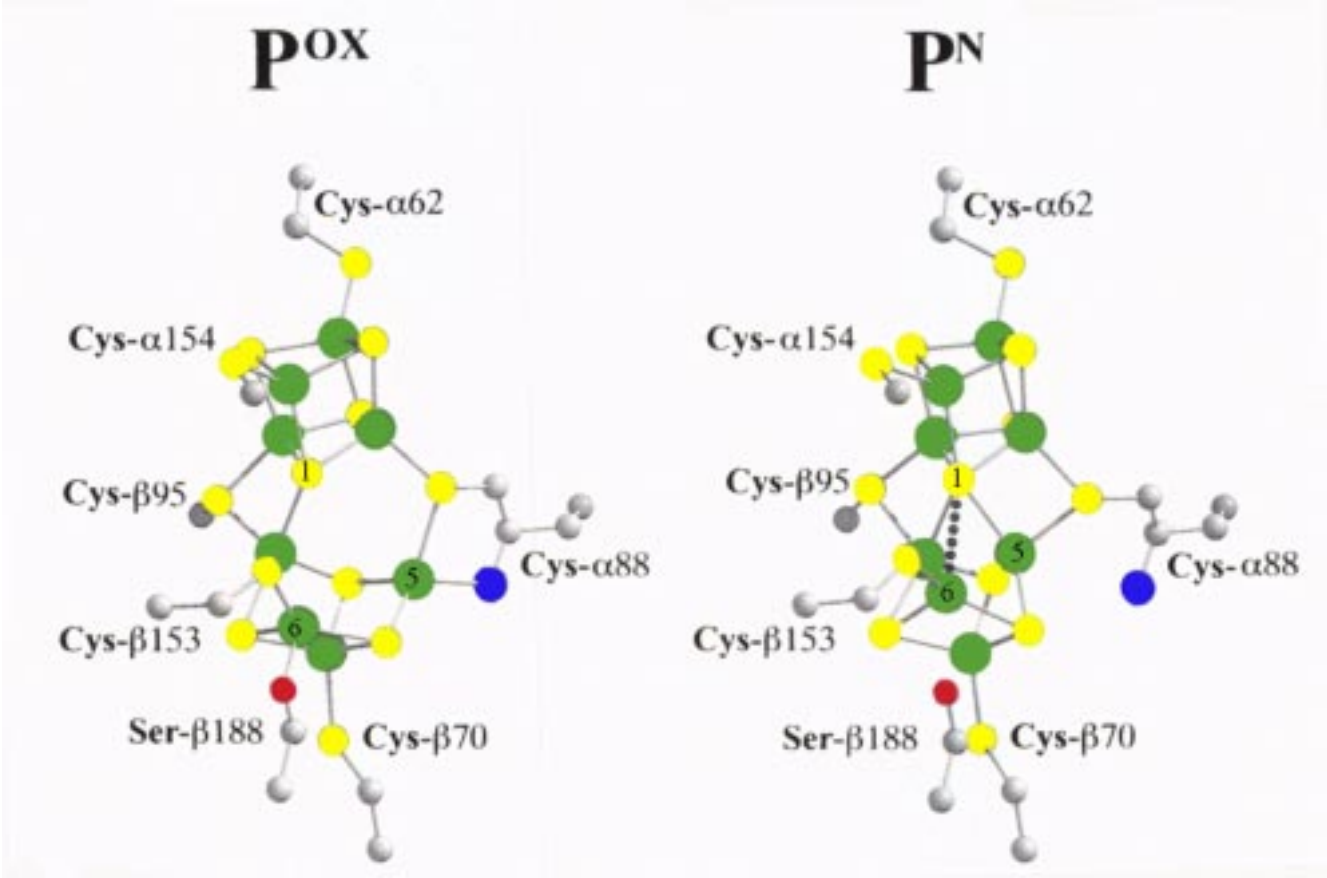

Figure 7: Updated Ball and Stick Model of the *A. vinelandii* P cluster and Surrounding Ligands in the P^{OX} and P^{N} Redox States

Fe atoms are shown in green, sulfur atoms in yellow, α-Cys88 main chain nitrogen atom in blue, and serinyl side group oxygen atom in red.

E. Protein-Protein Interaction

Complex formation between the MoFe and Fe proteins has been known for years to be a critical step in the overall mechanism of biological nitrogen fixation. It is a well established fact that only in the two-protein complex does MgATP hydrolysis and intermolecular electron transfer occur (Hageman & Burris, 1978a; Imam & Eady, 1980; Thorneley *et al*., 1991). Studies on the effects of salt inhibition of nitrogenase activity and chemical crosslinking experiments were two of the early indications of how the protein-protein interaction might transpire.

1. Chemical Cross-linking Studies

The Fe and MoFe proteins from A. vinelandii were found to be chemically-crossed linked by EDC (Willing *et al*., 1989) and it was subsequently found that the link is between Glu-112 of the Fe protein and β-Lys400 of the MoFe protein (Willing & Howard, 1990). Primary sequence comparisons of nitrogenases from various bacterial species, however, identified these two residues as variable and, therefore, unique to the *A. vinelandii* nitrogenase. The cross-linking reaction was found to be sensitive to high concentrations of salt, which led researchers to investigate this phenomenon further, and to predict that ionic interactions between component proteins dominant the coupling mechanism. NaCl inhibited the substrate reduction rate of H^+, C_2H_2, and N_2, and the inhibition pattern indicated cooperativity amongst several inhibitor sites (Deits & Howard, 1990). Increasing the salt concentration also appeared to decrease the binding affinity of MgATP and decreased the rate of MgATP-dependent Fe chelation by α, α'-bipyridyl. It is important to note that spectral analysis of the Fe_4S_4 cluster of the Fe protein revealed little effect by NaCl (Lindahl *et al*., 1987).

2. Av1-Cp2 Heterologous Crosses

Some of the earlier work exploring the interaction of the two component proteins of nitrogenase involved heterologous crosses of Fe and MoFe proteins from different nitrogen-fixing species. One particular cross, between Av1 and Cp2, stood out because, unlike most of the hybrid combinations, it was able to associate but then formed an

irreversible, tight complex and, therefore, would not support substrate reduction (Emerich *et al*., 1978). Examination of the primary amino acid sequences of Av2 and Cp2 revealed a significant difference in that Cp2 is thirteen amino acids shorter than Av2 at the carboxy-terminus. In order to ascertain if this terminal sequence was responsible for the tight Av1/Cp2 complex formation, the Cp2 carboxy-terminal residues were incorporated into Av2 (Jacobson *et al*., 1990). When this hybrid Av2 was assayed for activity with Av1, there was a 50% reduction in Av2 activity, however, no tight complex was formed, thus, the carboxy-terminus of Cp2 is not the cause of the inactive complex.

3. Post-translational Modification at Arg-100

The Arg-100 residue of *Azotobacter vinelandii* was the subject of inquiry prior to the solution of the x-ray structure of the Fe protein (Wolle *et al*., 1992a). In a series of experiments an arginine, Arg-101, in the Fe protein from the purple photosynthetic, nitrogen-fixing bacterium *Rhodospirillum rubrum* was found to be the site of a post-translation modification (Pope *et al*., 1984; Lowery *et al*., 1986). The Arg-101 residue was ADP-ribosylated in response to light and ammonium levels. All indications are that the ADP-ribosylation inactivates the Fe protein by blocking its association with the MoFe protein component. Based on this hypothesis and the fact that Cp2 has an analogous arginine residue, Arg96, at about the same position as the *R. rubrum* Arg-101, the effect of ADP-ribosylation was tested on Cp2 and its subsequent interaction with Av1 in a Av1/Av2 substrate-reduction assay (Murrell *et al*., 1988). Cp2 added to an Av1/Av2 activity assay inhibited substrate reduction, whereas ADP-ribosylated Cp2 was unable to inhibit Av1/Av2 activity. Conversely, Av1 incubated with Cp2 blocked ADP-ribosylation of the Cp2. Taken together, these findings argue for a direct role of the Arg-100 residue of Cp2 in Fe protein docking with the MoFe protein. The proximity of this residue to the Fe_4S_4 cluster ligand, Cys-98, agrees with a solvent-exposed location of both amino acids in the three-dimensional picture of the dimeric Fe protein.

4. Site-directed Mutagenesis Affecting Protein-Protein Interaction

The surface of the Fe protein that interacts with the MoFe protein and some of the residues integral to protein-protein docking were identified prior to as well as after the solution of the x-ray crystal structure. As in the cases of the ligands to the Fe_4S_4, FeMo-cofactor and P cluster, and the Walker type-A and type-B motif residues, identification utilized, among other techniques, site-directed mutagenesis and subsequent analysis and comparison of the altered MoFe and Fe proteins to their wild-type counterparts.

a. Substitutions in the Fe protein - Analysis of amino acid substitutions in the vicinity of the Fe_4S_4 cluster face of the Fe protein from *A. vinelandii* identified some likely candidates for involvement in protein-protein docking. Four charged residues, Arg-100, Glu-112, Arg-140, and Lys-143 stand out in the crystal structure as extending outward from the proposed docking surface. When altered Fe proteins were constructed with individual substitutions for Arg-100 replaced with histidine (R100H; Wolle *et al*., 1992), Arg-140 replaced by glutamine, or Lys-143 replaced with glutamine (R140Q and K143Q; Seefeldt, 1994), each of the altered Fe proteins was found to have decreased substrate reduction rates, increased inhibition of substrate reduction to excess concentrations of MoFe protein, increased sensitivity to increasing NaCl concentrations in activity assays, and substantial uncoupling of ATP hydrolysis from substrate reduction. These results, in addition to the chemical cross-linking data, support the contention that all four charged residues have a role in the docking mechanism that is necessary for nitrogenase catalytic action.

b. Substitutions in the MoFe protein - An interesting pattern of biochemical phenotypes occurs on substitution of a group of charged, possibly complementary amino acid residues on the surface of MoFe protein from *A. vinelandii*. The four aspartyl residues, α-Asp161, α-Asp162, β-Asp160, and β-Asp161 are all completely conserved in the primary sequences of at least five nitrogen fixers (Dean & Jacobson, 1992). Substitution by asparagine at α-Asp162, β-Asp160, or β-Asp161 has minimal effect on nitrogenase activity (Kim *et al*., 1993). This lack of effect is also true for a double substitution of asparagine at both α-Asp162 and β-Asp161. However, substitution of

Asn for α-Asp161 leads to phenotypic pattern nearly identical to an Arg-100-altered Fe protein. This result implicates the α-Asp161 residue as involved in protein-protein interaction even though the crystal structure of the MoFe protein has it in a non-exposed position. This contrast in phenotypes of substitutions at highly conserved and structurally symmetric positions demonstrates the possibility of functional inequality between α and β-subunits. It is worthwhile to point out that these conserved aspartates are connected through short α-helices to the P cluster ligands, α-Cys154 and β-Cys153. This linkage could function as a signal-transducing bridge between the protein surface and the metallocluster.

In addition to these charged residues, at least one hydrophobic residue, β-Phe125, on the MoFe protein from *K. pneumoniae* was found to be a recognition site for peptide cleavage by chymotrypsin (Fisher *et al*., 1993). Also, when this residue was replaced by isoleucine the resultant MoFe protein had ~70% reduction in primary electron transfer rate from the Fe protein (Thorneley *et al*., 1993). These facts, in addition to the β-Phe125 residue's status at the protein exterior, are evidence for hydrophobic as well as electrostatic interactions in component protein docking.

5. The Rees-Howard Model and the Variable Loop

The solution of the x-ray crystal structures of both the MoFe and Fe proteins from *A. vinelandii* spawned a nitrogenase component protein docking model (Howard, 1993; Howard & Rees, 1994) that also incorporated the results of amino acid substitution studies (Wolle *et al*., 1992b) and chemical cross-linking experiments (Willing & Howard, 1990). This model is referred to as the Rees-Howard model (Peters *et al*., 1994). Some of the salient features of this model include: 1. a region of the Fe protein, which includes the Fe_4S_4 cluster and two α-helices extending outward in the shape of a bent rod, can be directly aligned with a complementary groove formed by the αβ-subunit interface of the MoFe protein where the P cluster resides; 2. there is juxtaposition of several pairs of oppositely charged patches on the surfaces of the two nitrogenase component proteins; 3. the model positions the metalloclusters of the nitrogenase complex such that the shortest

distance between the Fe_4S_4 cluster of the Fe protein and the P cluster of the MoFe protein is ~18-❹, and that between the Fe_4S_4 cluster and the FeMo-cofactor is ~32-❹. This last feature suggests an electron transfer sequence of:

$$Fe_4S_4 \text{ cluster} \rightarrow \text{P cluster} \rightarrow \text{FeMo-cofactor} \rightarrow \text{substrate}$$

The docking model, based on the crystal structures of the Fe and MoFe proteins from *A. vinelandii*, has identified a polypeptide loop that includes residues 59 through 67 of the Fe protein as a part of the surface interaction with the MoFe protein (Peters *et al*., 1994). When the Av2 and Cp2 primary sequences were aligned and compared, this stretch of amino acids revealed notable differences, for this reason this oligopeptide is referred to as the "variable loop". In order to determine if this region of the Fe protein was responsible for the tight, inactive complex of the Av1-Cp2 heterologous mix, a hybrid Av2 was created that contained most of the Cp2 sequence for positions 59 through 67. The hybrid Fe protein (designated as AvCp2) yielded many of the same biochemical features found in other Fe proteins with substitutions in residues thought to be important for protein-protein interaction. The hybrid protein exhibited reduced substrate reduction rates, hypersensitivity to molar excesses of MoFe protein, disruption of the pattern of inhibition by moderate levels of NaCl concentrations, and uncoupling of ATP hydrolysis from substrate reduction when compared to wild-type Fe protein. In addition to these trademark characteristics of perturbation of protein-protein docking the AvCp2 hybrid dissociated from the MoFe protein at only half the rate (i.e., slower) than the wild-type proteins dissociated from each other. These results support the contention that the region delineated by residues 59 through 67 is involved in component protein interaction.

6. The ADP·AlF_4^--stabilized Nitrogenase Complex

The recent finding of a stabilized transition state complex of nitrogenase from *A. vinelandii* has had significant impact on the field. The experiments were based on the known inhibition of some nucleotide-dependent switch proteins by AlF_4^-, which with GDP or ADP present appears to act by mimicking the triphosphate (Chabre, 1990). MgADP with AlF_4^- was found to stabilize a tight, inactive complex between the MoFe and Fe proteins that probably corresponds to the transition state of one of the steps in the

turnover sequence of nitrogenase (Duyvis *et al*., 1996; Renner & Howard, 1996). Incubation experiments with a nitrogenase turnover system, AlF_4^- and either MgATP or MgADP showed that inhibition was time dependent and the rate of inhibition was more than 30-fold greater with MgATP than with MgADP. This fact indicated that MgATP hydrolysis influenced inhibition by the AlF_4^--trapped complex. This AlF_4^--inhibited complex was isolated by gel chromatography and its composition was determined. The approximate molecular weight was 370,000, and the ratio of Av2/Av1 was ~2, while the ratio of ADP/complex was 2.7 - 3.4. This finding suggests that not all nucleotide binding sites need to be occupied for complex stabilization. This complex was found to be slowly reversible with a $t_{1/2}$ for dissociation of ~21 hr at room temperature (Renner & Howard, 1996). Incubation of the complex at 50°C for 2 hr recovers 46% of the activity of the MoFe protein (Duyvis *et al*., 1996). Both sets of data confirm the existence of a stable transition state complex of nitrogenase.

The strength of the ADP·AlF_4^--stabilized nitrogenase complex made it an ideal candidate for crystallization and structural analysis. The x-ray crystal structure of the ADP·AlF_4^--stabilized nitrogenase complex from *A. vinelandii* was recently solved and refined to a 3-❹ resolution (Schindelin *et al*., 1997). The subunit composition of the nitrogenase complex is a $(\alpha\beta\gamma_2)_2$ octamer with one Fe protein γ_2-dimer per MoFe protein $\alpha\beta$-subunit pair and, therefore, two bound Fe proteins per MoFe heterotetramer. Each $\alpha\beta\gamma_2$ half of the complex is related by a non-crystallographic two-fold axis, and each Fe protein γ_2-dimer has a molecular two-fold axis that aligns with the pseudo-two-fold axis that runs through the P cluster and relates the α- and β-subunits of the MoFe protein.

The crystal structure of the complex agrees very well with the Rees-Howard docking model, however, there are some structural features that can only be described and quantified in detail by the crystal structure. When comparing the x-ray crystal structures of the complex with the static model, most of the movement due to protein-protein association occurs in the Fe protein. One consequence of this movement is that the closest atom-to-atom distance between the Fe_4S_4 cluster of Av2 and the P cluster of Av1

is ~14-❹, which is 4-❹ shorter than the distance approximated by the Rees-Howard model. This movement brings the P cluster into a position equidistant between the Fe_4S_4 cluster and the FeMo-cofactor, thus reinforcing the hypothesis of the P cluster as an electron transfer mediator. The area of surface contact between nitrogenase component proteins can be estimated at ~3,500-$❹^2$ per Av2/Av1 interface region. In this contact region, the Fe_4S_4 cluster is completely buried with many van der Waals contacts (~3.2 - 3.5-❹) to several α- and β-subunit residues. The substantial conformational change in the Fe protein upon complex formation can be described as a ~13° rotation of each γ-monomer towards the subunit interface. This results in contraction of the quaternary structure of the Fe protein as the two subunits close inwardly. The crystal structure of the nitrogenase complex exposes five separate regions of the Fe protein which differ noticeably in conformation when compared to the static model. These are: 1. the Walker A-type motif or phosphate-binding loop (P-loop); 2. the protein-protein interface region of residues 51 through 75, which differ in primary sequence between Av2 and Cp2 (see Section I.E.5); 3. the residues 88 through 118 that includes the Fe_4S_4 cluster ligand, Cys97, and the complex-docking residue Arg100; 4. the region that overlaps the carboxy-end of the Walker B-type motif and extends beyond the cluster ligand, Cys132; and 5. residues 151 through 176, which participate in an intersubunit salt bridge that also stabilizes the adenosine ring of the bound nucleotide.

The ADP·AlF_4^--stabilized nitrogenase complex structure supports the idea of nucleotide-induced conformational shifts as the catalytic driving force in the early steps of the nitrogenase mechanism. The net contraction of the subunit interface of the Fe protein may represent the conformation necessary for effective protein docking, ATP hydrolysis and electron transfer. After hydrolysis and phosphate release, many of the intersubunit contacts in the Fe protein would be severed and perhaps this would cause a relaxation into the more open conformation that could drive the complex dissociation process.

F. Mechanism of Nitrogenase

The minimum requirements for biological nitrogen fixation by nitrogenase are known. These include the MoFe and Fe proteins, the substrate N_2, a source of reductant (flavodoxin or ferredoxin *in vivo*, and sodium dithionite, $Na_2S_2O_4$, *in vitro*), MgATP in the presence of a ATP regenerating system, and an anaerobic environment. It is also widely accepted that the direction of electron flow is from reductant to Fe protein to MoFe protein and finally to bound substrate. What is not known, are the exact details of the mechanism of nitrogenase. However, a comprehensive kinetic model of nitrogenase action, the Thorneley & Lowe model, has described and quantitated many of the individual steps of the catalytic reaction of the nitrogenase from *K. pneumoniae*, and amazingly agrees with much of the experimental data available both prior and following its initial proposal (Thorneley & Lowe, 1985). The model can be broken down into two cycles, the Fe protein oxidation-reduction cycle, and the MoFe protein cycle.

1. The Fe Protein Cycle

The Fe protein cycle is a redox cycle that describes the single electron donation from the Fe protein to the MoFe protein and the concomitant hydrolysis of MgATP and the events necessary for re-reduction of the oxidized Fe protein in order to re-initiate another round of the cycle. The individual steps can be modeled as the four sides of a square (see Figure 8). The initial step is protein-protein association, followed by the electron transfer coupled to MgATP hydrolysis, followed by protein-protein complex dissociation, and finally Fe protein re-reduction and nucleotide exchange. A brief note on the nomenclature of the Fe protein cycle is appropriate. The MoFe and Fe proteins are designated by their genus-species initials, and component protein number, the oxidation state is denoted by the subscripts red or ox, the status of bound nucleotides is in parentheses with the number of nucleotides as a subscript to the parentheses, and the

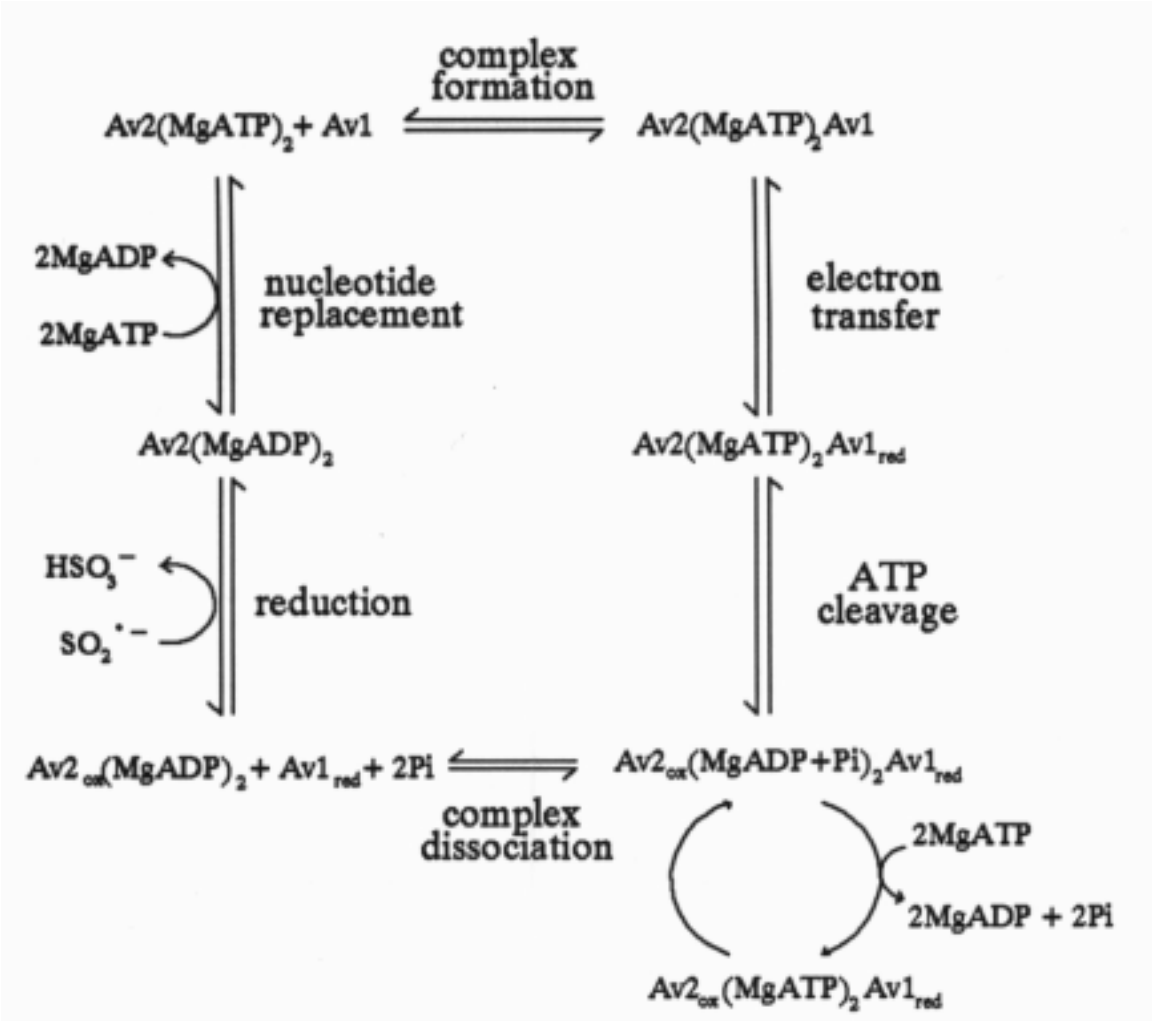

Figure 8: The Fe Protein Cycle

Av1 represents one αβ-subunit dimer of the two functionally equivalent halves of the MoFe protein, while Av2 represents the Feprotein. The redox states are indicated by the subscripts ox (oxidized) and red (one-electron-reduced). The reductant-independent ATPase cycle is depicted in the lower right-hand corner. Adapted from Thorneley & Lowe, 1983.

docked state of the complex is denoted as a hyphen (complexed) or plus sign (non-complexed). Because one Fe protein interacts with each α- and β-subunit dimeric half of the MoFe protein, the Fe protein cycle describes what is occurring on one of the functional halves.

a. Protein association rate (k_{+1}) - The first event that must occur before effective electron transfer is the association of the MoFe protein with the Fe protein in the formation of a complex. The rate of association, k_{+1}, was originally estimated to be $\geq 10^7 M^{-1}s^{-1}$ (Thorneley, 1975), and later a value of $k_{+1} \geq 5x10^7 M^{-1}s^{-1}$ was determined by monitoring the rate of electron transfer from $Kp2(MgATP)_2$ to Kp1 as a function of protein concentration (Lowe & Thorneley, 1984b). The increase in accuracy of the determination was partly dependent on the increased sensitivity of the computer-interfaced stopped-flow apparatus, which allowed lower protein concentrations to be used. The rapid association of these two proteins, as evidenced in the rate constant, k_{+1}, means that the reaction is occurring close to the diffusion limit of two molecules colliding in solution. The high value of k_{+1} is postulated to increase the efficiency of nitrogenase for N_2 reduction over H_2 evolution.

Previously, a "dilution effect" (Mortenson, 1964) had been noted as the disproportionate decrease in substrate reduction activity when nitrogenase component protein concentration was decreased below 0.5 μM. The data from the Thorneley-Lowe model found that the dilution effect was due to k_{+1} becoming the rate-limiting step at low protein concentrations (Thorneley, 1975; Thorneley & Lowe, 1984b). This example shows how the model has been used to explain experimental phenomena. Conversely, high concentrations (>100 μM) of nitrogenase component proteins were found to affect the lag time for H_2 evolution (see Sections I.F.2.a & b) such that as the protein concentration increased the lag time also increased (Lowe & Thorneley, 1984). The conclusion was that higher protein concentrations favor N_2 reduction relative to H_2 evolution and therefore the high component protein concentrations that are assumed to occur *in vivo* are a requirement for efficient nitrogen fixation.

b. Electron transfer coupled to MgATP hydrolysis (k_{+2}) - These two reactions are considered together because it is still not clear what the sequence of occurrence is. Early investigations utilized a combination of rapid quench analysis and stopped-flow spectrophotometry (Eady *et al*., 1978). The rapid quench technique allowed for measurement of Pi released upon MgATP hydrolysis. Stopped-flow spectrophotometry monitored the electron transfer from $Kp2(MgATP)_2$ to Kp1 at 10°C, because there is a significant absorbance increase at 430 nm when $Kp2_{red}$ is oxidized by Kp1 to yield $Kp2_{ox}$. The absorbance change of the Fe protein had been utilized prior to this study, and using stopped-flow spectrophotometry, the rate constant for electron transfer between Fe and MoFe proteins, k_{+2}, was accurately quantitated as 200 s^{-1} at 23°C (Thorneley, 1975). The conclusion of this study at lower temperatures was that MgATP hydrolysis and electron transfer occur concomitantly.

Stopped-flow microcalorimetry experiments with the nitrogenase from *K. pneumoniae* at 6°C found that protons are liberated from the MgATP hydrolysis reaction at a rate faster than the electron transfer rate (Thorneley *et al*., 1989). Therefore, MgATP hydrolysis would have to precede electron transfer. The opposite conclusion was derived from research that used a pH indicator to measure proton production (Mensink *et al*., 1992). The ATP-dependent proton production rate was observed to be slower than the electron transfer rate, although neither rates were rate-limiting for nitrogenase turnover. These results argue for a system where MgATP-binding actuates electron transfer between component proteins and MgATP hydrolysis drives the dissociation of the complex after electron transfer.

Recent evidence from the altered Fe protein from *A. vinelandii*, L127Δ, corroborates the latter premise of electron transfer preceding MgATP hydrolysis. The L127Δ Fe protein can transfer an electron to wild-type MoFe protein in the absence of bound MgATP, thus it seems that ATP hydrolysis is not a prerequisite for electron transfer (Lanzilotta *et al*., 1996). However, the nucleotide-free L127Δ Fe protein also

forms a tight irreversible complex with the MoFe protein which agrees with the proposal that ATP hydrolysis is necessary for dissociation.

c. Complex dissociation rate (k_{-3}) - The kinetics of the dissociation of the oxidized Fe protein from the one-electron-reduced MoFe protein from *K. pneumoniae* has been measured by an elegantly designed stopped-flow experiment (Thorneley & Lowe, 1983). The experiment employs the inhibition of dithionite reduction of $Kp2_{ox}(MgADP)_2$ by Kp1. The rate constant for complex dissociation was determined by reacting dithionite-free $Kp2_{ox}(MgADP)_2$-Kp1 with $Kp2_{red}$ and excess dithionite (10 mM) at 23°C. This mixture results in a decrease in absorbance at 430 nm as the $Kp2_{ox}$ is reduced by dithionite following release from Kp1. The measured rate constant, k_{-3}, was $6.4 \pm 0.8\ s^{-1}$, and was concluded to be the rate-limiting step in the catalytic cycle for substrate reduction. The value of k_{-3} was used to calculate the specific activity of Kp1 for H_2 evolution, and this calculated value agreed very well with the value obtained by the standard steady-state assay under equivalent conditions. The slow dissociation rate calculated in this study is also consistent with the observed lag period that occurs before H_2 formation in *A. vinelandii* nitrogenase (Hageman & Burris, 1978b). If each Fe protein donates one electron to one of the αβ-subunit functionally independent halves of the MoFe protein, then the lag period corresponds to the two slow dissociation steps that are necessary before the two-electron product H_2 is evolved.

There is an important additional conclusion from the complex dissociation data that relates the slow dissociation rate with efficient N_2 reduction. Because products are assumed to only evolve from the non-complexed substrate-reduction site on the MoFe protein (Lowe & Thorneley, 1984a), the slow dissociation rate may be necessary for the generation of low-potential metal hydride site capable of binding N_2 and thus displacing H_2 (see Figure 9). In other words, the value of k_{-3} may contribute to a preference for N_2 reduction over H_2 evolution.

d. Reduction of oxidized Fe protein by dithionite (k_{+4}) - The reduction of oxidized Fe protein by dithionite has been examined with *K. pneumoniae* nitrogenase (Thorneley

& Lowe, 1983). This study also confirmed that $SO_2^{\cdot -}$, a dissociation product of $S_2O_4^{2-} \leftrightarrow 2SO_2^{\cdot -}$, is the active reductant based on a linear dependence of k_{obs} on $[S_2O_4^{2-}]^{1/2}$. The rate constant for $Kp2_{ox}(MgADP)_2$ reduction by $SO_2^{\cdot -}$, k_{+4}, was measured by the stopped-flow technique at 23°C to be $3 \times 10^6\ M^{-1}\ s^{-1}$. $Kp2_{ox}(MgADP)_2$ reduction is followed by replacement of bound MgADP by MgATP (at a rate of ~200 s^{-1}) to complete the Fe protein cycle (Ashby & Thorneley, 1987; Thorneley & Cornish-Bowden, 1977). MgADP is a competitive inhibitor of the MgATP-induced electron transfer reaction from the Fe protein to the MoFe protein. The build-up of MgADP results in a decrease in $Kp2_{red}(MgATP)_2$ concentration and an increase in $Kp2_{ox}(MgADP)_2$, which gives rise to a lowered electron flux through the MoFe protein to reducible substrates.

2. MoFe Protein Cycle

The MoFe protein cycle is a redox cycle that depicts the sequence of the partial reactions that transpire during the net reduction of N_2 to $2NH_3$ and H_2 (Lowe & Thorneley, 1984a). Because N_2 reduction is an eight-electron-requiring process, there are eight individual partial reactions where each progressive step represents one turn of the Fe protein cycle (see Figure 9). In the nomenclature of the MoFe protein cycle, E represents one $\alpha\beta$-subunit functional dimer of the MoFe protein, and the numerical subscript represents the number of times the MoFe protein has completed the Fe protein cycle. In the species E_n, n also indicates the number of rate-limiting complex dissociation steps that the MoFe protein has undergone and, therefore, the number of electrons acquired. E_0 is the initial as-isolated, dithionite-reduced state of the MoFe protein. The three arrows between each redox state of the MoFe protein represent (i) the association, (ii) MgATP hydrolysis coupled electron transfer, and (iii) dissociation steps of the Fe protein cycle. It is important to note that a central tenet of the Thorneley-Lowe model is that the kinetics of the Fe protein cycle are independent of the oxidation state of the MoFe protein and this assumption has been demonstrated to hold for the first two oxidation states of the MoFe protein (Fisher *et al.*, 1991).

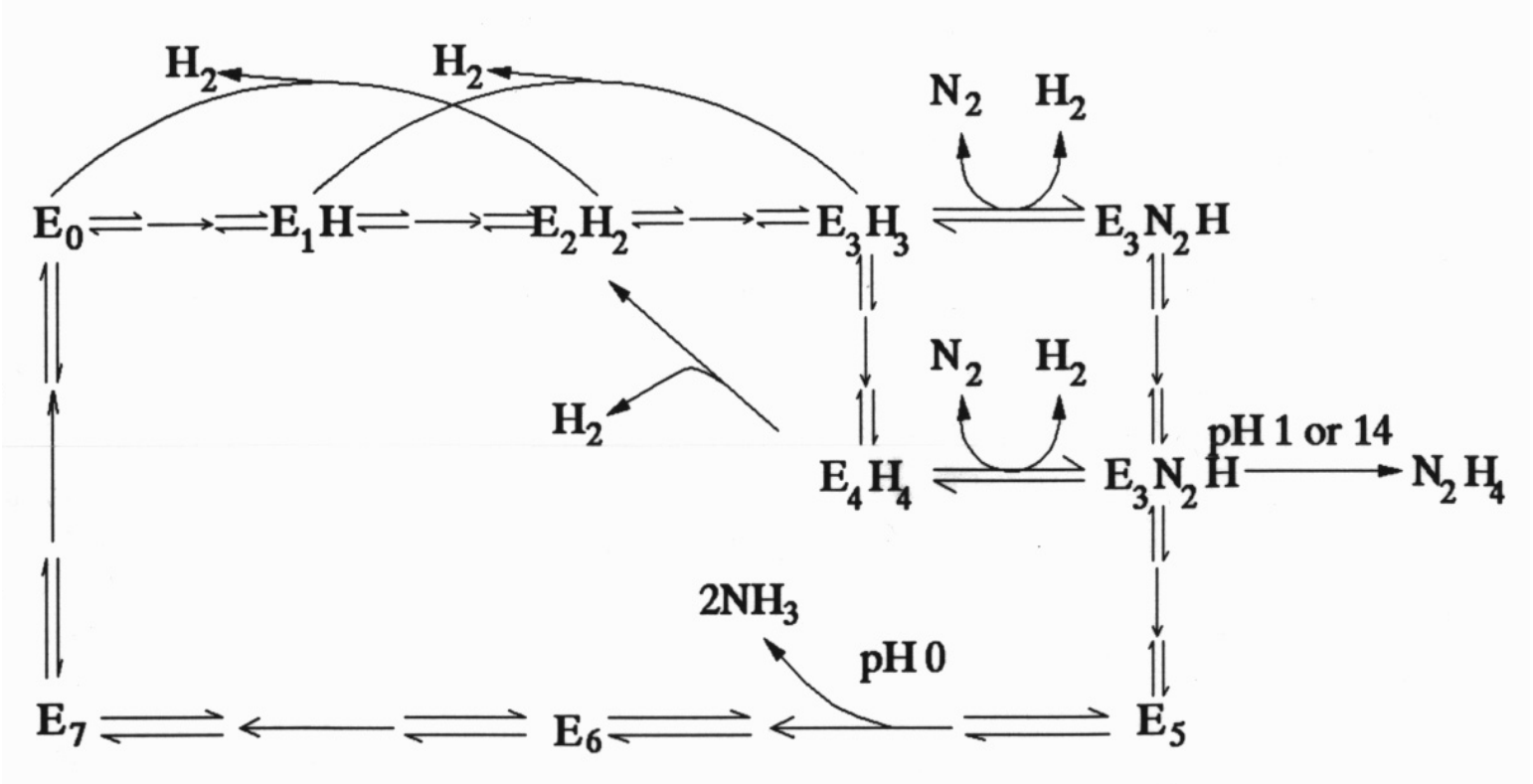

Figure 9: The MoFe Protein Cycle

E_n represents an αβ-subunit, functional half of the MoFe protein, which has been reduced by *n* electrons. The three intervening arrows between each step represent the protein association, electron transfer/ATP cleavage, and complex dissociation steps of Fe protein cycle.

a. H_2 evolution vs. N_2 reduction - Based on the model, the first redox state that is capable of evolving a product is E_2, which can release H_2, and thus revert to E_0. This aspect of the model conforms to the previously mentioned data suggesting that the lag phase in H_2 evolution is caused by two slow dissociation steps during nitrogenase turnover (Hageman & Burris, 1978b). H_2 evolution from the E_2 state is a consequence of the hydrogenase activity of nitrogenase under conditions where higher redox states of the MoFe protein cannot be reached, e.g., at low flux (Wherland *et al*., 1981; Guth & Burris, 1983). The model predicts that N_2 does not bind to the MoFe protein until the E_3 or E_4 redox state has been attained and that this binding results in the displacement of H_2, which explains the minimum requirement of one H_2 evolved for every N_2 reduced. The Thorneley-Lowe model asserts the importance of minimizing the concentration of E_2 and the need to quickly convert to the N_2-binding E_3 redox state. Hydrogen evolution for E_2 is minimized by the slow complex dissociation step, k_{-3}, and the rapid conversion of E_2 to E_3 is due to the diffusion-limited association rate, k_{+1}. A dire consequence of this proposal is that any artificial increase in the rate-limiting step of the nitrogenase mechanism would result in an decrease in N_2 reducing activity and an increase in H_2-evolving activity.

b. The "committed" N_2 reduction cycle - Hydrazine, N_2H_4, is released from MoFe protein, which is turning over in the presence of N_2, when the enzymatic reaction is quenched with either acid or base (Thorneley *et al*., 1978). Hydrazine is not released as a substrate reduction product of nitrogenase operating under physiological conditions, but arises from the reaction of protons or solvent in an acid/base catalyzed reaction with a bound intermediate. The Thorneley-Lowe model proposes that this MoFe protein-bound intermediate is a bound dinitrogen-hydride intermediate at the E_4 redox state (Thorneley & Lowe, 1984a). This proposal was supported using computer simulations of N_2H_4 release by quenching at either the E_3, E_4, or E_5 redox states of the MoFe protein. The prediction, based on the computer-simulated N_2H_4 release at E_4, was found to be 1,000 times more likely to fit the actual experimental data than at E_3 or at E_5.

The model suggests a hydrazido(2-) structure, $=N\text{-}NH_2$ for the enzyme-bound intermediate that yields hydrazine upon quenching based on related model chemistry. The first two electrons are supposed to be used in H_2 evolution, while the second pair of electrons would reduce bound N_2 to hydrazido(2-) level. Two more electrons, provided by the oxidation of metal centers in the MoFe protein upon acid or base quench, would convert the hydrazido(2-) intermediate to hydrazine. Additionally, the concentration of hydrazine released from nitrogenase equilibrated in a 50% H_2/50% N_2 atmosphere showed a distinct decrease relative to the hydrazine concentration derived from an 100% N_2 atmosphere. This evidence endorses the idea of H_2 inhibition of N_2 reduction by displacement at the active site, and that displacement occurs before formation of the hydrazido(2-) intermediate. Reduction of the MoFe protein beyond the N_2-bound E_3 or E_4 state represents the "committed" phase of the MoFe protein cycle where NH_3 evolution is assured.

A similar acid quench experiment was performed in order to measure the concentration of NH_3. Computer simulations, based on the calculated rate constants of the Thorneley-Lowe model, ascertained that the best fit to the experimental data was obtained when two moles of NH_3 were liberated from the E_5 or E_6 species. The results suggested that the first two electrons lead to H_2 formation, whereas the next three or four electrons reduce N_2 by cleavage of the nitrogen-nitrogen triple bond to give NH_3 and an MoFe protein-bound nitrido ($\equiv N$) or imido ($=NH$) intermediate (Thorneley & Lowe, 1982). The second mole of NH_3 would come from the acid-hydrolysis of the enzyme-bound intermediate, which yields one mole of NH_3 and an oxidized MoFe protein. This agrees with the theory that the N_2 triple bond is attacked by progressive protonation of the β-nitrogen atom, which is induced by an increase in bond order between Mo and the α-nitrogen atom (Chatt, 1980). Based on the acid-quench data, the overall pattern of product release from the nitrogenase system under a N_2 atmosphere is H_2, N_2H_4, and then NH_3. The Thorneley-Lowe model attempts to relate this sequence to the number of electrons transferred from the Fe protein to the MoFe protein.

c. The C_2H_2 reduction cycle - An extension of the Thorneley-Lowe model of the mechanism of nitrogenase action was applied to the mechanism of acetylene (C_2H_2) reduction. In a series of experiments, it was shown that the product of the two-electron reduction of C_2H_2, ethylene (C_2H_4) can be slowly reduced to ethane (C_2H_6) by nitrogenase (Ashby *et al*., 1987). Also, C_2H_4 was able to inhibit both total electron flux through nitrogenase and MgATP hydrolysis. It was concluded that C_2H_4 was evolved from the MoFe protein after three electrons had been transferred, i.e., from the E_3 redox state of the MoFe protein. Successive experiments discovered good fits of the acid quench data for C_2H_2 reduction by nitrogenase with the simulations of binding C_2H_2 at the E_1 or E_2 species and release of C_2H_4 at the E_3 or E_4 species (Lowe *et al*., 1990). Additionally, it was found that the apparent inhibition of C_2H_4 formation by high protein concentrations was due to binding and stabilizing effect of C_2H_2 on the $Kp2_{ox}Kp1$ complex, presumably by enhancing the protein association rate. The inhibitory effects of C_2H_2 on total electron flux was tested in conjunction with inhibition of C_2H_4 formation by CO. Under a 5% CO/95% C_2H_2 atmosphere, the amount of C_2H_4 formed was found to be constant at about 10% of the total flux as the component protein concentration was increased. However, the H_2 evolution was also inhibited as the component protein concentration is increased. Typically under a 10% CO/10% C_2H_2/90% Ar atmosphere, CO will divert the entire electron flux towards H_2 evolution without a decrease in total flux (Hardy *et al*., 1965). The results of the increasing protein concentration assays support the contention that CO and C_2H_2 are bound concurrently to distinct sites, because both gases are impacting different forms of inhibition simultaneously. CO is directing allocation of the majority of the electron flux to H_2 evolution, while C_2H_2 is depressing total flux at high component protein concentrations. Thus, CO does not appear to competitively inhibit C_2H_2 reduction by binding to the same site.

G. Summary and Comments

The preceding literature survey is a testament to the enormous effort and contribution made by many researchers in the pursuit of the complete understanding of the process known as biological nitrogen fixation and, more specifically, the mechanism of the nitrogenase enzyme system. Paramount in these efforts is the cogent use of molecular biological techniques for the purpose of manipulating the intricate workings of the system in order to understand each component and its role in the overall process. Site-directed mutagenesis of highly conserved amino acid residues has suggested both the function and importance of many of these targeted residues. Examples include residues in the vicinity of the Fe_4S_4 cluster and MgATP-binding sites of the Fe protein, in the environment of the FeMo-cofactor of the MoFe protein, and in the protein-protein docking region of both these proteins. In nearly every instance, the conclusions made from mutagenesis results were confirmed by the x-ray crystal structures that, in most cases, became available after the fact. One particular element of the nitrogenase complex that remains elusive to this type of analysis is the P clusters of the MoFe protein. This dissertation will reveal some interesting and wholly unexpected results from the site-directed mutagenesis of one particular P cluster bridging ligand, α-Cys88.

CHAPTER II.
MATERIALS AND METHODS

A. Construction of Site-directed Mutant Strains

1. Degenerate and Specific Oligonucleotide Synthesis

Automated oligonucleotide synthesis was utilized for the construction of either 18-mer or 21-mer single-stranded DNA polymers. A Beckman or Applied Biosystems DNA synthesizer was employed to create the desired sequences and the oligonucleotides were purified by disposable OPC column (ABI, Foster City, CA). The altered codon was always situated in the middle of the oligomer with 5'- and 3'- flanking complementary sequences. This arrangement increases the strength of the association of the oligonucleotide to the template DNA during annealing. When a specific codon substitution was desired, the codon bias for *A. vinelandii* was used when more than one codon choice was available. In the case of degenerate codons, the synthesizer was programmed to insert all four nucleotides at each of the three codon positions, thus, all sixty-four potential codons were constructed.

2. Plasmid Construction

Site-directed mutagenesis of the *nifD* gene, which encodes the α-subunit of the MoFe protein from *A. vinelandii*, utilized template DNA consisting of a 1.4-kilobase *Eco*RI endonuclease digested fragment cloned into the EcoRI site of bacteriophage vector M13mp18 (Messing & Vieira, 1982). Site-directed mutagenesis of the *nifK* gene, which encodes the β-subunit of the MoFe protein from *A. vinelandii*, utilized a 1.0 kilobase *Hind*III-*Kpn*I digested fragment cloned into pUC118 (Vieira & Messing, 1987) as a template. The oligonucleotide-containing, ligated *E. coli* plasmid DNA (5-10 μl) was added to 300 μl of competent *E. coli* 7118 cells. This mixture was placed on ice for 20 min, heat shocked at 42°C for 90 sec, then placed back on ice for 5 min. Serial dilutions (1x, 0.1x, 0.01x) of the transfected bacteria were spread on LB + Ampicillin (10 μg/ml) agar plates and allowed to grow overnight at 37°C. Individual colonies were picked and

transferred into 2 ml of YTA broth in sterile 50 ml flasks, and grown for 3-4 hrs at 37°C in a tabletop shaker at 300 rpm. 10 µl of each bacterial culture was then added to 2 ml of fresh a YTA + M1307 (0.01%) helper phage mixture and grown for an additional 1.5 hr. After this incubation time, 10 µl of kanamycin (20 mg/ml) was added to each flask and the cultures were grown for ~16 hrs in the shaker at 37°C and 300 rpm. These cell cultures were then subjected to single-strand plasmid DNA purification and this DNA was screened for mutations in the targeted codon by single-lane dideoxy sequencing (Sanger *et al*., 1977). Confirmation of potential mutants was performed by full sequencing of all four nucleotide dideoxy reactions, which also confirmed no additional mutations within 200 bases both 5' and 3' of the chosen codon. The resultant plasmid carrying the single codon mutation is referred to as the mutation vector DNA.

3. Transformation of *A. vinelandii*

The mutation vector DNA was used to transform either wild-type (Nif+) or a *nif* gene deletion strain (Nif-) of *A. vinelandii*. The selection of the transformable strain is dependent on the proposed phenotype of the transformed mutant strain. If the mutation causes loss of diazotrophy, then a wild-type *A.vinelandii* strain is used; if the mutation retains the diazotrophic trait, then rescue of a Nif^- *A.vinelandii* strain would verify its integration into the bacterial chromosome.

a. Growth of transformable *A. vinelandii* culture - The first step in transformation is growth of a *A. vinelandii* culture that is capable of taking up exogenous plasmid DNA. Using the molybdenum starvation method (Page & von Tigerstrom, 1979), competent cells were grown on Burk's media (see Section II.B.1) without molybdate or iron. The overnight culture was typically a bright, fluorescent green color due to the overproduction of Fe-importing, siderophores in the media.

b. Plasmid incorporation by congression - Transformable cells were then used in a transformation reaction mix containing 200 µl of competent cells, 20 µl of the mutation vector DNA and, 200 µl of 1x MOPS buffer. Potential Nif- transformants required an additional selectable marker, in this case rifampicin resistance (rif^R), which is introduced

into the *A. vinelandii* cells simultaneously with the mutation vector DNA by the method of congression. The technique involves the addition of *A. vinelandii* chromosomal DNA, which carries an uncharacterized rif^R marker to the transformation reaction. The concentration of mutation vector DNA is 20-fold higher than the rif^R DNA to insure that incorporation of mutation vector accompanies the acquisition of antibiotic resistance.

c. Screening for double reciprocal crossovers - Nif-, rif^R transformants were selected by outgrowth of the transformation reaction mixture on Burk's media + rifampicin (5 mg/L) agar plates with or without a fixed nitrogen source (urea or ammonium acetate). Double cross-over recombinants grew on the + fixed nitrogen, + Rif plates, but not on - fixed nitrogen, + Rif plates. At least two colony isolates were selected for each mutation and their phenotypes were verified prior to growing confluent agar plates, which were then freezer stocks for subsequent culturing.

B. Bacterial Growth and Derepression

1. Solid Media, Nif+/- Phenotype Screening

Initial screening of mutant *A. vinelandii* strains was accomplished by the qualitative method of growth on agar plates incubated at the optimal growth temperature of 30°C. Agar plates consisted of a 1.6 or 2% agar in Burk's modified media plus or minus a fixed nitrogen source, either 20 mM urea or 40 mM ammonium acetate. Unless noted otherwise, the fixed nitrogen source was always urea. Burk's modified media (Strandberg & Wilson, 1968) is a minimal bacterial growth medium comprised of 2% sucrose, phosphate buffer, pH 7.0 (0.2 g/L KH_2PO_4, 0.8 g/L K_2HPO_4), 0.2 g/L $MgSO_4 \cdot 7H_2O$, 0.5 mM $CaCl_2 \cdot 2H_2O$, 20 μM $FeCl_3 \cdot 6H_2O$, and 1 μM $Na_2MoO_4 \cdot 2H_2O$. The agar, sucrose, and Mg^{2+} and Ca^{2+} salts were added to distilled/deionized water and autoclaved. The phosphate buffer, Mo and Fe salts, and urea or ammonium acetate were filter-sterilized as concentrated solutions and were added separately to the autoclaved mixture after it has cooled below ~60°C. This procedure minimizes the formation of insoluble precipitates (e.g., $Ca_3(PO_4)_2$) during cooling of the steam-sterilized media.

Mutant strains from fresh freezer stocks that were Nif+ grew on nitrogen-free plates to thick colonies in 2-3 days, Nif^{Slow} typically took 4-7 days, and strictly Nif- strains showed no growth on nitrogen-free plates.

2. Liquid media & Doubling Times ($t_{1/2}$)

The next step in characterization of a mutant strain is to determine its doubling time during the logarithmic stage of growth on liquid Burk's media. The recipe for Burk's media was the same as above except that agar and a fixed nitrogen source were excluded. Mutant and wild-type (as a control) strains were first cultured on agar plates containing a fixed nitrogen source and then transferred to 250 ml Klett flasks filled with 50 ml of Burk's media plus a nitrogen source (denoted as BN-media). A Klett flask refers to a Erlenmeyer flask with a glass Klett tube annealed at an oblique angle to the top half of the flask. This design allows for turbidity measurement on the cell culture as a closed system and minimizes risk to contamination. Cell cultures were grown in a G-25 Incubator Shaker (New Brunswick Scientific Co. Inc., Edison NJ) operating at 30°C and aerated by shaking at 250-300 rpm. Turbidity measurements were taken on a Klett-Summerson colorimeter fitted with a green No. 54 filter (Klett Mfg. Co. Inc., NY). After the BN liquid cultures had grown to a Klett reading of 150-200, which corresponds to the mid- to late-logarithmic phase, the entire contents of the flask were centrifuged using a Sorvall RC-5B Refrigerated Superspeed Centrifuge (DuPont Instruments, Wilmington, DE) and a GSA-type rotor at 8,000xg for ~10 min at 4°C. The cell pellet was resuspended with ~10 ml of Burk's nitrogen-free media (denoted as B-media), centrifuged again, and the pellet was resuspended in ~10 ml of B-media and used as an inoculum for fresh, sterile Klett flasks. Enough inoculum was added to bring the fresh culture to a Klett reading of about 50. The flask was returned to the cabinet shaker and the turbidity was measured periodically. The doubling time, $t_{1/2}$, was calculated using the generation time (g) equation, where $g=\ln 2/\alpha$, and $\alpha=(\ln N - \ln N_0)/(t - t_0)$. The doubling time determination was derived from at least two independent cultures and at least two independent isolates of the same mutation, i.e., at least four separate growths of the same

strain. Wild-type *A. vinelandii*, whose doubling time is well established at ~2.5-3.0 hrs, served as a control.

3. Fernbach Batch Growth and Derepression

Once it was determined that the diazotrophic growth of a mutant strain was unlike that of wild-type, typically, the next step was to grow a large enough liquid culture to yield a few grams of derepressed cells for crude extract activity assays. Fernbach flasks (2.8-L capacity) are used due to their large bottom circumference which increases the culture aeration during cabinet shaker incubation. Each flask contained 500 ml of BN- or B-media and enough flasks (typically 1 L. worth) were used to obtain ~4 g of cell pellet. Fernbach cultures were initiated using cells from either 1 or 2 confluent agar plates that were had been growing for no more than 3 days. About 5-10 ml of BN-media was added to each plate and the cell lawn was resuspended into the liquid using a sterile "hockey-stick" plate scraper. The resuspended cells were grown on fixed nitrogen to a Klett of ~200 at which time the culture was harvested by centrifugation, rinsed with 10 ml B-media, re-centrifuged, and resuspended with another 10 ml aliquot of fresh B-media. Cells were then transferred into sterile Fernbach flasks, each containing a 500 ml. aliquot of fresh B-media. This second growth represented the derepression phase because lack of a fixed nitrogen source in the media results in activation of *nif* gene expression. The cultures were shaken for another 3-4 hrs during which time the cells synthesized nitrogenase. The cells were harvested and the cell pellet was scraped into small plastic zip-lock bags and stored in the -80°C freezer. Using this procedure, typical cell paste yields are 3-4 g per liter of cell culture.

4. Fermentor Batch Growth and Derepression

Results from crude extract activity assays from the derepressed cells provide the basis for the decision to grow larger-scale amounts of the strain of interest. A 24-L working capacity, MF-128S Microferm Fermentor (New Brunswick Scientific Co. Inc., Edison NJ) was used to grow enough cells (typically 100-200 g) for preparative-scale purification of the nitrogenase component proteins, i.e., in the range of 100-200 mg of

each protein. The Fermentor batch growth is accomplished using a similar methodology as the Fernbach growth except that the inoculum is larger and harvesting is via a tangential flow membrane harvester which utilizes a model 601S peristaltic pump (Watson-Marlow, Falmouth, Cornwall, UK) and a 0.45 μm Durapore Pellicon cassette (Millipore Corp., Bedford, MA). A 500 ml culture in a Fernbach flask was an inoculum for each 24-L fermentor batch. A typical inoculum is started from 1-2 confluent plates and this culture grew to a density of ~200 Klett units in 5-7 hrs when grown on Burk's media plus 20 mM urea in Fernbach flasks. Depending on the cell density, 150-500 ml of inoculum are added aseptically to 24-L of pre-sterilized Burk's media. Filter-sterilized phosphate buffer and urea was added at the same time as the inoculum. Fermentation consists of overnight (12-18 hrs) growth at 30°C, a 300 rpm agitation rate, and a 20-30 L/min aeration rate. Derepression of the culture was accomplished, using a membrane cassette filter apparatus, which filters the cells from the urea-containing media and concentrates the cell culture volume in the process. A 24-L batch is usually concentrated to less than 2 L. It is then washed 2-3 times with 2 L of phosphate buffer while still in the fermentor with concentration back to below 2 L after each wash. After the washing with phosphate buffer, the fermentor cell culture is replenished with 24 L of Burk's nitrogen-free media and the culture is allowed to derepress for 3-4 hrs. After derepression, the cells are harvested by concentration to ~1 L, using the membrane cassette filter, and then washed with 5 L of 50 mM Tris buffer, pH 8.0. The concentrated cell culture is then transferred to 500 ml centrifuge bottles and centrifuged in the Sorvall RC-5B in a GS-3 rotor at 6,000 x g for 15-20 min. The cell pellets are scraped into large plastic zip-lock bags and stored in the -80°C freezer.

5. ^{57}Fe-Incorporation Growth

In order to produce nitrogenase samples for analysis by Mössbauer spectroscopy, *A. vinelandii* strains were grown in the fermentor using the non-radioactive iron isotope, ^{57}Fe, as the sole source of iron in the media. This procedure was identical to the previously described fermentation method with the exception that the Fe was prepared

from a solid metal sample and the concentration of Fe in the media was 10 μM. ^{57}Fe solid was dissolved by boiling of a small piece of the metal (typically 27 mg) in a small volume (5-10 ml) of a mixture of 50% HCl and 50% HNO_3. The ^{57}Fe solid was completely dissolved in acid within 30 min or less. Typically, the amount of Fe dissolved equaled the amount needed to bring the concentration of a 24-L fermentor batch to 10 μM of ^{57}Fe. If a strain could grow diazotrophically, then just one nitrogen-free, ^{57}Fe-incorporated batch would be produced in order to minimize the expense of using the isotope during both repressed (+ urea) and derepressed (- urea) growth.

C. Crude Extract Preparation

A. vinelandii cells were broken open and their cytosolic extract was separated by a one of two procedures. However, additional steps may be included depending on the amount of cells and the fragility of the nitrogenase component proteins.

1. Sonication or Homogenization

For 400 g or less of cell paste, sonication in glass rosette cells was the usual course of action. Cell paste was resuspended in 50 mM Tris buffer, pH 8.0, 1-2 mM sodium dithionite ($Na_2S_2O_4$) in the range of 1:1 to 3:1 ratio of ml of buffer per g of cells. A model XL2015 sonicator (Heat Systems Inc., Farmingdale, NY) was mounted in a sound-dampening polyacrylic box. A low oxygen atmosphere was maintained by flushing the rosette cell with argon both prior to and during sonication. Small-scale sonication was performed in the 10-ml rosette cell using the micro-probe and a 50% power output. Sonication consisted of 5-7 cycles of 30 sec on/off intervals in order to minimize heating when the probe is activated. Heating was also minimized by immersion of the rosette cell in a ice water bath. Large-scale sonication was performed in the 200 ml rosette cell, using the large probe, with 100% power output. Sonication consisted of 6-7 cycles of 1 min on/off intervals. After sonication, the crude extract was transferred to a degassed, argon-flushed Schlenk flask if the DNase/RNase and/or heat treatment steps were required. The extract was drawn from the rosette cell through a large-bore transfer

line by applying a slight vacuum to the Schlenk flask connected to the other end of the line. Alternatively, the extract was transferred directly into 10, 30, or 70 ml argon-flushed ultracentrifuge tubes using a syringe rinsed with dithionite-containing buffer.

For cell amounts larger than 400 g, cells were homogenized using a Manton-Gaulin homogenizer. The cell paste was resuspended as described above, however, the total volume of cells plus buffer could be brought up to 1.5 L, if necessary. Dilute suspensions improved the percentage of broken cells by homogenization. The homogenizer was rinsed with chilled, dithionite-reduced 50 mM Tris buffer, pH 8.0, and all open vessels of the homogenizer were flushed with argon gas. Cell extract was passed through the homogenizer twice operating at a pressure of 10,000 psi. The resulting effluent was dark brown and was collected in a 2 L Schlenk flask that was also continually flushed with argon gas.

2. Nuclease and Heat Treatment

For nitrogenase component proteins that could tolerate the treatments, optional purification steps were available. The first option was a 30-min room-temperature incubation of the crude extract in the presence of 10 mg/L of both RNase and DNase. This procedure improved the clarification of the supernatant. The second option was a 5-min, 50-55°C heat step, followed by immediate immersion of the Schlenk flask and extract in an ice water bath to bring the extract temperature rapidly down to ~15°C. This second step removed approximately 50% of the soluble proteins from the extract during the centrifugation step.

3. Ultracentrifugation

The soluble cytosolic fraction of the crude extract was separated from the insoluble cellular debris by ultracentrifugation for ~90 min at 98,000xg and 4°C in a Beckman L5-50B ultracentrifuge (Beckman Instruments, Inc., Palo Alto, CA). The nitrogenase component proteins are located wholly in the dark brown supernatant that results as a consequence of centrifugation. This supernatant is typically transferred under

argon flushing to another degassed Schlenk flask or separatory funnel for further processing.

D. Protein Purification

1. Chromatographic Separation of Nitrogenase Components

Crude extract was typically in the volume range of 300-400 ml and had a protein concentration of 30-50 mg/ml. The crude extract was loaded onto either DEAE-cellulose (Whatman Biosystems Ltd., Maidstone, Kent, UK) or Q-Sepharose (Pharmacia LKB, Uppsala, Sweden), typically 5 x 15-20 cm. The column had been pre-equilibrated and made anaerobic by washing with ~4 L of 25 mM Tris, 1-2 mM dithionite, pH 7.4. Q-Sepharose column equilibration buffers also contained 50 mM NaCl to limit the strength of binding of dithionite to the column. Prior to crude-extract loading, the anaerobicity of the column was confirmed using 1 mM methylviologen- soaked filter paper, where development of a deep blue color indicates the presence of dithionite in the column effluent. The extract was loaded by a Rabbit Plus peristaltic pump (Rainin, Instruments Co. Inc., Woburn MA) at a rate of ~400 ml/hr. The loading was followed by a 1-2 column volume wash with 25 mM Tris buffer, pH 7.4, 2 mM dithionite, or until the zero baseline was re-established on the in-line UA-5 Absorbance/Fluorescence Detector (ISCO Lincoln, NE). The detector had a 5 mm pathlength detector cell with a 405 nm filter, which allowed detection of yellow-to- brown colored proteins. This method of detection is ideal for Fe-S cluster-containing proteins and was used exclusively throughout the nitrogenase purification schemes.

After the 25 mM Tris wash, a linear salt gradient was initiated using an additional peristaltic pump that added a 25 mM Tris, 1M NaCl (pH 7.4) solution into the low (50 mM) or salt-free buffer at half the rate of the pump loading onto the column. By this technique, a linear NaCl gradient passed over the column and resulted in separation of the MoFe and Fe proteins. On a DEAE-cellulose column, the gradient ranged from 0 to 0.5 M NaCl and the MoFe protein eluted at ~0.2-0.25 M NaCl, while the Fe protein elutes at ~ 0.3-0.35M NaCl. The strong anion exchanger, Q-Sepharose, utilized a 0.05 to 1.0 M

NaCl gradient where MoFe protein released at ~0.3-0.35 M NaCl, and the Fe protein eluted at 0.45-0.5 M NaCl. The two nitrogenase component proteins were collected in separate anaerobic Schlenk flasks, and each protein fraction was concentrated and then frozen in droplet form in liquid nitrogen. This method of anaerobic, low temperature storage was used for all nitrogenase proteins at all stages in their purification, with little or no loss of activity known to occur over years of storage. Concentration was achieved by use of 200 ml capacity Amicon stirred-cell, molecular weight cut-off (MWCO), membrane concentrators (Amicon Inc., Beverly, MA). These cells were made anaerobic by rinsing the cell with dithionite-reduced buffer. Anaerobiosis was verified by methylviologen paper. The MoFe protein was concentrated with a 100K MWCO membrane, while the Fe protein was concentrated via a 30K MWCO membrane.

2. MoFe Protein Purification

Further purification of the MoFe protein fraction involved multiple options that exploit a variety of physico-chemical properties of this protein.

a. Gel filtration chromatography - This method separates proteins based on molecular size and is a logical next step in purifying semi-pure protein mixtures. The MoFe protein fraction that elutes from the anion-exchange column contains some Fe protein as well as low molecular weight proteins. A large S-200 Sephacryl (Pharmacia LKB, Uppsala, Sweden) column (7.5 x 50 cm) or S-300 Sephacryl column (5 x 50 cm) was typically employed at this stage due to the relatively large amount of protein (~1.5-2.0 g.). The gel filtration columns were equilibrated and run in a 25 mM Tris, pH 7.4, 200 mM NaCl, and 1-2 mM dithionite buffer. The salt is necessary to limit protein-protein aggregation or precipitation, which would decrease separation over the column. The estimated molecular mass of MoFe protein is nearly four times that of Fe protein so it migrates faster than the Fe protein over a S-200 or S-300 Sephacryl column. A typical elution profile from one of these gel filtration columns consists of one large absorbance peak with one or two shoulders on either side of the apex. Thus, three or four fractions of ~50-100 ml were collected separately from this single major peak and associated shoulders, and the fractions with the best activity were selected for further purification.

b. Hydrophobic interaction chromatography - This separation technique relies on the presence of aliphatic and aromatic side groups on the surface of proteins including soluble, cytosolic proteins such as the nitrogenase component proteins. This technique relies on relatively weak binding interactions between the hydrophobic sites in the column resin and the hydrophobic patches on the protein surface. Therefore, this technique is only useful as a final purification step in this instance because the resin capacity is low and the separation of samples is diffuse. Some MoFe protein fractions from the gel filtration column were chromatographed over a ~ 100 ml (2.5 x 15-20 cm) Phenyl-Sepharose column (Pharmacia LKB, Uppsala, Sweden), which was pre-equilibrated with 2-4 L of 25 mM Tris, pH 7.4, 400-500 mM $(NH_4)_2SO_4$, 1-2 mM dithionite buffer. The addition of ammonium sulfate is necessary for binding of the relatively hydrophilic MoFe protein to the hydrophobic phenyl group on the resin matrix. The high concentration of ammonium sulfate forces an interaction to occur by the salting-out effect, which is the result of competition between the salt ions and the dissolved protein molecules for the molecules of solvation. Under high salt concentrations the strength of hydrophobic interaction between protein and the column resin phenyl groups are greater than the forces of protein hydration. The MoFe protein sample is diluted with a highly concentrated $(NH_4)_2SO_4$ solution in order to bring the sample to an equal salt concentration as the pre-equilibrated column, typically 350-500 mM $(NH_4)_2SO_4$. Proteins are eluted from the Phenyl-Sepharose column by a decreasing $(NH_4)_2SO_4$ gradient. A MoFe protein fraction was eluted near the end of the decreasing salt gradient at 0-0.1M $(NH_4)_2SO_4$. This peak was typically broad and of low absorbance, and was collected into two or three separate fractions. Each fraction was concentrated using an Amicon cell fitted with a 100K MWCO membrane, and the resulting concentrated sample was then frozen into liquid nitrogen in droplet form. A typical yield at this stage ranged from 50 to 100 mg of pure MoFe protein when starting from ~200 g of *A. vinelandii* cells. Purity was assessed by a combination of SDS-PAGE, specific activity enhancement, and metal analysis. The highest activity fraction was exchanged into 25 mM HEPES, pH7.4, 200 mM NaCl, 10 mM $MgSO_4$ buffer by either dialysis or a P6-DG desalting column (Bio-

Rad, Hercules, CA). The MoFe protein in this highly purified state was used for all structural, kinetic and spectroscopic characterizations.

c. Hydroxyapatite Chromatography

An alternative purification method was necessary for some of the more fragile forms of altered MoFe proteins, because the hydrophobic interaction technique resulted in mostly inactive protein. Hydroxyapatite chromatography provided the needed separation resolution without subjecting the protein sample to inactivating conditions. Hydroxyapatite can act as a weak anion or cation exchange resin, depending on the nature of the sample and the elution buffer. The resin consists of $Ca_3(PO_4)_2$ bound to a ceramic matrix, so the Ca^{2+} group can act as an anion exchanger and PO_4^{3-} group can act as a cationic exchanger. Due to the weak interaction between protein and hydroxyapatite, the binding capacity was very low and a large column volume was necessary. An approximately ~300 ml (5 x 15 cm) HA-Ultrogel column (IBF Biotechnics, Villeneuve-la-Garenne, France) was pre-equilibrated with ~4 L of 50 mM potassium phosphate buffer, pH 6.8, 1-2 mM dithionite. The protein sample was diluted to this same initial phosphate concentration prior to loading. The MoFe protein was eluted from the column using a 50-500 mM phosphate linear gradient, and came off as a broad dilute peak between 250 and 300 mM phosphate. Subsequent hydroxyapatite purifications utilized a step gradient of 150, 300, and 500 mM phosphate, where the MoFe protein eluted from the 300 mM step as a sharp, concentrated peak. Yields from this chromatographic step were similar to the hydrophobic interaction method, and had similar purity levels. The hydroxyapatite eluted fraction was concentrated and stored in liquid nitrogen by the aforementioned procedure.

d. Crystallization of MoFe protein - A method for microcrystalline precipitation of highly purified wild-type MoFe protein was developed in the past (Burgess *et al.*, 1980) and was used when maximally active MoFe protein was required. This technique starts with the concentration of a sample (typically with specific activity ≥1,800 nmoles H_2 $(min \cdot mg\ MoFe\ protein)^{-1}$) to ≥100 mg/ml. The protein is then diluted or dialyzed to a

NaCl concentration of ~25 mM at which point the sample appears cloudy due to protein precipitation at low salt concentrations. The sample is then transferred to anaerobic Beckman 30-ml capacity centrifuge tubes and, after a 1 hr incubation at 38°C, the sample is centrifuged in a Sorvall SA-600 at 20,000xg for 20 min again at 38°C. The pellet that forms is the pure MoFe protein and, after removal of the black, inactive supernatant, the pellet is rinsed with 25 mM Tris, pH 7.4, 25 mM NaCl buffer and centrifuged again for 20 min at 38°C. The supernatant is typically colorless and is discarded, while the pellet is resuspended with cold 25 mM Tris, pH 7.4, 250 mM NaCl buffer by maceration of the pellet with a canula and light vortexing. The resuspended pellet is centrifuged a final time at 20,000xg and 4°C for 20 min. This centrifugation typically results in a small whitish pellet, which is discarded, and a dark brown supernatant. The supernatant contains high purity MoFe protein with maximal activity in the range of 3,000 nmols H_2 (min·mg MoFe protein) $^{-1}$.

3. Fe Protein Purification

The Fe protein fraction, which separates from the MoFe protein fraction on anion-exchange, usually requires one or two more purification steps in order to obtain a sample with high specific activity (typically ≥2,000 nmoles H_2 (min·mg MoFe protein)$^{-}$1) for use in assays. The Fe protein fraction is purified via a second anion-exchange column, with the best results obtained from a Q-Sepharose column. Because the Fe protein fraction eluted from the first column in high salt (i.e., 400-500 mM NaCl), the fraction was diluted with 25 mM Tris buffer to reduce the salt concentration to ~100 mM prior to loading. A smaller Q-Sepharose column (~100 ml., 2.5 x 20 cm) was employed for the second step because the protein loading was substantially less than the first crude extract loading. An increasing NaCl gradient from 0.05 M to 1.0 M was utilized to elute the Fe protein from the column. A large absorbance peak was preceded by a smaller one, which contained contaminating MoFe protein. The larger peak eluted at 400-450 mM NaCl and was mainly Fe protein and some flavodoxin. The Fe protein peak was collected into 3-4 separate fractions. These fractions were concentrated using an Amicon cell fitted with a

30K MWCO membrane, and were stored in liquid nitrogen. The best activity fractions (2,000-2,500 nmols H_2 (min·mg Fe protein) $^{-1}$) were typically from the down slope side of the eluted peak and these fractions are buffer exchanged into 25 mM HEPES, 0-100 mM NaCl, 10 mM $MgSO_4$ as previously described.

4. Metal Affinity Chromatography

A recently developed protein purification technique has been exploited in order to expedite the purification of the MoFe protein from *A. vinelandii*. The method is particularly suited for isolation of altered forms of the MoFe protein that appear to be more susceptible to inactivation by protein denaturation and/or metallocluster extrusion. The method employs attaching a poly-histidine tail to the carboxy-terminus of the α-subunit of the MoFe protein. Poly-histidine polypeptides are known to bind selectively divalent metal cations, and this discovery was the basis for the creation of this purification method (Van Dyke *et al*., 1992). Metal affinity chromatography resin is saturated with a divalent metal salt and the bound metal ion acts as an exchange site for the retention and elution of proteins possessing the poly-His motif. Ni^{2+} is a particularly strong exchange site so $NiSO_4$ was chosen for MoFe protein purification.

The procedure used in purifying poly-His-modified MoFe proteins was taken from the His-Bind® Resin manufacturers recommendations (Novagen Inc., Madison WI). All metal affinity chromatography solutions consisted of various concentrations of imidazole combined with a 20 mM Tris, pH 7.9, 200-500 mM NaCl buffer solution. Dithionite was excluded from all solutions that would come in contact with the column because of the potential production of NiS precipitate. Therefore, all buffers were degassed thoroughly and the metal affinity column was run in an anaerobic glovebox (Vacuum Atmospheres Co., Hawthorne, CA). Preparation of the crude extract proceeded by the prescribed method except that 0.2% sucrose was included in the resuspension buffer because this technique is thought to stimulate respiratory protection of the nitrogenase component proteins. After centrifugation, the ultracentrifuge tubes were taken into the glovebox and the supernatants were pooled and then loaded onto the 50 mM $NiSO_4$-saturated metal

affinity column. The column had a typical resin volume of ~100 ml (2.5 x 20 cm) for ~200 g of frozen cell paste. This column would be pre-equilibrated overnight with 8-10 column volumes of the 20 mM Tris buffer containing 5 mM imidazole. Imidazole, which is the side group of the amino acid histidine, was used in a step gradient to separate the poly-His MoFe proteins from other column-bound proteins. After loading, the column was washed with 5 mM imidazole-containing 20 mM Tris buffer until the column effluent was clear. Next, the column was treated with a 40-60 mM imidazole, 20 mM Tris buffer, which resulted in the elution of a light brown band during the first 100 ml of this wash buffer. This fraction had very little MoFe protein activity in it. The column was washed with more 40-60 mM imidazole, 20 mM Tris buffer until the effluent was relatively clear as determined by visual inspection. The poly-His MoFe protein was eluted from the column using 250 mM imidazole, 20 mM Tris buffer. A dark brown band eluted during the first 100 ml of this elution buffer.

For some altered MoFe proteins, the metal-affinity-purified fraction was collected into salt-free, 2 mM dithionite-reduced Tris or HEPES buffer in order to dilute the imidazole and NaCl concentrations by 4-5 fold. This fraction could then be removed from the glovebox and purified further by anion-exchange chromatography. The yield from the metal affinity column was in the range of 150-300 mg. Thus, a small DEAE-Sepharose (Pharmacia LKB, Uppsala, Sweden) column of ~ 30 ml (1.5 x 15-20 cm) was adequate to bind and separate the remaining contaminants from the MoFe protein. The MoFe protein eluted from this column as one large peak, which was collected as three separate fractions, each of which was concentrated in an Amicon cell, and then stored in liquid nitrogen. The best activity fraction was usually the middle fraction, which yielded 50-200 mg of high specific activity MoFe protein. This entire procedure could be accomplished in 12-16 hrs as opposed to the 6-8 days required for the traditional purification procedure.

5. Determination of Protein Purity

At each stage of the purification process, it was necessary to establish the level of purity of the various fractions that were collected separately as they eluted from each

chromatography column. Both qualitative and quantitative methods were utilized to substantiate purity.

a. SDS-PAGE - This method was the most qualitative but was also the quickest and easiest method for estimating and comparing the purity of fractions. A model SE250 mini-gel apparatus (Hoefer Scientific Instruments, San Francisco, CA) utilized the discontinuous gel electrophoresis method (Laemmli, 1970). Optimal resolution conditions were obtained from a 4% T (total acrylamide) and 0.1% C (cross-linker) stacking gel and a 12% T, 0.32%C separating gel. Samples were denatured by boiling in SDS- and β-mercaptoethanol-containing buffer (5 min), and then 5-20 μg were loaded into each well. Mini-gel dimensions were 1.5 x 60 x 80 mm, and electrophoretic runs were 1-1.5 hrs. at 25-30 mA constant current with tap water cooling of the central core. Gels were stained at room temperature from 2-16 hrs. in a 0.1% R-250 Coomassie blue stain (Bio-Rad Laboratories, Richmond, CA), destained in a mixture of 40% methanol and 10% acetic acid, and then stored in 5% methanol, 7% acetic acid. A 667 instant film Polaroid photograph (Polaroid Corp., Cambridge, MA) was taken as a permanent record of each gel.

b. Specific activity - Protein were estimated using the Lowry method with the Folin-Ciocalteau modification for increased protein sensitivity (Lowry *et al*., 1951). Protein samples were routinely diluted 50 to 100-fold with distilled water to bring them into the linear range of the standard curve, i.e., 20-100 μg/ml. A bovine serum albumin (BSA) stock solution (1 mg/ml in 1% NaCl) was used to generate a standard curve, and an appropriately-diluted buffer blank was used to zero the model 8452 Diode Array Spectrophotometer (Hewlett-Packard, Palo Alto, CA). Absorbance readings at 750 nm were taken in disposable 1 cm pathlength cuvettes after uniform color development was achieved in ~35 min. Protein concentration calculations were via the spectrophotometer software package.

Specific activity measurements were obtained from steady-state H_2 evolution or C_2H_2 reduction assays. Either assay was adequate for highly purified protein fractions.

However, crude extract fractions required C_2H_2 reduction analysis because of the potential H_2 uptake activity in these extracts.

The substrate reduction rate, measured in nanomoles of product evolved per minute, was divided by the known amount of protein in the assay, calculated from the product of protein concentration and volume used in the assay. The resulting value was the specific activity for a particular product and protein. For purified component proteins, the specific activity was based on the concentration of the nitrogenase component, either Fe or MoFe protein, that was limiting in the assay. In crude extract assays, the activity measurement was based on the total protein contain of the extract because the actual percentage of nitrogenase was unknown.

c. Purification Table - Because some of the site-directed mutant strains produced nitrogenase component proteins with significantly reduced activity, a fair measure of purity was gained by comparison of activities between wild-type and altered proteins at various stages of purification. If the nitrogenase proteins from wild-type and mutant strains were purified by identical methods, then at each stage of the purification scheme, the specific activity should have retained the same relative ratio. Also, if the nitrogenase proteins from wild-type and mutant strains were equally responsive to the derepression process and were equally stable to the various purification strategies, then the total amount of protein should have been relatively equal throughout the purification scheme. The simplest way to compare the purity of the nitrogenase proteins from different strains at each stage of the purification is by means of a purification table. Such a table listed categories of total protein, total activity, specific activity, yield, and fold purification (see Section III.B).

d. Metal estimation - An alternative quantitative indicator of nitrogenase purity was gained from the metal concentration of the proteins. By measuring the molybdenum and/or iron concentrations from a known concentration of protein, it was possible to estimate the number of metal atoms per molecule of MoFe or Fe protein. Ideally, a pure sample of MoFe protein will have 2 g-atoms of Mo and 30 g-atoms of Fe per mole of protein. The closer a MoFe protein sample came to these ideal numbers for metal

content, the purer the sample was. The exception to this rule was MoFe proteins with substitutions that affect the synthesis, insertion, or ligation of the metalloclusters. These MoFe proteins may not have a full complement of clusters relative to the protein concentration, thus, even a highly purified sample could have metal concentration values far below the ideal amounts. The relative concentration of Mo and Fe in a MoFe protein sample was also used to estimate the concentration of the two types of metal centers, the FeMo-cofactor and the P cluster. Ideally, a sample had a Mo:Fe ratio of 1:15 if both cluster types were found in equal proportion. A significant deviation from this ratio may be evidence for loss of one cluster type.

Purified MoFe protein samples were analyzed for metal content using inductively coupled plasma atomic emission spectrometry (ICP-AES). All metal analyses were performed by J.T. Rinehart (Dept. of Human Nutrition and Foods, Virginia Tech) using a Plasma 400 Emission Spectrometer (Perkin-Elmer, Rockville, MD). Samples generally consisted of 5 mg of purified protein in 5 ml of 25 mM HEPES, pH 7.4, 200 mM NaCl buffer. This concentration and volume allowed for at least three replicate quantitations for Mo and Fe each with metal amounts significantly above the detection sensitivity of the equipment. Results were recorded as parts per million (ppm) of either Mo or Fe, which after subtraction of a buffer blank, were then converted into concentrations to yield g-atoms of Mo or Fe per sample.

6. FeMo-cofactor Reconstitution

In order to ascertain if the apoprotein of the α-Cys88 altered MoFe proteins was reactivatable by FeMoco insertion, a FeMoco reconstitution experiment was performed on the crude extracts of each strain. Prior to the FeMoco reconstitution experiment the FeMoco from wild-type *A. vinelandii* MoFe protein was extracted using a modification of the original published method (Shah & Brill, 1977).

a. FeMoco extraction - Purified MoFe protein was diluted with enough degassed, 2 mM dithionite distilled water to bring the protein concentration to ~5 mg/ml. The protein solution was kept on an ice water bath and the pH titration was monitored the a pH meter probe inserted through a side port of a three-armed round bottom flask. The

solution was continually flushed with argon throughout the procedure. The dilute MoFe protein solution was titrated to a pH of 2.2 with 0.25 M HCl and allowed to stand for 3 min. The solution was then titrated back up to pH 5.5 with 0.25M NaOH and allowed to stand on ice for 25 min.

The solution was transferred to 40 ml round bottom glass centrifuge tubes fitted with rubber stoppers and that had been previously degassed and flushed with argon. Balanced pairs of tubes were subjected to a Jouan refrigerated table top centrifuge at 900 rpm for 10 min and 4°C. The supernatant was discarded and 10 ml of cold dimethylformamide (DMF) was added to each tube and then vortexed briefly to resuspend the pellet. The tubes were centrifuged again in the Jouan at 1600 rpm for 10 min and 4°C with the brake off. The supernatant was again discarded and the DMF wash procedure was repeated.

To each tube 6 ml of 2 mM dithionite, alkaline (pH ~9-10) n-methylformamide (NMF) was added. The tubes were vortexed for 5 min and spun in the Jouan at 2200 rpm for 10 min and 4°C with the brake off. The supernatant from the spins was saved in a degassed and argon-flushed Schlenk flask. The centrifugation pellets were then washed with 4 ml of the alkaline NMF and the rest of the procedure was repeated. The second supernatant was pooled with the first. The NMF solution was dark green due to the presence of the FeMoco. The pooled supernatants were transferred to anaerobic 12 ml glass, conical centrifuged tubes, fitted with rubber stoppers and sealed with Saran wrap. The tubes were centrifuged in the Jouan at 3000 rpm for 30 min and 4°C with the brake off. The supernatant from this spin was transferred to a separate clean degassed and argon flushed Schlenk flask which was sealed and covered with Saran and placed in the -80°C freezer overnight.

The FeMoco/NMF solution is concentrated to a few ml via an anaerobic condensation apparatus. The cofactor solution and condenser apparatus were both taken into the anaerobic glovebox for assembly. Inside the glove box, the cofactor solution was transferred to a pear-shaped 150 ml flask, which was then attached to one end of the

condenser. After assembling the condenser and ensuring that all connections were sealed, the apparatus was removed from the glove box. The opposite end of the condenser consisted of a 250 ml Schlenk flask that was immersed into a dewar with liquid N_2, whereas the FeMoco-containing flask was immersed in a 35°C water bath. The Schlenk flask was attached to a direct drive vacuum pump and the condenser was recirculated with ice-cold water. This system allowed for boil-off of the volatile NMF solution by the water bath and vacuum, condensation of the NMF vapor as liquid by the condenser, and trapping of the condensed liquid NMF in as solid in the liquid N_2-cooled Schlenk flask. The entire condenser apparatus was then taken back into the glovebox where the concentrated FeMoco was aliquoted into 50 µl, 100 µl, and 200 µl volumes and stored in the -80°C freezer .

b. FeMoco Reconstitution Assay - The assay consisted of an incubation of the crude extract from a strain producing a potentially FeMoco-less MoFe protein and purified FeMoco. A volume of the crude extract that was adequate for the entire set of assays was taken into the anaerobic glovebox along with an aliquot of NMF-extracted FeMoco. A volume of FeMoco extract equal to 5% of the final total volume was added to the crude extract. The 5% limit was important because NMF can inhibit the nitrogenase reaction when concentrations exceed this limit. The crude extract-FeMoco mixture was allowed to incubate at room temperature for ~30 min. after which time a standard H_2 evolution (see Section II.E.1) or C_2H_2 reduction (see Section II.E.2) assay was performed. The crude extract was assayed in the presence and absence of added FeMoco extract in order to determine it's capacity for reconstitution of activity. Crude extract was assayed instead of purified MoFe protein because the reconstitution event requires the Fe protein, and ATP which were present in the crude extract.

E. Steady-state Assays of Purified Products

Once the purity of the nitrogenase component proteins was determined, the protein of interest was subjected to a battery of steady-state assays. All of the assays used have been well established in the characterization of wild-type nitrogenase.

1. H_2 Evolution

This assay was one of the two routinely used methods of measuring the hydrogenase activity of the nitrogenase complex. All assays were performed at 30°C in 9 ml septa-sealed vials containing the nitrogenase component proteins, sodium dithionite, an ATP-regenerating system, and an anaerobic, argon flushed gas atmosphere of ~1 atm. pressure. The precise procedure was outlined in the steps below.

a) The MgATP-regenerating system (also referred to as reaction mix) consisted of a final concentration of 2.5 mM ATP, 5 mM $MgCl_2$, 30 mM creatine phosphate, and 25 units of creatine phosphokinase (CPK) in 25 mM HEPES buffer. Each assay vial contained 0.3 ml of a 3.3 x reaction mix stock and enough distilled water to bring the total assay mixture to 1 ml. All vials were kept on ice both to minimize turnover of the regenerating system and to prevent denaturation of CPK during preparation.

b) The vials were then capped by crimping an aluminum seal over the rubber septum. The vials were subjected to five alternating cycles of 100 sec of vacuum-degassing and 10 sec of argon-flushing via a custom-made vacuum/gas manifold (Corbin, 1978).

c) During the preceding step, a 200 mM $Na_2S_2O_4$ solution was anaerobically prepared by addition of argon-flushed 25 mM HEPES buffer (~5 ml) to an argon-flushed vial containing the solid dithionite. The nitrogenase samples were removed from their liquid nitrogen storage and allowed to thaw in 1 ml crimp-sealed vials with argon-flushing through a vent needle placed in the septa-sealed top of the vial.

d) After the vials had been degassed and argon-flushed, they were placed back on ice and 100 μl of the 200 mM dithionite solution was added to each vial using a gas-tight syringe (Hamilton Co., Reno, NV). One of the two nitrogenase component proteins, typically MoFe protein or crude extract, was added next.

e) The vials were then placed in a model G76 Gyrotory Water Bath Shaker (New Brunswick Scientific Co. Inc., Edison NJ), for ~4 min at 30°C. At this time, each vial was vented to atmospheric pressure by piercing the septum with a hypodermic 26-gauge syringe needle. The needle was attached to a barrel-less syringe body with ~0.5 ml of distilled water in it to allow for visual monitoring of gas-venting by the formation of bubbles in the water. The venting apparatus was removed when bubble formation ceased.
f) The second nitrogenase component, usually purified Fe protein, was then added to each vial to initiate the nitrogenase catalytic reaction. Homogeneous mixing was ensured by swirling of the 1 ml reaction solution before replacement in the water bath.
g) After a preset time interval, reactions were stopped by addition of 250 µl of a 30% trichloroacetic acid or 500 mM EDTA solution by injection of the solution through the septa-seal.
h) The gas contents of each assay vial were analyzed by removal of a 200-400 µl gas sample using a Pressure-Lok, lockable gas-tight syringe (Precision Sampling Corp., Baton Rouge, LA), and injection of the sample into a Model 8A gas chromatograph (Shimadzu, Kyoto, Japan) fitted with a thermal conductivity detector (katharometer). H_2 produced during the nitrogenase reaction was determined by separation of the gas sample components over a 1 m x 2 mm I.D. molecular sieve 5-❹, 60/80 mesh column (Supelco Inc., Bellefonte, PA) operating at an oven temperature of 40°C. Argon was the carrier gas at a flow rate of ~60 ml/min. Peak heights were recorded and peak areas were integrated by a CR501 Chromatopac integrator (Shimadzu, Kyoto, Japan). Peak areas were calibrated by reference to a 1% H_2 in N_2 standard (Scott Specialty Gases, Plumsteadville, PA), and H_2 was identified by retention time and distinguished from O_2 and N_2 peaks as they passed through the detector.

2. C_2H_2 Reduction

The procedure for this steady-state assay of substrate reduction activity was essentially the same as the H_2 evolution assay with the following exceptions.

a) The gas atmosphere of the anaerobic assay vials was 10% C_2H_2/90% Ar. This assay requires preparation of C_2H_2 gas by the reaction of CaC_2 with water. After the venting of excess Ar pressure, 1 ml of C_2H_2 gas was added to each assay vial, and the vials are replaced in the shaker water bath for ~4 min. at 30°C. These vials were then vented to atmospheric pressure prior to initiation of the enzymatic reaction.

b) Assay samples were analyzed for C_2H_4 production on a model GC-14A gas chromatograph (Shimadzu, Kyoto, Japan) equipped with a flame ionization detector. A 200 µl gas sample was removed from each assay vial and injected into a 3 m x 2 mm Porapak N (Supelco Inc., Bellefonte, PA) column operating at a column oven temperature of 80°C and a helium carrier gas flow rate of ~95 ml/min. The injector temperature was set at 180°C, and the detector temperature was 200°C. The C_2H_4 peak eluted after 1.1 min and peak area was calibrated using a C_2H_4 gas standard of 1000 ppm C_2H_4 in He. A 200-400 µl gas sample was then assayed for H_2 content over the Shimadzu GC-8A gas chromatograph as previously described.

3. NH_3 Production

Nitrogenase ammonia production was assayed by a modification of the indophenol method (Chaney & Marbach, 1967). Although this colorimetric assay was specific and very sensitive, it was also prone to interference by reagents used in the nitrogenase *in vitro* catalytic reaction, e.g. dithionite ion, Tris buffer, and creatine. Interference by Tris buffer explains the need for buffer exchange into HEPES buffer for all purified nitrogenase component proteins. An improvement to the indophenol method (Dilworth *et al.*, 1992) included the passage of the liquid contents of a nitrogenase reaction vial over a Bio-Gel AG 1-X2 (Bio-Rad, Hercules, CA) anionic exchange resin. The resin removed most of the inhibitors of the color development reaction. Individual disposable columns (2.5 cm x 0.6 cm dia.) were used for each assay sample and were made from glass Pasteur pipettes plugged with Pyrex fiberglass wool (Corning Inc., Corning, NY). The nitrogenase enzymatic turnover phase of the ammonia assay was identical to both the H_2 evolution and C_2H_2 reduction assays with the exception that the

assay vials were evacuated and then flushed with N_2 instead of Ar. Because H_2 was an obligate product of N_2 reduction, gas samples were first injected onto the GC-8A gas chromatograph. The H_2 content was a useful value to have prior to ammonia estimation because the amount of ammonia produced during the reaction was predicted from the quantity of H_2 produced. The colorimetric detection procedure is described below.

a) After uncapping the assay vials, 0.5-1.0 ml of the reaction mixture was removed and loaded onto distilled water-rinsed Bio-Gel AG 1-X2 columns. Each column was then rinsed with two 0.5 ml aliquots of distilled water to ensure elution of ammonia.

b) A fraction of the column effluent was added to disposable 13 mm x 100 mm glass test tubes and the volume was brought up to 1.0 ml with distilled water. This procedure was done in duplicate for each assay vial mixture.

c) A 0.3 ml of a 5% phenol, 2.5% NaOH sodium phenate solution was then added to each test tube, followed by the simultaneous addition of 0.45 ml of 10% sodium hypochlorite and 0.45 ml. of 0.02% sodium nitroprusside. The phenate and hypochlorite combined with ammonia to produce a blue color, while the nitroprusside acted as a catalyst to increase the speed, intensity and stability of the colorimetric reaction.

d) After a 40 min incubation at room temperature, each sample was transferred to a 1 cm pathlength disposable cuvette and the sample's absorbance was measured at 630 nm in the model 8452 diode array spectrophotometer. Ammonia concentration was determined using an $(NH_4)_2SO_4$ standard curve, which was linear in the range of 0-400 nmols of NH_4^+.

e) Due to the presence of trace amounts of color-inhibiting substances in the assay, a spiked-blank was created and used as a color-inhibition correction factor for ammonia quantitation. A spiked-blank consisted of a nitrogenase activity assay that was inactivated with acid or EDTA prior to initiation of the enzymatic reaction. After passage over the exchange column, an appropriately diluted sample of this blank was added to a known concentration of ammonia standard and the indophenol reaction was carried out. The percentage decrease in absorbance of the spiked standard was the inverse of the

correction factor. The percentage decrease in absorbance was typically around 70%, thus a correction factor of 10/7 or 1.43 was applied to the ammonia concentration values.

4. ATP Hydrolysis Determination by Creatine Formation

For any steady-state assay containing the creatine phosphokinase ATP-regenerating system, ATP hydrolysis was measured indirectly by the creatine colorimetric detection method (Ennor, 1957). The protocol included the modification of using small anion exchange columns to remove interfering compounds from the nitrogenase reaction mix as described for the NH_3 assay. The enzymatic assays were always stopped with EDTA because addition of acid could result in hydrolysis of phosphocreatine, thus, giving false positive creatine estimations. All creatine fractions were kept on ice throughout the assay to minimize spurious generation of creatine after cessation of the enzyme activity assay. The complete procedure for creatine measurement is described below.

a) A 0.5 ml sample of each nitrogenase reaction mixture was applied to pre-rinsed anion exchange resin columns. Each column was rinsed twice with 0.5 ml of distilled water.

b) Anywhere from 50 to 200 μl of the column effluent was diluted to either 0.5 or 1.0 ml with distilled water in disposable 13 x 100 mm test tubes. Each sample was run in duplicate.

c) 1.0 ml of a 1% naphthol, 6% NaOH, and 16% $NaCO_3$ solution was added to each tube.

d) Addition of 0.5 ml of a 0.05% diacetyl solution initiates the colorimetric reaction.

e) After a 30 min incubation at room temperature, the creatine content was calculated by measurement of the absorbance of each sample at 530 nm in the spectrophotometer. A creatine standard curve ranging from 0 to 300 nmoles was used to calibrate the absorbance readings after correction of a killed blank.

5. Electron Flux Titration Assays

The response of the nitrogenase system to a varying electron flux has proven to be an important diagnostic of the overall mechanism. Alterations in total substrate reduction rates, ATP hydrolysis rates, and patterns of electron allocation to alternative products are some of the consequences of changing the electron flux of through nitrogenase. Electron flux was controlled by varying the molar ratio of Fe protein to MoFe protein in fixed total

protein activity assays. The total protein was fixed at either 0.5 or 1.0 mg per 1 ml assay mix. The amounts of Fe or MoFe protein varied in compensatory fashion to give the desired molar ratio while maintaining a constant total protein concentration. Electron flux ranged from a low flux-producing Fe protein:MoFe protein ratio of 1:10 to a high flux ratio of 80:1.

6. K_m for C_2H_2

The Michaelis constant, K_m, is the substrate concentration at which the specific activity of the enzyme of interest is half the value of the maximum specific activity (v_{max}). The value of K_m is an indirect indicator of the binding affinity of the substrate for the active site; the lower the K_m, the tighter the association between substrate and enzyme. The K_m for C_2H_2 was measured for wild-type and altered MoFe proteins as a probe for potential perturbations of the active site. The estimation of the K_m for C_2H_2 was obtained from nitrogenase activity assays in the presence of limiting C_2H_2 concentrations. The procedure is essentially the same as C_2H_2-reduction assay method except that non-saturating amounts of C_2H_2 were added to each vial. The volumes of gas added typically ranged from 5-1,000 μl of C_2H_2 with care to ensure that concentrations ranged about the K_m, from 5-10-fold higher to 5-10-fold lower. For each volume, duplicate assays were performed. Other than the amount of C_2H_2, each assay vial contained identical concentrations of nitrogenase activity assay reactants. The rate of C_2H_4 production was determined for each assay and a double reciprocal plot of substrate concentration versus specific activity of C_2H_4 production was constructed (Lineweaver-Burk plot). K_m and v_{max} values were derived from this plot. These values were reported in terms of atmospheres because of the difficulty in accurately measuring the concentrations of dissolved gases.

7. CO Inhibition

The pattern of CO inhibition of nitrogenase activity was discussed in section I.D.2.d. The comparison of wild-type and altered MoFe proteins in terms of their response to saturating (10%) concentrations of carbon monoxide was also employed as a

probe of disturbance of the enzyme active site. Nitrogenase activity assays were performed under the three gas atmospheres, 100% Ar, 10% C_2H_2/90% Ar, and 100% N_2, in the absence and presence of 10% CO. The procedure included the addition of 1 ml of 100% CO to assay vials containing the designated gas phase at atmospheric pressure. The assay vials were equilibrated in a shaker water bath for ~4 min at 30°C and then vented to atmospheric pressure prior to initiation of the enzymatic reaction.

8. NaCl Inhibition

The inhibitory effects of high salt concentrations on the substrate reduction rate by nitrogenase are well documented and discussed in Section I.E. Nitrogenase activity assays were performed in the presence of increasing concentrations of NaCl and the effect on maximum specific activity were recorded. The range of salt concentrations was 0-500 mM NaCl in addition to the amount of salt included in the purified nitrogenase component proteins. The desired salt concentration was provided by addition of the appropriate amount of a 5 M NaCl stock solution prior to the degassing/flushing step. All other parameters were equivalent for each activity assay sample. The assay results were plotted as the change in maximum specific activity with increasing NaCl concentration.

9. Limiting Dithionite

In a limiting dithionite assay, the final concentration of dithionite in each assay vial was either 0.5 or 1.0 mM. Under these conditions, the turnover of nitrogenase eventually consumed all of the available reductant by conversion of the supply of electrons into one or more substrate reduction products. Even if a particular altered MoFe protein had a decreased specific activity compared to wild-type MoFe protein, both proteins should generate the same total amount of product but over different periods of time. By following the time course for product evolution, it was determined whether all of the electrons from dithionite were accounted for in the form of product, i.e., whether or not there was an unknown product being formed by an altered MoFe protein.

10. C_2H_2 Concentration Titration

High concentrations of acetylene in nitrogenase activity assays are known to cause a decrease in maximum specific activity. The procedure for these assays involved

evacuation of the assay vials and flushing with either 100% Ar or 100% C_2H_2, followed by dilution with either acetylene or argon, respectively. Using this technique, a complete titration of 0-100% C_2H_2 was produced. These assays could ascertain whether an altered form of the MoFe protein was inhibited by C_2H_2 and by how much.

F. Pre-steady-state Kinetics

The steady-state assay methods described in the previous section were useful in gathering information on components of the overall nitrogenase mechanism, such as rates of substrate reduction, rates of ATP hydrolysis, electron allocation to products, and the effects of inhibitors. Pre-steady-state kinetic analysis was necessary to detail the individual steps in the nitrogenase mechanism, i.e., to study the changes in, and rates of, processes occurring on the milliseconds scale. Because the nitrogenase reaction involved electron transfer events between metalloclusters with absorbance maxima in the visible range of the spectrum, spectrophotometry has proven to be a valuable and sensitive detection method for measurement of the catalytic reaction.

1. Stopped-flow Spectrophotometry

Stopped-flow spectrophotometry is ideally suited for the detection and analysis of the absorbance changes that take place on a millisecond time scale in the nitrogenase component proteins before they reach steady-state. An SF-61 stopped-flow spectrophotometer was used for pre-steady-state kinetic studies (HiTech Scientific Ltd., Salisbury, UK). This unit consisted of a thermostated SHU-61 handling unit and a two component spectrometer unit comprised of an M-300 variable wavelength monochromator and an MSU-6- electronics unit. Thermostatic control was achieved with a FC-200 Flow Cooler and a C-85D Circulator (both Techne Ltd., Duxford, Cambridge, UK). The recording, analysis and storage of the absorbance spectra was via a computer equipped with IS-1 rapid kinetic analysis software. Due to the strict anaerobic environment required for the pre-steady-state assays, the handling unit resided in a high integrity glove box operating under an 100% N_2 atmosphere. Connections to the optical unit and temperature control apparatus were through sealed connections in the wall of the

glovebox. Glovebox anaerobicity was monitored by a model 316RA Trace Oxygen Analyzer (Teledyne Analytical Instruments, City of Industry, CA), and the N_2 atmosphere was purified, circulated and pressure regulated by a model M040-2 Dri-Train (Vacuum Atmospheres Co., Hawthorne, CA).

The handling unit consists of two gas tight 500 µl drive syringes that are encased in a thermostated observation chamber. The drive syringes were flushed and filled through the top of the unit where 1-5 ml reservoir syringes were attached via luer lock connections. The drive syringes were controlled either manually or by a pneumatic ram, which simultaneously pushed the syringe plungers upwardly from the bottom of the unit. The reactants in the two drive syringes were forced through a mixing chamber and into an observation cell and finally into the stopping syringe on the outside of the thermostatic chamber. The observation cell has an optional pathlength of either 2 or 10 mm and the volume between mixing and observation chambers resulted in a 1-4 msec "dead time". The dead time equals the time that the reaction has progressed from mixing till the first observation is made.

A typical stopped-flow shot was composed of 50 µl of reactant from each drive syringe, both of which are thermostated at 23°C. The optical unit was used to set the observation wavelength of 430 nm, which corresponded to the maximal change in absorbance of the Fe protein as it became oxidized by the MoFe protein. The length of observation was manipulated at the computer interface using the rapid kinetics software package. The number of data points taken in a single observation was fixed at 1,024, thus, the resolution between data points decreases for longer scans. When contact was made between the stopping syringe plunger and the stop block switch, the flow from the drive syringes was arrested, and the optical detection and recording devices were simultaneously activated. The sensitivity of the spectrophotometer was sufficiently high to detect absorbance changes as low as $\Delta A = 0.005$. Rate constants were obtained by curve-fitting the absorbance spectra from stopped-flow experiments to exponential functions using least squares minimization.

2. Primary Electron Transfer

As with most pre-steady-state experiments on the nitrogenase complex, the measurement of the primary electron transfer rate utilizes the 430 nm absorbance change of the Fe protein as its Fe_4S_4 cluster is oxidized from the +1 reduced state to the +2 oxidized state by the MoFe protein. The experiment consisted of an Fe protein-MoFe protein mixture in one drive syringe that was combined with MgATP from the other syringe. Both syringes contained dithionite and HEPES buffer. The molar ratio of Fe protein to MoFe protein is varied depending on the purpose of the experiment. The basic set-up of the primary electron transfer determination was exploited for different purposes.

a. Absorbance titration - This procedure was a necessary first step prior to calculation of the rate constant for primary electron transfer. The maximum absorbance was determined by increasing the molar ratio of a Fe protein-to-MoFe protein mix in the single drive syringe. The concentration of MoFe protein remained fixed whereas the concentration of Fe protein was increased until the change in absorbance that occurs upon mixing with MgATP saturates out. A molar ratio titration typically ranged from 1:1 up to a 6:1 Fe protein-to-MoFe protein ratio. Saturation of the absorbance increase occurred at about 4:1.

b. Estimation of the rate constant for primary electron transfer - The change in absorbance over the time course of the stopped-flow experiment resulted in an exponential curve. This curve was fit to a first exponential equation ($Y = -dY \cdot e^{-kx} + Y$) from which the rate constant for primary electron transfer, k_{+2}, was obtained. The absorbance curve saturated within the first 50 msec. of mixing the contents of the two drive syringes, and the rate constant was usually estimated from the linear portion of the curve within this time period. Because the electron transfer was a first-order reaction, the unit of the rate constant was in sec^{-1}.

c. Longer time absorbance changes - The quantitation of the rate constant, k_{+2}, usually required observing the reaction for ~100 msec. However, if the primary electron transfer reaction was scanned for longer time intervals (in the range of 500-1,000 msec), additional absorbance changes occurred that were dependent on the gas substrate in the

stopped-flow experiment. As was mentioned in Section I.D.3.d, these absorbances have been proposed to be produced by the oxidation of the P clusters of the MoFe protein.

3. Secondary Electron Transfer

Primary electron transfer refers to the donation of a single electron from the Fe protein to the dithionite-reduced E_0 redox state of the MoFe protein. Thus, the electron transfer results in the transition of the MoFe protein from the E_0 to the E_1 redox state. Secondary electron transfer describes the subsequent electron transfer event, namely the donation of an electron from the Fe protein to the E_1 redox state of the MoFe protein to produce the E_2 state. One of the central tenets of the Thorneley-Lowe model is that the redox status of the MoFe protein does not influence the rate constants of the Fe protein cycle, and this assumption has been proven to be true for the first two intermolecular electron transfer steps of the MoFe protein cycle (Fisher *et al*., 1991).

The secondary electron transfer rate was measured using stopped-flow spectrophotometry and was similar to the primary rate determination with a few modifications. In order to measure the transition from E_1 to E_2, the redox state of the MoFe protein in the drive syringe must be poised at the E_1 state and then mixed with reduced Fe protein in the other drive syringe. Attainment of the E_1 state was accomplished by establishing a one-electron reduction reaction between the Fe and MoFe proteins in one of the drive syringes. A very low Fe protein to MoFe protein molar ratio of 1:100 in the presence of dithionite and an ATP-regenerating system resulted in an accumulation with time of the E_1 redox state of the MoFe protein.

The design of this stopped-flow experiment included a two-syringe mixing-block apparatus connected to one of the drive syringes. In one of the syringes was the 1:100 Fe protein-to-MoFe protein mixture, while in the other syringe was the ATP-regenerating system. The contents of the two syringes were mixed together by injection into one of the drive syringes and a timer was started to follow the progression of the one-electron reduction reaction. At designated time intervals, the contents of this one-electron reduction reaction were mixed with a molar excess of reduced Fe protein and MgATP, and the stopped-flow spectrum was recorded. Initial stopped-flow traces corresponded to

the E_0 to E_1 electron-transfer transition, because the mixture of Fe and MoFe proteins in one of the drive syringes had not had sufficient time to react and, therefore, the population of MoFe protein was almost entirely in the E_0 redox state. However, as the time since the initial mixing progressed, the E_1 redox state of the MoFe protein accumulated and the stopped-flow traces were recording the intermolecular electron-transfer rate for the E_1 to E_2 transition, or secondary electron transfer rate. As in the primary electron transfer experiment, the rate constant determination utilized the equation $Y = -dY \cdot e^{-kx} + Y$.

4. Complex Dissociation

Pre-steady-state kinetic analysis of the nitrogenase complex has produced invaluable insight into the mechanism of the overall reaction by quantitating the rates of some of the individual steps. The Fe protein-MoFe protein complex dissociation step is the proposed rate-limiting step in the overall catalytic mechanism. Therefore, all altered MoFe proteins were subjected to the complex dissociation rate experiment. Again, stopped-flow spectrophotometry was used to estimate the rate constant for protein complex dissociation, k_{-3} using the equation $Y = -dY \cdot e^{-kx} + Y$. The experimental design was significantly more complex than the primary and secondary electron transfer rate procedures. The intricate nature of this stopped-flow experiment was due to the necessarily cautious preparation of the nitrogenase component proteins as described below.

a. Preparation of dithionite-free MoFe protein - Sodium dithionite was removed from concentrated, purified MoFe protein samples on a Bio-Gel P-6DG desalting resin column (Bio-Rad Laboratories, Hercules, CA). The size of the column was dependent on the size of the sample; a rule of thumb for the column volume was five times the sample volume. The P-6DG column was equilibrated with 5-10 column volumes of 25 mM HEPES, 10 mM $MgCl_2$, dithionite-free buffer. The MoFe protein had a tendency to stick to the desalting resin, therefore, 200 mM NaCl was always included in the column buffer. The column was run in a high integrity anaerobic glovebox (<0.1 ppm O_2), and the elution of the protein was detected visually by its dark brown color. The dithionite-free

MoFe protein was collected in about twice the volume of the original loading volume. The absence of dithionite in the MoFe protein sample was confirmed with methylviologen paper, and the subsequent elution of dithionite from the column was also confirmed with methylviologen paper. A portion of the dithionite-free MoFe protein sample was reserved for later protein concentration determinations.

b. Preparation of oxidized Fe protein - Fe protein was oxidized by passage over indigocarmine, which was bound to a Dowex AG1-X8 anion exchange resin (Bio-Rad Laboratories, Hercules, CA). This resin was prepared by saturation of the resin with an indigocarmine solution, followed by filtration and rinsing of the resin with distilled water in a sintered glass funnel. The redox-active column consisted of a base of P-6DG desalting resin, followed by a thin layer of AG1-X8 resin, with the indigocarmine-bound anion exchange resin layer on the top. The volumes of the P-6DG and dye-bound resins were dependent on the sample volume and were typically five-fold greater. The thin layer of unbound AG1-X8 resin sandwiched between the other two types of resin served to bind any potentially displaced indigocarmine during protein elution.

The column was equilibrated with 5-10 column volumes of 25 mM HEPES, 10 mM $MgCl_2$, dithionite-free buffer. Fe protein was loaded onto the dye-bound phase of the column and the column was then clamped shut so that the Fe protein would remain in contact with the indigocarmine for a 30-min incubation period. Sodium dithionite in the Fe protein sample turns the very top of the dye-bound resin a bright yellow color, however, the majority of the dye remains blue. The large excess of oxidized indigocarmine ensured that the Fe protein was sufficiently oxidized during the 30-min incubation. The Fe protein was eluted with buffer and detected, collected, and absence of dithionite confirmed by the method previously described for dithionite-free MoFe protein. A small sample of the eluted Fe protein was saved for protein concentration estimation.

c. Calculation of the rate constant for complex dissociation, k_{-3} - Essentially, the stopped-flow spectrophotometric experiment involved the establishment of a complex between dithionite-free Av1 and dye-oxidized $Av2_{ox}(MgADP)_2$ in a 1:1 molar ratio in one drive syringe (see Section I.F.1.c). This mixture was combined with the contents of

the other drive syringe, a molar excess of $Av2_{red}$ in the presence of excess MgADP and excess dithionite. The resulting stopped-flow spectrum demonstrated an exponential decrease in absorbance at 430 nm as the oxidized Fe protein was reduced by dithionite upon dissociation from the MoFe protein. The rate constant for protein complex dissociation, k_{-3}, was calculated from the linear portion of this absorbance decrease.

G. Spectroscopy

As discussed in Sections I.C.2, I.D.2b & 3b, the utility of various spectroscopic techniques has yielded a wealth of data on the structure, metal content, redox activity, and the mechanism of nitrogenase. It was a natural consequence that some of these techniques would be used to analyze altered MoFe proteins for comparison to wild-type MoFe protein.

1. Electron Paramagnetic Resonance

In addition to charge and mass, an electron also has angular momentum or spin. A spinning electron generates a magnetic field and the strength of this magnetic field is referred to as the magnetic moment of the electron. An externally applied magnetic field forces the magnetic moment of an electron to assume one of two possible orientations. Either the electron is aligned with the external magnetic field and is said to have a -1/2 spin, or the electron is aligned against the magnetic field and is said to have a +1/2 spin. When two electrons are paired, their spins oppose and cancel each other resulting in a diamagnetic state. If a molecule contains one or more unpaired electrons, the molecule is paramagnetic and can, therefore, be studied by electron paramagnetic resonance (EPR) spectroscopy. The EPR spectrum reveals information about the immediate environment of an unpaired electron. For a free electron, $g = 2.0023$ and perturbation of its electronic environment can shift the *g*-value away this value. EPR has proven useful in the study of Fe-S cluster-containing proteins because of the existence of unpaired electrons in unique and various electronic surroundings.

The EPR spectra of the Fe and MoFe proteins of nitrogenase can only be observed at temperatures below 30 K or less. For the most part, EPR samples were run in the

laboratory of Dr. Dick Dunham at the University of Michigan (Ann Arbor, MI) on a Varian E-line spectrometer (Varian Associates, Palo Alto, CA). The EPR spectra of individual samples were typically recorded at a microwave frequency of 9.2 GHz and a microwave power of 20 mW with a 100-kHz field modulation of 10 G at 12 K maintained by liquid helium boil-off.

Nitrogenase protein samples were prepared for EPR analysis in an anaerobic glovebox operating under a 100% N_2 atmosphere and <0.1 ppm O_2. Sample concentrations varied but were typically 20 mg/ml or greater for MoFe protein. Sample volumes of ~250 μl were injected into ~20 cm x 3 mm I.D. quartz EPR tubes using a stainless steel canula fitted with a plastic tip protector to avoid scratching the tube. The sample tubes were then frozen in a methanol bath at -30°C. The methanol bath consisted of a hollow copper block connected to copper pipe which passed through sealed ports in the wall of the glove box. Outside the glovebox, the copper pipe was connected to a N_2 gas cylinder. The N_2 gas was cooled as it passed through a coiled section of the copper pipe that was immersed in a filled liquid N_2 dewar. The cooled N_2 gas in turn cooled the methanol-filled copper block. EPR samples were flash frozen in this methanol bath in less than a minute and remained frozen during transfer from the glovebox to liquid N_2 storage dewars.

EPR samples for direct comparison of spectral intensity were placed in calibrated quartz EPR tubes (Wilmad Glass Co. Inc., Buena, NJ) to avoid differences that might arise from differences in tube diameter collecting more sample within the spectral window. Tubes were calibrated by measuring the column height of a known amount of water placed in a tube. The tube diameter could then be calculated by rearrangement of the equation for the volume of a cylinder, $d^2 = 4V/\pi h$, where d is the tube diameter, V is the volume of water, and h is the height of the water column.

2. Mössbauer Spectroscopy

Mössbauer spectroscopy is a nuclear resonance technique involving the absorption of γ-ray photons by a sample capable of low energy nuclear transitions (Huynh, 1994). The

most significant detectable transition applicable to a biological system is that observed in the ^{57}Fe isotope. Mössbauer spectroscopy is ideally suited to measure hyperfine interactions, both magnetic and electric, between the Fe nucleus and its surrounding electrons because of the extreme resolution allowed through the transition energy of 14.4 keV between the ground and first excited state of the ^{57}Fe nucleus. An absorption spectrum is generated by moving the γ-ray source, ^{57}Co (Rh), relative to the absorber, causing a Doppler shift in the frequency of emitted radiation. Therefore, the Mössbauer spectra is expressed in terms of source velocity (in mm/sec) versus transmission or absorbance (in percent, %). There are two possible transitions for ^{57}Fe from the ground state to the excited state; this situation results in a spectrum consisting of two equal-intensity absorption lines called a quadrupole doublet. The shift of the center of the two lines from 0 mm/sec is known as δ, the isomer shift. The energy separation between the two absorption lines is called $\Delta\mathbf{E_Q}$, the quadrupole splitting.

Previous Mössbauer spectroscopic investigations of the MoFe proteins from *A. vinelandii* (Zimmerman *et al*., 1978) and *C. pasteurianum* (Huynh *et al*., 1980) demonstrated the utility of low-temperature (4 K) and small applied magnetic field (500 G) spectra in describing the P clusters in the dithionite-reduced state. Systems with even numbers of electrons require an applied magnetic field in order to produce the characteristic quadrupole doublets of the Mössbauer spectrum. Also low temperature measurements allow for the direct correlation between Mössbauer absorption and concentration of the iron site in the sample. Such measurements have distinguished two types of iron sites in the P^N state of wild-type MoFe protein; the first is designated as "Fe^{2+}" with a large quadrupole splitting ($\Delta\mathbf{E_Q}$= 3 mm/sec and isomer shift, δ = 0.66 mm/sec) that represents 25% of the P cluster iron, and the second designated as "D" with a smaller quadrupole splitting ($\Delta\mathbf{E_Q}$= 0.8 mm/sec and isomer shift, δ = 0.63 mm/sec) that represents 75% of the P cluster iron.

All Mössbauer spectroscopic analyses were performed in the laboratory of Prof. Vincent Huynh in the Department of Physics at Emory University (Atlanta, GA). In order

to obtain ^{57}Fe-enriched nitrogenase component proteins, the strains that produce these proteins had to be grown on ^{57}Fe-enriched media (see Section II.B.5). The nitrogenase proteins were purified as previously described and then concentrated to ~200 mM (46 mg/ml). About 350-450 μl were added to special Mössbauer cuvettes and frozen on the liquid N_2-cooled methanol bath located in the anaerobic glove box. Mössbauer spectra were recorded in either a weak-field spectrometer equipped with a Janis 8DT variable-temperature cryostat or a strong-field spectrometer furnished with a Janis CNDT/SC super-Varitemp cryostat encasing an 8T superconducting magnet. The zero velocity of the spectra refers to the centroid of a room temperature spectrum of a metallic iron foil. All spectra were recorded at either 4.2 K in the presence of a magnetic field of 500 Gauss in either the parallel or perpendicular mode to the direction of the radiation source, or at 150 K in the absence of an external magnetic field. In order to more easily compare the altered and wild-type P-cluster spectra, the FeMoco contribution (47% of the total Fe) was subtracted out of the low temperature (4 K) spectra. The Mössbauer spectra were analyzed using the WMOSS program (WEB Research Co., Edina MN).

3. Magnetic Circular Dichroism Spectroscopy

Magnetic Circular Dichroism, or MCD, exploits the circular polarization of the ground and excited states of electronic transitions in molecules. MCD measures the differential molar absorptivity of left and right circularly polarized light, $\Delta\varepsilon$, as a function of wavelength in the presence of a magnetic field applied parallel to the direction of light propagation. Variable- temperature MCD, or VTMCD, can provide additional information because this technique is a selective optical probe for paramagnetic chromophores like transition metal centers. Because the paramagnetism of the FeMo cofactors and P clusters is a direct consequence of the oxidation state of the MoFe protein, VTMCD spectra can be used to selectively compare both cluster types in wild-type versus altered MoFe proteins (Johnson, 1988).

In collaboration with Prof. Michael K. Johnson in the Department of Chemistry at the University of Georgia (Athens, GA), we have collected and compared the VTMCD

spectra of various MoFe proteins under dithionite-reduced and thionine-oxidized conditions. The VTMCD spectra were recorded using Oxford Instruments SM3 or SM 4000 split-coil superconducting magnets (1.5-300 K and 0-7 T) mated to a Jasco J-500C or J-715 spectropolarimeters. All samples contained 50-60% (v/v) glycerol in order to form optically transparent glass on freezing.

CHAPTER III.
SUBSTITUTION OF THE P CLUSTER BRIDGING CYSTEINES

A. Introduction

In the mid-1980's, a site-directed mutagenesis project was initiated in our laboratory that centered on the conserved cysteine residues of the MoFe protein of *A. vinelandii* (Brigle *et al*. 1987a; Dean *et al*., 1990). The goal of the project was to identify which of the various cysteines were metallocluster ligands and specifically to assign the cysteine ligands to either the FeMo-cofactor or the P cluster. An additional product of the project was the ranking of the importance of conserved cysteine residues based on the mutant strain's retention of diazotrophic capability. By using degenerate oligonucleotide directed mutagenesis, a variety of amino acid substitutions was generated for each particular residue position. The percentage of Nif $^{+}$ strains that resulted from this mutation was taken as a measure of the importance of the substituted cysteine in the functioning of the MoFe protein in the nitrogenase mechanism. By this methodology, α-Cys275, α-Cys62, and α-Cys154 were determined to be critical to MoFe protein function due to the inability of mutant strains with substitutions at these residues to grow diazotrophically. Two other conserved cysteines, α-Cys88 and β-Cys153, fell into a separate class because they survived moderate replacement, i.e., 2-3 strains with amino acid replacements at either of these residues which retained lower but significant levels of diazotrophy. The β-Cys70 and β-Cys95 residue replacements made in the initial studies were strictly Nif $^{-}$. However, only 1-2 amino acid replacement strains were produced in the initial study. Therefore, the importance of these residues could not be gauged by this method. This research, along with similar results in *K. pnuemoniae* (Kent *et al*. 1989; 1990), led to the proposal of α-Cys62, α-Cys88, α-Cys154, β-Cys70, β-Cys95, and β-Cys153 as P cluster ligands and α-Cys275 as the sole thiol ligand to FeMoco (Brigle *et al*., 1987a; Dean *et al*., 1990).

The strains with substitutions for the conserved cysteines α-Cys88 and β-Cys153 became the foundation for a corollary project. This project seeks to investigate the nature of the perturbation of the nitrogenase reaction that is a result of amino acid replacement at these conserved cysteine positions. The β-Cys153-substituted strains were selected for the initial investigations based on the relatively high levels of diazotrophic growth and substrate reduction activity, as well as the intensity of the FeMoco S=3/2 EPR signal. The enzymatic characterization of the altered MoFe protein that was purified from one of these strains has already been described in detail (see Section I.D.3.c). The next logical step in this project was to investigate the altered MoFe proteins from the strains with substitutions at the α-Cys88 site.

Of the nine mutant strains containing amino acid substitutions generated at the α-Cys88 position, three were able to grow diazotrophically (Dean *et al*., 1990). These strains produced MoFe proteins with either aspartate, glycine, or threonine in place of α-Cys88. Subsequent analysis of the purified MoFe proteins from these three mutant strains is the focus of this project. However, additional site-specific mutagenesis was necessary to investigate different aspects of this project, namely, site-directed mutagenesis of β-Cys95 and construction of mutant strains producing poly-His-tagged, α-Cys88-substituted MoFe proteins. Each of these molecular biological manipulations is described below along with an explanation for creating the particular strains.

B. Site-directed Mutagenesis of β-Cys95

Prior to the solution of the x-ray crystal structure of the MoFe protein from *A. vinelandii*, two of the α-Cys88-substituted forms of the MoFe protein had been purified to ~90% homogeneity. The *A.vinelandii* strains, DJ399 and DJ396, produced MoFe proteins with α-88CD and α-88CG substitutions, respectively. After the crystal structure of the MoFe protein revealed that the α-Cys88 and β-Cys95 residues both serve as bridging ligands between the protein and the two cubane-halves of the 8-Fe P cluster

structure (Kim & Rees, 1992), it also seemed pertinent to determine if β-Cys95 would tolerate the same amino acid replacements as the α-88 site.

1. Construction of the Mutant Strains

The technique used to create mutations at the β-95 site was identical to that described in the Materials and Methods section (see Section II.A.2). Degenerate oligonucleotide mutagenesis resulted in five different plasmids with sequences coding for amino acid replacements for the β-Cys95 residue. DNA dideoxy-sequencing was used to screen and identify the amino acid substitutions as arginine, lysine, glutamate, tryptophan, and valine. Additional mutant strains generated by site-specific oligonucleotide mutagenesis included serine, aspartate, and threonine. The purified plasmids were separately transformed into competent wild-type *A. vinelandii* cells as previously described (see Section II.A.3) and the recombinants were screened based on the diazotrophic phenotype. Two separate, yet identical, isolates of each genotype were cultured and made into freezer stocks (see Table 3).

2. Results of Doubling Times Analysis

Each mutant strain constructed was subjected to a diazotrophic growth experiment for the purpose of determining the Nif phenotype and, if applicable, the doubling time ($t_{1/2}$) of the strain. The doubling time procedure was performed as described in Section II.B.2. The results are seen in Table 3.

C. Construction of Poly-His-Tagged, α-Cys88-substituted MoFe Producing Strains

An improved procedure for purification of the fragile α-Cys88-altered MoFe protein utilized an *A. vinelandii* strain, DJ995, that produces a MoFe protein with seven histidines residues attached to the carboxy terminus of the α-subunit. The *E. coli* plasmids, pDB459 (α-88CG), pDB460 (α-88CT), and pDB461 (α-88CD) used to create the original *A.vinelandii* mutant strains, were used to transform the DJ995 strain. The resulting recombinants were screened for diazotrophic growth and the new *A. vinelandii* strains were made into freezer stocks. The doubling times for the poly-His-tagged, α-

Cys88 altered MoFe proteins were determined and compared to the non-Poly-His-tagged containing mutant strains as controls (see Table 4).

D. Discussion

One conclusion drawn from the diazotrophic growth studies is that the β-Cys95 site does not tolerate the same range of substitutions as the α-Cys88 site. The DJ1096 strain, which produces a β-95CD-substituted MoFe protein, demonstrates a much slower doubling time and a substantially lower level of nitrogenase activity than the DJ399 strain, which also produces an aspartate-for-cysteine substitution at the seemingly complementary P cluster bridging ligand position at α-88. Subsequent purification of the MoFe protein from this mutant strain yields an enzyme with poor substrate reduction activity (H. Xie, personal communication).

Based on the preliminary results of doubling time comparisons between strains, which only differ in the presence or absence of a poly-histidine tail, it was concluded that the poly-histidine tail did not adversely affect the functioning of the MoFe protein in the nitrogen fixation process.

Table 3: Construction and Diazotrophic Growth of *A. vinelandii* βCys95 Mutant Strains

Strain	**β-95 Codon**	**Plasmid**	**Substitution**	**Doubling Times (hrs)**
Wild-type	UGC	-	None	2.5
DJ1096, 1097	GAC	pDB934	β-95CD	20
DJ1094, 1095	ACC	pDB935	β-95CT	NG
DJ1080, 1081	AGA	pDB925	β-95CR	NG
DJ1082, 1083	GAA	pDB926	β-95CE	NG
DJ1084, 1085	AAA	pDB927	β-95CK	NG
DJ1090, 1091	UGG	pDB929	β-95CW	NG
DJ1092, 1093	GUA	pDB930	β-95CV	NG
DJ120	UCC	pDB	β-95CS	NG

NG = no growth

Table 4: Comparison of Diazotrophic Growth Rates of α-Cys88 Mutant Strains

Strain	**α-88 Position Codon**	**Plasmid**	**Substitution**	**Doubling Time (hrs)**
DJ995*	UGC	pDB827	His_7	2.5
DJ399, 400	GAC	pDB461, 462	α-88CD	7.2
DJ1008*	GAC	pDB461	α-88CD, His_7	7.0
DJ395, 396	GGA	pDB459	α-88CG	9.6
DJ1019*, 1020*	GGA	pDB459	α-88CG, His_7	10.0
DJ397, 398	ACU	pDB460	α-88CT	17.0
DJ1021*, 1022*	ACU	pDB460	α-88CT, His_7	14.0

*Strains contain the Poly-His tail codon $^{5'}$CACCACCAUCACCACCACCAU$^{3'}$

CHAPTER IV.

PURIFICATION OF α-CYS88-ALTERED MOFE PROTEINS

A. Introduction

Initial attempts to purify the α-Cys88-altered MoFe proteins were based on the purification scheme that was successful in isolating the β-153CS-substituted MoFe protein from *A. vinelandii* (May *et al*., 1991). This scheme included sonication to break open the cells, a 5 min 56°C heat step to precipitate contaminating proteins and chromatographic steps that utilized strong anion exchange and hydrophobic interaction columns. However, the heat treatment and hydrophobic interaction steps resulted in inactivation of the MoFe proteins and alternative methods had to be developed. The results from two separate purification schemes are described and their effects on the nature of the substitutions are proposed.

B. Purification by Traditional Chromatographic Methods

The α-Cys88-altered MoFe protein from *A. vinelandii* mutant strain DJ399 was selected as the first target for purification. This decision was based on the relatively high substrate reduction activity and strong S=3/2 EPR signal found in crude extracts of this strain. It was immediately obvious, however, that this altered MoFe protein was substantially less stable than its β-153CS counterpart. DJ399 was inactivated by heat treatment above 40°C and, therefore, this purification step was excluded. Also, hydrophobic interaction chromatography resulted in inactivation of a large fraction of the MoFe protein from this strain as demonstrated by the dramatic reduction in the yield of both enzyme and activity from this column. A higher level of purity, as determined by specific activity, was obtained by eliminating the heat step and replacing the hydrophobic interaction step with gel filtration and hydroxyapatite chromatographic steps. This scheme gave a 20-35% recovery of total activity, ~20-fold enrichment of specific activity over crude extract, and a maximum specific activity of ~600 nmols H_2 (min·mg MoFe

protein)$^{-1}$ (see Table 5). Lower yields and enrichment were obtained when this purification procedure was applied to the DJ396 strain, which produces an α-88CG-substituted MoFe protein with a specific activity of ~120 nmols H_2 (min·mg MoFe protein)$^{-1}$.

Although this scheme proved successful, it was very labor intensive and time consuming. Another problem encountered during this purification scheme was the irreversible precipitation of the MoFe protein during the later stages. Precipitation seemed to be associated with concentration of column eluants and liquid N_2 freeze/thaw cycles that are a part of the usual protocol for protein storage between purification steps. For these reasons, a novel technique was developed for the isolation of these fragile altered MoFe proteins. It is described below.

C. Purification by Metal Affinity Chromatography

As previously discussed in Sections II.D.4 and III.C, the combination of molecular biological and chromatographic techniques were exploited in the development of a highly specific and rapid purification technique. Attachment of a seven histidyl residue tail to the carboxy terminus of the α-subunit of the MoFe protein allows for tight binding to a $NiSO_4$-saturated metal affinity chromatography column.

The poly-His-tagged, α-88CD MoFe protein-producing strain DJ1008 was selected as the first of the mutant strains to be subjected to this new purification technique. Following the procedure described in Section II.D.4, the purified poly-His-tagged, α-88CD MoFe protein was obtained with a 25-40% yield, a 30-fold enrichment of specific activity over crude extract, and a maximum specific activity of ~1,000 nmols H_2 (min·mg MoFe protein)$^{-1}$ (see Table 5). Also the purified protein product was ~95% pure as determined by SDS-PAGE gel analysis (data not shown). Thus, the metal affinity method resulted in a 66% increase in specific activity over the traditional method.

Table 5: Comparison of Purification Methods for α-Cys88 Altered MoFe Proteins

Strain	**Wild-type**	**DJ995**	**DJ399**	**DJ1008**	**DJ396**	**DJ1019**	**DJ1021**
Substitution	None	His_7	α-88CD	α-88CD His_7	α-88CG	α-88CG His_7	α-88CT His_7
Purification Method	Traditional	Metal Affinity	Traditional	Metal Affinity	Traditional	Metal Affinity	Metal Affinity
SPA (H_2)*	1900 ± 200	2500 ± 200	600 ± 150	1,100 ± 100	120 ± 10	300 ± 30	200 ± 20
Yield (%)	30-40	45-55	20-35	25-40	10-20	25-30	25-30
Mo/MoFe	1.2 ± 0.2	1.6 ± 0.2	1.5 ± 0.1	0.9 ± 0.1	1.0 ± 0.3	0.65 ± 0.2	0.65 ± 0.2
Fe/MoFe	19 ± 2	24 ± 2	12.5 ± 3	12 ± 1	6.7 ± 2	9.1 ± 2	8.7 ± 2
Fe/Mo	15	15	8.5	13	6.7	14	14
SPA (Mo)**	350	360	92	270	28	110	73

All values are the result of at least five replicate measurements

* Specific Activity = nmoles H_2 (min·mg MoFe protein)$^{-1}$

** Specific Activity = nmoles H_2 (min·ng atom Mo)$^{-1}$

† g atoms of Mo or Fe per mole of MoFe protein

Similar percentage increases in yield, enrichment, and maximum specific activity were obtained from purification of strain DJ1019, which expresses a poly-His-tagged, α-88CG MoFe protein. Finally, the metal affinity method was used exclusively in the purification of a third *A.vinelandii* mutant strain, DJ1021, which expresses a poly-His-tagged, α-88CT MoFe protein (see Table 5).

D. Metal Analysis of Purified Products

Inductively coupled plasma atomic emission spectroscopy was utilized to determine the Mo and Fe contents of the purified MoFe proteins from wild-type and α-Cys88-mutant strains. As seen in Table 5, the metal contents of the α-Cys88-altered MoFe proteins are substantially lower than wild-type MoFe protein, which has metal contents closer to the theoretical values of 2 molybdenum and 30 iron atoms per MoFe tetramer.

E. FeMoco Reconstitution Assays

The metal analysis results brought up the possibility that the α-Cys88-altered MoFe proteins did not have a full complement of metalloclusters relative to wild-type. Possibilities for this result include the extrusion of FeMoco during purification or perhaps inefficiency in the metal-insertion processes in these mutant strains. FeMoco reconstitution assays (see Section II.D.6.b) were performed on crude extracts of each of the α-Cys88-substituted mutant strains in order to test whether the apoprotein fractions could accomodate insertion of exogenous FeMoco. This experiment was performed in order to address the question of whether insertion of FeMoco into an apoprotein containing amino acid substitutions at the α-88 position occurred as readily as FeMoco insertion into apoprotein with cysteine at this position. A difference in ease of FeMoco insertion among these two types of apoprotein would indicate an importance of the α-Cys 88 in metallocluster biosynthesis and/or insertion. If FeMoco reconstitution were possible in these crude extracts, an increase in substrate reduction activity would be expected. The assays were performed on crude extracts of each of the α-Cys88-

substituted mutant strains as well as on the control strain DJ42, which has a deletion for the FeMoco biosynthetic genes *nifENX*. Although the control showed significant C_2H_2 reduction activity, none of the mutant strain crude extracts showed any measurable increase in activity. In fact, there was a slight reduction in activity for all three, which was attributable to the presence of NMF in the assay.

F. Discussion

The improvements in yield and maximum specific activity of the metal-affinity purification scheme over the traditional chromatographic method are attributable to a number of factors. The reduced number of column chromatography steps and elimination of repeated freeze/thaw cycles for the affinity-purified samples are undoubtedly contributing factors because the nitrogenase component proteins are highly O_2-sensitive. Also, the aforementioned precipitation that occurs upon concentration and repeated freeze-thaw cycles is substantially reduced during the affinity method. Gel electrophoretic analysis of the MoFe protein subunits from the two purification options do not reveal any noticeable differences in amounts of contaminating bands. However, this technique, by itself, is a very qualitative and subjective estimation of purity. Another possibility for the improvements is that the traditional chromatographic methods may cause loss of either one or both of the metalloclusters during purification. This possibility is difficult to appraise because there are limited metal analysis results for altered MoFe proteins purified by the traditional methods. However, the lowered Fe/Mo ratios for the α-88CD and α-88CG MoFe protein from strains DJ399 and DJ396, respectively, could be due to loss of P clusters and retention of FeMoco during purification. This possibility could also explain the increased amounts of precipitated protein accumulated during the concentration steps because the P clusters reside at the αβ-subunit interface of the MoFe protein and could influence accurate quaternary structure formation. The overall result would be a higher total Mo content and a lower Fe/Mo ratio because a large fraction of the protein product is P cluster-less.

The ICP-AES results for the Mo and Fe concentrations of the three α-Cys88 altered proteins purified by the affinity chromatography are at the same time both disturbing and interesting because all three proteins display reduced Mo/MoFe protein values compared to wild-type but nearly ideal Fe/Mo numbers. These results lend credence to the premise that P cluster insertion into the newly synthesized $\alpha_2\beta_2$ tetramer is a prerequisite for FeMoco insertion. This idea is supported by the fact that FeMoco-deficient MoFe proteins with P clusters have been identified (Paustian *et al.*, 1990; Dean *et al*., 1993; Howard & Rees, 1996), but not a P cluster-less MoFe protein with intact FeMo cofactors. Additionally, these findings support the hypothesis that effective P cluster assembly may require the αβ-subunit interface as a scaffold for correct insertion.

CHAPTER V.

STEADY-STATE KINETICS OF α-CYS88 ALTERED MOFE PROTEINS

A. Introduction

The next step, after the successful purification of any altered form of a nitrogenase component protein, was the characterization of the kinetic parameters of that protein in the multitude of enzymatic reactions performed by nitrogenase. Such a characterization was necessary to answer the question of how these α-Cys88 altered MoFe proteins compare to wild-type and, therefore, assess the importance of this residue in a number of nitrogenase catalytic reactions. These reactions include H_2 evolution, C_2H_2 reduction, N_2 reduction, ATP hydrolysis, and response to inhibitors, CO and NaCl. It is also often informative to adjust the conditions of the assays, such as the electron flux or limiting a crucial reaction compound, and observe potential differences from wild-type nitrogenase. All of these steady-state kinetic experiments were applied to each of the three α-Cys88 altered MoFe proteins in an attempt to delineate how changes in this P cluster ligand might affect these reactions.

B. Maximum Specific Activities under Argon, Acetylene, and Nitrogen

Following the procedures described in Sections II.E.1-3, the maximum specific activities of each α-Cys88 substituted MoFe protein was assayed with wild-type Fe protein under a 100% Ar, a 10% C_2H_2/90% Ar, and a 100% N_2 atmosphere. To ensure that maximum activity was attained, a high flux condition of a 20:1 molar ratio of Fe protein to MoFe protein was used. It was assumed that only the wild-type nitrogenase products would evolve from the altered MoFe proteins. Thus, under 100% Ar, only H_2 was determined, under 10% C_2H_2/90% Ar, only C_2H_4 and H_2 were measured, and under 100% N_2, only NH_3 and H_2 were quantified. This assumption was confirmed in a limiting dithionite experiment

Table 6: Specific Activities and Electron Allocation of Wild-type and α-Cys88 Altered MoFe Proteins

Substrate	Product(s)	DJ995, Wild-type		DJ1008, α-88CD		DJ1019, α-88CG		DJ1021, α-88CT	
		Spec. Act.*	%e-	Spec. Act.*	%e-	Spec. Act.*	%e-	Spec. Act.*	%e-
100% Ar	H_2	2,500 ± 200	100	1,100 ± 100	100	300 ± 39	100	200 ± 20	100
10%C_2H_2/	H_2	350 ± 50	14	150 ± 20	15	40 ± 5	14	10 ± 3	6
90% Ar	C_2H_4	2,150 ± 200	86	850 ± 100	85	240 ± 20	86	160 ± 20	94
100%	H_2	650 ± 50	30	250 ± 20	30	80 ± 10	30	50 ± 10	29
N_2	NH_3	1,000 ± 200	70	400 ± 100	70	100 ± 20	70	80 ± 20	71

All values are the result of at least three replicate measurements

* nmoles product (min·mg MoFe protein)$^{-1}$

(see Section V.D). All activities were determined in parallel with the purified MoFe protein from strain DJ995, which produces a wild-type MoFe protein with a poly-His tail. The maximum specific activities under a 100% Ar, a 10% C_2H_2/90% Ar, and a 100% N_2 atmosphere are listed in Table 6.

Because of the lowered Mo content of the α-Cys88-altered MoFe proteins, it is informative to relate the specific activities of the these proteins in terms of nanomoles of Mo present as well as on a protein concentration basis. This description of activity is based on the assumption that the Mo content is an indirect measurement of the concentration of nitrogenase active sites, i.e., FeMoco, in an assay. Table 5 expresses the specific activities of the wild-type and altered MoFe proteins based on Mo content. Based on these calculations, the difference in specfic activity between the wild-type and the α-88CD MoFe proteins is much less then the activity differences based on total protein. However, the specific activity based on Mo content for the α-88CG and α-88CT MoFe proteins are significantly lower than the wild-type MoFe protein activity.

A common method for comparison of nitrogenase activities under various substrates is to convert all products into pairs of electrons (often denoted as $2e^-$), and to quantitate the specific activities in terms of total electron pairs per minute per milligram of MoFe protein. When this conversion is applied to the wild-type nitrogenase, the maximum specific activity for the production of total electron pairs is relatively independent of the gas substrate. This same independence of substrate was demonstrated by all three of the α-Cys88 altered MoFe proteins (see Table 7).

C. Electron Flux Titration Under Argon, Acetylene, and Nitrogen

Substrate reduction activities were performed at a variety of Fe protein to MoFe protein molar ratios as a method for titrating the electron flux through the nitrogenase complex in question. The patterns of saturation of specific activity, allocation of

Table 7: Specific Activities of Wild-type and α-Cys88 Altered MoFe Proteins Based on Total Electron Pairs under Argon, Acetylene, and Nitrogen

Substrate	DJ995 Wild-type	DJ1008 α-88CD	DJ1019 α-88CG	DJ1021 α-88CT
100% Argon*	2,500 ± 200	1,100 ± 100	300 ± 30	200 ± 20
10% C_2H_2/ 90% Argon**	2,500 ± 200	1,000 ± 100	280 ± 30	170 ± 20
100% N_2†	2,150 ± 300	850 ± 100	230 ± 50	170 ± 20

All values are the result of at least five replicate measurements

***** nmoles of H_2 $(min \cdot mg\ MoFe\ protein)^{-1}$

****** (nmoles of C_2H_4 + nmoles of H_2) $(min \cdot mg\ MoFe\ protein)^{-1}$

† (nmoles of NH_3 x 1.5 + nmoles of H_2) $(min \cdot mg\ MoFe\ protein)^{-1}$

electrons to products, and ATP hydrolysis for each α-Cys88-altered MoFe protein were determined and compared to wild-type nitrogenase. The procedure used is described in Section II.E.5, where the electron flux titration ranged from a 1:10 up to an 80:1 molar ratio of Fe protein to MoFe protein. The total protein per assay was fixed at 0.5 mg, but the time duration of each assay was dependent on the maximum activity of the MoFe protein.

1. Specific Activity vs. Electron Flux

The pattern of increasing specific activity with increasing electron flux (i.e. Fe protein:MoFe protein) was approximately the same for wild-type and the three altered MoFe proteins. In all cases, there was a linear increase in specific activity until a maximum was reached, at which point the titration curve saturated at that maximum value. The only difference being the absolute value of that maximum for each MoFe protein. There was also essentially no difference in the shape of the saturation curves for the three gas substrates for any one particular MoFe protein. When products were converted to electron pairs, there was no difference between absolute values of the titration curves for each of the MoFe proteins analyzed under a 100% Ar, a 10% C_2H_2/90% Ar, and a 100% N_2 atmosphere.

2. Electron Allocation to Alternative Products

One noticeable difference did appear for one of the altered MoFe proteins when comparing the pattern of electron allocation to products during an electron flux titration. The α-88CT MoFe protein had an unusual pattern of electron allocation to H_2 evolution under a 10% C_2H_2/90% Ar gas atmosphere (see Table 6). Only ~5% of the total electrons moving through this protein were diverted to H_2 formation, and this proportion was independent of the electron flux. Under equivalent assay conditions, the wild-type MoFe protein will favor H_2 formation over C_2H_4 formation at low flux and the reverse is true for high flux assays. At a 1:10 low flux ratio, nitrogenase allocates ~40 % of its electron flux to H_2 evolution and the remainder to C_2H_4 formation while, at a 40:1 high flux ratio, only ~10-15% of its electron flux ends up as H_2.

3. ATP Hydrolysis

The measurement of creatine generated during a steady-state assay of nitrogenase activity has been discussed in Section II.E.4. This quantification requires that a creatine phosphokinase ATP-regenerating system be included in the assay mix. Under high flux conditions of wild-type nitrogenase turnover, the hydrolysis of MgATP is tightly coupled to substrate reduction, such that a minimum of 2 MgATPs are hydrolyzed for each electron transferred through the nitrogenase complex. Because product evolution from nitrogenase requires the transfer of at least two electrons, the coupling of ATP hydrolysis and substrate reduction is often denoted as the number of molecules of ATP hydrolyzed per electron pair transferred (ATP/$2e^-$).

The coupling of ATP hydrolysis and substrate reduction can be perturbed by a number of factors, including pH, temperature, and electron flux. However, the ATP/$2e^-$ ratio has been shown to be independent of the substrate reduced (Watt *et al*. 1975). With these facts in mind, the measurement of the ATP/$2e^-$ ratio under various substrate and electron flux conditions has been an informative device in the comparisons of wild-type and altered MoFe proteins. Several altered MoFe proteins have been described where the uncoupling of ATP hydrolysis from substrate reduction has been elicited by shifting the composition of the gas atmosphere, e.g., with α-195HQ and β-98YH MoFe proteins. In wild-type nitrogenase under adverse component protein ratios (very low flux), MgATP hydrolysis becomes uncoupled from substrate reduction resulting in an ATP/$2e^-$ ratio greater than 4. The three α-Cys88 substituted MoFe proteins were evaluated for ATP hydrolysis as the electron flux was increased (see Table 8). One of the altered MoFe proteins, α-88CG, stood out as noticeably different from the other altered and wild-type MoFe proteins. In this protein, as electron flux increases, the ATP/$2e^-$ also increases, i.e., ATP hydrolysis and substrate reduction become uncoupled. This pattern is in stark contrast to the wild-type MoFe protein, which becomes more tightly coupled as electron flux increases. The

Table 8: Flux Dependencies of ATP/2e- Ratio for Wild-type and α-Cys88 Altered MoFe Proteins

Substrate	DJ995 Wild-type	DJ1008 α-88CD	DJ1019 α-88CG	DJ1021 α-88CT
100% Argon†	4.5 ± 0.5	4.5 ± 0.5	10 ± 1	6.5 ± 1
10% C_2H_2/ 90% Argon†	4.5 ± 0.5	4.5 ± 0.5	10 ± 1	6.5 ± 1
100% N_2†	5.0 ± 0.5	5.5 ± 0.5	12 ± 1	7.5 ± 1
Flux dependency*	Independent	Independent	Dependent	Independent

All values are the result of at least five replicate measurements
* ATP/2e- as Fe protein:MoFe protein ratio increases from 1:10 to 80:1
† 0.5 mg assays, 20:1 Fe protein-to-MoFe protein molar ratio

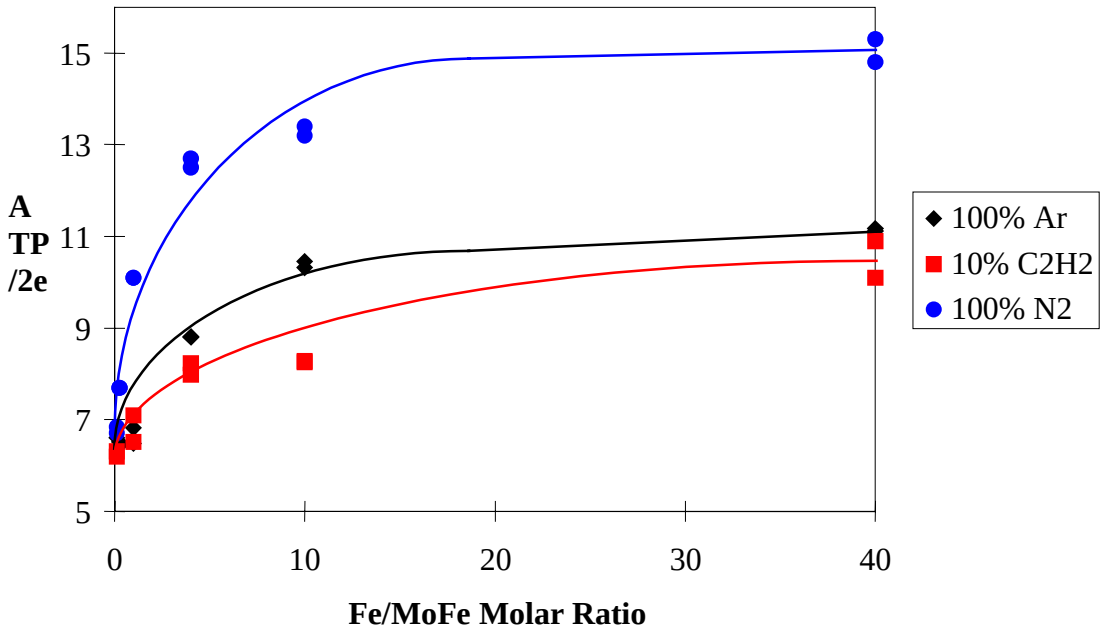

Figure 10: Electron Flux vs. ATP/2e- for the ∝-88CG MoFe Protein under Various Gas Substrates

uncoupling pattern of the α-88CG MoFe protein is approximately the same for each of the three gas substrates examined (see Figure 10).

D. Total Product Evolution Under Limiting Assay Conditions

One of the possible explanations for a decreased rate of substrate reduction in the three α-Cys88 altered MoFe proteins could be that electrons are consumed by the generation of novel products that are not detected by traditional nitrogenase assay methods. In order to test this possibility, steady-state H_2 evolution assay were performed under limiting dithionite concentrations. The goal of these experiments was to measure the amount of H_2 evolved during a time course experiment up to point where the limiting dithionite is completely consumed and no more product is evolved. If H_2 is the only product, then both wild-type and α-Cys88 altered MoFe proteins will accumulate the same total amount of H_2, although the time to dithionite exhaustion may be different due to the slower rates of reduction for the modified proteins.

Steady-state assays performed in the presence of limiting-dithionite levels (1 mM) were run on the wild-type and α-88CG altered MoFe proteins. The results of the time course experiments are displayed in Figure 11. Each assay contained 0.5 mg of total protein and a high flux component protein ratio of 20:1. Both MoFe proteins evolved the same total amount of H_2, while the slopes of the linear portion of the progression curves reflected the difference in the rates of product evolution for each protein.

Creatine assays were run on each of the preceding limiting dithionite assays. The pattern of ATP hydrolysis versus H_2 evolution (i.e., ATP/2e-) revealed a dramatic difference between the wild-type and α-88CG altered MoFe proteins (see Figure 12). As the dithionite concentration approached exhaustion during the time course experiment, ATP hydrolysis and H_2 evolution became more coupled for the α-88CG MoFe protein, i.e. the ATP/2e- decreased from ~11 to ~7.5. The wild-type MoFe protein under identical conditions remained coupled at ~ 5.5 ATP/2e- during the first 20 min of the experiment until dithionite was exhausted. After dithionite exhaustion, the ATP/2e- ratio increases (after ~20 min) for

the wild-type MoFe protein due to reductant-independent ATPase activity. Reductant-independent ATP hydrolysis is also the cause of the increase in the ATP/2e- ratio that occurs in the α-88CG altered MoFe protein after 40 min.

E. Inhibition of Nitrogenase Activity

The pattern of response to various inhibitors by the nitrogenase complex has also been a useful diagnostic of detailing the possible mechanism of the catalytic reaction. Two types of inhibitors, carbon monoxide and NaCl, elicit specific and distinct responses in the component proteins

1. Effect of CO

The effect of CO on the allocation of electrons to alternative products by nitrogenase has been discussed in Section II.E.7. The wild-type pattern of diversion of all electrons to H_2 formation has not always held in certain mutationally-altered variants with substitutions of critical amino acid residues in the vicinity to the FeMo-cofactor, e.g., α-195HN and α-277RH. Therefore, the effect of CO was tested on the α-Cys88 altered MoFe proteins in order to determine if alteration of the P cluster peptide environment resulted in any disruption of the pattern of electron allocation. When assays were run under the three gas substrates in the presence and absence of 10% CO, there was no difference in the pattern of electron allocation from that of wild-type nitrogenase (see Table 9). Because CO is believed to bind at the FeMo-cofactor, the lack of any differences in the CO inhibition patterns between the wild-type and α-Cys88 altered MoFe proteins supports the contention that the substitutions at the P cluster ligand have no effect on inhibitor binding at the FeMoco.

2. NaCl Inhibition

Inhibition of nitrogenase substrate reduction activity has been discussed in relation to protein-protein interaction (see Section I.E). The uncoupling of ATP

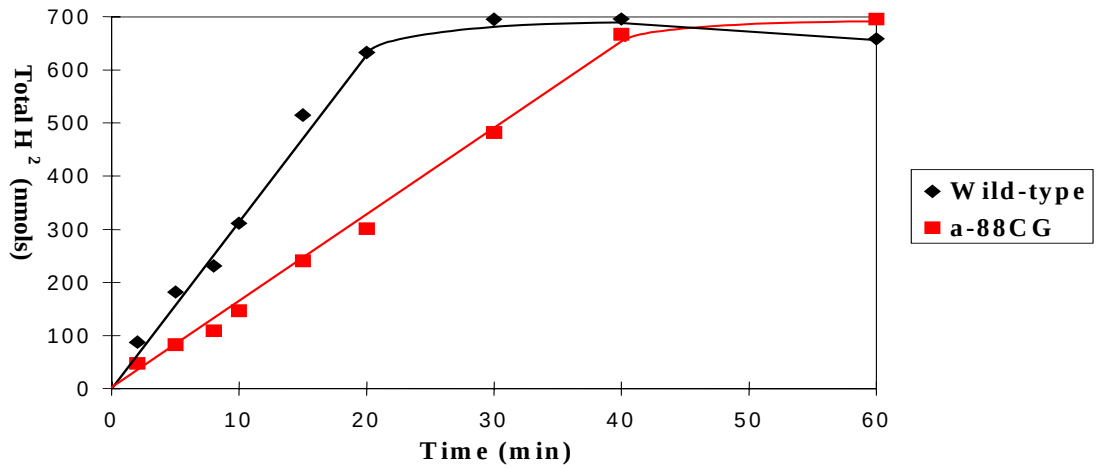

Figure 11: H_2 Evolution under Limiting Ditionite

for Wild-type and α-88CG MoFe Proteins

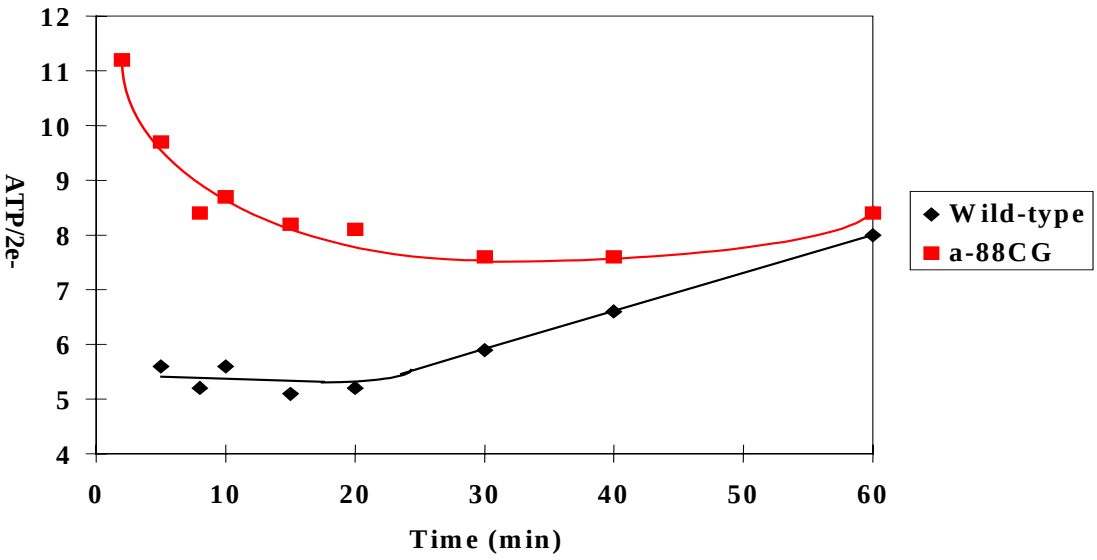

Figure 12: ATP Hydrolysis vs. H2 Evolution under Limiting

Dithionite for Wild-type and α-88CG MoFe Proteins

Table 9: CO Inhibition for Wild-type and α-Cys88 Altered MoFe Proteins under Argon, Acetylene, and Nitrogen

Substrate	DJ995, Wild-type		DJ1008, α-88CD		DJ1019, α-88CG		DJ1021, α-88CT	
	Spec. Act.*	% H_2	Spec. Act.*	% H_2	Spec. Act.*	% H_2	Spec. Act.*	% H_2
100% Ar	2,500	100	1,050	100	300	100	220	100
90% Ar/10% CO	2,700	100	1,100	100	320	100	230	100
10% C_2H_2/90% Ar	2,500	15	1,000	15	300	15	240	15
10% C_2H_2/ 80% Ar/10% CO	2400	100	950	100	270	100	210	100
100% N_2	2,200	30	850	30	250	30	200	30
90% N_2/10% CO	2,200	100	800	100	240	100	210	100

All values are the average of at least three replicate measurements with a standard deviation of ≤10%
* nmoles total electron pairs (min·mg MoFe protein)$^{-1}$

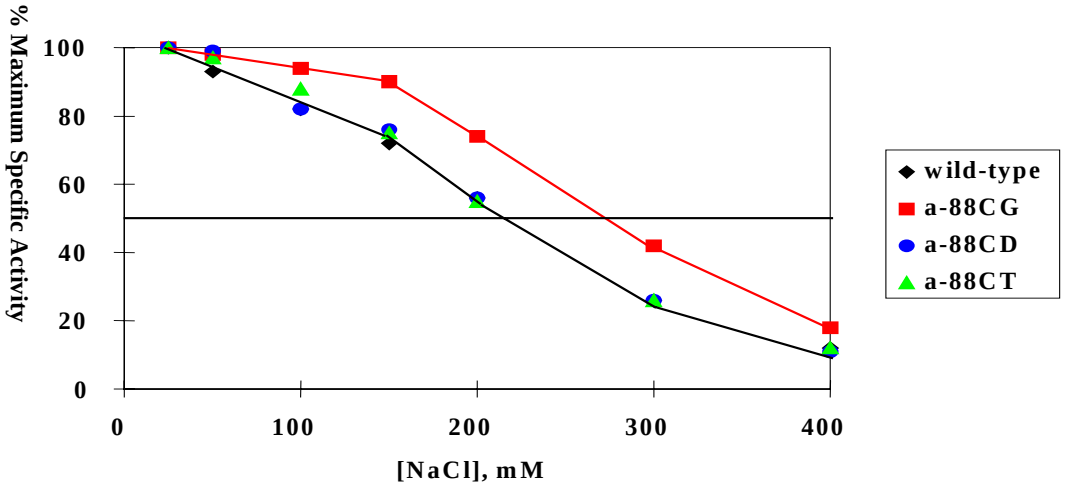

Figure 13: NaCl Inhibition of H_2 Evolution for Wild-type and α-Cys88 altered MoFe Proteins

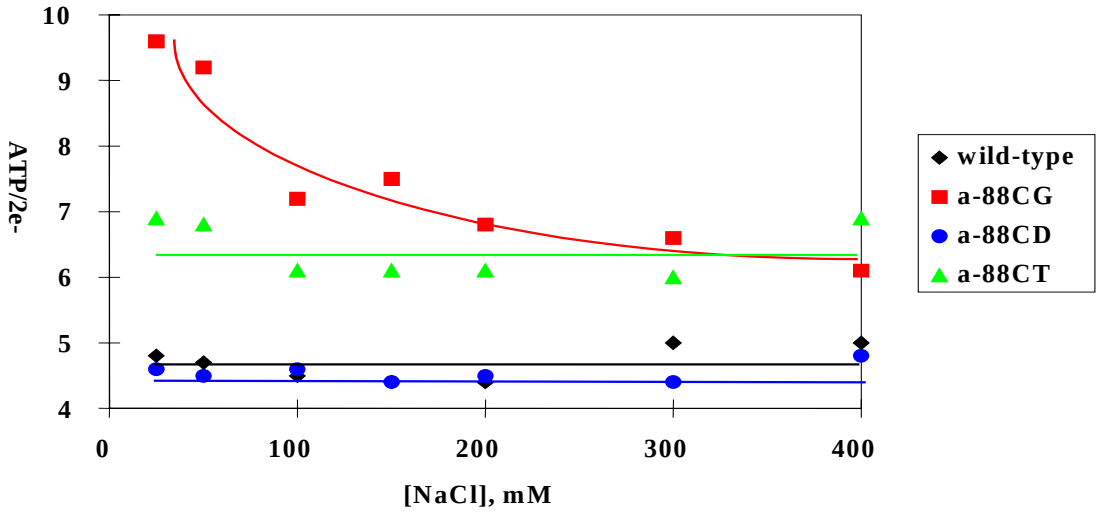

Figure 14: Effect of NaCl on ATP Hydrolysis vs. H_2 Evolution for Wild-type and α-Cys88 altered MoFe Proteins

hydrolysis from substrate reduction, which is a characteristic of perturbation of protein-protein interaction, was assayed for the α-88CG MoFe protein in the presence of increasing concentrations of NaCl under a fixed, high flux Fe protein-to-MoFe protein molar ratio of 20:1. Wild-type, α-88CD, and α-88CT MoFe proteins were also subjected to the same NaCl inhibition assays. The effect on maximal specific activity as well as the effect on the ATP/$2e^-$ ratio was determined for each MoFe protein (see Figures 13 & 14). Based on the decrease in maximal specific activity with increasing NaCl concentration, the α-88CG MoFe protein demonstrated a slightly reduced sensitivity to NaCl inhibition relative to the wild-type, α-88CD, and α-88CT MoFe proteins. The same high flux steady-state assays of the α-88CG MoFe protein revealed a unique pattern when the ATP/$2e^-$ ratio was plotted against increasing NaCl concentration. The uncoupling of ATP hydrolysis from substrate reduction decreased with increasing salt concentration for the α-88CG MoFe protein. The three other MoFe proteins showed no change in ATP/2e- ratio throughout the NaCl titration assays.

3. C_2H_2 Self Inhibition

A more subtle form of inhibition of nitrogenase activity is demonstrated in activity assays containing high concentrations of C_2H_2. In wild-type nitrogenase assays run in the presence of increasing concentrations of C_2H_2, the specific activity as measured by total product evolution, i.e., H_2 plus C_2H_4, is decreased to ~70% at 100% C_2H_2 compared with the maximum specific activity, which occurs at 100% Ar/0% C_2H_2. The maximum specific activity for ethylene production occurred under a 80% Ar/20% C_2H_2 atmosphere. Steady-state assays were performed under high flux (20:1) conditions and a total protein concentration of 0.5 mg/ml for wild-type and α-88CD MoFe proteins. The pattern of product evolution for these proteins were nearly identical as shown in Figure 15. The pattern of ATP/2e- with increasing acetylene concentration was also similar for the two MoFe proteins as seen in Figure 16. The reasoning for performing these assays on the α-88CD MoFe protein will become evident from the results of the pre-steady-state kinetic analysis of this protein (see Section VI.C).

F. Determination of K_m for C_2H_2 Reduction

Quantitation of the Michaelis constant, K_m, of a particular substrate for the altered MoFe protein can be used as an indirect measurement of any disturbance of the active site. The K_m for C_2H_2 reduction is the easiest measurement to make from the available substrates reduced by nitrogenase. The K_m for C_2H_2 was determined to be 0.0062 atm for wild-type MoFe protein, and 0.0051 atm. for the α-88CD, 0.0045 atm. for the α-88CG, and 0.0040 for the α-88CT MoFe proteins.

G. Discussion of Steady-state Kinetics of the α-Cys88 Altered MoFe Proteins

A significant decrease in nitrogenase activity is evident in each of the three α-Cys88 altered MoFe proteins when these are compared to the activity levels of the wild-type nitrogenase complex. However, the source of the diminished activity might be attributed to a number of factors. These possibilities are divided into five categories: 1. diminished metallocluster content; 2. alteration of the substrate reduction site; 3. perturbation of protein-protein interaction; 4. decreased intermolecular electron transfer rate; and 5. reduced intramolecular electron transfer rate. The first three possibilities are addressed below as they were investigated by the steady-state characterization data, whereas the last two are addressed in Section VI.E.

1. Metallocluster Content

As previously discussed in Section IV.D. the metal content of the α-Cys88 altered MoFe proteins were substantially reduced relative to the highly purified fractions of the poly-

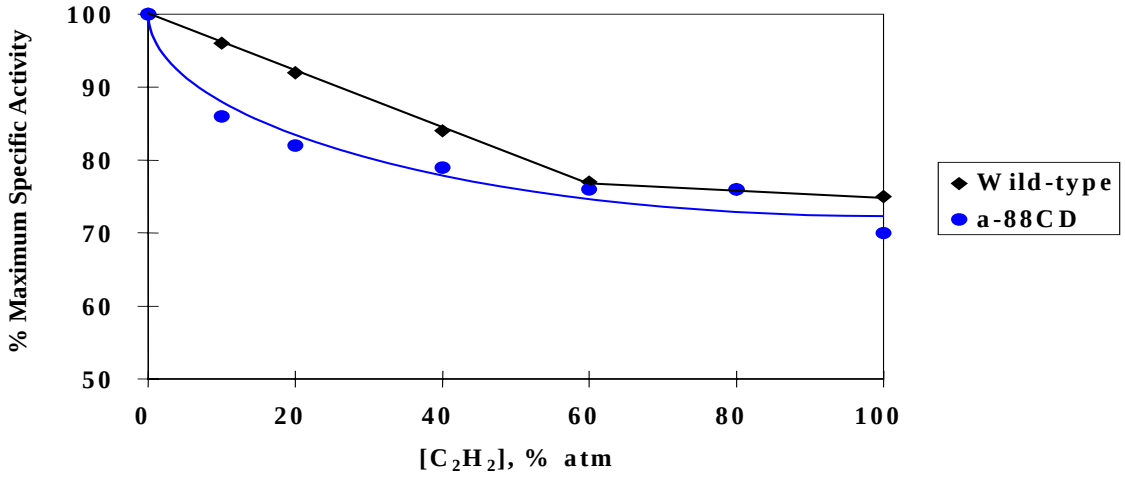

Figure 15: C_2H_2 Inhibition of Total Product Evolution for Wild-type and α-88CD MoFe Proteins

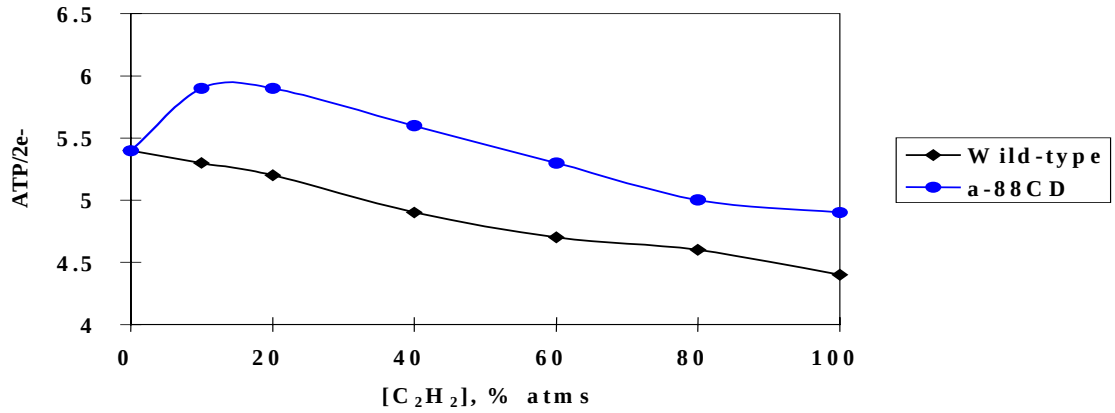

Figure 16: C_2H_2 Inhibition of ATP Hydrolysis vs. Product Evolution for Wild-type and α-88CD MoFe Proteins

His-tagged wild-type MoFe protein from the *A. vinelandii* strain DJ995. Because the molybdenum content of the MoFe protein is often a good indicator of the level of activity, perhaps the lowered substrate reduction activity of the α-Cys88 altered MoFe proteins is due to loss of the FeMo-cluster. If this possibility were true, it might be expected that when activity is expressed in terms of active site concentration, the altered and wild-type MoFe proteins would be equivalent for substrate reduction activity. These calculations can be seen in Table 7. When specific activity is quantified in terms of g. atoms of Mo, the α-88CD MoFe protein exhibits 75% of the wild-type MoFe protein specific activity, whereas the α-88CG and α-88CT MoFe proteins are 33% and 20% of wild-type MoFe protein activity, respectively. Therefore, the loss of active sites from the α-88CG and α-88CT MoFe proteins is an inadequate explanation for the lowered substrate reduction activity levels in these last two site-substituted nitrogenase components. However, the α-88CD MoFe protein is quite similar to the wild-type MoFe protein when activity is calculated in terms of Mo content. Perhaps these two proteins only differ in the amounts of cluster-less apoprotein produced during derepression and which co-purify with the holoprotein on the metal-affinity column..

2. Modified Substrate Reduction Site(s)

A simple explanation for diminished enzyme activity is that these substitutions somehow affect the active site of the MoFe protein. Perhaps a conformational change at the P cluster is communicated through the peptide backbone to the FeMo-cofactor, which in turn could affect either substrate binding or rates of reduction. Two inhibitors of nitrogenase activity, CO and C_2H_2, are both believed to bind to and exert their influence at the FeMoco. The three altered MoFe proteins had identical patterns of inhibition to the wild-type protein. Additionally, the K_m for C_2H_2 values are nearly identical for all four MoFe proteins. Because acetylene binds at the FeMo-cofactor, the lack of any difference in K_m for C_2H_2 values is strong evidence for an unperturbed FeMoco site in the α-Cys88 altered MoFe proteins.

Changes in the peptide environment of the FeMoco have been shown to alter, among other things, the pattern of electron allocation to alternative products and differences in the total electron pair production under various substrates. For the most part, the well-documented patterns of electron distribution to products in the wild-type nitrogenase are duplicated by the α-88CD, α-88CG, and α-88CT MoFe proteins, although the absolute values of rates of product evolution are different. The one exception to this general trend is the allocation of electrons to H_2 under a 10% C_2H_2/90% Ar atmosphere by the α-88CT MoFe protein. These findings substantiate the conclusion that the FeMoco structure and function are generally unaffected by the substitutions at the α-Cys88, P cluster bridging residue.

3. Disruption of Protein-Protein Interaction

The most significant deviations from wild-type MoFe protein kinetic parameters occur in the α-88CG MoFe protein during electron flux titration and NaCl inhibition assays. In both these experiments, the uncoupling of ATP hydrolysis from substrate reduction in the α-88CG MoFe protein revealed a pattern that was markedly different from that of wild-type MoFe protein. Both of these assays may be considered indicators of the strength of interaction between the component proteins of nitrogenase. Thus, the substitution of glycine for cysteine at the α-88 P cluster bridging position may alter some aspect of the protein-protein association and/or dissociation mechanism. In order to explain how ATP hydrolysis might become uncoupled from substrate reduction in the altered MoFe proteins, it is useful to first review how uncoupling might occur in the wild-type nitrogenase complex. There are basically two different mechanisms that rationalize the uncoupling that occurs under conditions of a very high molar excess of MoFe protein relative to Fe protein.

a. The "back-reaction" - In the first model (Hageman & Burris, 1978), the specific activity of the enzyme complex is substantially reduced due to the accumulation of a catalytically-incompetent, one-electron reduced MoFe protein. The decreased availability of the reduced Fe protein electron donor explains the accumulation of the one-electron

reduced MoFe species and the limited procession to the two-electron, product-evolving species. According to the model, the one-electron reduced form of MoFe competes with dithionite for the $Av2_{ox}(MgADP)_2$ form of the Fe protein that results from the dissociation of the nitrogenase complex in the Fe protein cycle of the nitrogenase mechanism (Thorneley & Lowe, 1984b; see Section I.F.1). This competition causes the formation of a catalytically inactive complex of oxidized Fe protein with the one-electron reduced MoFe protein and, thus, results in a decrease in the rate of substrate reduction. This situation is often referred to as the "back-reaction" because it represents the reversal of the dissociative step (k_{-3}) in the Fe protein cycle, i.e. it corresponds to k_{+3}. An increase in dithionite concentration or a decrease in total protein concentration has been shown to suppress the back-reaction by favoring the reduction of the $Av2_{ox}(MgADP)_2$ form of the Fe protein (Hageman & Burris, 1978; Thorneley & Lowe, 1984b). The back-reaction could then lead to back-donation of an electron from $Av1_{red}$ to $Av2_{ox}(MgADP)_2$ within the two-protein complex, followed by displacement of MgADP by MgATP. In this proposed scheme, an electron could continue to shuttle back and forth between the component proteins within the nitrogenase complex in a futile cycle where MgATP is hydrolyzed without substrate reduction (Orme-Johnson & Davis, 1977).

b. Reductant-independent ATP hydrolysis - The second mode for uncoupling is often referred to as reductant-independent MgATP hydrolysis. The *in vitro* ATPase activity of the nitrogenase complex in the absence of reductant has been demonstrated in *A. vinelandii* (Hadfield & Bulen, 1969), *C. pasteurianum* (Jeng *et al*. 1970), and *K. pnuemoniae* (Imam & Eady, 1980). The amount of phosphate released in these dithionite-free assays varies greatly and is dependent on pH (Jeng *et al*. 1970; Imam & Eady, 1980), as well as the molar ratio of the component proteins (Ljones & Burris, 1972).

At neutral pH, the reductant-independent ATPase activity has been reported to vary from 5% (in *A.v*. and *K.p*.) to 33% (in *C.p*.) of the rate of reductant-dependent ATP hydrolysis. Later experiments using *C. pasteurianum* nitrogenase showed a rate of reductant-independent ATP hydrolysis that was 6-10% of the reductant-dependent rate

(Ljones & Burris, 1972). The slightly higher values were attained when dithionite was exhausted by nitrogenase turnover prior to the phosphate release measurement, while the lower values derived from experiments where dithionite was excluded completely. This same range in activity was also found by altering the component protein ratio in the assay. In assays with a molar excess of Fe protein, the reductant-independent ATPase was 6% of the reductant-dependent rate and the ATP/$2e^-$ was found to be ~4 during reductant-dependent conditions. Assays run with a molar excess of MoFe protein had a reductant-independent ATPase relative rate of 10% and an ATP/$2e^-$ of >20 during reductant-dependent assay conditions. The conclusion of these experiments is that excess MoFe protein inhibits electron transfer but not ATP hydrolysis. Perhaps two types of ATP-hydrolyzing complexes between Fe protein and MoFe protein exist, one which is coupled to electron transfer and another which is uncoupled. Excess MoFe protein would then favor the ATP-hydrolyzing complex that is uncoupled from substrate reduction.

Some of the earliest work on reductant-independent ATP hydrolysis in the nitrogenase complex demonstrated a pH dependence on the relative rates of the coupled and uncoupled ATPase activities. It was found that, in the *C. pasteurianum* nitrogenase complex as the pH of steady-state assays decreased from 6.6 to 5.2, the relative rate of phosphate release due to reductant-independent ATP hydrolysis increased from 33% to 100% of the reductant-dependent phosphate release rate (Jeng *et al*. 1970). A more thorough investigation of the pH-dependence of reductant-independent ATP hydrolysis utilized the nitrogenase complex of *K. pnuemoniae* (Imam & Eady, 1980). These results agreed with the pH titration assays from *Cp*, and noted a Mg^{2+} and ATP concentration-dependent inhibition for reductant-independent ATPase activity. Additionally, a constant value for ATP/$2e^-$ was found for the pH range of 5.4 to 7.2, when the total phosphate formation values were corrected by subtracting the reductant-independent ATP hydrolysis values. The conclusion is that the uncoupling of ATP hydrolysis and electron transfer, which occurs at lower pH values, is due entirely to reductant-independent ATPase activity.

More recent research investigated the reversibility of the reductant-independent MgATP hydrolytic reaction in the nitrogenase complex from *K. pneumoniae* (Thorneley *et al*., 1991). The goal of this study was to compare the reductant-independent and -dependent ATPase reactions in order to determine if both reactions occur at the same sites on the protein complex. Using the kinetics of phosphate/water oxygen exchange, the ATP-binding site was probed and the reversibility of reductant-independent ATP cleavage was examined. Reductant-independent phosphate release rates maximized at a $Kp2_{ox}$ to Kp1 of 3:1 (or a $Kp2_{ox}$ to Mo of 2.2:1). MgADP was found to be a competitive inhibitor of reductant-independent ATP hydrolysis and bound more tightly to the $Kp2_{ox}$Kp1 complex than did MgATP. However, MgADP binds free $Kp2_{ox}$ more tightly than $Kp2_{ox}$Kp1 and this fact may be the driving force for the protein complex dissociation step. ^{18}O exchange between phosphate and water under reductant-independent ATPase conditions revealed a rate enhancement in the presence of MgADP, which was interpreted to support the reversible nature of ATP breakdown and formation on the $Kp2_{ox}$Kp1 complex in the absence of reductant.

It is difficult to reconcile these two possible explanations for the ATPase/electron transfer-uncoupling phenomenon in wild-type nitrogenase with the pattern of uncoupling demonstrated by the α-88CG MoFe protein. In both models, an excess of MoFe protein over Fe protein in a steady-state assay is found to increase the rate of ATP hydrolysis relative to the substrate reduction rate. However, the α-88CG MoFe protein exhibits uncoupling under high flux conditions, i.e. with excess amounts of Fe protein over MoFe protein. Uncoupling is observed in α-88CG MoFe protein steady-state assays when dithionite is in abundance, which should inhibit any significant contribution of reductant-independent ATPase activity.

Table 10: Comparison of Electron Flux Effects on Substrate Reduction and ATP Hydrolysis for the Wild-type and α-88CG MoFe Proteins

Strain	**DJ995, wild-type MoFe protein**			**DJ1019, α-88CG MoFe protein**		
e^- Flux, Fe:MoFe	**Low, 1:10**	**High, 40:1**	**Fold increase**	**Low, 1:10**	**High, 40:1**	**Fold increase**
ATP/2e^-	4.5	4.5	1	5.5	12	2.2
ATP SPA*	450	10,000	22	280	3,600	13.0
H_2 SPA**	100	2,200	22	50	300	6.0

Table 11: Comparison of NaCl Inhibitory Effects on Substrate Reduction and ATP Hydrolysis for the Wild-type and α-88CG MoFe Proteins

Strain	**DJ995, wild-type MoFe protein**			**DJ1019, α-88CG MoFe protein**		
[NaCl], mM	**Low, 25 mM**	**High, 400 mM**	**Fold decrease**	**Low, 25 mM**	**High, 400 mM**	**Fold decrease**
ATP/2e^-	6.0	6.0	1	10.0	6.0	1.7
ATP SPA*	12,500	1,500	8.3	2,600	310	8.4
H_2 SPA**	2,100	250	8.4	270	50	5.4

* ATP Hydrolysis rate = nmoles Creatine $(min \cdot mg \text{ MoFe protein})^{-1}$

** H_2 Evolution rate = nmoles H_2 $(min \cdot mg \text{ MoFe protein})^{-1}$

The increased uncoupling of ATP hydrolysis from substrate reduction with increasing electron flux exhibited by the α-88CG MoFe protein is quantitated by the ratio of ATP/$2e^-$. There are several ways to obtain an increase in a ratio value. Firstly, the ratio numerator, i.e., the absolute rate of ATP hydrolysis, could be increasing more rapidly than the wild-type rate with increasing electron flux. Secondly, the ratio denominator, i.e., the absolute rate of substrate reduction could be decreasing more rapidly than the wild-type rate with increasing electron flux. Thirdly, the numerator and denominator could both be increasing but the numerator increases more rapidly than the denominator. Fourthly, both the numerator and denominator could be decreasing but the numerator decreases less rapidly than the denominator. When the wild-type and α-88CG MoFe proteins are compared under low and high flux conditions, it is apparent that all rates are higher for both proteins under high flux conditions (see Table 10). However, the change in substrate reduction rate for the α-88CG MoFe protein going from a low to a high electron flux condition is much lower than the equivalent change in wild-type MoFe protein under low and high electron flux conditions. Therefore, the uncoupling of ATP hydrolysis from substrate reduction in the α-88CG MoFe protein is due to a lowered substrate reduction rate relative to the ATP hydrolysis rate as electron flux increases, i.e., the situation described in the third scenario above.

As discussed previously, (see Section V.E.2), the α-88CG MoFe protein is less inhibited by high concentrations of NaCl during high-electron-flux steady-state assays of H_2 evolution when compared to the wild-type, α-88CD and α-88CT MoFe proteins. Perhaps more interesting is the pattern of "re-coupling" of the ATP hydrolysis rate to the electron transfer rate for the α-88CG MoFe protein as the NaCl concentration increases, i.e., as the NaCl concentration increases, the ATP/2e- decreases from ~10 to 6. As in the previous example, it is important to examine the individual changes in the absolute rate of ATP hydrolysis and the substrate reduction rate in order to delineate which rate is more affected by the increasing NaCl concentration. As shown in Table 11, the major

difference between the wild-type and α-88CG MoFe proteins is the relatively lower inhibition of substrate reduction activity in the altered form of the MoFe protein.

A third example for the re-coupling of ATP hydrolysis and substrate reduction in the α-88CG MoFe protein is the time course assay in the presence of limiting dithionite. As in the previous two examples, as electron flux is decreased, the rate of ATPase activity decreases relative to the rate of substrate reduction and, therefore, the ATP/2e- value decreases. In this experiment, electron flux decreases as the limiting concentration of dithionite is depleted over time. Wild-type MoFe protein remains coupled during the same stage where the α-88CG MoFe protein is uncoupled, and becomes uncoupled only after complete exhaustion of the reductant source. This increase in the rate of ATP hydrolysis for the wild-type MoFe protein is undoubtedly due to reductant-independent ATPase activity.

A common theme seems to exist in each of the situations in which uncoupling of ATPase activity from electron transfer occurs with the α-88CG MoFe protein. In all three nitrogenase activity assays, the ATP/2e- ratio is high when there is the availability of excess reduced Fe protein over MoFe protein. The α-88CG MoFe protein is incapable of converting a high flux of electrons into products as efficiently as the wild-type MoFe protein, thus, lowered relative rates of substrate reduction are observed for this altered MoFe protein. The result is a waste of ATP molecules relative to the amount of product(s) evolved. When either the relative concentration of Fe protein to α-88CG MoFe protein (i.e., low flux) is decreased or the relative concentration of a competing counterion (e.g. NaCl) is increased in steady-state H_2 evolution assays, the result in both cases is a decrease in the rate of efficient electron transfer from the Fe protein to the altered MoFe protein and, therefore, a decrease in the ATP/$2e^-$. These data suggest that Fe protein can dock with the α-88CG MoFe protein and hydrolyze ATP without transferring an electron.

This conclusion is itself not a complete answer to how the α-Cys88 to Gly substitution affects the substrate reduction rate. A likely explanation is that the amino

acid substitution in the α-88CG MoFe protein has perturbed a conformational state that normally functions in the efficient transfer of electrons. Because the P cluster mediates electron transfer between nitrogenase component proteins, this perturbance must exist somewhere in the pathway from the Fe_4S_4 cluster of the Fe protein to the substrate bound at the FeMo-cofactor. The decrease in steady-state substrate reduction rate could result from a disturbance in either the intermolecular electron transfer rate or the intramolecular electron transfer rate or both. However, steady-state kinetic analysis is not able to probe perturbations of these electron transfer processes. Therefore, the next logical step was to subject all of the MoFe proteins to pre-steady state kinetic analyses. The results and discussion of these experiments are the topic of the next chapter.

CHAPTER VI.

PRE-STEADY-STATE KINETICS OF α-CYS88 ALTERED MOFE PROTEINS

A. Introduction

Although the steady-state kinetic analysis of the α-Cys88 altered MoFe proteins revealed a variety of significant differences from the wild-type MoFe protein, these analyses did not delineate a specific root for the changes in the nitrogenase mechanism caused by substitutions at the P cluster bridging cysteine α-88. However, the electron transfer process in the altered MoFe proteins was clearly implicated as a source of perturbation in the catalytic reaction. Over a decade earlier, the work of Thorneley and Lowe had detailed the individual steps in the intermolecular electron transfer cycle between the Fe protein and MoFe protein of the nitrogenase complex (see Section I.F.1). One of the many findings that eventuated from this work was the determination that dissociation of the nitrogenase complex was the rate-limiting step in the overall mechanism. Therefore, the next reasonable course of action was to subject the α-Cys88 altered MoFe proteins to similar pre-steady-state kinetic analyses in order to ascertain if differences existed in the value and/or the location of the rate-limiting step between wild-type and altered MoFe proteins. The technique of stopped-flow spectrophotometry was used exclusively in these kinetic experiments (see Section II.F.1).

B. Primary Electron Transfer Rate, k_{+2}

The primary electron-transfer rates of each of the α-Cys88 altered MoFe proteins were calculated using the same methodology that established the electron transfer rate for wild-type nitrogenase from *K. pneumoniae* (Thorneley, 1975). An absorbance titration experiment was necessary to resolve the maximum absorbance change at 430 nm for the Fe protein as it is oxidized during the electron donation event. There were essentially no differences between the wild-type and altered MoFe proteins for the component protein ratio at which maximum absorbance change occurred; all MoFe proteins maximized (see Figure 17) at a Fe protein-to-MoFe protein ratio of 4:1. In order to insure maximization of

the absorbance change during the rate constant calculation, a 5:1 Fe protein-to-MoFe protein was used in each primary electron-transfer measurement. Table 12 lists the rate constants, k_{+2}, for primary electron transfer for the wild-type and α-Cys88 altered MoFe proteins. Although the rates are lower for the α-88CD, α-88CG and α-88CT when compared to wild-type MoFe protein, none of these rates was sufficiently slow to fully account for the lowered steady-state substrate reduction rates determined for these altered MoFe proteins.

Although the absolute value for the protein-complex association rate cannot be determined from the primary electron transfer experiment, it is possible to conclude that because the subsequent electron-transfer step is not rate-limiting and the two component proteins must associate before electron transfer occurs, then the association rate may also be excluded as a potential rate-limiting step.

Additional data pertaining to the α-Cys88 altered MoFe proteins can be gleaned from the primary electron-transfer rate determinations. Because the Fe protein, reductant source, and ATP are all present in excess concentrations, the ΔA is, therefore, proportional to the fraction of MoFe protein that is capable of accepting an electron from the Fe protein within the 100 millisecond time frame of this stopped-flow spectrophotometric experiment. In other words, ΔA is proportional to the fraction of catalytically active MoFe protein. When the ΔA for the wild-type MoFe protein primary-electron transfer scan is compared to the ΔA values for the α-88CD, α-88CG and α-88CT MoFe proteins, the differences closely match the differences in Mo content between these proteins (see Table 13 & Figure 17). This correlation provides additional evidence for the contention that these substitutions at the α-88 P cluster bridging cysteine affect the metallocluster content of the MoFe protein.

Table 12: Primary Electron Transfer Rate Constant, k_{+2}, for the Wild-type and α-Cys88 Altered MoFe Proteins

MoFe Protein	100% N_2	100% C_2H_2	100% Argon
Wild-type	170 sec^{-1}	200 sec^{-1}	170 sec^{-1}
α-88CD	110 sec^{-1}	200 sec^{-1}	110 sec^{-1}
α-88CG	150 sec^{-1}	180 sec^{-1}	ND
α-88CT	130 sec^{-1}	140 sec^{-1}	ND

ND = Not Determined

Table 13: Comparisons of Absorbance Change for Primary Electron Transfer Reactions and Mo Content for the Wild-type and α-Cys88 Altered MoFe Proteins

MoFe Protein	ΔAbs*	%WT**	Mo Content†	%WT**
Wild-type	0.10	100	1.6	100
α-88CD	0.05	50	0.9	56
α-88CG	0.025	25	0.6	38
α-88CT	0.023	23	0.6	38

* Absorbance change at 430 nm for 10 μM of MoFe protein.
** Percent of the wild-type MoFe protein value
† g atoms of Mo per mole of MoFe protein

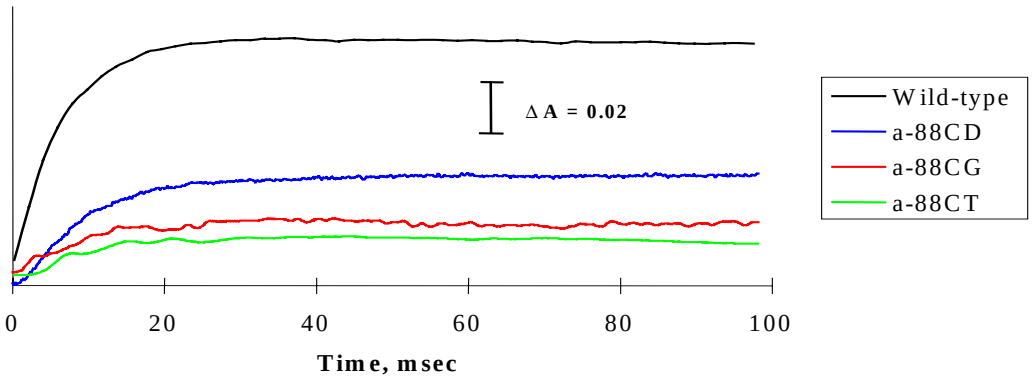

Figure 17: Primary Electron Transfer Spectra for Wild-type and ∝-Cys88 Altered MoFe Proteins

The anaerobic glovebox in which all of the pre-steady-state kinetic measurements were taken operates under a 100% N_2 atmosphere. Therefore, initial rate constants were based on the MoFe protein's electron transfer abilities under a N_2 environment. Additional information can potentially be gained from examination of a particular nitrogenase complex primary electron-transfer reaction under a 100% C_2H_2 atmosphere. The absorbance changes, which occur after the first 200 msec under a N_2 atmosphere but are absent under an C_2H_2 atmosphere, have been interpreted to be due to an oxidation of the P clusters that occurs when highly reduced states of the MoFe protein (E_4, see Section I.D.3.d) are acheived. Because the altered MoFe proteins in this study possess substitutions at a P-cluster ligand, the primary electron-transfer analyses were also performed under a 100% C_2H_2 atmosphere and, in some cases, the spectrophotometric scans were allowed to extend as long as 1 sec. Table 12 lists the primary electron-transfer rate constants, k_{+2}, for the four MoFe proteins of interest. An interesting and serendipitous discovery was that the α-88CD MoFe protein had a primary electron-transfer rate constant under an atmosphere of 100% C_2H_2 that was double the rate constant under a 100% N_2 atmosphere. In contrast, the wild-type, α-88CG and α-88CT MoFe proteins revealed no significant differences in their values of k_{+2} for a either 100% C_2H_2 or 100% N_2 atmosphere. Subsequently, the wild-type and α-88CD MoFe proteins were subjected to the same electron-transfer experiment under a 100% Argon atmosphere (see Table 12), where the observed rate constants were similar to those observed under 100% N_2. However, in all cases, none of the primary electron-transfer rates appeared to be rate-limiting.

An interesting result was obtained from comparisons of the slower absorbance changes that occur under nitrogen and acetylene atmospheres. The α-88CG MoFe protein revealed a distinct absorbance decrease under both N_2 and C_2H_2 atmospheres following the initial absorbance increase during primary electron transfer (see Figures 18

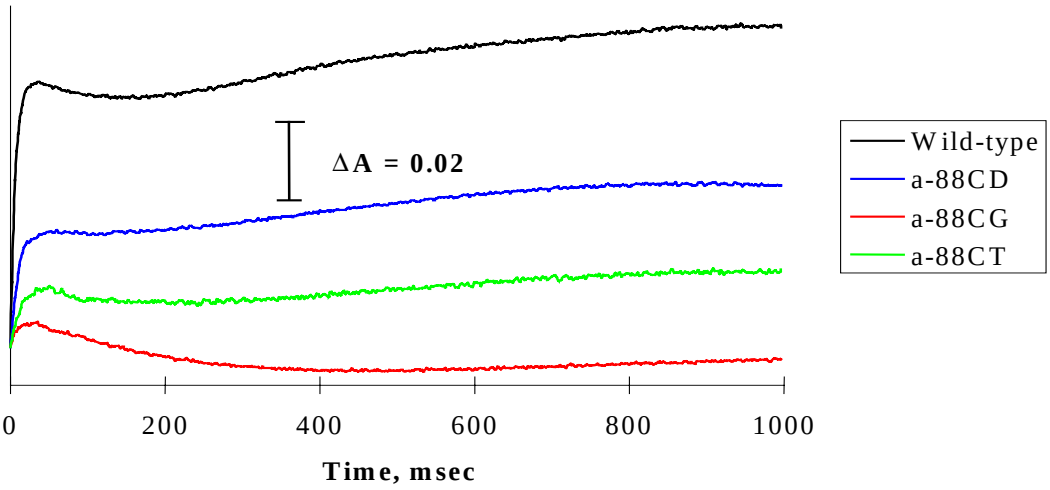

Figure 18: Long Time Absorbance Changes during Nitrogenase Turnover under N_2 for Wild-type and α-Cys88 Altered MoFe Proteins

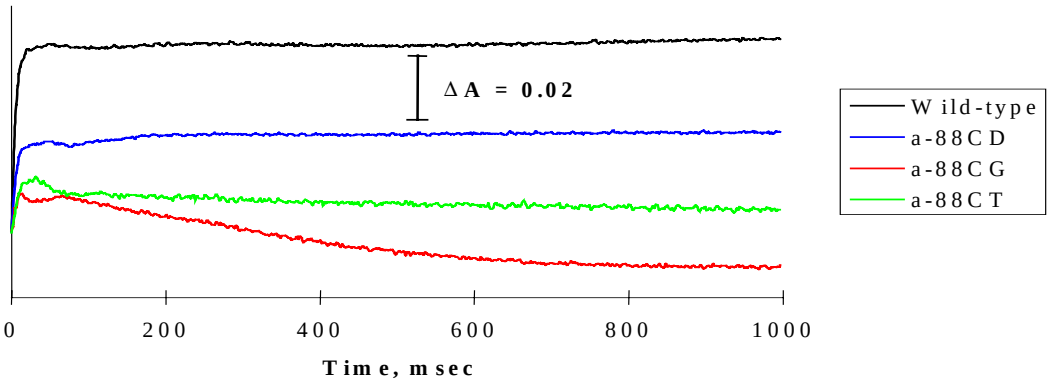

Figure 19: Long Time Absorbance Changes during Nitrogenase Turnover under C_2H_2 for Wild-type and α-Cys88 Altered MoFe Proteins

& 19). Meanwhile, the wild-type, α-88CD, and α-88CT MoFe proteins exhibited both similar patterns for the small, slower absorbance change that occurs under the 100% N_2 condition, and the absence of an additional absorbance change that occurs under the 100% acetylene condition.

C. Protein Complex Dissociation Rate, k_{-3}

Inspection of the protein-dissociation rates for the α-Cys88 altered MoFe proteins was a high priority experiment because of the fact that, in the wild-type nitrogenase complex, Fe protein-MoFe protein dissociation is the rate-limiting step. Although the experiment was technically more difficult than the primary electron transfer experiment due to the necessity of using dithionite-free nitrogenase component proteins, the wild-type controls agreed favorably with the published values of 6.4 ± 0.8 sec^{-1} for k_{-3}. Dissociation rates were determined for the wild-type and α-Cys88 altered MoFe proteins under both 100% N_2 and 100% C_2H_2 atmospheres (see Table 14). As evidenced by the rate constants measured under a 100% N_2 atmosphere, there is no significant difference in the dissociation rate of MoFe/Fe protein complexes containing either the wild-type or the α-Cys88 altered MoFe proteins. When dissociation rates were measured under a 100% C_2H_2 atmosphere, the rates for wild-type, α-88CG and α-88CT MoFe protein were similar to each other and about 50% as fast as those under N_2, whereas the α-88CD MoFe protein had a k_{-3} value that was almost twice that of the other three proteins, and the rate was nearly the same as the rate under a 100% N_2 atmosphere.

These differences in rate constants for the α-88CD MoFe protein compared to wild-type and the other altered MoFe proteins under N_2 and C_2H_2 atmospheres provided the motivation for conducting a set of substrate-reduction assays under high acetylene concentrations and various component-protein concentrations. The goal of these experiments was to ascertain whether the differences in rate constants observed using the

Table 14: Protein Complex Dissociation Rate, k_{-3}, for Wild-type and α-Cys88 Altered MoFe Proteins under N_2 and C_2H_2 Atmospheres

MoFe Protein	100% N_2*	100% C_2H_2*	$k_{-3}N_2/k_{-3}C_2H_2$
Wild-type	6.4	3.6	1.8
α-88CD	7.0	6.0	1.2
α-88CG	6.1	3.2	1.9
α-88CT	6.7	3.5	1.9

* rate constants in units of sec^{-1}

Table 15: Rapid Quench Product Evolution for Wild-type and α-88CD MoFe Proteins under N_2 and C_2H_2 Atmospheres

MoFe Protein	Total nmoles of product/min		Product under Ar / Product under C_2H_2
	100% Argon*	100% C_2H_2**	
Wild-type	410	200	2.0
α-88CD	300	250	1.2

* nmoles of H_2 for 10 μM of MoFe protein, 50 μM of Fe protein assay

** nmoles of H_2 + C_2H_4 for 10 μM of MoFe protein, 50 μM of Fe protein assay

two gases were also manifested in differences in substrate-reduction rate. Assays measuring inhibition due to C_2H_2 concentration have been discussed previously (see Section V.E.3), and revealed no significant differences between the wild-type and α-88CD MoFe proteins in their patterns of inhibition of total electron flux (see Figure 15). However, a critical difference between the stopped-flow spectrophotometric experiment and the C_2H_2-concentration-inhibition assays was the component-protein concentrations. In order to maximize the absorbance change in the pre-steady-state kinetics experiment, a 10 μM MoFe protein and 50 μM Fe protein mixture was utilized in the spectrophotometric scans. In the steady-state C_2H_2-reduction assays, the protein concentrations were 30-fold lower for MoFe protein and 7.5-fold lower for Fe protein. In order to simulate the conditions of the stopped-flow spectroscopy, several high-protein-concentration, small-volume, rapid-quench assays were performed under 100% Argon and 100% C_2H_2 atmospheres (see Section II.E.10.b). In these assays, an argon atmosphere was used in place of an 100% N_2 atmosphere due to the ease and sensitivity with which H_2 can be measured by gas chromatography and because the wild-type and α-88CD MoFe proteins each have similar primary electron-transfer rates under an 100% argon and 100% N_2 atmosphere. As demonstrated by the results in Table 15, the ratio of product evolution under an argon vs. an C_2H_2 atmosphere is equivalent to the ratio of k_{-3} under a nitrogen vs. an C_2H_2 atmosphere for both the wild-type and α-88CD MoFe proteins. Thus, the rapid-kinetic results are in agreement with the substrate-reduction rates when measured under identical conditions for these two MoFe proteins.

D. Secondary Electron Transfer Rate

Although there are significant differences in some of the rate constants for both primary electron transfer and protein complex dissociation for the wild-type and the α-Cys88 altered MoFe proteins, neither of these rate constants could be ascribed as the rate-limiting step in the overall catalytic mechanism of the α-88CG and α-88CT MoFe proteins. Therefore, it was necessary to look beyond the first electron transferred between

the nitrogenase component proteins in search of a potential rate-limiting step in the site-substituted MoFe proteins. Due to the transient nature and multiplicity of the reduced states of the MoFe protein beyond the E_1 redox stage, detailed quantification of the abundance and rate constants of these more reduced states are exceedingly difficult to obtain. However, one technique has recently proved useful in gauging the electron-transfer rate between the Fe protein and the one-electron-reduced MoFe protein from *K. pneumoniae* (i.e., from the E_1 to the E_2 redox states of the MoFe protein; see Section I.F.2), and is referred to as secondary electron transfer. The stopped-flow technique utilized for these measurements has been described in Section II.F.3.

Table 16 lists the rate constants for secondary electron transfer for the four MoFe proteins under investigation for both 100% N_2 and 100% C_2H_2 atmospheres. Based on these results, it can be concluded that the wild-type and α-88CD MoFe proteins demonstrate no significant changes in the rates of electron transfer for the E_0-to-E_1 and E_1-to-E_2 transitions. Additionally, the primary and secondary electron-transfer rates are the same irrespective of the two gaseous substrates employed for both of these MoFe proteins. However, the α-88CG and α-88CT MoFe proteins both display a more than 10-fold decrease in the rate of electron transfer over a 1-hr time period during stopped-flow spectrophotometric analysis. Figure 20 details the change in the rate constant value with time for the wild-type and the α-Cys88 altered MoFe proteins; a decreasing rate constant value means a slower electron-transfer rate or fewer electron-transfer events per unit time. It is important to note that, in each secondary electron-transfer rate determination, the total change in absorbance for each scan remains approximately the same at each time point for each MoFe protein. This constancy in the absorbance change is important in the interpretation of the rate-constant decrease and is also an issue that recurs in Chapter VIII.

E. Discussion of Pre-steady-state Kinetics of the α-Cys88 Altered MoFe Proteins

The pre-steady-state analysis of the α-Cys88 altered MoFe proteins had two goals. The first goal was to determine whether differences existed between the wild-type and the

altered MoFe proteins in any of the quantifiable rate constants of the Fe-protein cycle. The second goal was to determine if any of these differences represented the rate-limiting step and so could account for the reduced substrate-reduction rates observed in the steady-state analyses. The rapid-kinetic data permits a number of conclusions to be drawn concerning the perturbations of the nitrogenase reaction in the α-Cys88 altered MoFe proteins. These conclusions are divided into four categories: 1. intermolecular electron-transfer rates; 2. intramolecular electron-transfer rates; 3. effects of C_2H_2 on the α-88CD MoFe protein; and 4. alternative explanations.

1. Intermolecular Electron-Transfer Rates

Based on the primary electron-transfer rate-constant data, it can be concluded that, under a 100% N_2 atmosphere, there is a significant reduction (~40%) in the intermolecular electron-transfer capability of the α-88CD MoFe protein when compared to wild-type MoFe protein. Although this difference is significantly large, the electron transfer rate is still much faster than the complex dissociation rate and, therefore, cannot explain the overall lowered substrate-reduction rate in this altered MoFe protein. Also, the differences in k_{+2} between the wild-type and the α-88CG and α-88CT MoFe proteins were slight and probably inconsequential.

A potentially important pre-steady-state kinetic measurement is the dissociation rate of the nitrogenase component-protein complex because this rate is the proposed rate-limiting step in the wild-type nitrogenase mechanism. Because the dissociation rate of the nitrogenase complex is significantly slower than the majority of the other steps in the Fe-protein cycle and, if intermolecular electron transfer is the rate-limiting process in an altered MoFe protein, then quantitation of the complex-dissociation rate is a logical first

Table 16: Comparison of Primary and Secondary Electron Transfer Rate Constants under N_2 and C_2H_2 Atmospheres for Wild-type and α-Cys88 Altered MoFe Proteins

MoFe Protein	Primary Electron Transfer Rate*		Secondary Electron Transfer Rate**	
	100% N_2	100% C_2H_2	100% N_2	100% C_2H_2
Wild-type	170	200	160	180
α-88CD	110	200	100	200
α-88CG	150	180	10	ND
α-88CT	130	140	10	ND

ND = not determined

*Rate constants in units of sec^{-1}, determined from ~50 msec curve fit.

**Rate constants in units of sec^{-1}, determined from ~50-500 msec curve fit ≥1 hr after mixing.

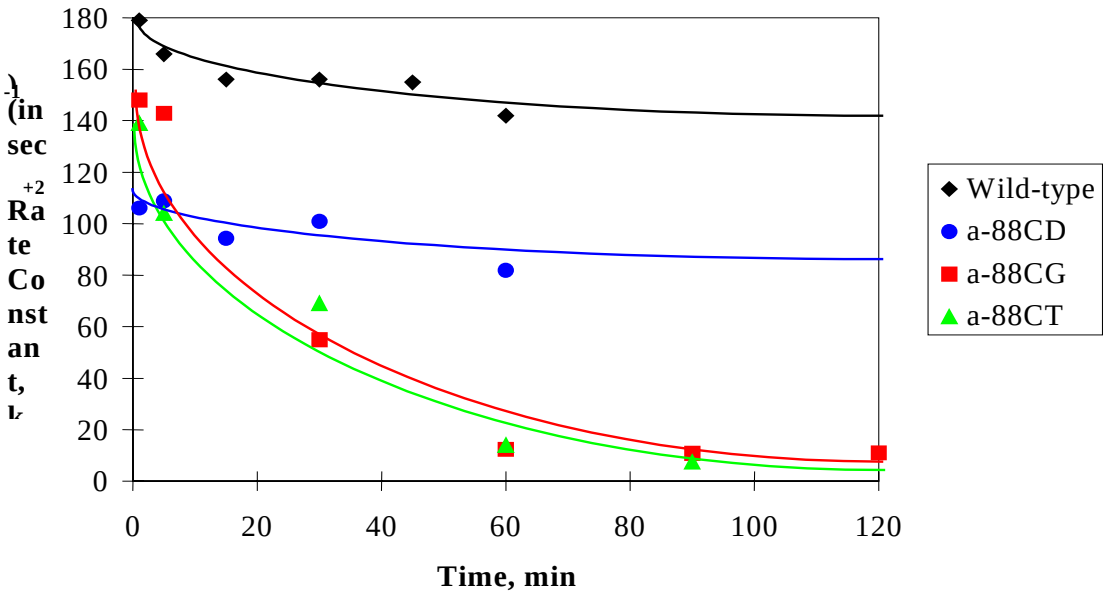

Figure 20: Change in Electron Transfer Rate Constant, k_{+2}, with Time for Wild-type and ∝-Cys88 Altered MoFe Proteins under a N_2 atmosphere

step. However, there were essentially no differences in the rate constant, k_{-3}, between the wild-type and the three site-substituted MoFe proteins. Thus, although substitution at the α-88 P cluster-bridging cysteine has demonstrated effects on the intermolecular electron-transfer process, these effects do not result in any rate constants less than the value of ~6 sec^{-1} that represents the rate-limiting step for the wild-type nitrogenase catalyzed reaction.

An additional consequence of the analysis of the rate of complex dissociation concerns the uncoupling of ATPase activity from substrate-reduction activity in the α-88CG MoFe protein. The discussion of the steady-state kinetic analyses (see Section V.G) included possible explanations for the significant uncoupling that occurs when the Fe protein-MoFe protein complex is slow in dissociating, namely initiation of the back reaction and reductant-independent ATP hydrolysis. The k_{-3} rate-constant determination for the α-88CG MoFe protein, because it is nearly identical to the wild-type MoFe protein rate, supports the conclusion that the uncoupling of ATP hydrolysis from product evolution is not due to increased ATPase activity from a slowly-dissociating nitrogenase complex.

2. Intramolecular Electron-Transfer Rate

A likely explanation for the reduction in substrate-reduction activity in the α-88CG and α-88CT MoFe proteins is the disruption of the intramolecular electron-transfer mechanism. As previously mentioned in Section VI.D, due to the heterogeneity of MoFe protein redox states that exists during turnover of the nitrogenase enzyme system, intramolecular electron transfer is not susceptible to direct measurement. However, the secondary electron-transfer technique has been utilized as an indirect method for the quantification of subsequent electron-transfer events because secondary electron transfer cannot proceed any faster than the intramolecular events that precede it.

The secondary electron-transfer rate data for the α-88CG and α-88CT MoFe proteins reveals a substantial decrease in the rate constant over the time course of the experiment. A legitimate explanation of this phenomenon involves the current hypothesis that electrons are accepted from the Fe protein by the P clusters and then shuttled

intramolecularly to the FeMoco. In the glycine- and threonine-α-88-substituted MoFe proteins, this intramolecular transfer is somehow diminished, resulting in a decrease in both the intermolecular electron-transfer rate to the E_2 redox state and in the subsequent production of the more reduced states of the MoFe protein. This scenario is reminiscent of the situation in the β-98YH MoFe protein (see Section I.D.3.c), where the second phase of the biphasic turnover rate of this protein was estimated to occur after the accumulation of two electrons at the P cluster. The smaller rate constant of the second phase was interpreted to be due to disruption of the intramolecular electron-transfer process in the β-98YH MoFe protein. A similar explanation is consistent with the data observed in this work.

When the primary electron-transfer spectrophotometric scans are extended to 1 sec, a noticeable absorbance decrease occurs in the α-88CG MoFe protein under either 100% N_2 or 100% C_2H_2 atmosphere (see Figures 18 & 19). The absorbance decrease that occurs in the α-88CG MoFe protein is reminiscent of similar patterns found in the β-98YH altered MoFe protein of *A. vinelandii* (Peters *et al*., 1995b) and the β-124FI altered MoFe protein from *K. pneumoniae* (Thorneley, 1992). All of these absorbance decreases occur after the initial absorbance increase due to the primary electron-transfer event that is complete within the first 50 msec. Each of the absorbance decreases can be fit to a single exponential curve, although the rate constant associated with the curve is different for each of the above altered MoFe protein. Coincidentally, the rate constant associated with the α-88CG MoFe protein slow, longer time, absorbance change is equal to the protein rate of complex dissociation, namely 6.5 sec^{-1}. However, the interpretation of these absorbance decreases is the same for each altered protein. The decrease means that, in the steady-state, a much higher percentage of the Fe protein is in its reduced state. This increase in reduced Fe protein concentration is not due to a decrease in the protein complex dissociation rate, k_{-3}, because this would result in a higher concentration of oxidized Fe protein which has a higher absorption at 430 nm. Therefore, some other reaction has become rate-limiting and this slows down the oxidation of Fe protein in the

second cycle of electron transfer. A disruption of an intramolecular electron-transfer event is a plausible explanation for these experimental results.

3. Effects of C_2H_2 on the α-88CD MoFe Protein

A conclusion drawn from the steady-state kinetic examination of the α-88CD MoFe protein is that its lowered substrate-reduction activity is due to the presence of metallocluster-deficient MoFe protein. This conclusion is supported by the pre-steady-state kinetic data. None of the rate constants for either primary or secondary electron transfer or for protein-complex dissociation proved to be rate-limiting for this aspartate-for-cysteine-substituted MoFe protein. However, an unexpected, yet interesting, finding is the effect of an 100% C_2H_2 atmosphere on both the primary-electron-transfer and protein-dissociation rates.

In the steady-state C_2H_2 self-inhibition assays, both wild-type and α-88CD MoFe proteins exhibit similar patterns of inhibition of total electron flux by high concentrations of acetylene. These assay results indicate that, at the protein concentrations and component-protein ratios used in these assays, acetylene inhibits substrate reduction by both MoFe proteins in an equivalent fashion. When substrate-reduction assays are performed at the high protein concentrations used in the stopped-flow spectrophotometry experiments, the activity of the α-88CD MoFe protein is nearly equal under 100% C_2H_2 to its substrate-reduction activity under 100% N_2. Whereas, when wild-type MoFe protein is subjected to the same high-protein-concentration rapid-quench assays, the product-evolution rate under 100% C_2H_2 is about half the rate under 100% N_2. These results correlate with the pattern of rate constants for protein-complex dissociation under acetylene and nitrogen.

A simple explanation for the effect of acetylene on the α-88CD MoFe protein is that it has a higher affinity for the active site and this could account for the differences in substrate-reduction rates under 100% C_2H_2. However, this explanation does not conform with the observations that the K_m for acetylene reduction is the same for both proteins and

that the patterns of C_2H_2 self-inhibition in lower-protein-concentration assays are very similar (see Section V.E.3; Figure 15).

Perhaps a better explanation includes the observation that acetylene is both a substrate and an inhibitor of nitrogenase turnover and that these two functions are elicited differentially under various assay conditions. Apparently, the high-protein and high-acetylene concentrations used in the stopped-flow analyses are optimal for the inhibitory function of C_2H_2. The differences between the wild-type and α-88CD MoFe protein then are due to a decreased sensitivity to the inhibitory effects of acetylene on the altered MoFe protein relative to the wild-type MoFe protein. The alteration of the P-cluster peptide environment has somehow altered the ability of acetylene to act as an inhibitor. The aspartyl-substitution at the α-88 position of the MoFe protein results in the alteration of an C_2H_2-binding site that, in the wild-type MoFe protein, either blocks or limits electron flux through the MoFe protein when the C_2H_2 concentration is high.

It is believed that the inhibitory effect of C_2H_2 at high component-protein concentrations is due to an enhancement of the binding affinity between MoFe protein and oxidized Fe protein by C_2H_2 (see Section I.F.2.c; Lowe *et al*. 1990). Working under this hypothesis, the α-88CD substitution could be inducing a conformational change in the structure of the MoFe protein such that it reduces the strength of the $Av2_{ox}$ Av1 associative complex that is normally enhanced by acetylene. The alteration in this P-cluster ligand provides a compensatory conformational change that permits nitrogenase component-protein dissociation even in the presence of high acetylene concentrations.

It is possible that the apoprotein fraction of the α-88CD MoFe protein diminishes the inhibitory effects of acetylene by binding and sequestering a percentage of the gas molecules, thereby relieving some of the holoenzyme to function normally. However, this possibility seems unlikely when one considers that the α-88CG and α-88CT MoFe proteins both contain a higher percentage of apoprotein and yet respond identically to wild-type MoFe protein under an 100% C_2H_2 atmosphere.

4. Alternative Explanations

The evidence for a rate-limiting intramolecular electron-transfer step has been demonstrated for both the α-88CG and α-88CT MoFe proteins. However, the possibility exists that there are rate-limiting steps in the intermolecular electron-transfer process of the Fe-protein cycle that could not be measured in our analyses. Two such steps are the rate of ATP hydrolysis and the rate of phosphate release. Previous research with the nitrogenase complex from *K. pneumoniae* has determined the rate of ATP hydrolysis to be 50 sec^{-1} (Thorneley *et al*., 1989), and the rate of phosphate release to be 22 sec^{-1} (Lowe *et al*., 1995). Due to the unavailability of the specialized equipment required for phosphate release measurements in the millisecond time scale, it was not possible to attempt to determine these rate constants for the α-Cys88 altered MoFe proteins.

However, from the steady-state creatine assays, it could be estimated that the rates of ATP hydrolysis in the wild-type and altered MoFe proteins were approximately equal when these rates were recorded in terms of Mo content. Therefore, it seems unlikely that ATP hydrolysis is the rate-limiting step in these site-directed MoFe-protein variants. Estimation of the rate of phosphate release is not possible using the data obtained thus far for the α-Cys88 altered MoFe proteins. It has been suggested that phosphate release represents the key work step in the energy-transduction process, and this has been found to be the case for a number of ATPases (Thorneley, 1992). Furthermore, it has been speculated that the energy transduced by phosphate release could be used to modulate the redox potential of the P clusters and/or FeMo-cofactors. Perhaps examination of the phosphate release rates for both the α-Cys88 altered MoFe proteins and for related altered MoFe proteins could contribute to the resolution of this interesting hypothesis.

CHAPTER VII.
SPECTROSCOPIC TECHNIQUES APPLIED TO THE α-CYS88 ALTERED MOFE PROTEINS

A. Introduction

The employment of sophisticated spectroscopic techniques has traditionally yielded a wealth of information in the realm of metalloenzyme research. Data obtained include estimation of midpoint potentials of redox centers, determinations of oxidation and spin states of individual atoms in metalloclusters, and the effect(s) of the peptide environment on the electromagnetic properties of metal centers. As discussed in previous sections (see Sections I.C.2, I.D.2b & 3b, and II.G), three types of spectroscopy have been invaluable in nitrogenase research because of their sensitivity in detecting minute changes in the electronic and magnetic properties of the Fe-S centers of the enzyme complex. These three types of spectroscopy are electron paramagnetic resonance, Mössbauer, and magnetic circular dichroism spectroscopies. In each case, the technique reveals specific details of the electromagnetic properties of either the FeMoco or P cluster or both. Differences in the spectra of the various wild-type and α-Cys88 altered MoFe protein are discussed in the following sections as are the potential consequences of these differences.

B. Electron Paramagnetic Resonance (EPR) Spectroscopy

The initial impetus for applying EPR to the α-Cys88 altered MoFe proteins was to determine whether the S=3/2 FeMoco signal of these proteins was altered in line shape, *g* value, and/or peak intensity. Such an examination reveals potential perturbation of the immediate environment of the unpaired electrons of the FeMo-cofactor that is indicative of structural, compositional, and/or electromagnetic properties of this metallocenter.

Additionally, a S=1/2 EPR signal has been found by various researchers that arises from “apo-or demolybdo-” MoFe protein that lacks FeMoco but possesses the P clusters. Sources of this signal include an inactive Mo-deficient form of *C. pasteurianum*

MoFe protein (Zumft & Mortenson, 1973), the *ΔnifH A. vinelandii* strain DJ54 (Gavini *et al*., 1994), and a Nif B^- strain of K. pneumoniae (Hawkes & Smith, 1983). This relatively broad signal has *g*-values at 2.04 and 1.94 and is believed to arise from the P cluster and, when integrated, the signal works out to only ~0.1 spin per MoFe tetramer.

1. Spectra of Dithionite-reduced Wild-type and α-Cys88 Altered MoFe Proteins

The EPR spectra of wild-type and α-Cys88 altered MoFe proteins were recorded in the laboratories of Dr. W.R. Dunham, University of Michigan, on a Varian E-line spectrometer under the experimental conditions described in Section II.G.1. Figure 21 shows the relative S=3/2 EPR signals for the four MoFe proteins studied. As expected, because the S=3/2 EPR arises in FeMoco, there are no detectable differences in the spectra of the wild-type and α-Cys88 altered MoFe proteins in terms of either line shape or *g* value of the characteristic FeMoco EPR signal, however, the peak intensity of the *g*=3.7 deflection is noticeably smaller in the α-88 site-substituted MoFe proteins when compared to a wild-type MoFe protein sample of equal protein concentration as determined by the Folin colorimetric assay.

An important discovery was revealed during inspection of the dithionite-reduced EPR spectrum of the α-88CG MoFe protein. In addition to the typical S=3/2 FeMoco signal, there was a S=1/2 signal with *g*=2.08, 1.95, and 1.83 that integrated to the same peak area as the S=3/2 signal, thus indicating a 1:1 ratio of these two paramagnetic species (see Figure 22). This S=1/2 EPR signal was identical to a one-electron-oxidized P-cluster-derived signal that has been shown to be a transient species in the oxidative titration of the MoFe protein from *A. vinelandii* (see Section I.D.3.b; Tittsworth & Hales, 1993). Recognition of the similarities between these EPR signals led to the hypothesis that substitution of α-Cys88 with Gly results in this S=1/2 signal and, therefore, this spectrum could be the first demonstration of a non-integer EPR signal associated with the P cluster in the dithionite-reduced state of the MoFe protein.

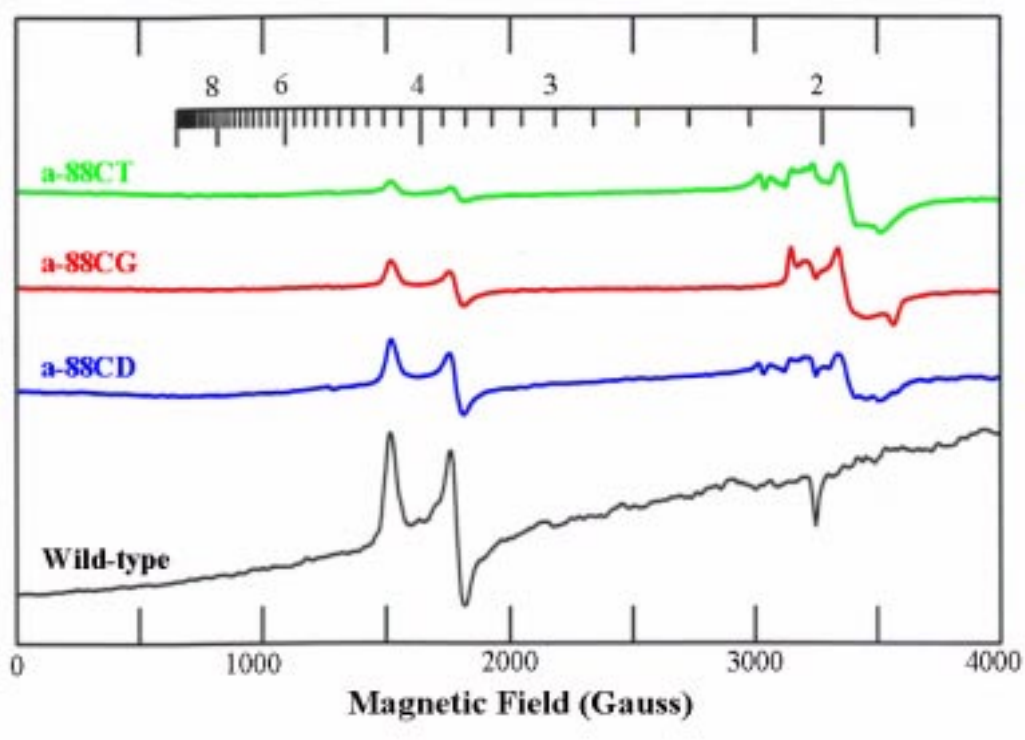

Figure 21: EPR Spectra Comparison for the Wild-type and α-Cys88 Altered MoFe Proteins

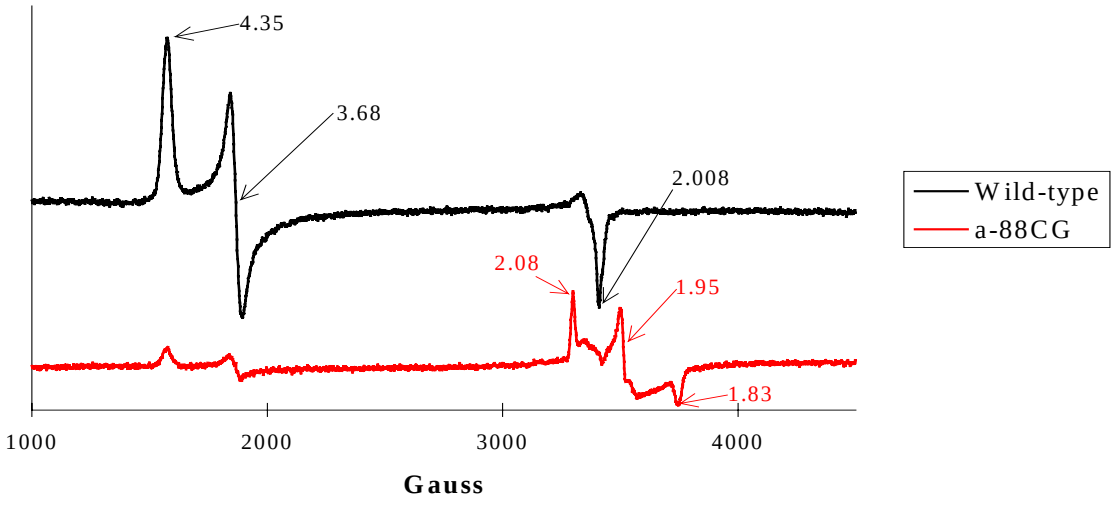

Figure 22: EPR Spectra Comparison of Dithionite-reduced Wild-type and a-88CG MoFe Proteins

2. Slow Turnover Spectra for Wild-type and α-88CG MoFe Proteins

The possibility of a detectable EPR signal associated with the P clusters of the α-88CG MoFe protein provided the opportunity to test the hypothesis that the P clusters were the primary acceptor of electrons from the Fe protein. In this nitrogenase turnover experiment, the α-88CG MoFe protein was combined with Fe protein, excess dithionite and an ATP-regenerating system. An adverse molar ratio of 1:100 Fe protein-to-MoFe protein was used in order to slow the electron-transfer reaction sufficiently so that the reaction could be stopped by the freeze-quench method at various time points. Figure 23 shows the EPR spectra for samples that were stopped at 0, 5, 30, or 60 min after initiation of this slow turnover reaction. The S=1/2 EPR signal disappears within 5 min and does not reappear in either the 30- or 60-min samples, whereas the S=3/2 FeMoco EPR signal intensity decreases by more than half over the first 5 min and then slowly increases from the 5-min sample to 60-min sample. The results of this time-course experiment showed that the S=1/2 EPR signal was lost as predicted but the results were inconclusive in determining whether the S=1/2 EPR signal was a part of the turnover cycle of the nitrogenase reaction.

In the wild-type control experiment, the S=3/2 EPR signal diminishes to ~30% of the initial (0 min) peak intensity during the first 5 min of the reaction. The signal intensity slowly increases to 50% at 30 min and 70% at 60 min, respectively, of the initial S=3/2 peak intensity. These results are in line with the expected decrease in the signal intensity as FeMoco is reduced from the semi-reduced, EPR-active state, to the fully-reduced EPR-silent state during the early stages of the turnover experiment. As the reaction continues beyond 30 min, the product is evolved and FeMoco returns to the semi-reduced, EPR active state, which results in a gradual increase in the S=3/2 EPR signal peak intensity.

3. Single-electron Turnover Spectra for Wild-type and α-88CG MoFe Proteins

In order to more carefully dissect the sequence of the electron-transfer reaction between the Fe protein and the α-88CG MoFe protein, an additional turnover experiment

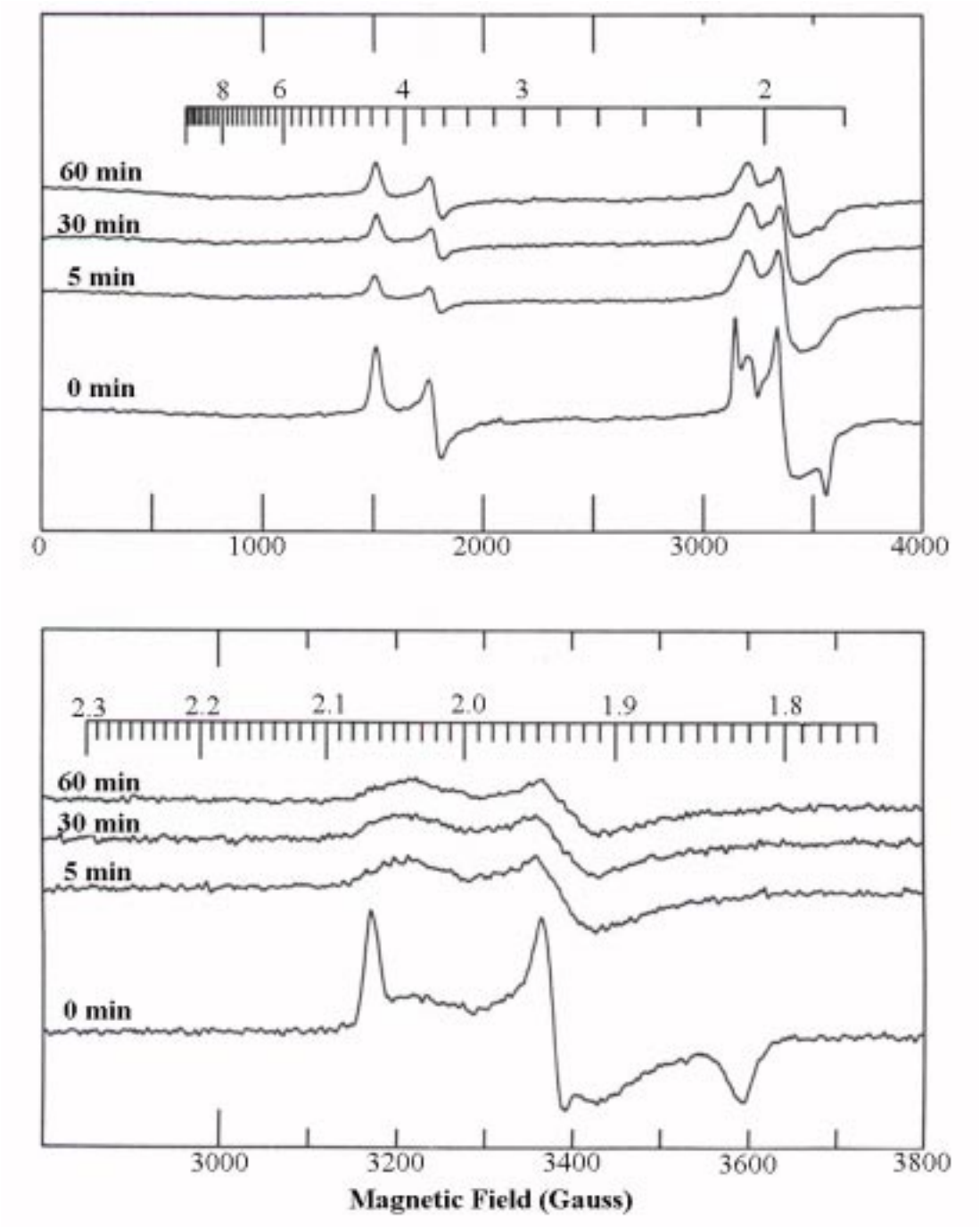

Figure 23: EPR Spectra of the α-88CG MoFe Protein During Slow Turnover

Overlay scans of the time-course experiment. Top: EPR spectra through both S=3/2 (FeMoco) and S=1/2 (P cluster) signals. Bottom: Magnification of the EPR spectra of the S=1/2 signal.

was performed. In this experiment, dithionite-reduced Fe and α-88CG MoFe proteins were run over P6-DG desalting columns in order to remove excess dithionite. The two proteins were then mixed at an Fe protein-to-MoFe protein molar ratio of 1:2 in order to compensate for the inactive fraction of α-88CG MoFe protein and so achieve an effective 2:1 molar ratio of active holoproteins.. The electron-transfer reaction was initiated by addition of a 100 mM ATP solution, and 250 μl aliquots were removed from the reaction vial and placed into quartz EPR tubes. The reactions taking place in each tube were halted by the freeze-quench method at 0, 1, or 5 min after addition of ATP. In the absence of exogenous reductant, each α-88CG MoFe protein should receive on average a single electron from the available pool of reduced Fe protein. Figure 24 clearly demonstrates that the S=1/2 P cluster EPR signal diminishes over the 5-min time course, while the S=3/2 FeMoco EPR signal remains unchanged over the same time course, indicating that the P cluster received the first electron.

In the wild-type control experiment, the S=3/2 EPR signal that arises from the semi-reduced FeMoco is unchanged in signal intensity after the first minute of the single electron turnover reaction. After 5 min, the signal intensity increases by ~50% relative to the initial (0 min) time sample. However, the reduced Fe protein EPR signal in the g=2 region of the spectra disappears completely upon addition of MgATP and does not reappear throughout the 5 min time-course experiment, thus verifying that the Fe protein is not re-reduced. These results do not completely agree with the expected results of a one-electron reduction of wild-type MoFe protein. A gradual diminution of the S=3/2 EPR signal should occur if an adequate supply of reduced MoFe protein is available in the reaction mixture. However, if a fraction of the MoFe protein is in a partially-oxidized state, then the single-electron donation event would result in an increase in the S=3/2 EPR signal with time as the oxidized MoFe protein is reduced. Another possibility is that there was an inadequate supply of Fe protein relative to the concentration of MoFe protein in the mix and the reduction of MoFe protein by Fe protein took place unusually slowly.

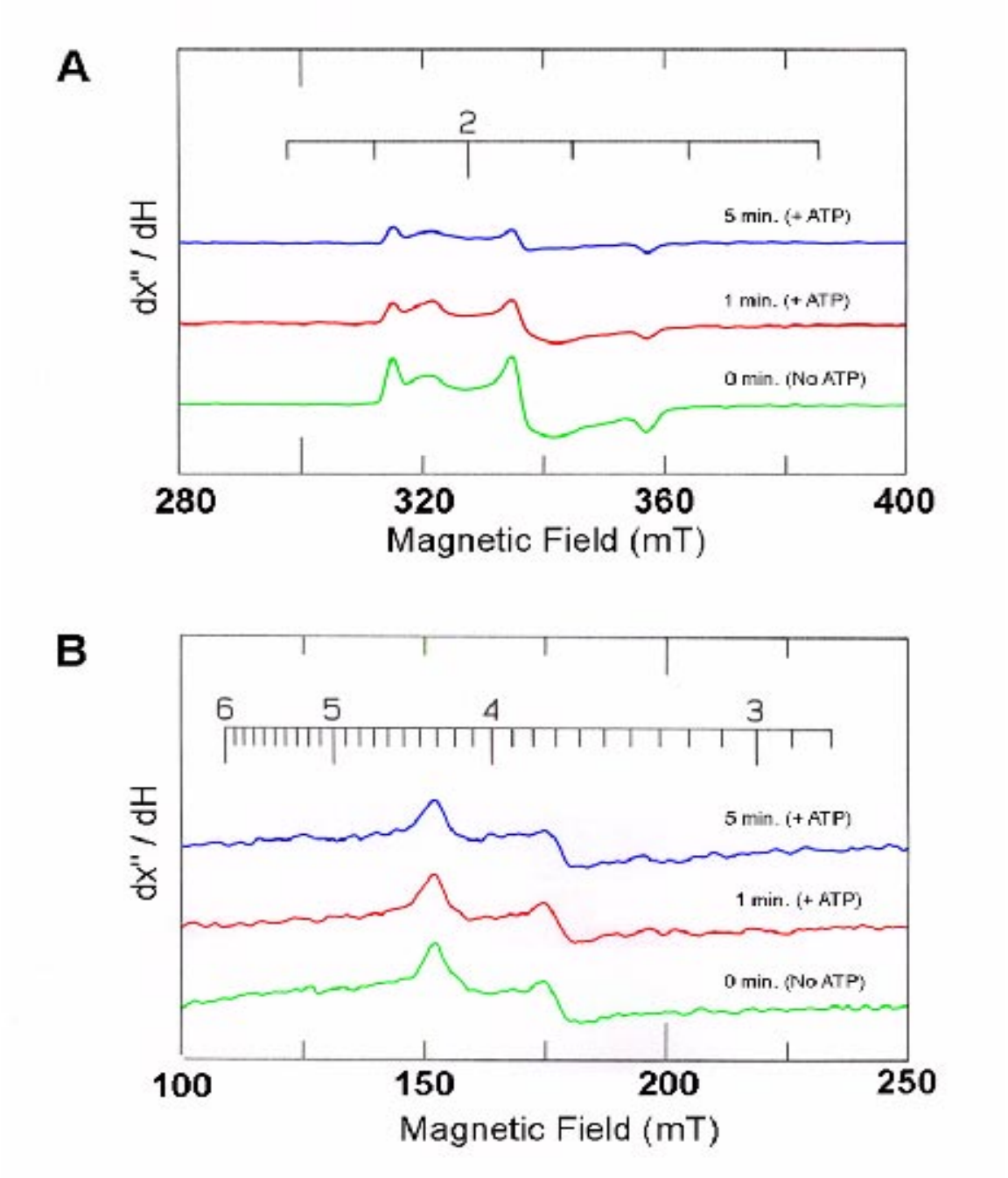

Figure 24: EPR Spectra of the α-88CG MoFe Protein During Single Electron Turnover Overlay scans of the time-course EPR spectra. A: The S=1/2 P Cluster EPR signal. B: The S=3/2 FeMoco EPR signal.

C. Mössbauer Spectroscopy

Unlike EPR spectroscopy, Mössbauer spectroscopy can be utilized to detect spectroscopic features arising from P clusters in the dithionite-reduced state of the wild-type MoFe protein. As discussed in Section II.G.2, Mössbauer spectroscopy is sensitive to energy transitions from the atomic nucleus and, unlike EPR, does not depend on unpaired valence electrons. Therefore, the diamagnetic P clusters of dithionite-reduced wild-type MoFe protein yield a Mössbauer spectrum when the isotope, ^{57}Fe, has been incorporated into their structure.

Each of the *A. vinelandii* strains that produce the polyHis-tagged, α-Cys88 altered and wild-type MoFe proteins were grown on ^{57}Fe-containing media and their MoFe proteins were purified as described. Figure 25 shows the Mössbauer spectra of each of these proteins at 4 K and an applied magnetic field of 500 G and after subtraction of the FeMoco contribution. For comparative purposes, the wild-type P cluster Mössbauer spectrum is overlaid with each of the altered MoFe protein P cluster spectra. Of the three altered MoFe proteins, the Mössbauer spectrum of the P clusters of the α-88CD MoFe protein is the most similar to that of the wild-type spectrum. The quadrupole splitting, $\Delta\mathbf{E_Q}$, and the isomer shift, δ, for these two proteins are nearly identical for each Fe subspecies. The Mössbauer spectra of the α-88CG and α-88CT MoFe protein P-clusters show distinct differences from the wild-type spectrum. In particular, both altered proteins demonstrate either a splitting (in α-88CT) or a shifting (in α-88CG) of one of the quadrupole doublet peaks that, in the wild-type spectrum, is assigned to the D subspecies of P cluster Fe atoms. The Mössbauer data confirm that all of the amino-acid substitutions at the α-88 position affect the electromagnetic environment of the P clusters, and that each substitution affects the environment differently.

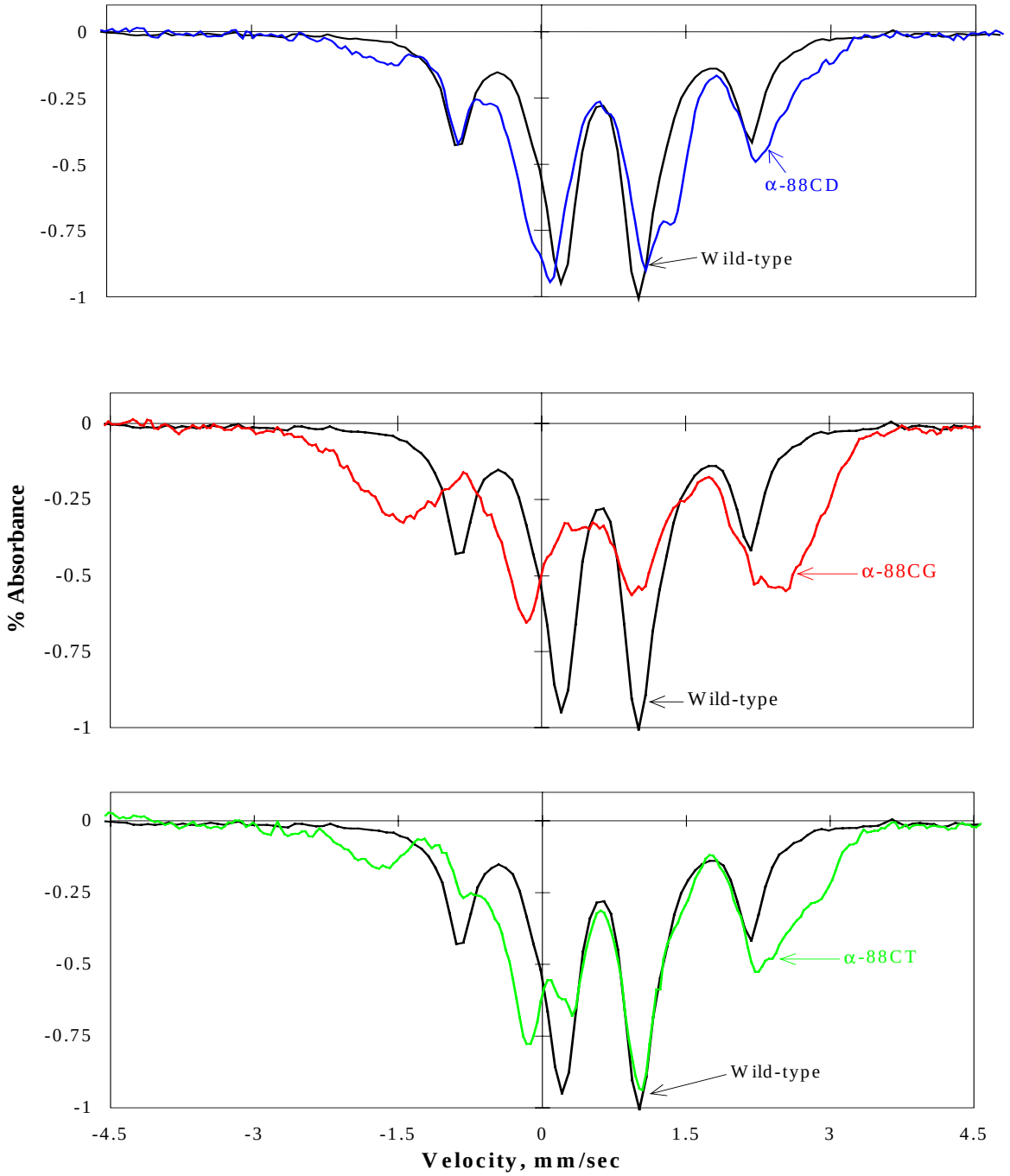

Figure 25: Mossbauer Spectra of P cluster Contribution from the Wild-type and ∝- Cys88 Altered MoFe Proteins

D. Variable Temperature Magnetic Circular Dichroism (VTMCD) Spectroscopy

In the early 1980's, the spectroscopic technique of low temperature magnetic circular dichroism was first used in the investigation of metal centers of the MoFe protein from *K. pneumoniae* (Johnson *et al*., 1981). In this study, it was determined that the variable temperature MCD spectra of the dithionite-reduced MoFe protein was due to the paramagnetism of the FeMo-cofactor, while the variable temperature MCD spectra of the thionine-oxidized MoFe protein arose from the half-integer spin state of the P clusters. In collaboration with Prof. M.K. Johnson of the Chemistry Department at the University of Georgia, Athens, GA, the VTMCD spectra of the both thionine-oxidized and dithionite-reduced forms of three α-Cys88 altered MoFe proteins were collected and each compared to the wild-type MoFe protein spectra under identical redox states.

1. Dithionite-reduced Spectra for Wild-type and α-Cys88 Altered MoFe Proteins

Because the VTMCD spectra of the dithionite-reduced MoFe proteins detects only the iron-molybdenum cofactor, it was predicted that each of the altered MoFe proteins would yield a spectrum similar to that of the wild-type MoFe protein. As observed with the Mössbauer spectra, of the three α-Cys88 altered MoFe proteins, the α-88CD MoFe protein's dithionite-reduced MCD spectrum was the most similar to the wild-type spectrum (see Figure 26). However, the two spectra are not identical; a noticeable decrease in the peak intensity at ~580 nm occurs in the α-88CD MoFe protein. The MCD spectra of the dithionite-reduced α-88CG and α-88CT MoFe proteins are generally similar and also show some loss of intensity at 580 nm. The trough that occurs between 420 and 450 nm in the wild-type spectrum is also less well defined (see Figure 27).

2. Spectra for Thionine-oxidized Wild-type and α-Cys88 Altered MoFe Proteins

These MoFe protein samples were prepared by treatment with enough excess thionine dye such that the blue color was retained. Excess dye was then removed anaerobically on a Sephadex G-25 column. Unfortunately, one of the α-Cys88 altered MoFe proteins, α-88CT, did not survive the thionine treatment and was, therefore, unavailable for analysis. As before, the VTMCD spectrum of thionine-oxidized α-88CD

MoFe protein was nearly identical to the wild-type spectrum, although the peak intensities of the α-88CD spectrum were ~50% of wild-type for samples with equal protein concentrations (see Figure 28). The VTMCD spectrum of thionine-oxidized α-88CG MoFe protein shows essentially the same peak positions and temperature-dependence as the wild-type MCD spectrum but with only approximately one-third of the wild-type spectrum's intensity for the two major peaks. These intensity differences probably reflect the lower metal and, therefore, cluster content of the altered MoFe proteins.

E. Discussion of Spectroscopic Analyses of the α-Cys88 Altered MoFe Proteins

The original purpose of the spectroscopic analyses of the α-Cys88 altered MoFe proteins was to determine if differences existed in the unique spectra arising from the FeMoco and P cluster. From the available evidence, a number of conclusions can be made concerning the amino-acid substitutions at the α-Cys88 P cluster-bridging residue.

1. Effects of α-Cys88 Substitution on the Spectroscopic Signals of FeMoco

a. EPR - The S=3/2 EPR signal is one of the best spectroscopic fingerprints for detecting the presence of the iron-molybdenum cofactor in the MoFe protein of the nitrogenase complex. Based on the EPR spectra of equally concentrated samples of dithionite-reduced wild-type and α-Cys88 altered MoFe proteins, there is no difference in the lineshape and position of the S=3/2 signals. Each sample exhibits the typical 4.3 and 3.7 *g*-values associated with the FeMoco EPR signal. The only differences between samples are the intensities of the signals, which are reflections of the relative concentration of the FeMo-cofactor per total protein concentration. These differences in EPR peak intensities match the differences in Mo content and the ΔA values for primary electron transfer for each of the four MoFe protein samples. These three estimations of metallocluster content support the hypothesis that the α-Cys88 position of the MoFe protein is involved in cluster biosynthesis, maturation and/or insertion.

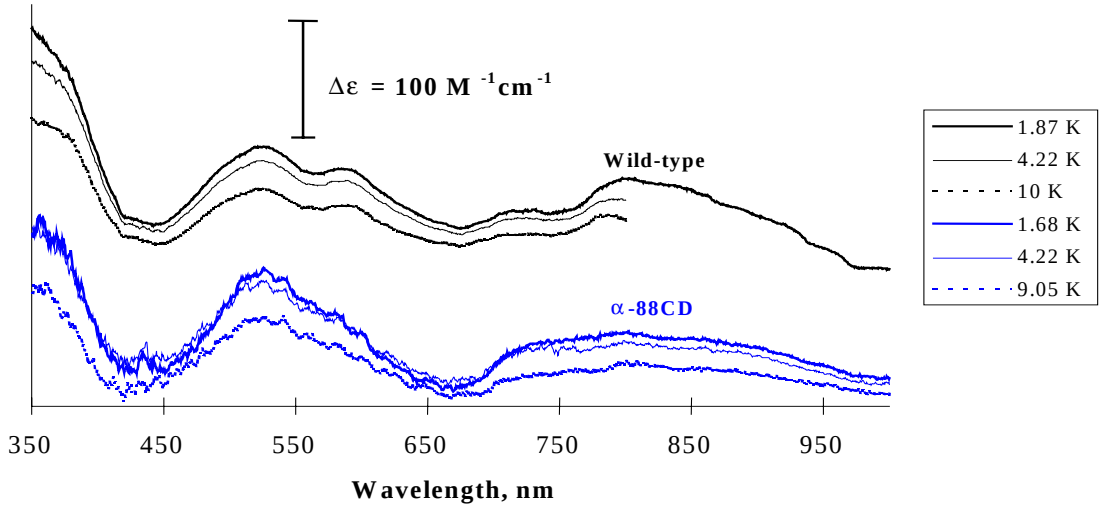

Figure 26: Variable Temperature Magnetic Circular Dichroism Spectra of Dithionite-reduced Wild-type and ∝-88CD MoFe Proteins

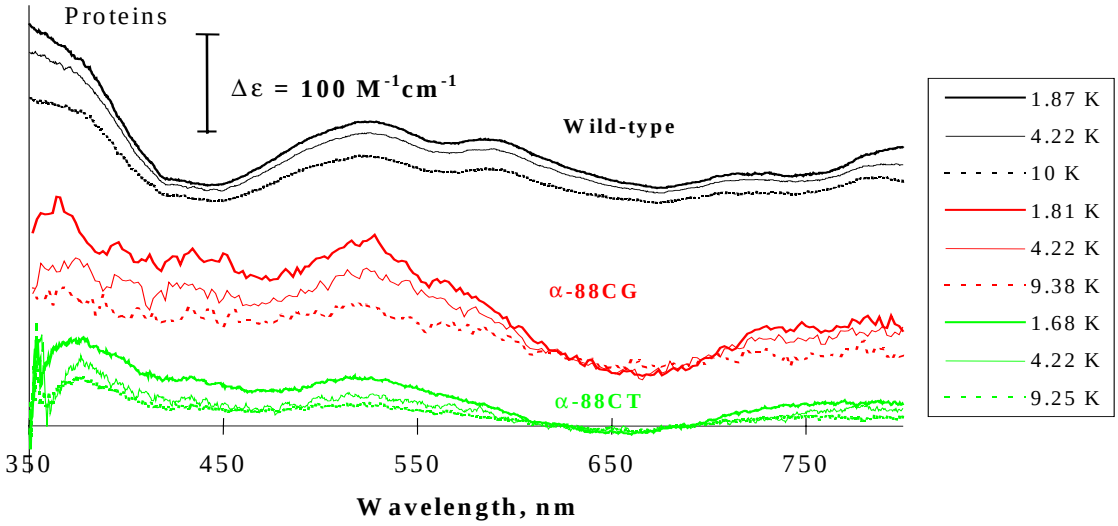

Figure 27: Variable Temperature Magnetic Circular Dichroism Spectra of Dithionite-reduced Wild-type, ∝-88CG, and ∝-88CT MoFe Proteins

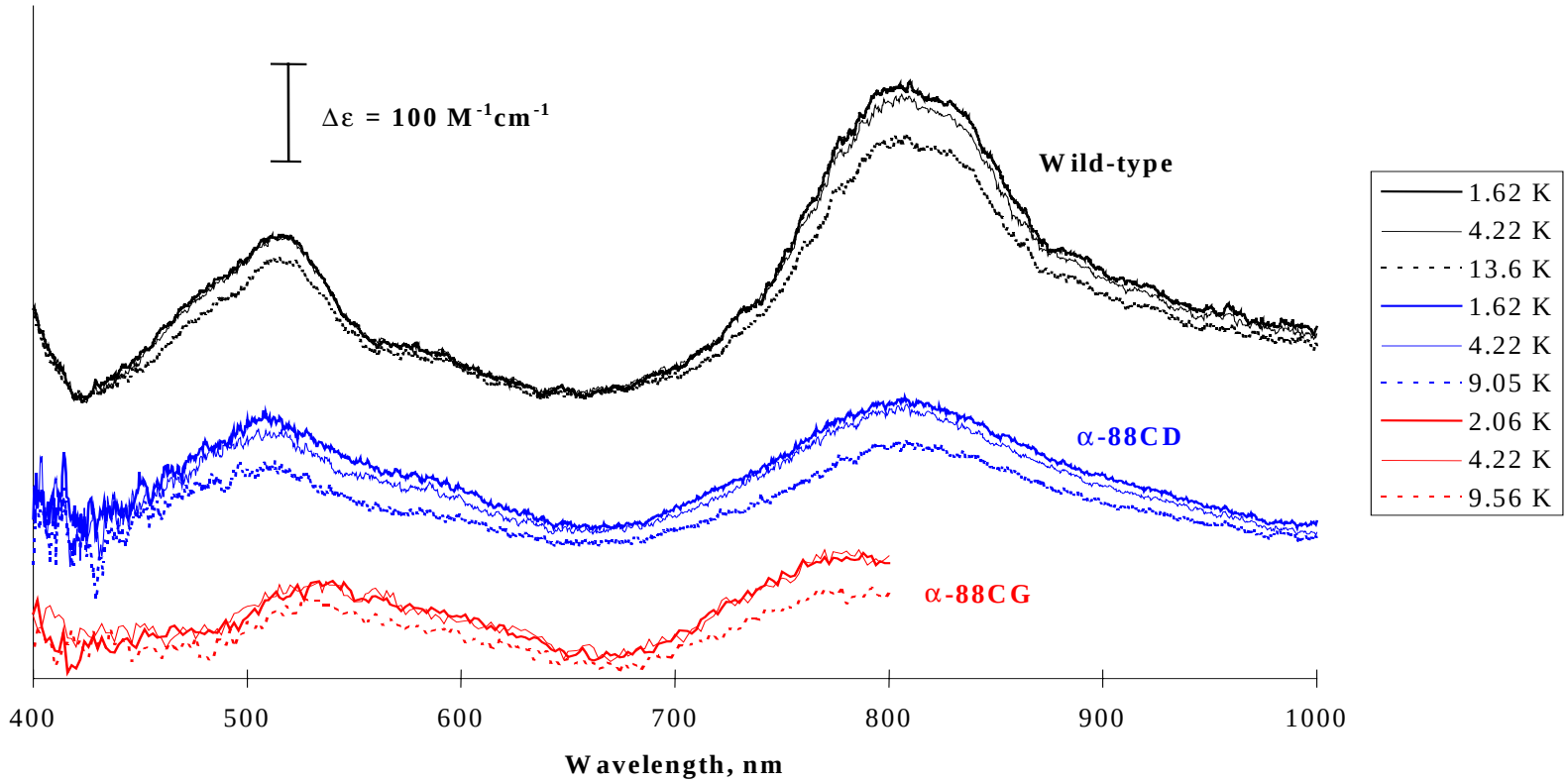

Figure 28: Variable Temperature Magnetic Circular Dichroism Spectra of Thionine-oxidized Wild-type, ∝-88CD, and ∝-88CG MoFe Proteins

b. MCD - As previously discussed, the variable temperature MCD spectra of the dithionite-reduced MoFe protein is a product of paramagnetic centers that exist under those redox conditions, which in wild-type MoFe protein means the FeMo-cofactor. The similarity of the wild-type and α-88CD MoFe proteins MCD spectra is an endorsement for the hypothesis that, of three viable alterations of the P cluster, the aspartyl substitution is the least disruptive to the electromagnetic properties of the FeMo-cofactor. However, the MCD spectra of the dithionite-reduced wild-type and α-88CD MoFe proteins are not identical. The α-88CD MoFe protein spectrum exhibits decreased peak intensities at 580 and 800 nm relative to the wild-type MoFe-protein spectrum. Although these peaks cannot be assigned to a particular metal atom within the paramagnetic center, these differences can be interpreted as a generalized perturbation of the magnetic environment of the FeMoco caused by the structural alteration of the P cluster (M.K. Johnson, personal communication).

2. Effects of α-Cys88 Substitution on the Spectroscopic Signals of the P cluster

a. EPR - As discussed in Section I.D.3.b, the P cluster is normally diamagnetic in the dithionite-reduced redox state and, therefore, has no EPR signal. However, a most interesting discovery is that of a S=1/2 EPR signal in the dithionite-reduced α-88CG MoFe protein. Based on signal integration, comparison with the S=3/2 FeMoco EPR signal, and its similarity to a transient, one-electron-oxidized P-cluster EPR signal from wild-type MoFe protein, it was concluded that this signal is associated with the P cluster of this altered MoFe protein. Successive experiments that attempted to follow the sequence of electron transfer from the Fe protein to the MoFe protein established that the α-88CG MoFe protein P cluster was the immediate electron acceptor from the electron-donating Fe protein. However, it remains to be shown whether the S=1/2 EPR signal returns upon completion of a substrate-reduction cycle, i.e., upon exhaustion of the reductant source and total conversion of available electrons into product(s). If the S=1/2 signal returns at the end of the redox cycle for the α-88CG MoFe protein its reappearance would indicate that the one-electron oxidized P cluster functions at some stage of the electron transfer process in the nitrogenase complex, and that this signal is not just an artifact of the amino acid substitution.

b. Mössbauer - The Mössbauer spectra of the P clusters from the α-Cys88 altered MoFe proteins reveal noticeable shifts in the peak position and peak intensity for both of the quadrupole doublets when these are compared to the wild-type spectrum. Although past research involving the Mössbauer spectra of the P clusters from wild-type MoFe protein has identified 2 or 3 different species of Fe atom, analysis by our collaborators has been unable to assign any of the Mössbauer spectral differences of these altered MoFe proteins to any of these Fe atom species (B.H. Huynh & P. Tavares, personal communication). However, it is possible to assign these shifts in the Mössbauer spectra to a generalized perturbation of the P cluster electromagnetic properties that results from amino-acid substitution at the α-Cys88 position.

c. MCD - The variable temperature MCD spectrum of thionine-oxidized MoFe protein has been interpreted to result from the paramagnetic centers that exist under these redox conditions, namely the P clusters. Examination of the MCD spectra of thionine-oxidized wild-type, α-88CD, and α-88CG MoFe proteins reveal no significant differences in the positions of the two major absorbance peaks at 520 and 800 nm, whereas the relative intensities of the 800 nm peak differ in accordance with the relative metal content of each MoFe protein.

The differences in the MCD spectra of the dithionite-reduced α-88CG and α-88CT MoFe proteins are interpreted in terms of P cluster paramagnetism. The MCD spectra of these two altered MoFe proteins are more similar to each other than they are to either the wild-type or α-88CD MoFe proteins. In particular, the MCD spectra of both α-88CG and α-88CT MoFe proteins MCD spectra lack a well-defined absorbance minimum at ~430-450 nm, which is prominent in both the wild-type and α-88CD MoFe proteins. Expert MCD interpretation concludes that these spectral differences could mean an additional paramagnetic center in the dithionite-reduced state of the α-88CG and α-88CT MoFe proteins (M.K. Johnson, personal communication). The dithionite-reduced EPR spectrum of the α-88CG MoFe protein would certainly support this interpretation of the MCD spectrum.

No one type of spectroscopy can stand alone in its interpretation of metalloenzyme structure and function. It is always important to corroborate the results from one spectroscopic technique with other spectroscopic techniques that detect different resonance signals within the same samples. In the spectroscopic investigation of the α-Cys88 altered MoFe proteins, three distinct spectroscopic detection methods were utilized. There was general agreement from all of the spectroscopic analyses that each of the three altered MoFe proteins possess perturbations of their electromagnetic environments and so of the specific spectroscopic signals that are attributable to the P clusters.

CHAPTER VIII.

ANALYSIS OF THE α-88CG MOFE PROTEIN-L127Δ FE PROTEIN COMPLEX

A. Introduction

Once the S=1/2 EPR signal of the α-88CG MoFe protein had been ascribed to the P cluster, the next step was to utilize this signal as a P-cluster redox indicator during turnover of the nitrogenase complex. Because of the fast rate of electron transfer, it was necessary to adjust the reaction conditions in order to limit the turnover process to a single electron-transfer event. Through collaboration, it was possible to obtain an altered Fe protein from *A. vinelandii* that was ideally suited for just such a purpose. The L127Δ Fe protein (see Section I.C.3.b) has the unique ability to form a tight irreversible complex with wild-type MoFe protein and to transfer a single electron in the absence as well as in the presence of MgATP. The rate of primary electron transfer between the L127Δ Fe protein and wild-type MoFe protein in either the absence or presence of MgATP is more than 100-fold slower than in the wild-type nitrogenase complex, which requires MgATP for component-protein association and electron transfer.

B. Initial EPR Experiment

A series of experiments in which the α-88CG MoFe protein was combined with the L127Δ Fe protein were performed in the attempt to delineate the electron-transfer process. In an initial experiment, the two altered nitrogenase component proteins were combined in either the presence or absence of MgATP, transferred into quartz EPR tubes and then freeze quenched after an appropriate time period. The EPR spectra of this mixture were essentially no different than a composite spectrum of those of the two individual proteins, α-88CG MoFe protein and L127Δ Fe protein, prior to mixing. Possible explanations for this result include: 1. the two component proteins do not form a complex or; 2. the two component proteins associate but do not transfer an electron. These experimental results were the impetus for the subsequent inquiries.

C. Binding Affinity of the α-88CG MoFe Protein-L127Δ Fe Protein Complex

A straight forward and simple experiment was performed in order to determine if the α-88CG MoFe protein and L127Δ Fe protein could form a tight irreversible complex similar to the complex between the L127Δ Fe protein and wild-type MoFe protein. A component protein mixture consisting of a 2:1 Fe protein-to-MoFe protein ratio was combined in an anaerobic vial in either the presence or absence of MgATP. The mixture was allowed to incubate for at least 5 min and then loaded onto a S-300 Sephacryl gel filtration column. The eluting peak(s) were collected and then subjected to SDS-PAGE analysis from which the components in each elution sample were identified by comparison to MoFe protein and Fe protein standards. The MoFe protein/Fe protein combinations, which were subjected to this treatment, included the wild-type, or α-88CG, or β-188SG MoFe proteins mixed individually with either wild-type or L127Δ Fe protein. The results of the complex-formation analysis are shown in Table 17. As expected, the mixture of wild-type MoFe and Fe protein separated clearly whereas the wild-type MoFe protein and L127Δ Fe protein eluted as a single peak. The β-188SG MoFe protein was included as a control for terminally-substituted P clusters and behaved like wild-type MoFe protein. However, it appeared that the α-88CG MoFe protein and L127Δ Fe protein were either unable to associate to form a protein complex or any complex that formed readily dissociated. In order to discern between these two possibilities, this nitrogenase component-protein combination was subjected to steady-state assays to test whether substrate reduction and/or ATP hydrolysis occurs. Distinction between these two possibilities was necessary to determine if this protein complex should be subjected to subsequent pre-steady-state rate constant determinations.

D. Substrate Reduction and ATP Hydrolysis

The α-88CG MoFe protein-L127Δ Fe protein combination as well as the wild-type MoFe protein-L127Δ Fe protein combination were subjected to typical steady-state

Table 17: Nitrogenase Complex Binding Affinities

Nitrogenase Mixture		# of Peaks off S-300 column	Peak Identity*	
MoFe Protein	Fe Protein		Peak 1	Peak 2
Wild-type	Wild-type	2	MoFe	Fe
Wild-type	L127Δ	1	MoFe & Fe	-
α-88CG	Wild-type	2	MoFe	Fe
α-88CG	L127Δ	2	MoFe	Fe
β-188SG	L127Δ	1	MoFe & Fe	-

* Determined by co-migration with MoFe protein and Fe protein standards on SDS-PAGE gels.

Table 18: Pre-steady-state Kinetic Analysis of Wild-type and Altered Nitrogenase Complexes

Nitrogenase Mixture		Primary Electron Transfer, k_{+2}, (in sec^{-1})		Complex Dissociation Rate, k_{-3} (in sec^{-1})
MoFe Protein	Fe Protein	+ MgATP	- MgATP	
Wild-type	Wild-type	160	-	6.5
α-88CG	Wild-type	150	-	6.1
Wild-type	L127Δ	6.0*	0.4*	- *
α-88CG	L127Δ	13	1.2	2.4

*Determined by Lanzilotta *et al*., 1996

assays under 100% Argon (see Section II.E.1&4). In order to measure the anticipated low levels of H_2 evolution and/or ATPase activity, some of the assays were allowed to incubate at 30°C for up to 8 hr. Although no substrate-reduction activity was detected in any of the assay samples, a fairly constant level of ATP hydrolysis, as measured by creatine production, was found throughout the time-course experiment. The α-88CG MoFe protein-L127Δ Fe protein combination produced an ATP hydrolysis rate of ~23 nmoles of creatine (min·mg MoFe protein)$^{-1}$ whereas the wild-type MoFe protein-L127Δ Fe protein combination exhibited an ATP hydrolysis rate of ~27 nmoles of creatine (min·mg MoFe protein)$^{-1}$. Neither MoFe proteins nor Fe proteins alone was unable to hydrolyze ATP.

A second set of steady-state assays was performed in which methyl viologen was included in the assay reaction solution as a potential electron-transfer mediator between reductant and oxidized Fe protein. The results of these experiments were identical to the previous set, no substrate reduction and an ATPase rate of ~20 nmoles of creatine (min·mg MoFe protein)$^{-1}$.

It has been well established that neither nitrogenase component protein can hydrolyze MgATP in the absence of the other but can only do so as a protein-protein complex. Because the α-88CG MoFe protein-L127Δ Fe protein combination was able to hydrolyze MgATP, it can be safely concluded that these two proteins can associate to form a complex but cannot reduce substrate. Therefore, the next logical step in the overall analysis of this protein-protein interaction was to determine whether electron transfer occurs and at what rate, and also whether this nitrogenase component-protein complex can dissociate and what the rate of this reaction is.

E. Pre-steady-state Kinetic Analysis

All pre-steady-state kinetic analyses were performed as described in Sections II.F.1-4 with the exception that the L127Δ Fe protein was used in place of wild-type Fe protein and that, in some instances, MgATP was excluded from some of the stopped-flow spectrophotometric experiments. Appropriate controls were run on the same day and rate

constant quantitation of controls agreed with previously determined values for all controls.

1. Primary Electron Transfer Rate +/- MgATP

The α-88CG MoFe protein-L127Δ Fe protein primary-electron-transfer rate was determined in the presence and absence of MgATP and the rate constants were determined using the curve-fitting software package. The primary electron-transfer rate constants, k_{+2}, are listed in Table 19, which includes the published values for the primary-electron-transfer rates for the wild-type MoFe protein-L127Δ Fe protein combination for comparison (Lanzilotta *et al*., 1996). Based on the rate constants, it appears that the α-88CG MoFe protein is able to accept an electron from the L127Δ altered Fe protein approximately 3-fold faster than wild-type MoFe protein in the absence of MgATP and about 2-fold faster than wild-type MoFe protein when MgATP is included in the reaction. Thus, the L127Δ Fe protein was able to transfer an electron to the α-88CG MoFe protein. The altered MoFe protein's ability to dissociate from the altered Fe protein was tested in the following set of stopped-flow experiments.

2. Protein Complex Dissociation Rate

The dissociation rate of the α-88CG MoFe protein-L127Δ Fe protein complex was determined under identical conditions to those described in Section II.E.4. The rate constants, k_{-3}, for complex dissociation are shown in Table 18 along with the control rate constants, which were reconfirmed at the same time. Unlike the wild-type MoFe protein, the α-88CG MoFe protein demonstrated the ability to dissociate from the L127Δ Fe protein at a rate that was only ~2.5-fold slower than the dissociation of wild-type MoFe protein from wild-type Fe protein.

3. Secondary Electron Transfer Rate

It is difficult to reconcile some aspects of the α-88CG MoFe protein-L127Δ Fe protein complex analyses. Even though the two proteins demonstrate the ability to associate to form a complex, hydrolyze MgATP, transfer an electron and dissociate from each other, there is no evidence of substrate reduction in this altered protein pairing. The possibility existed that some event occurs after the first round of the Fe protein cycle that prevents further interaction between the two component proteins. In order to further

examine these possibilities, the α-88CG MoFe protein-L127Δ Fe protein complex was subjected to the secondary electron-transfer rate experiment (see Section II.F.3). The procedure for this experiment was identical to previous rate determinations with the exception that the L127Δ Fe protein was present in both drive syringes of the stopped-flow apparatus as opposed to wild-type Fe protein. Figure 29 displays the change in absorbance at 430 nm that was measured for the electron-transfer reaction occurring between the α-88CG MoFe protein and the L127Δ Fe protein over the 90-min time course experiment. From the stopped-flow spectra, an additional plot of the change in absorbance versus time was created and is seen in Figure 30. This plot represents an exponential decrease in absorbance with increasing time and can be fitted to a first-order curve with a rate constant of 0.6 min^{-1}. The rate constant is an indirect measurement of the rate at which the pool of L127Δ Fe protein has lost the ability to be oxidized by donation of an electron to the α-88CG MoFe protein.

The rate constants that are derived from each of the spectra taken during the earliest time points (i.e., 0.5 and 1 min) are in close agreement with the primary electron transfer rate constant of 13 sec^{-1} determined in the presence of MgATP. Later time points reveal a decrease in the rate constant values as time increases, however, this decrease may be due in whole or in part to the decreasing absorbances upon which the rate constants are based.

F. Discussion of α-88CG MoFe Protein-L127Δ Fe Protein Complex Analyses

The steady-state, and pre-steady-state kinetic analysis of the α-88CG MoFe protein-L127Δ Fe protein complex has demonstrated that, like the wild-type MoFe protein- L127Δ Fe protein complex, these two altered nitrogenase component proteins are able to associate to form a complex, hydrolyze MgATP, and transfer a single electron.

Figure 29: Absorbance Scans of Electron Transfer Reaction for the α-88CG MoFe Protein-L127 Δ Fe Protein Complex

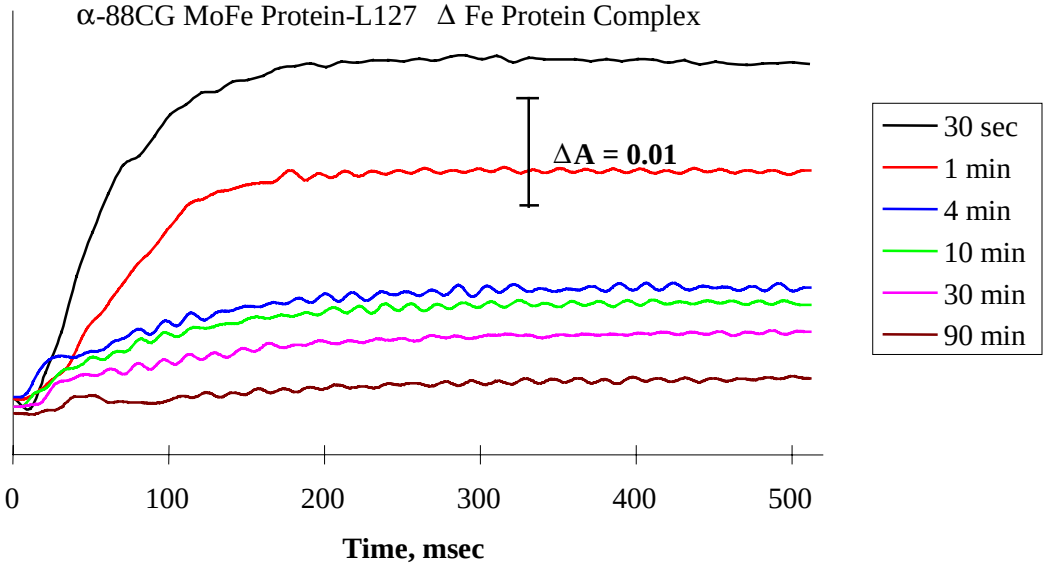

Figure 29: Absorbance Scans of Electron Transfer Reaction for the ∝-88CG MoFe Protein-L127ΔFe Protein Complex

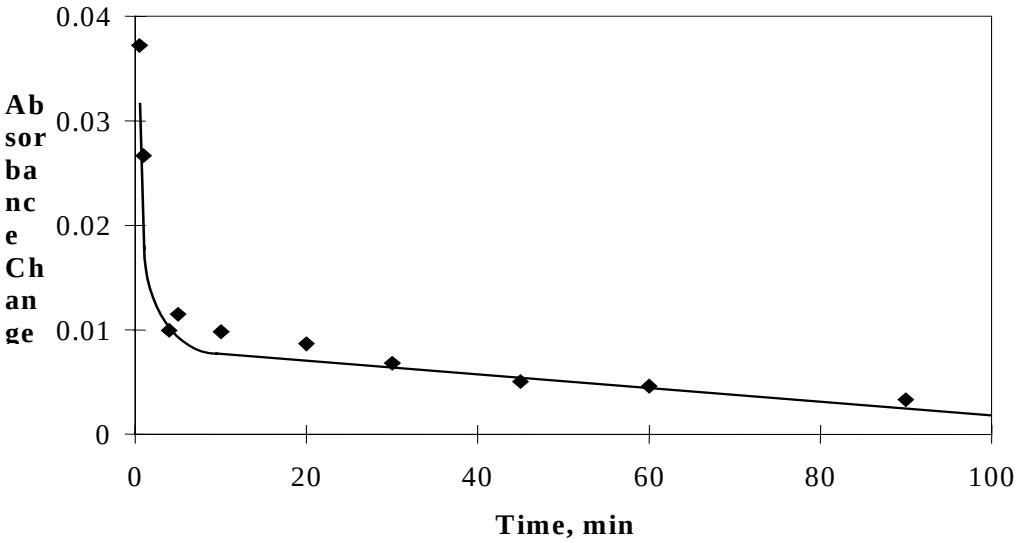

Figure 30: Absorbance Change vs. Time for Electron Transfer Reaction of ∝-88CG MoFe Protein-L127ΔFe Protein Complex

However, unlike the wild-type MoFe protein- L127Δ Fe protein complex, the α-88CG MoFe protein-L127Δ Fe protein complex is able to dissociate at a rate that is somewhat slower than the rate-limiting step of the wild-type nitrogenase complex. However, neither wild-type nor the α-88CG MoFe protein has demonstrated the ability to reduce substrate while using the L127Δ Fe protein as an electron donor.

The secondary electron-transfer experiment may provide a reasonable explanation for the difference in dissociation capabilities between the wild-type and α-88CG MoFe proteins. The decrease in absorbance at 430 nm that occurs with time in the α-88CG MoFe protein-L127Δ Fe protein electron-transfer reaction can be interpreted as arising from a decrease in the concentration of α-88CG MoFe protein that is capable of accepting an electron from the L127Δ Fe protein. Because the L127Δ Fe protein is in excess over the α-88CG MoFe protein in this experiment, the formation of a tight, non-dissociating component-protein complex effectively removes the α-88CG MoFe protein from the reaction. Perhaps the L127Δ Fe protein is able to complete two electron-transfer cycles with the α-88CG MoFe protein before becoming a tightly-bound complex that is incapable of further turnover.

The number of electrons that can be accepted from the L127Δ Fe protein by either the wild-type or α-88CG MoFe proteins before becoming a tight complex may be a direct consequence of the redox state of the P clusters. Each αβ-subunit dimeric half of the α-88CG MoFe protein is initially in the one-electron oxidized state and the first electron received from the L127Δ Fe protein reduces the P clusters to the fully-reduced, P^N redox state that normally occurs in dithionite-reduced wild-type MoFe protein. The second round of electron donation from the L127Δ Fe protein to the α-88CG MoFe protein would then bring the α-88CG MoFe protein to a redox state equivalent to the one-electron-reduced wild-type MoFe protein. It is this redox state of the MoFe protein to which the L127Δ Fe protein binds tightly and irreversibly. In terms of the Thorneley-Lowe model of the MoFe protein cycle, the as-isolated, dithionite-reduced α-88CG MoFe protein is in the "E_{-1}" redox state while the as-isolated, dithionite-reduced wild-type

MoFe protein is in the E_0 state. Continuing this analogy to the Thorneley-Lowe model, the L127Δ Fe protein binds tightly to the E_1 redox state of either wild-type or α-88CG MoFe proteins.

Using a chemically-oxidized wild-type MoFe protein, evidence has been gathered that demonstrates that the first electron transferred from either wild-type or L127Δ Fe protein is accepted at the P cluster (Lanzilotta & Seefeldt, 1996). It would be interesting to determine if the L127Δ Fe protein can dissociate from this oxidized wild-type MoFe protein and if the rate of primary electron transfer between the L127Δ Fe protein and this wild-type MoFe protein with its P cluster in the P^{+1} redox state is faster than when its P cluster is in the P^N redox state.

CHAPTER IX.
SUMMARY AND PROSPECTIVES

This dissertation research has described the role of the P cluster in the electron transfer mechanism within the nitrogenase complex of *A. vinelandii*. Site-directed mutagenesis has revealed that the cluster-bridging residue, α-Cys88, is responsible for controlling the rates of inter- and intramolecular electron transfer. This residue was substituted by nine amino acids. Three of these amino acid substitutions, Asp, Gly, and Thr, resulted in mutant strains which retained diazotrophic growth capability although at reduced rates relative to the wild-type strain. Metal analysis of the purified proteins from these strains revealed that all three substitutions result in noticeably lower Mo content. This result was concluded to mean that the α-88 position affects metallocluster insertion.

Steady-state kinetic analyses revealed that none of the α-Cys88 altered MoFe proteins affected the catalytic properties of the substrate reducing active site, the FeMo-cofactor. The α-88CG MoFe protein demonstrated a unique pattern of uncoupling of the rate of ATP hydrolysis from the rate of substrate reduction. It was determined that as the availability of reduced Fe protein increased, the substrate reduction rate decreased relative to the ATPase activity. This phenomenon was due to inhibition of electron flow through the MoFe protein.

Pre-steady-state kinetic analyses relied on stopped-flow spectrophotometry and determined that the intermolecular rates were affected particularly in the α-88CD MoFe protein. However, none of the intermolecular electron transfer rate constants were found to be rate-limiting, i.e., these processes were not responsible for the lower catalytic activity of these α-Cys88 altered MoFe proteins. The α-88CG and α-88CT MoFe protein were found to have signifcantly decreased intramolecular electron transfer rates and this explained their lowered substrate reduction rates.

The α-88CD MoFe protein was nearly identical in catalytic functioning to the wild-type MoFe protein, and it was concluded that it only differed with respect to concentration of metalloclusters per total protein. However, this altered MoFe protein had an interesting response to high concentrations of acetylene. There were significant

increases in both primary electron transfer and complex dissociation rate constants under 100% C_2H_2 relative to a 100% N_2 atmosphere. This was determined to be due to alteration of an acetylene inhibitory binding site that is normally occupied under high acetylene concentrations.

A new S=1/2 paramagnetic signal was discovered in the dithionite-reduced α-88CG MoFe protein. Creation of this signal was evidence for the influence exerted by the α-Cys88 residue on the electromagnetic properties of the P cluster. It was determined that this S=1/2 signal arose from a one-electron-oxidized P cluster in the dithionite-reduced α-88CG MoFe protein. This signal was exploited to prove that the P cluster are indeed the immediate electron acceptor from the reduced Fe protein during intermolecular electron delivery.

Finally, it was shown that, unlike the wild-type MoFe protein, the α-88CG MoFe protein was able to dissociate from the L127Δ Fe protein after donation of a single electron. Pre-steady-state kinetic analysis revealed that these two altered nitrogenase component proteins could interact through two cycles of electron transfer before becoming tightly bound. These findings demonstrate the role of the redox state of the P cluster in the regulation of electron transfer and complex dissociation.

A number of fascinating areas of inquiry concerning the mechanism of nitrogenase have been illuminated during the course of this research project. Many of the experimental discoveries hold promise for further research and for understanding a number of questions that still surround the involvement of the P clusters in the overall process of nitrogen fixation. A few of these promising areas of inquiry are described below.

Biosynthesis - The α-Cys88 position has been shown to have an effect on P cluster biosynthesis, maturation, and/or insertion. Perhaps the α-Cys88 altered MoFe proteins and other mutant strains with amino-acid substitutions for conserved residues proximal to the P cluster can be exploited in order to reveal the sequence of metal cluster insertion, and to reveal modification of P cluster composition or structure. Such discoveries may have important consequences on attempts to synthesize an artificial nitrogenase for commercial production of nitrogen fertilizers.

Substrate Reduction - Alterations at the α-Cys88 position have demonstrated effects on: 1. the coupling of substrate reduction and ATP hydrolysis for the α-88CG MoFe protein and; 2. acetylene concentration effects on the α-88CD MoFe protein. Perhaps these altered proteins could be used to study further the involvement of the two associated phenomena, uncoupling of substrate reduction from ATP hydrolysis and C_2H_2 self-inhibition. An understanding of these two specific phenomena may provide insight into some of the general processes necessary for accurate nitrogenase functioning.

Electron Transfer - Both the α-88CG and α-88CT MoFe proteins have lowered substrate-reduction rates that result in part in a decreased rate of intramolecular electron transfer within the MoFe protein. Although the intermolecular electron-transfer mechanism of nitrogenase is an active and fruitful target of research, the mechanism of intramolecular electron transfer from P cluster to FeMoco is just now being investigated. Site-directed mutagenesis appears to be an excellent tool in pursuit of these questions and examination of altered MoFe proteins, like the α-88CG, α-88CT, β98YH, and β124FI (in Kp), will undoubtedly play a part in obtaining some of the answers.

Spectroscopy - The α-88CG MoFe protein S=1/2 signal can be utilized to further study the electron-transfer sequence in nitrogenase and to understand the interaction of redox changes in the various metallocenters of nitrogenase and their effects on the conformational changes that are necessary for accurate functioning in nitrogenase.

By the same token, the variable temperature MCD and Mössbauer spectra of the α-Cys88 altered MoFe proteins might provide more structural information for what happens at the P cluster and FeMoco during the individual steps of nitrogenase turnover. Various freeze-quench methods exist which might be useful in these types of pursuits. In addition, there is always the chance that another spectroscopic signal, like the α-88CG MoFe protein S=1/2 signal, might be discovered.

Interaction of Altered Nitrogenase Component Proteins - The analysis of the α-88CG MoFe protein-L127Δ Fe protein complex demonstrates the utility of combining altered nitrogenase proteins of known or suspected defects in order to obtain more information about one or both altered proteins. A large number of site-specific alterations

of the nitrogenase component proteins have been generated over the last decade. In many cases, individual altered proteins represent specific disturbances in a step or capability necessary for normal nitrogenase functioning. There is great potential in this synergistic approach for dissecting the precise sequence of redox and conformational changes that must occur during protein-protein interaction, electron transfer, substrate binding, and product release.

P cluster Structure - With the advent of the new x-ray crystal structure of the P cluster under different redox conditions, there are new implications for the functioning of P clusters in the coupling of electron transfer and proton transfer to the FeMoco. Examination of the x-ray crystal structures of some or all of the α-Cys88 altered, as well as other P-cluster-ligand substituted, MoFe proteins might aid in the elaboration of this hypothesis of coupled proton and electron transfer and perhaps lead to explanations for the lowered substrate-reduction activity of these altered MoFe proteins. For example, the role of the α-Cys88 main chain N atom, which coordinates the Fe5 atom of the P cluster might be revealed by examination of the α-88CG MoFe protein. This altered MoFe protein lacks the bridging cysteine residue and must rely on this N atom for coordination from the α-88 residue. This alteration allows for isolation and, therefore, examination of the function of this NH-Fe bond in the nitrogenase-catalyzed electron-transfer mechanism. Alternatively, the dithionite-reduced α-88CG MoFe protein may represent an intermediate structure of the P cluster between the P^{OX} and P^{N} redox states and could be utilized as a trapped transition state in the conformational switching mechanism that is necessary for efficient functioning of nitrogenase.

REFERENCES

Alberty RA. 1994. Thermodynamics of the nitrogenase reactions. *J. Biol. Chem*. 269:7099-102

Allen RM, Homer MJ, Chatterjee R, Ludden PW, Roberts GP, Shah VK. 1993. Dinitrogenase reductase- and MgATP-dependent maturation of apodinitrogenase from *Azotobacter vinelandii*. *J. Biol. Chem*. 268:23670-74

Ashby GA, Dilworth MJ, Thorneley RNF. 1987. *Klebsiella pneumoniae* nitrogenase: Inhibition of hydrogen evolution by ethylene and the reduction of ethylene to ethane. *Biochem. J.* 247:547-554

Bishop PE, Premakumar R, Dean DR, Jacobson MR, Chisnell JR, Rizzo TM, Kopczynski J. 1986. Nitrogen fixation by *Azotobacter vinelandii* strains having deletions in structural genes for nitrogenase. *Science* 232:92-94

Bolin JT, Ronco AE, Mortenson LE, Morgan TV, Williamson M, Xuong N-H. 1990. Structure of the nitrogenase MoFe-protein: Spatial distribution of the intrinsic metal atoms determined by X-ray anomalous scattering. Pp. 117-22 in *Nitrogen Fixation: Achievements and Objectives.* 1992. Greshoff PM, Roth LE, Stacey G, Newton WE eds. New York: Chapman & Hall

Bolin JT, Ronco AE, Morgan TV, Mortenson LE, Xuong N-H. 1993. The unusual metal clusters of nitrogenase: Structural features revealed by x-ray anomalous diffraction studies of the MoFe protein from *Clostridium pasteurianum. Proc. Natl. Acad. Sci., USA* 90:1078-82

Braaksma A, Haaker H, Grande H, Veeger C. 1982. The effect of the redox potential on the activity of the nitrogenase and on the Fe protein of *Azotobacter vinelandii. Eur. J. Biochem.* 121:483-491

Brigle KE, Newton WE, Dean DR. 1985. Complete nucleotide sequence of the *Azotobacter vinelandii* nitrogenase structural gene cluster. *Gene* 37:37-44

Brigle KE, Setterquist RA, Dean DR, Cantwell JS, Weiss MC, Newton WE. 1987a. Site-directed mutagenesis of the nitrogenase MoFe protein of *Azotobacter vinelandii*. *Proc. Natl. Acad. Sci. USA* 84:7066-69

Brigle KE, Weiss MC, Newton WE, Dean DR. 1987b. Products of the iron-molybdenum cofactor-specific biosynthetic genes, *nifE* and *nifN*, are structurally homologous to the products of the nitrogenase molybdenum-iron protein genes, *nifD* and *nifK*. *J. Bacteriol.* 169:1547-53

Buchanan-Wollaston V, Cannon MC, Beynon JL, Cannon FC. 1981. Role of the *nifA* gene product in the regulation of *nif* expression in *Klebsiella pneumoniae*. *Nature* 294:776-78

Bui PT, Mortenson LE. 1968. Mechanism of the enzymic reduction of N_2: The binding of adenosine 5'-triphosphate and cyanide to the N_2-reducing system. *Proc. Natl. Acad. Sci. USA* 61:1021-27

Bulen WA, Burns RC, LeComte JR. 1965. Nitrogen fixation: Hydrosulfite as electron donor with cell-free preparations of *Azotobacter vinelandii* and *Rhodospirillum rubrum. Proc. Natl. Acad. Sci. USA* 53:532-539

Bulen WA, LeComte JR. 1966. The nitrogenase system from *Azotobacter*: Two enzyme requirements for N_2 reduction, ATP dependent H_2 evolution and ATP hydrolysis. *Proc. Natl. Acad. Sci. USA* 56:979-986

Burgess BK, Jacobs DB, Stiefel EI. 1980. Large-scale purification of high activity *Azotobacter vinelandii* nitrogenase. *Biochim. Biophys. Acta* 614:196-209

Burns RC, Hardy RWF. 1975. *Nitrogen fixation in bacteria and higher plants*. New York: Springer-Verlag

Burns RC, Bulen WA. 1965. ATP-dependent hydrogen evolution by cell-free preparations of *Azotobacter vinelandii. Biochim. Biophys. Acta* 105:437-45

Chabre M. 1990. Aluminofluoride and beryllofluoride complexes: a new phosphate analogs in enzymology. *Trends Biochem. Sci*. 15:6-10

Chan MK, Kim J, Rees DC. 1993. The nitrogenase FeMo-cofactor and P-cluster pair: 2.2A resolution structures. *Science* 260:792-94

Chaney AL, Marbach EP. 1962. Modified reagents for determination of urea and ammonia. *Clin. Chem.* 8:130-32

Chatt J. 1980. Chemistry relevant to the biological fixation of nitrogen. Pp. 1-18 in *Proc. Phytochem. Soc. Eur*. Stewart WDP, Gallon JR eds. London: Academic Press

Chisnell JR, Premakumar R, Bishop PE. 1988. Purification of a second alternative nitrogenase from a *nifHDK* deletion strain of *Azotobacter vinelandii. J. Bacteriol.* 170:27-33

Christiansen J, Tittsworth RC, Hales BJ, Cramer SP. 1995. Fe and Mo EXAFS of *Azotobacter vinelandii* nitrogenase in partially oxidized and singly reduced forms. *J. Am. Chem. Soc*. 117:10017-24

Conradson SD, Burgess BK, Newton WE, Mortenson LE, Hodgson KO. 1987. Structural studies of the molybdenum site in the MoFe protein and its FeMo cofactor by EXAFS. *J. Am. Chem. Soc.* 109:7507-15

Corbin JL. 1978. A simple, automated apparatus for the rapid multiple flush of reaction (assay) vessels with gases. *Anal. Biochem.* 84:340-2

Dean DR, Setterquist RA, Brigle KE, Scott DJ, Laird NF, Newton WE. 1990. Evidence that conserved residues Cys-62 and Cys-154 within the *Azotobacter vinelandii* nitrogenase MoFe protein a-subunit are essential for nitrogenase activity but conserved residues His-83 and Cys-88 are not. *Mol. Microbiol.* 4:1505-12

Dean DR, Jacobson MR. 1992. Biochemical genetics of nitrogenase. See Stacey *et al.*, 1992. pp. 763-834

Dean DR, Bolin JT, Zheng L. 1993. Nitrogenase metalloclusters: Structures, organization, and synthesis. *J. Bacteriol*. 175:6737-44

Deits TL, Howard JB. 1990. Effects of salts on *Azotobacter vinelandii* nitrogenase activities. *J. Biol. Chem.* 265:3859-67

Dilworth MJ. 1966. Acetylene reduction by nitrogen-fixing preparations from *Clostridium pasteurianum. Biochim. Biophys. Acta* 127:285-94

Dilworth MJ, Eady RR, Robson RL, Miller RW. 1987. Ethane formation from acetylene as a potential test for vanadium nitrogenase *in vivo. Nature* 327:167-8

Dilworth MJ, Eldridge ME. 1992. Correction for creatine interference with the direct indophenol measurement of NH_3 in steady-state nitrogenase assays. *Anal. Biochem.* 207:6-10

Dixon RA, Eady RR, Espin G, Hill S, Iaccarino M, Kahn D, Merrick M. 1980. Analysis of regulation of *Klebsiella pneumoniae* nitrogen fixation (*nif*) gene cluster with gene fusions. *Nature* 286:128-32

Duyvis MG, Wassink H, Haaker H. 1996. Formation and characterization of a transition state complex of *Azotobacter vinelandii* nitrogenase. *FEBS Lett.* 380:233-6

Eady RR, Lowe DJ, Thorneley RNF. 1978. Nitrogenase of *Klebsiella pneumoniae*: A pre-steady-state burst of ATP hydrolysis is coupled to electron transfer between the component proteins. *FEBS Lett*. 95:211-13

Eidsness MK, Flank AM, Smith BE, Flood AC, Garner CD, Cramer SP. 1986. EXAFS of *Klebsiella pneumoniae* nitrogenase MoFe protein from wild-type and *nifV* mutant strains. *J. Am. Chem. Soc*. 108:2746-48

Emerich DW, Ljones T, Burris RH. 1978. Nitrogenase: Properties of the catalytically inactive complex between the *Azotobacter vinelandii* MoFe protein and the *Clostridium pasteurianum* Fe protein. *Biochem. Biophys. Acta* 527:359-69

Ennor AH. 1957. Determination and preparation of N-phosphates of biological origin. *Methods in Enzymol*. 3:850-56

Filler WA, Kemp RM, Ng JC, Hawkes TR, Dixon RA, Smith BE. 1986. The *nifH* gene product is required for synthesis or stability of the iron-molybdenum cofactor of nitrogenase from *Klebsiella pneumoniae. Eur. J. Biochem.* 160:371-7

Fisher K, Lowe DJ, Thorneley RNF. 1991. *Klebsiella pneumoniae* nitrogenase: The pre-steady-state kinetics of MoFe protein reduction and hydrogen evolution under conditions of limiting electron flux show that the rates of association with the Fe-protein and electron transfer are independent of the oxidation level of the MoFe-protein. *Biochem. J.* 279:81-5

Fisher K, Lowe DJ, Pau RN. 1993. *Klebsiella pneumoniae* nitrogenase MoFe protein: Chymotryptic proteolysis affects function by limited cleavage of the β-chain and provides high-specific-activity MoFe protein. *Biochem. J.* 291:309-14

Fu W, Jack RF, Morgan TV, Dean DR, Johnson MK. 1994. *nifU* gene product from *Azotobacter vinelandii* is a homodimer that contains two identical [2Fe-2S] clusters. *Biochemistry* 33:13455-63

Gavini N, Watt GD, Ma L, Burgess BK. 1994

Georgiadis MM, Komiya H, Chakrabarti P, Woo D, Kornuc JJ, Rees DC. 1992. Crystallographic structure of the nitrogenase iron protein from *Azotobacter vinelandii. Science* 257:1653-59

Govezensky D, Zamir A. 1989. Structure-function relationships in the α-subunit of *Klebsiella pneumoniae* nitrogenase MoFe protein from analysis of *nifD* mutants. *J. Bacteriol*. 171:5729-35

Guth JH, Burris RH. 1983. Inhibition of nitrogenase-catalyzed NH_3 formation by H_2. *Biochemistry* 22:5111-22

Hadfield KL, Bulen WA. 1969. Adenosine triphosphate requirement of nitrogenase from *Azotobacter vinelandii. Biochemistry* 8:5103-8

Hageman RV, Burris RH. 1978a. Kinetic studies on electron transfer and interaction between nitrogenase components from *Azotobacter vinelandii. Biochemistry* 17:4117-24

Hageman RV, Burris RH. 1978b. Nitrogenase and nitrogenase reductase associate and dissociate with each catalytic cycle. *Proc. Natl. Acad. Sci. USA* 75:2699-702

Hageman RV, Burris RH. 1980. Electron allocation to alternative substrates of *Azotobacter* nitrogenase is controlled by the electron flux through dinitrogenase. *Biochim. Biophys. Acta* 591:63-75

Hagen WR, Wassink H, Eady RR, Smith BE, Haaker H. 1987. Quantitative EPR of an S=7/2 system in thionine-oxidized MoFe proteins of nitrogenase. *Eur. J. Biochem.* 169:457-65

Hardy RWF, Knight E Jr, D'Eustachio AJ. 1965. An energy-dependent hydrogen-evolution from dithionite in nitrogen-fixing extracts of *Clostridium pasteurianum*. *Biochem. Biophys. Res. Commun.* 20:539-44

Hardy RWF, Knight E Jr. 1967. ATP-dependent reduction of azide and HCN by N_2-fixing enzymes of *Azotobacter vinelandii* and *Clostridium pasteurianum*. *Biochim. Biophys. Acta* 139:69-90

Hardy RWF. 1993. Biological nitrogen fertilization: Present and future applications. Pp. 109-117 in *Agriculture and Environmental Challenges.* Srivastava JP, Aldermans H, eds. Proc. 13th Agric. Sector Symp. Washington D.C.:The World Bank

Hausinger RP, Howard JB. 1983. Thiol reactivity of the nitrogenase Fe-protein from *Azotobacter vinelandii. J. Biol. Chem.* 258:13486-92

Hawkes TR, Smith BE. 1983. Purification and characterization of the inactive MoFe protein ($NifB^-$ Kp1) of the nitrogenase from *nifB* mutants of *Klebsiella pneumoniae. Biochem. J.* 209:43-50

Hawkes TR, McLean PA, Smith BE. 1984. Nitrogenase from *nifV* mutants of *Klebsiella pneumoniae* contains an altered form of the iron-molybdenum cofactor. *Biochem. J.* 217:317-21

Hoch GE, Schneider KC, Burris RH. 1960. Hydrogen evolution and exchange, and conversion of N_2O to N_2 by soybean root nodules. *Biochim. Biophys. Acta* 37:273-79

Homer MJ, Paustian TD, Shah VK, Roberts GP. 1993. The *nifY* product of *Klebsiella pneumoniae* is associated with apodinitrogenase and dissociates upon activation with the iron-molybdenum cofactor. *J. Bacteriol.* 175:4907-10

Hoover TR, Robertson AD, Cerny RL, Hayes RN, Imperial J, Shah VK, Ludden PW. 1987. Identification of the V factor needed for synthesis of the iron-molybdenum cofactor of nitrogenase as homocitrate. *Nature* 329:855-57

Hoover TR, Imperial J, Ludden PW, Shah VK. 1988. Homocitrate cures the $NifV^-$ phenotype in *Klebsiella pneumoniae. J. Bacteriol.* 170:1978-79

Howard JB, Davis R, Moldenhauer B, Cash VL, Dean DR. 1989. Fe-S cluster ligands are the only cysteines required for nitrogenase Fe-protein activities. *J. Biol. Chem.* 264:11270-74

Howard JB. 1993. Protein component complex formation and adenosine triphosphate hydrolysis in nitrogenase. See Stiefel *et al*., 1993, pp. 271-89

Howard JB, Rees DC. 1994. Nitrogenase: A nucleotide-dependent molecular switch. *Ann. Rev. Biochem.* 63:235-64

Howard JB, Rees DC. 1996. Structural basis of biological nitrogen fixation. *Chem. Rev.* 96:2965-82

Howard KS, McLean PA, Hansen FB, Lemley PV, Koblan KS, Orme-Johnson WH. 1986. *Klebsiella pneumoniae nifM* gene product is required for stabilization and activation of nitrogenase iron protein in *Escherichia coli. J. Biol. Chem.* 261:772-78

Huynh BH, Henzl MT, Christner JA, Zimmermann R, Orme-Johnson WH, Münck E. 1980. Nitrogenase XII. Mössbauer studies of the MoFe protein from *Clostridium pasteurianum W5. Biochim. Biophys. Acta.*623:124-38

Huynh BH. 1994. Mössbauer spectroscopy in study of cytochrome cd_1 from *Thiobacillus denitrificans*, desulfoviridin, and iron hydrogenase. Pp. 523-543 in *Methods in Enzymology, Volume 243, Inorganic Microbial Sulfur Metabolism*. Peck HD, LeGall J, eds.

Hwang JC, Chen CH, Burris RH. 1973. Inhibition of nitrogenase-catalyzed reductions. *Biochim. Biophys. Acta* 292:256-70

Imam S, Eady RR. 1980. Nitrogenase of *Klebsiella pneumoniae*: Reductant-independent ATP hydrolysis and the effect of pH on the efficiency of coupling of ATP hydrolysis to substrate reduction. *FEBS Lett*. 110:35-38

Imperial J, Ugalde RA, Shah VK, Brill WJ. 1984. Role of the *nifQ* product in the incorporation of molybdenum into nitrogenase in *Klebsiella pneumoniae. J. Bacteriol.* 158:187-94

Jacobson MR, Brigle KE, Bennet LT, Setterquist RA, Wilson MS, *et al*. 1989a. Physical and genetic map of the major *nif* gene cluster from *Azotobacter vinelandii. J. Bacteriol.* 171:1017-27

Jacobson MR, Cash VL, Weiss MC, Laird NF, Newton WE, Dean DR. 1989b. Biochemical and genetic analysis of the *nifUSVWZM* cluster from *Azotobacter vinelandii. Molec. Gen. Genet.* 219:49-57

Jacobson MR, Cantwell JS, Dean DR. 1990. A hybrid *Azotobacter vinelandii-Clostridium pasteurianum* nitrogenase iron protein that has *in vivo* and *in vitro* catalytic activity. *J. Biol. Chem*. 265:19429-19433

Jeng DY, Morris JA, Mortenson LE. 1970. The effect of reductant in inorganic phosphate release from adenosine 5' triphosphate by purified nitrogenase of *Clostridium pasteurianum. J. Biol. Chem*. 245:2809-13

Jensen BB, Burris RH. 1986. N_2O as a substrate and as a competitive inhibitor of nitrogenase. *Biochemistry* 25:1083-88

Johnson MK, Thomson AJ, Robinson AE, Smith BE. 1981. Characterization of the paramagnetic centres of the molybdenum-iron protein from *Klebsiella pneumoniae* using

low temperature magnetic circular dichroism spectroscopy. *Biochim. Biophys. Acta* 671:61-70

Johnson MK. 1988. Variable-temperature magnetic circular dichroism studies of metalloproteins. In *Metal Clusters in Proteins.* ed. L Que pp. 326-42 Washington DC:ACS Books Symposium Series. 413 pp.

Kelly M, Lang G. 1970. Evidence from Mössbauer spectroscopy for the role of iron in nitrogen fixation. *Biochim. Biophys. Acta* 223:86-104

Kent HM, Ioannidis I, Gormal C, Smith BE, Buck M. 1989. Site-directed mutagensis of *Klebsiella pneumoniae* nitrogenase. *Biochem. J.* 264:257-64

Kent HM, Baines M, Gormal C, Smith BE, Buck M. 1990. Analysis of site-directed mutations in the α- and β-subunits of *Klebsiella pneumoniae* nitrogenase. *Mol. Microbiol.* 4:1497-1504

Kentemich T, Danneberg G, Hundeshagen B, Bothe H. 1988. Evidence for the occurrence of the alternative, vanadium-containing nitrogenase in the cyanobacterium *Anabaena variabilis. FEMS Microbiol. Lett.* 51:19-24

Kim C-H, Zheng L, Newton WE, Dean DR. 1993. Intermolecular electron transfer and substrate reduction properties of MoFe proteins altered by site-specific amino acid substitution. See Palacios *et al*., 1993, pp. 105-10

Kim C-H, Newton WE, Dean DR. 1995. Role of the MoFe protein α-subunit histidine-195 residue in FeMo-cofactor binding and nitrogenase catalysis. *Biochemistry* 34:2798-2808

Kim J, Rees DC. 1992a. Structural models for the metal centers in the nitrogenase molybdenum-iron protein. *Science* 257:1677-82

Kim J, Rees DC. 1992b. Crystallographic structure and functional implications of the nitrogenase molybdenum-iron protein from *Azotobacter vinelandii. Nature* 360:553-60

Kim J, Woo D, Rees DC. 1993. X-ray crystal structure of the nitrogenase molybdenum-iron protein from *Clostridium pasteurianum* at 3.0-A resolution. *Biochemistry* 32:7104-15

Kim S, Burgess BK. 1994. Purification and characterization of nitrogenase from a Δ*nifW* strain of *Azotobacter vinelandii. J. Biol. Chem.* 269:4215-20

Kirschner EM. 1996. Fertilizer makers anticipate strong U.S. demand. *Chem. Eng. News* 74 (15):16-17

Koonin EV. 1993. A superfamily of ATPases with diverse functions containing either classical or deviant ATP-binding motif. *J. Mol. Biol.* 229:1165-74

Kurtz DM, McMillan RS, Burgess BK, Mortenson LE, Holm RH. 1979. Identification of iron-sulfur centers in the iron-molybdenum protein of nitrogenase. *Proc. Natl. Acad. Sci. USA* 76:4986-89

Laemmli UK. 1970. Cleavage of structural proteins during assembly of the head of bacteriophage T_4. *Nature* 227:680-85

Lanzilotta WN, Ryle MJ, Seefeldt LC. 1995. Nucleotide hydrolysis and protein conformational changes in *Azotobacter vinelandii* nitrogenase iron protein: Defining the function of aspartate 129. *Biochemistry* 34:10713-10723

Lanzilotta WN, Fisher K, Seefeldt LC. 1996. Evidence for electron transfer from the nitrogenase iron protein to the molybdenum-iron protein without MgATP hydrolysis: Charaterization of a tight protein-protein complex. *Biochemistry* 35:7188-7196

Lanzilotta WN, Seefeldt LC. 1996. Electron transfer from the nitrogenase iron protein to the [8Fe-(7/8)S] clusters of the molybdenum-iron protein. *Biochemistry* 35:16770-16776

Lawson DM, Roe SM, Mayer S, Gormal C, Yousafzai FK, *et al*. 1997. Structure of *Klebsiella pneumoniae* nitrogenase. In *Nitrogen Fixation for the 21st Century*. Elmerich C, Kondorosi A, Newton WE, eds. Kluwer Academic Press, Dordrecht, The Netherlands, 1997, In Press

Li J-G, Burgess BK, Corbin JL. 1982. Nitrogenase reactivity: Cyanide as a substrate and inhibitor. *Biochemistry* 21:4393-4402

Liang J, Madden M, Shah VK, Burris RH. 1990. Citrate substitutes for homocitrate in the nitrogenase of a *nifV* mutant of *Klebsiella pneumoniae. Biochemistry* 29:8577-81

Lindahl PA, Day EP, Kent KA, Orme-Johnson WH, Münck E. 1985. Mössbauer, EPR, and magnetization studies of the *Azotobacter vinelandii* Fe protein. *J. Biol. Chem*. 260:11160-73

Lindahl PA, Gorelick NJ, Münck E, Orme-Johnson WH. 1987. EPR and Mössbauer studies of nucleotide-bound nitrogenase iron protein from *Azotobacter vinelandii. J. Biol. Chem*. 262:14945-54

Lindahl PA, Papaefthymiou V, Orme-Johnson WH, Münck E. 1988. Mössbauer studies of solid thionin-oxidized MoFe protein of nitrogenase. *J. Biol. Chem*. 263:19412-18

Ljones T, Burris RH. 1972. ATP hydrolysis and electron transfer in the nitrogenase reaction with different combinations of the iron protein and the molybdenum-iron protein. *Biochim. Biophys. Acta* 275:93-101

Lowe DJ. 1978. Simulation of the electron paramagnetic resonance spectrum of the iron protein of nitrogenase: A prediction of the existence of a second paramagnetic center. *Biochem. J*. 175:955-7

Lowe DJ, Thorneley RNF. 1984. The mechanism of *Klebsiella pneumoniae* nitrogenase action. Pre-steady-state kinetics of H_2 formation. *Biochem. J.* 224:877-86

Lowe DJ, Fisher K, Thorneley RNF. 1990. Nitrogenase of *Klebsiella pneumoniae*. Mechanism of acetylene reduction. *Biochem. J*. 272:621-625

Lowe DJ, Fisher K, Thorneley RNF. 1993. *Klebsiella pneumoniae* nitrogenase: pre-steady-state absorbance changes show that redox changes occur in the MoFe protein that depend on substrate and component protein ratio; a role for P-centres in reducing dinitrogen? *Biochem. J*. 292:93-98

Lowe DJ, Ashby GA, Brune M, Knights H, Webb MR, Thorneley RNF. 1995. ATP hydrolysis and energy transduction by nitrogenase. Pp. 103-8 in *Nitrogen Fixation: Fundamentals and Applications*. Tikhonovich IA, Provorov NA, Romanov VI, Newton WE, eds. Dordrecht, Netherlands: Kluwer Academic. 824 pp.

Lowery RG, Chang CL, Davis LC, McKenna M-C, Stephens PJ, Ludden PW. 1989. Substitution of histidine for arginine-101 of dinitrogenase reductase disrupts electron transfer to dinitrogenase. *Biochemistry* 28:1206-12

Lowry OH, Rosebrough NJ, Farr AL, Randall RH. 1951. Protein measurement with the folin phenol reagent. *J. Biol. Chem*. 193:265-75

Ludden PW, Davis R, Petrovich R, Roberts GP. 1993. Purification and analysis of the alternative nitrogenase from the photosynthetic bacterium *Rhodospirillum rubrum*. See Palacios *et al*. 1993, pp. 143

Ma L, Gavini N, Liu H, Hedman B, Hodgson KO, Burgess BK. 1994. Large scale isolation and characterization of the molybdenum-iron cluster from nitrogenase. *J. Biol. Chem.* 269:18007-15

Ma L, Brosius MA, Burgess BK. 1996. Construction of a form of the MoFe protein of nitrogenase that accepts electrons from the Fe protein but does not reduce substrate. *J. Biol. Chem*. 271:10528-32

Masepohl B, Angermüller S, Hennecke S, Hübner P, Moreno-Vivian C, Klipp W. 1993. Nucleotide sequence and genetic analysis of the *Rhodobacter capsulatus* ORF6-*nifU*$_l$*SVW* gene region: Possible role of NifW in homocitrate processing. *Mol. Gen. Genet.* 238:369-82

May HD, Dean DR, Newton WE. 1991 Altered nitrogenase MoFe proteins from *Azotobacter vinelandii*. *Biochem. J.* 277:457-64

McLean PA, Dixon RA. 1981. Requirement of *nifV* gene for production of wild-type nitrogenase enzyme in *Klebsiella pneumoniae*. *Nature* 292:655-6

McLean PA, Papaefthymiou V, Orme-Johnson WH, Münck E. 1987. Isotopic hybrids of nitrogenase. Mössbauer study of MoFe protein with selective ^{57}Fe enrichment of the P clusters. *J. Biol. Chem*. 262:12900-3

Mensink RE, Wassink H, Haaker H. 1992. A reinvestigation of the pre-steady-state ATPase activity of the nitrogenase from *Azotobacter vinelandii. Eur. J. Biochem.* 208:289-94

Merrick M, Filser M, Dixon R, Elmerich C, Sibold L, Houmard J. 1980. The use of translocatable genetic elements to construct a fine-structure map of the *Klebsiella pneumoniae* nitrogen fixation (*nif*) gene cluster. *J. Gen. Microbiol.* 117:509-20

Merrick M, Hill S, Hennecke H, Hahn M, Dixon RA, Kennedy C. 1982. Repressor properties of the *nifL* gene product of *Klebsiella pneumoniae*. *Mol. Gen. Genet.* 185:75-81

Messing J, Vieira J. 1982. A new pair of M13 vectors for selecting either DNA strand of double-digest restriction fragments. *Gene* 19:269-76

Miller RW, Eady RR. 1988a. Cyanamide: A new substrate for nitrogenase. *Biochim. Biophys. Acta* 952:290-96

Miller RW, Eady RR. 1988b. Molybdenum and vanadium nitrogenases of *Azotobacter chroococcum*: Low temperature favours N_2 reduction by vanadium nitrogenase. *Biochem. J.* 256:429-32

Minchin SD, Austin S, Dixon RA. 1989. Transcriptional activation of the *Klebsiella pneumoniae nifLA* promoter by NTRC is face-of-the-helix dependent and the activator stabilizes the interaction of sigma 54-RNA polymerase with the promoter. *EMBO J.* 8:3491-99

Morett E, Buck M. 1989. *In vivo* studies on the interaction of RNA polymerase-σ^{54} with the *Klebsiella pneumoniae* and *Rhizobium meliloti nifH* promoters: The role of NifA in the formation of an open promoter complex. *J. Mol. Biol.* 210:65-77

Mortenson LE. 1964. Ferredoxin and ATP, requirements for nitrogen fixation in cell-free extracts of *Clostridium pasteurianum*. *Proc. Natl. Acad. Sci. USA* 52:272-9

Münck E, Rhodes H, Orme-Johnson WH, Davis LC, Brill WJ, Shah VK. 1975. Nitrogenase. VIII. Mössbauer and EPR spectroscopy. The MoFe protein component from *Azotobacter vinelandii OP. Biochim. Biophys. Acta* 400:32-53

Murrell SA, Lowery RG, Ludden PW. 1988. ADP-ribosylation of dinitrogenase reductase from *Clostridium pasteurianum* prevents its inhibition of nitrogenase from *Azotobacter vinelandii. Biochem. J.* 251:609-12

Orme-Johnson WH, Hamilton WD, Jones TL, Tso M-YW, Burris RH, Shah VK, Brill WJ. 1972. Electron paramagnetic resonance of nitrogenase and nitrogenase components from *Clostridium pasteurianum W5* and *Azotobacter vinelandii OP. Proc. Natl. Acad. Sci. USA* 69:3142-45

Orme-Johnson WH, Davis LC. 1977. Current topics and problems in the enzymology of nitrogenase. In *Iron-Sulfur Proteins,* ed. W Lovenberg, pp 15-60. New York:Academic Press. 443 pp.

Page WJ, von Tigerstrom M. 1979. Optimal conditions for transformation of *Azotobacter vinelandii. J. Bacteriol.* 139:1058-61

Palacios R, Mora J, Newton WE, eds. 1993. *New Horizons in Nitrogen Fixation*. Dordrecht, Netherlands: Kluwer Academic. 788 pp.

Pau RN, Mitchenall LA, Robson RL. 1989. Genetic evidence for an *Azotobacter vinelandii* nitrogenase lacking molybdenum and vanadium. *J. Bacteriol.* 171:124-29

Paustian TD, Shah VK, Roberts GP. 1989. Purification and characterization of the *nifN* and *nifE* gene products from *Azotobacter vinelandii* mutant UW45. *Proc. Natl. Acad. Sci. USA* 86:6082-86

Paustian TD, Shah VK, Roberts GP. 1990. Apodinitrogenase: Purification, association with a 20-kilodalton protein, and activation by the iron-molybdenum cofactor in the absence of dinitrogenase reductase. *Biochemistry* 29:3515-22

Peters JW, Fisher K, Dean DR. 1994. Identification of a nitrogenase protein-protein interaction site defined by residues 59 through 67 within the *Azotobacter vinelandii* Fe protein. *J. Biol. Chem.* 269:28076-83

Peters JW, Fisher K, Dean DR. 1995a. Nitrogenase structure and function: A biochemical-genetic perspective. *Annu. Rev. Microbiol.* 49:335-66

Peters JW, Fisher K, Newton WE, Dean DR. 1995b. Involvement of the P cluster in intramolecular electron transfer within the nitrogenase MoFe protein. *J. Biol. Chem.* 270:27007-27013

Peters JW, Stowell MHB, Soltis SM, Finnegan MG, Johnson MK, Rees DC. 1997. Redox-dependent structural changes in the nitrogenase P-cluster. *Biochemistry* 36:1181-1187

Pierik AJ, Wassink H, Haaker H, Hagen WR. 1993. Redox properties and EPR spectroscopy of the P clusters of *Azotobacter vinelandii* MoFe protein. *Eur. J. Biochem.* 212:51-61

Pope MR, Murrell SA, Ludden PW. 1985. Covalent modification of the iron protein of nitrogenase from *Rhodospirillum rubrum* by adenosine diphosphoribosylation of a specific arginine residue. *Proc. Natl. Acad. Sci. USA* 82:3173-77

Rawlings J, Shah VK, Chisnell JR, Brill WJ, Zimmerman R, Münck E, Orme-Johnson WH. 1978. Novel metal cluster in the iron-molybdenum cofactor of nitrogenase. *J. Biol. Chem.* 253:1001-4

Renner KA, Howard JB. 1996. Aluminum fluoride inhibition of nitrogenase: Stabilization of a nucleotide·Fe-protein·MoFe-protein complex. *Biochemistry* 35:5353-58

Reitzer LJ, Movsas B, Magasanik B. 1989. Activation of *glnA* transcription by nitrogen regulator I (NR_I)-phosphate in *Escherichia coli*: Evidence for a long-range physical interaction between NR_I-phosphate and RNA polymerase. *J. Bacteriol*. 171:5512-22

Robson RL. 1984. Identification of possible adenine nucleotide-binding sites in nitrogenase Fe- and MoFe-proteins by amino acid sequence comparison. *FEBS Lett.* 173:394-98

Robson RL. 1986. Nitrogen fixation in strains of *Azotobacter chroococcum* bearing deletions of a cluster of genes coding for nitrogenase. *Nature* 322:388-90

Robson RL, Woodley PR, Pau RN, Eady RR. 1989. Structural genes for the vanadium nitrogenase from *Azotobacter chroococcum. EMBO J.* 8:1217-24

Robinson AC, Burgess BK, Dean DR. 1986. Activity, reconstitution, and accumulation of nitrogenase components in *Azotobacter vinelandii* mutant strains containing defined deletions within the nitrogenase structural gene cluster. *J. Bacteriol.* 166:180-86

Robinson AC, Dean DR, Burgess BK. 1987. Iron-molybdenum cofactor biosynthesis in *Azotobacter vinelandii* requires the iron protein of nitrogenase. J. Biol. Chem. 262:14327-32

Robinson AC, Chun TW, Li J-G, Burgess BK. 1989. Iron-molybdenum cofactor insertion into the apo-MoFe protein of nitrogenase involves the iron protein-MgATP complex. *J. Biol. Chem.* 264:10088-95

Roll JT, Shah VK, Dean DR, Roberts GP. 1995. Characteristics of NifEN in *Azotobacter vinelandii* strains. *J. Biol. Chem.* 270:4432-37

Rudd KE, Sofia HJ, Koonin EV, Plunkett G, Lazar S, Rouviere PE. 1995. A new family of peptidyl-prolyl isomerases. *Trends Biochem. Sci.* 20:12-14

Ryle MJ, Seefeldt LC. 1996. Elucidation of a MgATP signal transduction pathway in the nitrogenase iron protein: Formation of a conformation resembling the MgATP-bound state by protein engineering. *Biochemistry* 35:4766-4775

Sanger F, Nicklen S, Coulson R. 1977. DNA sequencing with chain-terminating inhibitors. *Proc. Natl. Acad. Sci. USA* 74:5463-67

Schindelin H, Kisker C, Schlessman JL, Howard JB, Rees DC. 1997. Structure of $ADP{\cdot}AlF_4^-$-stabilized nitrogenase complex and its implications for signal transduction. *Nature* 387:370-6

Schneider K, Müller A, Schramm U, Klipp EW. 1991. Demonstration of a molybdenum- and vanadium-independent nitrogenase in a *nifHDK*-deletion mutant of *Rhodobacter capsulatus*. *Eur. J. Biochem.* 195:653-61

Schöllhorn R, Burris RH. 1967. Reduction of azide by the N_2-fixing enzyme system. *Proc Natl. Acad. Sci. USA* 57:1317-23

Schulz GE, Elzinga M, Marx F, Schimer RH. 1974. Three-dimensional structure of adenyl kinase. *Nature* 250:120-23

Scott DJ, May HD, Newton WE, Brigle KE, Dean DR. 1990. Role for the nitrogenase MoFe protein a-subunit in the FeMo-cofactor binding and catalysis. *Nature* 343:188-90

Scott DJ, Dean DR, Newton WE. 1992. Nitrogenase-catalyzed ethane production and CO-sensitive hydrogen evolution from MoFe proteins having amino acid substitutions in an α-subunit FeMo cofactor-binding domain. *J. Biol. Chem.* 267:20002-20010

Seefeldt LC, Morgan TV, Dean DR, Mortenson LE. 1992. Mapping the site(s) of MgATP and MgADP interaction with the nitrogenase of *Azotobacter vinelandii*. *J. Biol. Chem.* 267:6680-6688

Seefeldt LC, Mortenson LE. 1993. Increasing nitrogenase catalytic efficiency for MgATP by changing serine 16 of its Fe protein to threonine: Use of Mn^{2+} to show interaction of serine 16 with Mg^{2+}. *Protein Sci.* 2:93-102

Seefeldt LC. 1994. Docking of nitrogenase iron- and molybdenum-iron proteins for electron transfer and MgATP hydrolysis: The role of arginine 140 and lysine 143 of the *Azotobacter vinelandii* iron protein. *Protein Sci.* 3:2073-2081

Shah VK, Brill WJ. 1977. Isolation of an iron-molybdenum cofactor from nitrogenase. *Proc. Natl. Acad. Sci. USA* 74:3249-53

Shah VK, Imperial J, Ugalde RA, Ludden PW, Brill WJ. 1986. *In vitro* synthesis of the iron-molybdenum cofactor of nitrogenase. *Proc. Natl. Acad. Sci. USA* 83:1636-40

Shah VK, Allen JR, Spangler NJ, Ludden PW. 1994. *In vitro* synthesis of the iron-molybdenum cofactor of nitrogenase. Purification and characterization of NifB cofactor, the product of NifB protein. *J. Biol. Chem*. 269:1154-58

Shah VK, P Rangaraj, Ludden PW. 1997. Requirement of NIFX for the in vitro biosynthesis of the iron-molybdenum cofactor of nitrogenase. In *Nitrogen Fixation for the 21st Century*. Elmerich C, Kondorosi A, Newton WE, eds. Kluwer Academic Press, Dordrecht, The Netherlands. In Press

Shen J, Dean DR, Newton WE. 1997. Evidence for multiple substrate-reduction sites and distinct inhibitor-binding sites from an altered *Azotobacter vinelandii* nitrogenase MoFe protein. *Biochemistry* 36:4884-4894

Smith BE, Lowe DJ, Bray RC. 1972. Nitrogenase of *Klebsiella pneumoniae*: Electron paramagnetic resonance studies on the catalytic mechanism. *Biochem. J.*130:641-643

Smith BE, Lowe DJ, Bray RC. 1973. Studies by electron paramagnetic resonance on the catalytic mechanism of nitrogenase of *Klebsiella pneumoniae. Biochem. J.* 135:331-41

Stacey G, Burris RH, Evans HJ, eds. 1992. *Biological Nitrogen Fixation*, New York:Chapman and Hall. 943 pp.

Stephens PJ, McKenna CE, Smith BE, Nguyen HT, McKenna M-C, Thomas AJ, Devlin F, Jones JB. 1979. Circular dichroism and magnetic circular dichroism of nitrogenase proteins. *Proc. Natl. Acad. Sci. USA* 76:2585-90

Stiefel EI, Coucouvanis D, Newton WE, eds. 1993. *Molybdenum Enzymes, Cofactors and Model Systems.* Washington DC: Am. Chem. Soc. 387 pp.

Strandberg GW, Wilson PW. 1968. Formation of the nitrogen-fixing enzyme system in *Azotobacter vinelandii. Can. J. Mircrobiol*. 14:25-31

Surerus KR, Hendrich MP, Christie PD, Rottgardt D, Orme-Johnson WH, Münck E. 1992. Mössbauer and integer-spin EPR of the oxidized P-clusters of nitrogenase: P^{OX} is a non-Kramers system with a nearly degenerate ground doublet. *J. Am. Chem. Soc*. 114:8580-90

Thorneley RNF. 1975. Nitrogenase of *Klebsiella pneumoniae:* A stopped-flow study of magnesium-adenosine triphosphate-induced electron transfer between the component proteins. *Biochem. J.* 145:391-396

Thorneley RNF, Cornish-Bowden A. 1977. Kinetics of nitrogenase of *Klebsiella pneumoniae:* Heterotropic interactions between magnesium-adenosine 5'-diphosphate and magnesium-adenosine 5'-triphosphate. *Biochem. J.* 165:255-262

Thorneley RNF, Eady RR, Lowe DJ. 1978. Biological nitrogen fixation by way of an enzyme-bound dinitrogen-hydride intermediate. *Nature* 272:557-8

Thorneley RNF, Lowe DJ. 1983. Nitrogenase of *Klebsiella pneumoniae:* Kinetics of the dissociation of oxidized iron protein from molybdenum-iron protein: Identification of the rate-limiting step for substrate reduction. *Biochem. J.* 215:393-403

Thorneley RNF, Lowe DJ. 1984a. The mechanism of *Klebsiella pneumoniae* nitrogenase action: Pre-steady-state kinetics of an enzyme-bound intermediate in N_2 reduction and of NH_3 formation. *Biochem. J.* 224:887-894

Thorneley RNF, Lowe DJ. 1984b. The mechanism of *Klebsiella pneumoniae* nitrogenase action: Simulation of the dependences of H_2-evolution rate on component-protein concentration and ratio and sodium dithionite concentration. *Biochem. J.* 224:903-909

Thorneley RNF, Lowe DJ. 1985. Kinetics and the mechanism of the nitrogenase enzyme system. Pp. 222-284 in *Molybdenum Enzymes.* Spiro TG, ed. New York: Wiley

Thorneley RNF, Ashby GA, Howarth JV, Millar NC, Gutfreund H. 1989. A transient kinetic study of the nitrogenase of *Klebsiella pneumoniae* by stopped-flow calorimetry. *Biochem. J.* 264:657-661

Thorneley RNF, Ashby GA, Julius C, Hunter JL, Webb MR. 1991. Nitrogenase of *Klebsiella pneumoniae.* Reversibility of the reductant-independent MgATP-cleavage reaction is shown by MgADP-catalysed phosphate/water oxygen exchange. *Biochem. J.* 277:735-41

Thorneley RNF. 1992. Nitrogenase of *Klebsiella pneumoniae:* An MgATP hydrolysing energy transduction system with similarities to actomyosin and p21ras. *Phil. Tans. R. Soc. Lond. B* 336:73-82

Thorneley RNF, Ashby GA, Fisher K, Lowe DJ. 1993. Electron-transfer reactions associated with nitrogenase from *Klebsiella pneumoniae.* See Stiefel *et al*., 1993, pp. 290-302

Tittsworth RC, Hales BJ. 1993. Detection of EPR signals assigned to the 1-equiv-oxidized P-clusters of the nitrogenase MoFe-protein from *Azotobacter vinelandii. J. Am. Chem. Soc.* 115:9763-67

Ugalde RA, Imperial J, Shah VK, Brill WJ. 1984. Biosynthesis of iron-molybdenum cofactor in the absence of nitrogenase. *J. Bacteriol*. 159:888-93

Van Dyke MW, Sirito M, Sawadogo M. 1992. Single-step purification of bacterially expressed polypeptides containing an oligo-histidine domain. *Gene* 111:99-104

Vaughn SA, Burgess BK. 1989. Nitrite, a new substrate for nitrogenase. *Biochemistry* 28:419-24

Vieira J, Messing J. 1987. Production of single-stranded plasmid DNA. *Methods in Enzymol*. 153:3-11

Walker GA, Mortenson LE. 1974. Effect of magnesium adenosine 5'-triphosphate on the accessibility of the iron of clostridial azoferredoxin, a component of nitrogenase. *Biochemistry* 13:2382-88

Walker JE, Saraste M, Runswick MJ, Gay NJ. 1982. Distantly related sequences in the alpha- and beta-subunits of ATP synthase, myosin, kinases and other ATP-requiring enzymes and a common nucleotide binding fold. *EMBO J.* 1:945-51

Watt GD, Bulen WA, Burns A, Hadfield KL. 1975. Stoichiometry, ATP/2e values, and energy requirements for reactions catalyzed by nitrogenase from *Azotobacter vinelandii. Biochemistry* 14:4266-72

Watt GD, Burns A, Lough S, Tennent DL. 1980. Redox and spectroscopic properties of oxidized MoFe protein from *Azotobacter vinelandii. Biochemistry* 19:4926-32

Watt GD, Burns A, Tennent DL. 1981. Stoichiometry and spectral properties of the MoFe cofactor and noncofactor redox centers in the MoFe protein of nitrogenase from *Azotobacter vinelandii. Biochemistry* 20:7272-77

Watt GD, MacDonald JW. 1985. Electron paramagnetic resonance spectrum of the iron protein of nitrogenase: Existence of a $g = 4$ spectral component and its effect on spin quantization. *Biochemistry* 24:7226-31

Watt GD, Wang Z-C, Knotts RR. 1986. Redox reactions of and nucleotide binding to the iron protein of *Azotobacter vinelandii. Biochemistry* 25:8156-62

Watt GD, Reddy KRN. 1994. Formation of an all ferrous Fe_4S_4 cluster in the iron protein component of *Azotobacter vinelandii* nitrogenase. *J. Inorg. Biochem*. 53:281-94

Wherland S, Burgess BK, Stiefel EI, Newton WE. 1981. Nitrogenase reactivity: Effects of component ratio on electron flow and distribution during nitrogen fixation. *Biochemistry* 20:5132-40

Willing A, Georgiadis MM, Rees DC, Howard JB. 1989. Cross-linking of nitrogenase components. *J. Biol. Chem.* 264:8499-503

Willing A, Howard JB. 1990. Cross-linking site in *Azotobacter vinelandii* complex. *J. Biol. Chem.* 265:6596-99

Wolle D, Dean DR, Howard JB. 1992a. Nucleotide iron-sulfur cluster signal transduction in the nitrogenase iron-protein: The role of Asp125. *Science* 258:992-95

Wolle D, Kim C-H, Dean DR, Howard JB. 1992b. Ionic interactions in the nitrogenase complex: Properties of Fe-protein containing substitutions for Arg-100. *J. Biol. Chem.* 267:3667-73

Yates MG. 1992. The enzymology of molybdenum-dependent nitrogen fixation. See Stacey *et al*., 1992, pp. 685-735

Yousafzai FK, Buck M, Smith BE. 1996. Isolation and characterization of nitrogenase MoFe protein from the mutant strain pHK17 of *Klebsiella pneumoniae* in which the two bridging cysteine residues of the P-clusters are replaced by the non-coordinating amino acid alanine. *Biochem. J.* 318:111-18

Zheng L, White RH, Cash VL, Jack RF, Dean DR. 1993. Cysteine desulfurase activity indicates a role for NIFS in metallocluster biosynthesis. *Proc Natl. Acad. Sci. USA* 90:2754-58

Zheng L, Dean DR. 1994. Catalytic formation of a nitrogenase iron-sulfur cluster. *J. Biol. Chem.* 269:18723-26

Zimmermann R, Münck E, Brill WJ, Shah VK, Henzl MT, Rawlings J, Orme-Johnson WJ. 1978. Nitrogenase X: Mössbauer and EPR studies on reversibly oxidized MoFe protein from *Azotobacter vinelandii OP*. *Biochim. Biophys. Acta* 537:185-207

Zumft WG, Mortenson LE. 1973. Evidence for a catalytic-centre heterogeneity of molybdoferredoxin from *Clostridium pasteurianum. Eur. J. Biochem.*35:401-9

Zumft WG, Mortenson LE, Palmer G. 1973. Electron paramagnetic resonance studies on nitrogenase. II. Interaction of Adenosine 5'-triphosphate with azoferredoxin. *Biochim. Biophys. Acta* 292:413-21

VITA

John Sidney Cantwell was born on March 25, 1960 in Redwood City, California as the seventh child and third son of Sidney Herbert Cantwell Jr. and Carol Virginia Cantwell. He spent the first eighteen years of his life growing up in Menlo Park, California, a suburb on the southern end of the San Francisco peninsula. He received a B.A. degree in Genetics from the University of California, Berkeley in June of 1983. After working in the biotechnology industry for one year, he joined the Nitrogen Fixation Research group of Dr. William E. Newton at the Western Regional Research Center of the U.S. Dept. of Agriculture in Albany, California. After five years of working as a Laboratory Specialist, John accompanied Dr. Newton to the Dept. of Biochemistry and Nutrition at Virginia Tech in Blacksburg, Virginia. There he entered the graduate degree program in June 1991, studying the mechanism of nitrogenase from *Azotobacter vinelandii*. After receiving his PhD. from Virginia Tech, he will join the research laboratories of Profs. Patricia C. Babbitt and George L. Kenyon in the Dept. of Pharmaceutical Chemistry at the University of California, San Francisco where he will continue research in the area of protein engineering.

_____

John S. Cantwell